PUBLICAÇÃO ESPECIAL Nº 10
1988

ESTUDO DE ESTRUTURAS EM GRANDE ESCALA NO HEMISFÉRIO SUL

Paulo Sérgio de Souza Pellegrini

Tese de Doutorado
Rio de Janeiro, Maio/88

CONSELHO NACIONAL DE DESENVOLVIMENTO CIENTÍFICO E TECNOLÓGICO
OBSERVATÓRIO NACIONAL
DEPARTAMENTO DE ASTRONOMIA

TESE

apresentada para obtenção do grau de

DOUTOR EM ASTROFÍSICA

ESTUDO DE ESTRUTURAS EM GRANDE ESCALA NO HEMISFÉRIO SUL

por

PAULO SÉRGIO DE SOUZA PELLEGRINI

Defendida em 8 de Junho de 1988

perante banca composta por:

Luis Alberto Nicolaci da Costa

Hugo Vicente Capelato

Ronaldo Eustáquio de Souza

Sayd José Codina Landaberry

Jorge Ramiro de la Reza

Para Maíra,

que quer saber

onde é o fim do Universo.

ÍNDICE

AGRADECIMENTOS

Esta tese representa o resultado de um trabalho que envolveu um número apreciável de pessoas e, portanto, os agradecimentos devem ser extensos.

A concepção do projeto "Southern Sky Redshift Survey" (SSRS) se deu a partir de uma discussão científica de L. Nicolaci da Costa com pesquisadores do CfA. A necessidade de estender o levantamento recém concluído no norte já era óbvia então e restava encontrar uma forma de torná-lo uma realidade. Daí surgiu uma frutífera colaboração entre o O.N. e o CfA.

O mérito de levar adiante a parte brasileira do projeto cabe principalmente a Nicolaci com o ímpeto e o profissionalismo que o caracterizam. Sua atuação foi desde os problemas instrumentais ao direcionamento científico do projeto. Os resultados científicos obtidos com os dados acumulados com o SSRS e aqui apresentados, tiveram sua orientação segura, participação efetiva e incentivo constante.

David Latham foi em todos os momentos um suporte incansável. Propiciou um desenvolvimento instrumental significativo para o O.N., participou efetivamente das implementações, incentivou continuamente, discutiu os resultados e, especialmente, confiou em nossa capacidade.

Marc Davis foi um dos idealizadores do SSRS e colaborou significativamente para as observações em Las Campanas, bem como em parte da análise aqui apresentada.

Christopher Willmer teve uma participação especialmente importante. Nas observações, na redução de dados, no desenvolvimento de programas de análise, na revisão de textos, etc.

Reinaldo de Carvalho contribuiu para as observações e particularmente para o desenvolvimento da rotina de análise dos "voids".

John Huchra tornou disponível dados observacionais do CfA, o que permitiu uma análise ampla da calota polar sul.

O SSRS como um todo foi multi-institucional e envolveu vários pesquisadores do O.N., CfA, Berkeley, Caltech e SAAO. Além dos já mencionados, M. Maia, J. Tonry, A. Meiksin, W. Sargent, J. Menzies e I. Coulson.

Para um projeto como esse que teve um grande conteúdo observacional, a participação técnica foi essencial. Marcos Nunes, além de construir o detector Reticon reproduzindo a última geração de detectores intensificados que estava sendo desenvolvida no CfA, foi o responsável pela sua implantação e manutenção eficientíssimas, participando também de observações. John Geary prestou um importante apoio para a constante atualização e modernização do sistema.

A eficiência do detector se deve em grande parte ao seu acoplamento à computação, onde Charles Rite (no "software") e Darcy do Nascimento (no "hardware") foram essenciais, desenvolvendo, implementando e adaptando partes do sistema. Ambos foram também fundamentais para a implementação dos atuais recursos de redução. Charles, além de participar de observações, auxiliou em alguns recursos gráficos utilizados neste trabalho. Bill Wyatt possibilitou a implementação e atualização do "software".

A todos, muito obrigado.

I. INTRODUÇÃO

Teoria e observação tem concorrido de uma forma extremamente positiva para o avanço do estudo da formação e evolução de grandes estruturas no Universo. Em particular, o grande avanço alcançado nos últimos anos se deve em grande parte aos resultados obtidos por extensos levantamentos de velocidades radiais iniciados na década passada e completados recentemente. Estes levantamentos provocaram uma profunda revisão das idéias correntes sobre a distribuição espacial de galáxias, revelando uma estrutura não homogênea (pelo menos numa escala de $100h^{-1}$ Mpc, $H_0 = 100h$ km/s/Mpc) onde as galáxias se apresentam concentradas em estruturas filamentares e planares, delineando grandes regiões aparentemente vazias de galáxias brilhantes. Um resumo dos principais levantamentos é descrito por Huchra e Geller (1986) e o impacto destes trabalhos pode ser aferido pelo fato de que até 1978 velocidades radiais foram determinadas para cerca de 1000 galáxias, enquanto atualmente existem dados acumulados para mais de 20000 objetos. Este números refletem de maneira contundente a importância dos vários programas conduzidos nos últimos anos.

As estratégias observacionais destes levantamentos são pelo menos de 3 tipos diferentes e tem fornecido importantes informações complementares:

- Levantamentos "uni-dimensionais" consideram pequenas regiões angulares e amostras fundas de galáxias até magnitudes $m_B \approx 17 - 22$. Este tipo de

levantamento vem sendo utilizado extensivamente por Kirshner et al. (1981, 1987) para investigar a extensão e o contraste de densidade associado ao "void" de Boots, o primeiro grande "void" descoberto. Este tipo de levantamento se mostrou bastante eficiente para identificar regiões vazias e estabelecer, pelo menos, um limite superior para a escala de tamanho dos "voids", que até agora continuam sem uma caracterização adequada de suas dimensões. Estes levantamentos tem sido utilizados, também, para estudar a possível evolução temporal das propriedades de aglomeração da matéria luminosa no Universo (e.g. Koo et al. 1986).

- Levantamentos "bidimensionais" consideram grandes regiões angulares ($\approx$ 100°) em faixas de declinação estreitas ($\approx$ 6°) e são moderadamente profundos como o que vem sendo realizado por de Lapparent et al. (1986) e Geller et al. (1987). A principal vantagem deste tipo de levantamento é permitir o estudo mais eficiente das características geométricas de algumas estruturas individuais, especialmente os "voids".

- Levantamentos "tridimensionais" consideram grandes regiões angulares e modestas distâncias radiais permitindo estudar e analizar a topologia da distribuição de galáxias (Huchra et al. 1983). Este é o tipo de levantamento apresentado e discutido nesta tese.

O primeiro levantamento completo e importante do tipo "tridimensional" foi o CfA Redshift Survey (CfA1), realizado pelo Harvard-Smithsonian Center for Astrophysics, que determinou velocidades radiais para uma amostra de galáxias no Hemisfério Norte limitada em magnitude 14.5. Este levantamento foi também o primeiro a se extender além do

aglomerado de Virgo e amostrar um volume do espaço suficientemente grande para, pelo menos, se aproximar de uma amostra representativa do Universo em grande escala. Além de Virgo, este levantamento inclui outros aglomerados como Coma, A1367, A2197, A2199, A194 e A400 e uma inspeção nos mapas projetados revela uma distribuição bastante irregular, com as galáxias concentradas em estruturas lineares que delineam grandes regiões vazias. Entretanto, uma constatação importante foi que o tamanho das estruturas observadas é comparável à profundidade efetiva do levantamento ($\approx$ 5000 km/s), sugerindo que o volume observado ainda não seja suficientemente grande para conter uma amostra adequada e representativa para estudos estatísticos da distribuição de galáxias. Este resultado demonstrou a imediata necessidade de se extender o CfA1, tanto em profundidade, como em outras direções do céu, de forma a evitar a grande concentração de galáxias associada ao aglomerado de Virgo. Programas observacionais para realizar estas extensões foram iniciados em 1981-82 por diferentes grupos, com observações sendo realizadas no Hemisfério Norte pelo CfA em faixas de declinação de 6° até uma magnitude limite m_B = 15.5 (CfA2), e no Sul considerando uma amostra com uma cobertura angular de 1.75 steradianos, comparável à da porção norte da amostra do CfA1.

Do CfA2 surgiram as primeiras evidências de que as galáxias se concentram preferencialmente em estruturas bidimensionais. De fato, de Lapparent et al. (1986) interpretaram os mapas de redshift como sendo seções de corte de "bolhas" em contato. Esta explicação se deve em grande parte às estruturas encontradas na primeira faixa de declinação observada, centrada em δ = 29.5° e contendo o proeminente aglomerado

de Coma. As galáxias, nesta faixa, se distribuem preferencialmente em filamentos curvos e contínuos, aproximadamente circulares, delimitando regiões vazias. O aparecimento destas estruturas foi interpretado como uma possível evidência de que as formas atualmente observadas das estruturas em grande escala foram geradas via explosões como no cenário proposto por Ostriker e Cowie (1981). Entretanto, a informação limitada disponível nos levantamentos "bidimensionais" não permite uma afirmação mais conclusiva. Mesmo assim, os resultados deste levantamento, bem como uma análise posterior dos dados de levantamentos mais fundos, em áreas restritas na direção de Corona Borealis (Postman et al. 1986), sugerem que a existência de grandes regiões vazias, com dimensões comparáveis às do "void" de Bootes ($\approx 60h^{-1}$ Mpc) são relativamente frequentes e requerem uma explicação adequada por parte das teorias de formação de grandes estruturas no Universo.

Uma maior quantidade de informação está certamente contida em levantamentos de profundidade moderada e grande cobertura angular. Com eles pode-se determinar algumas questões importantes como: 1) estimar a densidade média de galáxias; 2) medir o campo de velocidades peculiares, em combinação com resultados de estimadores secundários de distância; 3) procurar evidências para a formação de galáxias com "bias"; 4) testar os modelos para a origem da estrutura em grande escala pelo confronto direto com os resultados obtidos em simulações numéricas de N-corpos.

Desta forma se justifica o interêsse crescente num levantamento completo do Universo próximo, no Hemisfério Sul. Em primeiro lugar ele representa uma amostra estatísticamente independente, o que permite

avaliar a importante questão da representatividade das amostras até agora existentes. Em segundo lugar uma amostra na Calota Polar Sul evita grandes concentrações de galáxias, como o aglomerado de Virgo, permitindo uma visão mais clara das estruturas de menor contraste de densidade. Em terceiro lugar ele pode ser decisivo para a busca de uma evidência da existência de uma grande concentração de galáxias na direção l = 307°, b = 9°, que corrobore o modelo do Grande Atrator proposto por Lynden-Bell et al. (1988) para explicar o campo de velocidades peculiares observado a partir de uma amostra de galáxias elípticas em todo o céu (Burstein et al. 1986, Dressler et al. 1987).

Como mencionado anteriormente, uma das grandes motivações para a realização de levantamentos "tridimensionais" é a possibilidade de confrontar os dados observacionais com os modelos de distribuição obtidos em simulações de N-corpos aplicados à evolução de estruturas no Universo. Essas simulações numéricas tem sido amplamente utilizadas por terem se mostrado uma ferramenta poderosa para fornecer previsões objetivas das estruturas que se formam a partir de diferentes cenários cosmogônicos.

Os modêlos clássicos para a origem das estruturas no Universo supõem que estas se desenvolvem a partir de pequenas perturbações de natureza Gaussiana e fase aleatória. A evolução subsequente depende da natureza das perturbações (isotérmicas ou adiabáticas) e do tipo de matéria existente no Universo. Perturbações de densidade de pequena amplitude se expandem mais lentamente que o Universo como um todo, por efeito do aumento local do campo gravitacional em relação ao campo

medio. Desta forma, o contraste de densidade da perturbação evolui no tempo, formando condensações do material aglutinado. O meio onde são formadas as perturbações é a mistura de matéria e radiação do plasma original do Universo e dois tipos básicos de desvios da homogeneidade são considerados. Se matéria e radiação são perturbados mantendo a mesma proporção número de fotons/número de barions que o meio ambiente esta perturbação é chamada adiabática. Por outro lado, se apenas a componente material é perturbada, mantendo a componente fotônica inalterada, e portanto a mesma temperatura, a perturbação é chamada isotérmica. A evolução temporal dessas flutuações de densidade será determinada pelo seu tamanho característico comparado a 3 escalas importantes: a escala de tamanho do horizonte, a escala de tamanho de Jeans e uma escala característica de dissipação (escala de tamanho de Silk). Estas escalas estão associadas a massas características M_H, M_J e M_S que representam respectivamente a massa bariônica dentro do horizonte, a massa necessária para formar uma perturbação autogravitante e a massa mínima que resiste aos processos dissipativos do fluido cósmico (viscosidade e difusão dos fótons).

Perturbações de diferentes naturezas implicam em cenários bem distintos para a formação das estruturas. Para uma perturbação adiabática de massa M, nos instantes iniciais $M > M_H > M_J$ e esta cresce em relação ao meio ambiente. Se ao entrar no horizonte tal perturbação tem massa maior que a massa de Jeans, seu crescimento permanece. Se ao entrar no horizonte $M < M_J$ a perturbaçao oscila como uma onda acústica até a era de recombinação, quando a massa de Jeans decresce abruptamente. Se a perturbação não é dissipada até a era de recombinação ($M > M_S$), sua

amplitude volta a crescer. Neste caso as primeiras estruturas a entrarem no regime não-linear teriam massas da ordem de 10^{14} - 10^{15} $M_{\odot}$ (Silk 1968), que correspondem a aglomerados de galáxias e superaglomerados. O caminho evolutivo dessas perturbaçãoes seguiria, então, a teoria proposta por Zel'dovich (1970) para a formação de "panquecas". A idéia básica é de que se existe na perturbacão recém formada uma escala de coerência, esta domina o colapso gravitacional que se realiza preferencialmente numa direção, formando uma estrutura preferencialmente planar. Numa etapa posterior essas "panquecas" se fragmentariam formando galáxias, que neste caso, seriam mais recentes que as grandes estruturas.

Perturbações isotérmicas não evoluem nem se dissipam até a era de recombinação, mantendo as suas amplitudes iniciais. Comno após a recombinação a massa de Jeans cai para um valor da ordem de 10^{6} $M_{\odot}$, as primeiras estruturas a se formar são sistemas subgalácticos na escala de aglomerados globulares. A formação de galáxias, aglomerados de galáxias e superaglomerados se daria por aglutinação hierárquica, como sugerido por Peebles e colaboradores.

A origem de perturbações iniciais no Universo é ainda uma questão incerta em muitos detalhes. Entretanto, a teoria da inflação tem se mostrado de grande utilidade para a resolução deste problema. Esta teoria talvez seja um dos resultados mais importantes da cosmologia moderna. Ela prevê uma expansão exponencial do Universo durante uma transição de fase prevista pelos modelos de Grande Unificação (Guth, 1981), que descrevem as interações entre partículas elementares em altas energias. Sem entrar nos detalhes dos modelos inflacionários, que fogem

ao escopo do presente trabalho, eles tem como principal virtude explicar o alto grau de homogeneidade e isotropia do Universo como um todo, refletido pelas observações da radiação de fundo, a assimetria de barions e anti-barions observada e prevê um valor de $\Omega = 1$. Da mesma forma ela prevê o surgimento de flutuações quânticas a partir da transição de fase, que podem ser responsáveis pelo surgimento das perturbações iniciais de natureza adiabática. A inflação prevê também um espectro de perturbações inicias de curvatura constante que, como argumentado por Harrison (1970) e Zel'dovich (1972), é o único que pode ser interpretado sem problemas em pequena e grandes escalas.

A enorme quantidade de dados acumulada até hoje permitiu a astronomia moderna realizar uma importante descoberta com relação ao material constituinte do Universo. Determinações dinâmicas de massa do material luminoso em diferentes escalas tem levado sistematicamente à evidência da existência de material invisível, mas dinamicamente significativo. Essas conclusões derivam das curvas de rotação de galáxias espirais (Bosma 1981, Rubin et al. 1980) que indicam a existência de material escuro provavelmente na forma de um halo externo à porção luminosa dessas galáxias. Em escalas maiores, como no caso de núcleos de aglomerados de galáxias ricos, os dados observacionais relativos à dinâmica e luminosidade desses sistemas (ver Blumenthal et al. 1984) indicam que a parte visível perfaz um total de cerca de 10% do material com o restante 90% constituido de materia escura (DM). Na verdade, diferentes linhas de argumento sugerem que o material escuro não é bariônico. Se o Universo fosse constituido apenas de barions, vínculos impostos pela teoria de nucleosíntese e a abundância observada de

deutério implicam num valor de $\Omega_b \leq 0.1$. Num Universo aberto com $\Omega = \Omega_b = 0.1$, perturbações que resultariam em sistemas na escala de galáxias e aglomerados tem pouco tempo para crescer, exigindo grandes amplitudes iniciais na época de recombinação. As amplitudes necessárias, no entanto, induziriam flutuações na temperatura de fundo uma ordem de magnitude maior do que as observadas. Por outro lado, se a natureza da matéria escura for de interação fraca, perturbações inicias de grande amplitude poderiam existir sem interação com a componente fotônica. Essas perturbações "escuras" agiriam como formadoras de futuras estruturas.

Estes argumentos levaram ao desenvolvimento de teorias de formação de grandes estruturas envolvendo matéria não bariônica. Genericamente estas teorias podem ser divididas em duas classes associadas à matéria escura quente (HDM) e matéria escura fria (CDM), dependendo se as partículas são relativísticas ou não quando as perturbações com massas da ordem de galáxias entram no horizonte. Modelos de HDM geralmente consideram a existência de neutrinos massivos ($\approx$ 30 eV), que enquanto relativísticos tem sua distribuição homogenizada por "free-streaming" em escalas da ordem do horizonte. Perturbações com massas menores que a massa característica de dissipação (e.g. Bond e Szalay 1983) são então impedidas de se desenvolver, dando origem a um espectro de perturbações truncado. As estruturas que sobrevivem a esta dissipação tem escalas da ordem de superaglomerados e podem ser identificadas com as "panquecas". Modêlos de CDM consideram partículas massivas ($\approx$ 1 GeV) como fotinos e gravitinos, previstas pelas teorias de supersimetrias grande-unificadas e axions que embora leves, são criados com baixa velocidade. Estas partículas se tornam não relativísticas antes de escalas de tamanho da

ordem de galáxias e superaglomerados entrarem no horizonte e, portanto, os efeitos de "free-streaming" não são importantes. Desta forma o espectro de perturbações iniciais é suave, sem apresentar cortes, dando origem a sistemas num grande domínio de escalas. Como esse espectro declina monotonicamente em todas as escalas, o modêlo de CDM implica numa aglutinação hierárquica. Em resumo, os modelos canônicos assumem, atualmente, que a massa do Universo é dominada por espécies de matéria escura, estáveis e de fraca interação; que as estruturas se desenvolveram por instabilidade gravitacional de flutuações primordiais geradas adiabaticamente na fase de inflação, com um espectro invariante de escala (truncado no caso HDM) e fases aleatórias.

A evolução das estruturas nestes dois cenários diferentes vem sendo exploradas extensivamente em simulações numéricas de N-corpos. Nestas simulações o cenário HDM tem apresentado alguns problemas de interpretação, principalmente quanto à escala de tempo de formação das estruturas. Se o requerimento de que a função de correlação obtida seja semelhante à observada atualmente for utilizado para determinar a época atual neste modêlo, os resultados indicam que a formação de "panquecas" é um fenômeno relativamente recente ($z \approx 1 - 2$ para $\Omega \approx 0.1 - 1$). Isto está em desacôrdo com a observação de quasares (que se imagina estejam associados a núcleos ativos de galáxias) a $z > 3$. Outros problemas encontrados neste cenário são: 1) explicar a existência de galáxias longe das grandes estruturas observadas, já que os pequenos sistemas neste modêlo tem sua origem na fragmentação das "panquecas"; 2) a aparente inexistência de correlações entre as propriedades das galáxias e as estruturas em grande escala 3) o vínculo imposto na massa dos neutrinos

(> 100 keV) pelo tamanho dos halos de galáxias anãs.

Atualmente os modêlos mais populares para a formação das estruturas são os modêlos de CDM extensamente estudados por (e.g. Frenk et al. 1983, Davis et al. 1985, White et al. 1987). Uma das principais características destes modêlos é, ao contrário dos modêlos de HDM, fazer previsões bem específicas sobre a estrutura das galáxias. A evolução das estruturas neste cenário foram estudadas por Davis et al. (1985) para modêlos com $\Omega \leq 1$. Em particular, os modêlos com $\Omega = 1$ se mostraram mais consistentes com as observações desde que se assuma que as galáxias se formam em picos de densidade com maior contraste sobre a média o que exige a existência de algum processo de formação de galáxias com "bias".

Outros modêlos alternativos para a origem de estruturas no Universo foram propostos mas ainda não estão tão desenvolvidos como os discutidos acima, que apresentam previsões específicas que podem ser confrontadas com as observações que vem sendo acumuladas nos últimos anos. Para completeza, vale a pena citar: 1) o modêlo de cosmic strings, que são defeitos topológicos que surgem durante a transição de fase nos primórdios do Universo (Albrecht 1987); 2) cenários envolvendo explosões nucleares dos primeiros objetos massivos que se formaram (Ostriker e Cowie 1981); 3) strings supercondutores (Ostriker et al 1986). Uma característica desta classe de modêlos é que, ao contrário das flutuações Gaussianas, eles não apresentam fase aleatória, o que se reflete nas propriedades topológicas da distribuição de galáxias em escalas ainda no regime linear (Weinberg et al. 1987).

A confrontação das previsões dos modêlos numéricos com as observações é sem dúvida o principal instrumento disponível para discriminar o cenário mais provável para a origem das estruturas no Universo. Ao mesmo tempo isto exige o desenvolvimento de estatísticas mais adequadas que permitam a análise quantitativa dos modêlos teóricos e das observacões. O resultado de um confronto deste tipo, para o caso do modêlo de CDM, usando diferentes estatísticas é discutido por Davis et al. (1985) e White et al. (1987).

Este desenvolvimento da capacidade de previsão dos modêlos teóricos gerou, por sua vez, um interêsse no aumento da base de dados com a qual essa confrontação pode ser feita e justifica o grande esfôrço na realização de levantamentos de velocidades radiais nos últimos anos. Entre os principais resultados obtidos até agora se destacam: 1) a provável existência de grandes estruturas "bi-dimensionais", (relativamente finas) onde se concentram a maioria das galáxias; 2) e existência, talvez bastante frequente, de "voids" com dimensões $\approx 60h^{-1}$ Mpc e com um contraste de densidade da ordem de 0.75; 3) a existência de movimentos peculiares com velocidades da ordem de 600 km/s em regiões de aproximadamente $60h^{-1}$ Mpc. Estes dados observacionais devem ser explicados por qualquer teoria viável.

Neste trabalho são apresentados e discutidos os resultados de um extenso levantamento de velocidades radiais no Hemisfério Sul. Este projeto foi iniciado pelo Observatório Nacional (ON) em 1981, com o desenvolvimento de um detector intensificado Reticon, similar ao utilizado

pelo CfA para a realização dos levantâmentos CfA1 e CfA2. Atualmente mais de 2000 espectros de galáxias foram observados neste programa, para completar diversas amostras. No capítulo II estas diferentes amostras são apresentadas, bem como detalhes sobre as observações e as qualidades das velocidades radiais obtidas. No capítulo III são apresentados os resultados do Southern Sky Redshift Survey (SSRS) que representa uma das maiores amostras disponíveis no Hemisfério Sul para estudos estatísticos. No capítulo IV são apresentadas duas extensões do SSRS: a primeira procura definir uma amostra homogênea para a Calota Polar Galáctica Sul, permitindo investigar a extensão das estruturas observadas no SSRS; a segunda considera uma amostra mais funda, numa faixa de declinação de 10° onde estão presentes as estruturas mais proeminentes do SSRS. No capítulo V são apresentados os resultados de análise quantitativas através das quais pretende-se estudar as propriedades dos "voids" observadas no SSRS e verificar se as amostras do CfA1 e SSRS são estatísticamente similares. Neste capítulo é também apresentado o cálculo da velocidade peculiar induzida gravitacionalmente sobre o Grupo Local pelo material em nossa vizinhança. Este cálculo extende aos resultados preliminares obtidos por Davis e Huchra (1982) a contribuição do Hemisfério Sul. Condições de auto-consistência fornecem algumas estimativas dinâmicas para o parâmetro de densidade Ω. Finalmente, no capítulo VI é apresentado um resumo dos principais resultados do trabalho e as linhas gerais da pesquisa que se prentende dar continuidade.

REFERÊNCIAS

Albrecht, A. 1987, in Nearly Normal Galaxies: From the Planck Time to the Present, Proceedings of the UCSC Summer Astrophysics Workshop, ed. S. M. Faber, Springer: New York, p. 423

Blumenthal, G. R., Faber, S. M., Primack, J. R. and Rees, M. 1984, Nature, **311**, 517.

Bond, J. R. and Szalay, A. S. 1983, Ap. J. **274**, 443.

Bosma, A. 1981, Astron. J., **86**, 1825.

Burstein, D. Davies, R., Dressler, A. Faber, S. M., Lynden-Bell, R., Terlevich, R. and Wegner, G. 1986, in Galaxy Distances and Deviations from the Universal Expansion, eds. B. F. Madore and R. B. Tully (Dordrecht: Reidel), p. 123.

Davis, M., Efstathiou, G., Frenk, C. S. and White S. 1985, Ap. J., **292**, 371.

Davis, M. and Huchra, J. 1982, Ap. J., **254**, 437.

de Lapparent, V., Geller, M. and Huchra, J. P. 1986, Ap. J. (Letters), **302**, L1 (LGH).

Dressler, A., Lynden-Bell, D., Burstein, D, Davies, R. L., Faber, S. M., Terlevich, R. J. and Wegner, G. 1987, Ap. J. (Letters), **313**, 137.

Frenk, C. S., White, S. and Davis, M. 1983, A. J. **271**, 417.

Geller, M. J., Huchra, J. P. and de Lapparent, V. 1987, IAU Symp. 124, Observational Cosmology, ed. A. Hewitt, G. Burbidge and L. Z. Fang (Dordrecht: Reidel), p. 301.

Guth, A. H. 1981, Phys. Rev, **D23**, 347.

Harrison, E. R. 1970, Phys. Rev., **D1**, 2726.

Huchra, J. P., Davis, M., Latham, D. and Tonry, J. 1983, Ap. J. Suppl.,

52, 89.

Huchra, J. P. and Geller, M. (1987). To appear in "The Proceedings of the 13th Texas Symposium on Relativistic Astrophysics".

Kirshner, R. P., Oemler, A., Schechter, P. L. and Shectman, S. A. 1981, Ap. J. (Letteres), 248, 493.

Kirshner, R. P., Oemler, A., Schechter, P. L. and Shectman, S. A. 1987, Ap. J., 314, 493.

Koo, D., Kron, R. and Szalay, A. 1986 in 13th Texas Symposium on Relativistic Astrophysics, ed. M. Ulmer (World Scientific: Singapore).

Lynden-Bell, D., Faber, S. M., Burstein, D., Davies, R. L., Dressler, A., Terlevich, R. J. and Wegner, G. 1987, Ap. J., in press.

Ostriker, J. P. and Cowie, L. L. 1981, Ap. J. (Letters), 243, L127.

Ostriker, J. P., Thompson, C. and Witten, E. 1986, Phys. Lett. B, 180, 231.

Rubin, V. C., Ford, W K. and Thonnard, N. 1980, Ap. J. 238, 471.

Postman, M., Huchra, J. P. and Geller, M. J. 1986, A. J. 92, 1238.

Silk, J., 1968 Ap. J. 151, 459.

Weinberg, D., Gott, R. and Melott, A. 1987, Ap. J. 321, 2.

White, S., Frenk, C. S., Davis, M. and Efstathiou, G. 1987, Ap. J., in press.

Zel'dovich, Ya. B. 1970, Astron. Astrophys. 5, 84.

Zel'dovich, Ya. B. 1972, M. N. R. A. S., 160, 1P.

II. DADOS OBSERVACIONAIS

II.1 LEVANTAMENTOS DE VELOCIDADES RADIAIS NO HEMISFÉRIO SUL

O esfôrço realizado no Observatório Nacional no sentido de se obter amostras apropriadas para o estudo de estruturas em grande escala no Hemisfério Sul foi iniciado em 1981 e vem se concretizando através da realização de levantamentos de velocidades radiais de áreas extensas selecionadas neste hemisfério. Dois fatores são importantes para a seleção de uma amostra de galáxias adequada para o tipo de análise que se pretende realizar: por um lado, ela deve ser bastante extensa no sentido de ser representativa do Universo como um todo; por outro lado, dado um parâmetro de seleção bem definido, e um limite para esse parâmetro, ela deve ser o mais completa possível de forma a incluir, se não todos, a grande maioria dos objetos até esse limite. Somente atendendo a estas duas condições uma amostra pode ser considerada adequada para uma análise estatística confiável. Amostras deste tipo, utilizadas para o estudo de grandes estruturas no Universo, tem sido geralmente selecionadas em magnitude, entre estas o levantamento CfA1. Como esse levantamento representa, até o momento, a amostra angularmente extensa e completa mais bem estudada, seria de grande interesse a obtenção, no Hemisfério Sul, de um levantamento com características idênticas e que possa compor com os dados do Norte uma amostra homogênea "todo-céu".

Entretanto, no Hemisfério Sul não existe um catálogo como o compilado por Zwicky et al. (CGCG, 1961-1968) a partir do qual se possa

extrair diretamente uma amostra extensa e bem definida, até uma magnitude limite 14.5. Por outro lado, é possivel obter-se a partir do catálogo ESO-Uppsala (Lauberts 1982), que cobre declinações abaixo de-17.5°, uma amostra bem definida, selecionada em diâmetro e se extendendo até um limite de profundidade comparável ao da amostra do CfA1. Embora tal critério de seleção impeça que uma amostra assim determinada seja utilizada em conjunto com a amostra do CfA1 para uma análise "todo-céu", o seu estudo e intercomparação com o Norte é, por si só, de grande interesse pois permitirá, pela primeira vez, o exame de uma amostra extensa e moderadamente profunda no Hemisfério Sul. Mais ainda, como será mostrado neste capítulo, é possivel também determinar-se, a partir deste catálogo, amostras aproximadas, limitadas em magnitude, utilizando-se relações médias entre os diâmetros e as magnitudes das galáxias. Mesmo com os problemas envolvidos nesta determinação, esta tentativa é importante no sentido de resolver de modo aproximado o problema da unificação dos dados nos dois hemisférios e produzir uma amostra que possa fornecer resultados globais.

O trabalho apresentado nesta tese é voltado para a análise de amostras localizadas na Calota Polar Sul ($b \leq -30°$) onde está concentrado o maior esfôrço observacional. O levantamento realizado nesta área perfaz um total de cerca de 2000 galáxias já observadas em colaboraçao com o CfA, o Las Campanas Observatory e o South African Astronomical Observatory. Na seção II.2 é apresentado e discutido o critério de seleção da amostra situada abaixo de $\delta \leq -17.5°$, limitada em diâmetro e que constitui o Southern Sky Redshift Survey (SSRS). Esta amostra é a que pode ser melhor definida partindo dos catálogos atualmente

existentes e, desta forma, será utilizada para análises mais detalhadas nos capítulos seguintes. Nesta seção é também descrita a metodologia de observação e redução dos dados bem como os resultados relativos à qualidade das velocidades radiais obtidas. Na seção II.3 é apresentado o sistema de magnitudes desenvolvido para produzir amostras limitadas em magnitude no Hemisfério Sul e discutido, em particular, a obtenção de uma amostra comparável à do CfA1 na mesma região do SSRS.

O levantamento limitado em magnitude realizado nesta região, juntamente com a parte sul do levantamento CfA1 deixam apenas 0.55 steradianos da calota polar sul não cobertos, até agora, por qualquer esforço sistemático de determinação de velocidades radiais. Esta região permite a composição de todos os levantamentos limitados em magnitude na calota sul numa área contígua de 3.13 steradianos, facilitando a visualizão da extensão das estruturas identificadas no SSRS para o norte, em direção ao superaglomerado de Hydra-Centaurus. Com este intuito o ON e o CfA concluiram recentemente um levantamento limitado em magnitude 14.5 na faixa não explorada até agora ($-17.5° \lesssim \delta \leq -2.5°$) utilizando o catálogo de Vorontsov-Velyaminov e Arhipova (MCG, 1963-1968) na seleção de galáxias. Embora as magnitudes quotadas no MCG sejam de qualidade discutível (já que são na maioria determinadas visualmente em intervalos de 0.5 mag), a sua utilização se faz necessária pois este é o único catálogo moderadamente profundo nesta região. Os resultados desse mapeamento serão mostrado no capítulo IV.

Por outro lado, a conclusão dos levantamentos das amostras comparáveis à do CfA na região de $\delta \leq -17.5°$ mostrou a necessidade de

um mapeamento mais preciso de algumas estruturas e "voids", que se presupõe existir a partir dos dados daquelas amostras. Neste sentido, foram também iniciados, recentemente, levantamentos mais fundos, limitados em magnitude 15.5 na calota polar sul, em faixas de 10° de declinação. As magnitudes adotadas para esta seleção são aquelas determinadas por relações médias diâmetro-magnitude a partir do catálogo ESO-Uppsala (ver seção II.3) e os resultados para a primeira faixa examinada, $-40° \leq \delta \leq -30°$, que contem um dos mais interessantes "voids" detectados no SSRS serão mostrados no capítulo IV. A estratégia de observação em fatias de 10° de declinação é similar àquela que vem sendo realizada pelo CfA no Norte (de Lapparent et al. 1986) e a conclusão de ambos os levantamentos resultará na mais extensa amostra de galáxias produzida até então. Na verdade, os dados de velocidades radiais no Hemisfério Sul já superam em quantidade os dados fotométricos e quando uma melhor e mais extensa base de dados fotométricos estiver disponível neste hemisfério os dados provenientes das extensões destes levantamentos aqui descritos permitirão a determinação de uma amostra mais precisa e completa, até um limite próximo à magnitude 15.5.

Finalmente, convem mencionar que também vem sendo realizado um levantamento de velocidades radiais no superaglomerado de Hydra-Centaurus, devido ao crescente interêsse que esta região do espaço tem despertado entre os pesquisadores interessados no estudo de grandes estruturas no Universo. Recentemente este interêsse se acentuou graças à proposta da existência, nesta direção, de uma grande concentração de massa (Dressler 1987), responsável pelo deslocamento global da nossa vizinhança no Superaglomerado Local. Embora as análises por nós

realizadas, nesta região, com uma amostra limitada em magnitude, estejam voltadas para as propriedades de aglomeração da região de Hydra-Centaurus, é interessante mencionar o fato apontado por Lynden-Bell et al. (1987) de que no levantamento realizado pelo ON a presença desta grande massa já se fazia sentir como um excesso de galáxias a 4000 km/s. Os principais resultados obtidos nesta região, por pesquisadores do ON não são tratados aqui e são descritos por da Costa et al. (1986, 1987).

REFERÊNCIAS

da Costa, L. N., Nunes, M. A., Pellegrini, P. S., Willmer, C., Chincarini, G. and Cowan, J. 1986, Astron. J. **91**, 6.

da Costa, L. N., Willmer, C., Pellegrini, P. S. and Chincarini, G. 1987, Astron. J. **93**, 1338.

de Lapparent, V., Geller, M. and Huchra, J. P. 1986, Ap. J. (Letters), **302**, L1 (LGH).

Dressler, A. 1987 preprint.

Lauberts, A. 1982, The ESO/Uppsala Survey of the ESO(B) Atlas (Munchen: European Southern Observatory).

Lynden-Bell, D., Faber, S. M., Burstein, D., Davies, R. L., Dressler, A., Terlevich, R. J. and Wegner, G. 1987, Ap. J., in press.

Vorontsov-Velyaminov, B. A. and Arhipova, V. P. (1963-1974). Morphological Catalogue of Galaxies (Moscow). Parts 2 to 5.

Zwicky, F., Herzog, E., Wild, P., Karpowicz, M. and Kowal, C. (1961-1968). Catalog of Galaxies and Clusters of Galaxies Vols. 1-6 (Pasadena, California Institute of Technology).

II.2 AMOSTRA LIMITADA EM DIÂMETRO

THE ASTRONOMICAL JOURNAL VOLUME 89, NUMBER 9 SEPTEMBER 1984

REDSHIFTS FOR 228 SOUTHERN GALAXIES

L. N. DA COSTA, P. S. PELLEGRINI, M. A. NUNES, AND C. WILLMER
Department of Astronomy, CNPq/Observatório Nacional, Rua General Bruce, 586, Rio de Janeiro, R. J., 20921, Brazil

D. W. LATHAM
Harvard-Smithsonian Center for Astrophysics, 60 Garden Street, Cambridge, Massachusetts 02138
Received 29 March 1984; revised 29 May 1984

ABSTRACT

In this paper, we present new redshifts for 228 galaxies located south of declination $-30°$. The observations were made with a photon-counting Reticon detector on the Observatório Nacional (ON) 60-in. telescope. The detector is identical to the one used at Mount Hopkins for the CfA Redshift Survey, and the redshifts were derived using the same data-analysis system. A preliminary comparison with published 21-cm redshifts indicates that our velocities have a zero-point offset of about -4 km s^{-1}, with a typical uncertainty of 40 km s^{-1}. The observations reported here are the initial results of the ON-CfA Redshift Survey currently being undertaken in the southern hemisphere.

I. INTRODUCTION

Recent redshift surveys of galaxies have had a great impact on observational cosmology, considerably altering our view of the large-scale distribution of matter in the universe. Results from deep surveys on small fields (e.g., Kirshner *et al.* 1979; Kirshner *et al.* 1983), and wide-angle surveys of nearby galaxies (e.g., Huchra *et al.* 1983a) have clearly shown that galaxies tend to concentrate primarily in the form of long, interconnected linear filaments which surround large regions apparently devoid of luminous matter.

The resulting picture of cellularlike structures contrasts with earlier expectations on the nature of the large-scale galaxy distribution, stimulating a number of theoretical investigations about the nonlinear development of structures in the expanding universe. In recent years, the clustering process has been studied by means of extensive N-body simulations with initial conditions similar to those expected for the isothermal (e.g., Aarseth *et al.* 1979; Efstathiou 1979; Efstathiou and Eastwood 1981; Miller 1983) and the adiabatic (Klypin and Shandarin 1983; Frenk *et al.* 1983) scenarious of galaxy formation. In addition, several attempts have been made (e.g., Hausman *et al.* 1983; Hoffman *et al.* 1983; Pebbles 1983) to explain the formation of voids as a result of the growth of underdense regions in the initial distribution of matter. This question is particularly important since the existence of large voids has been commonly used as an argument against the gravitational instability scenario. Comparison between the results of these theoretical works with the properties of the presently observed galaxy distribution may provide a better understanding of the physical processes at work in the clustering of galaxies and to what extent the observed distribution reflects the distribution of matter at earlier epochs.

The results of previous observational work have also motivated efforts to sample larger volumes of space, trying to come as close as possible to a fair sample volume of the universe. Recently, Davis and Huchra (1982) have argued that the sample of galaxies brighter than $m_B = 14.5$ perhaps already satisfies this requirement. However, the structures revealed by the recently published CfA Redshift Survey (Huchra *et al.* 1983a) are as large as the survey depth, indicating that deeper surveys and additional sky coverage are necessary to fully map the observed structures. It is especially important to extend the observations into the southern skies, complementing the northern sample with galaxies in the opposite direction of the Virgo Supercluster. The southern sample may also help to improve current estimates of the space density of galaxies and contribute towards more accurate measurements of the cosmological density parameter, based on the Virgocentric infall.

At the present time, the Revised Shapley-Ames Catalog (Sandage and Tammann 1981) is the only existing magnitude limited sample of galaxies over the entire sky. However, the sampled volume is relatively small and the catalog includes high-quality redshifts, with uncertainties less than 10 km s^{-1}, as well as low-quality data with velocity uncertainties greater than 100 km s^{-1}. New optical redshifts and 21-cm radial velocities have become available since the publication of the Revised Shapley-Ames Catalog and can be found in the several redshift catalogs that have been recently compiled (e.g., Lauberts 1982; Rood 1980; Fairall *et al.* 1983; Huchra *et al.* 1983b; Huchtmeier *et al.* 1983; Palumbo *et al.* 1983). However, the data in these catalogs were obtained by several authors for a variety of reasons and do not represent an attempt to define a magnitude limited sample that could be used in cosmological investigations. This situation has motivated us to undertake a survey of galaxy redshifts, extending the CfA Redshift Survey into the southern hemisphere. In order to achieve this goal, we plan to use both Mount Hopkins and the Observatório Nacional telescopes with similar photon-counting Reticon detectors. An important aspect of utilizing identical detector systems and the same reduction techniques is that we may expect to produce a homogeneous sample of accurate redshifts, covering a large fraction of the whole sky. In this paper, we present the first results of this joint effort, representing the data accumulated during the observing period of 1982–1983.

II. OBSERVATIONS

The observations reported in this paper were made using a Cassegrain spectrograph and a photon-counting Reticon detector on the 60-in. telescope at the Observatório Astrofísico Brasileiro (OAB) of the Observatório Nacional. The detector employs a dual 936 Reticon system coupled to a high-gain image tube package, and it is identical to the latest version of the photon-counting detectors developed at the Harvard-

 0004-6256/84/091310-09$00.90

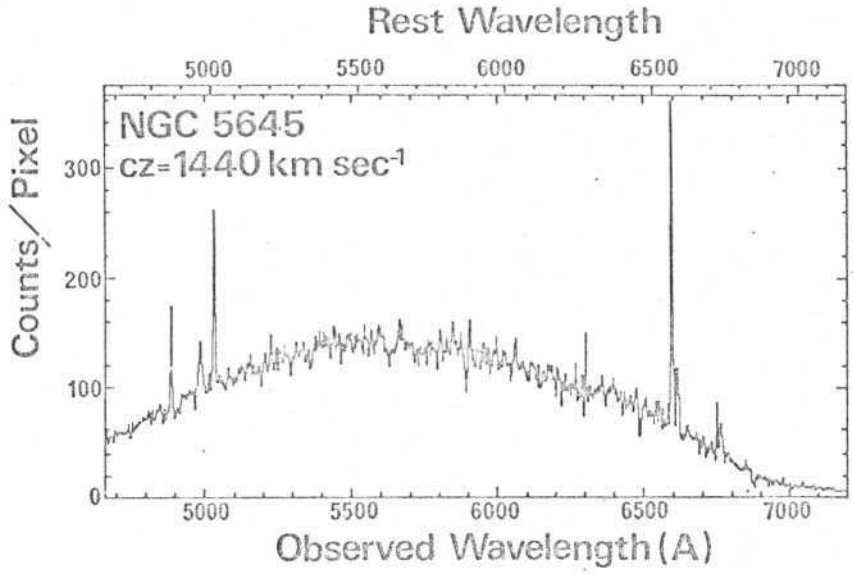

FIG. 1. Typical emission-line galaxy spectrum, showing the spectral coverage used in our observations, which extends from H β at 4861 Å to the forbidden line of [S II] at 6731 Å. The spectrum has not been corrected for the instrumental response and thus does not represent the true energy distribution.

Smithsonian Center for Astrophysics. The main characteristics of the detector system are similar to those described by Latham (1982).

The observations were made through a pair of 3×12-arcsec entrance apertures separated by 30 arcsec on the sky for simultaneous object and sky exposures. Most observations were made using a 900-line/mm grating, giving a dispersion of ~ 100 Å/mm with a typical resolution of 6 Å (FWHM). The wavelength coverage was from about 4700 to 7100 Å, in contrast to the range 4400–7200 Å adopted at Mount Hopkins. Although the spectral coverage in the present case is smaller, it includes all the important absorption features in the green, suitable for correlation analysis and, at the same time, the emission lines of Hα at 6563 Å, [N II] at 6548 and 6583 Å and [S II] at 6717 and 6731 Å that are used to determine an emission redshift. In the early phases of this program, a small number of galaxies were observed using a 1200-line/mm grating, with a dispersion of ~ 60 Å/mm and a resolution of ~ 4 Å. The spectral range was chosen to be 5700–7100 Å in order to include the most common emission lines in the red part of the spectrum. We note that the correlation redshifts obtained for the 60-Å/mm spectra have, in general, slightly larger intrinsic errors because with the 1200-line/mm grating the spectrum spans only ~ 1400 Å, substantially decreasing the number of features that can be matched to the standard template.

A complete galaxy exposure consists of two equal time exposures with the source placed on each of the two channels. In order to get reliable pixel-wavelength solutions, comparison exposures are made, using a helium-argon lamp and a neon lamp, just before and after a galaxy exposure. Usually, 55 to 60 He-Ne-Ar and sky lines are used in a seventh-order polynomial fit of the wavelength solution with typical rms residuals of 0.4 Å. Finally, incandescent lamp exposures are taken at the end of each night, to remove the fixed pattern noise arising in the readout electronics (Davis

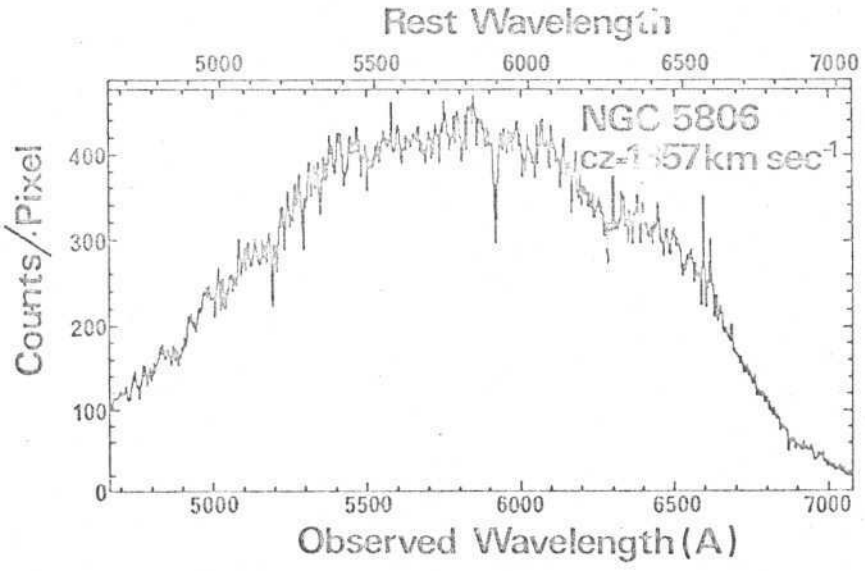

FIG. 2. Spectrum of NGC 5806 showing the absorption features important for the correlation analysis, such as the Mgb lines at ~ 5180 Å, Fe I at 5269 Å and the NaD lines at 5890 Å. As in Fig. 1, the spectrum is not corrected for the instrumental response.

and Latham 1979). We note that the procedures outlined above for the observation of galaxies are the same as those adopted at the CfA (Tonry and Davis 1979).

The observations are made under the control of a Data General Nova 3 minicomputer, which accumulates the spectrum in a separate memory buffer. The data are accessible during the observation and the real-time operating system provides routines to process and display the spectrum as it accumulates, helping to optimize exposure times, typically 10–30 min. A second computer system has been set up in Rio de Janeiro for data reduction, using the data-analysis software developed over the years at the CfA. The radial-velocity analysis, described in more detail by Tonry and Davis (1979) and Tonry (1980), is as follows. After a preliminary preparation of the data, the spectrum is examined for possible emission lines. The identified lines are fitted and the fit parameters are later used to calculate an emission redshift. Next, the emission lines are removed and the spectrum is cross-correlated against both a stellar and a galaxy template. These templates consist of a combination of high signal-to-noise spectra of a large number of stars and galaxies, with accurate published velocities. In the present analysis, we have used the original templates created for the CfA data. The final redshift is a weighted average between the emission and correlation redshifts, using the inverse-squared probable errors as weights (Tonry and Davis 1979). The redshift analysis is done automatically and the results are checked by examining plots of each individual spectrum, showing the main spectral features, which are used to confirm the redshift determination. Examples of typical galaxy spectra are shown in Figs. 1 and 2.

III. RESULTS

The ultimate goal of this project is to observe all galaxies brighter than $m_B = 14.5$ south of declination $-30°$ and below galactic latitude $-30°$. However, the limited number of published magnitudes for galaxies in the southern hemisphere makes it difficult to draw a magnitude limited sample from the available catalogs. The alternative has been to select galaxies from the ESO/Uppsala Survey of the ESO(B) Atlas, now available on tape copies (Lauberts 1982). The ESO catalog includes all galaxies down to a limiting diameter of about 1.0 arcmin and provides information about morphological types and diameter sizes for all galaxies. Using a tape copy of this catalog kindly supplied by Dr. R. West, magnitudes for the galaxies were roughly estimated using approximate relationships between apparent magnitudes and major angular diameters for the different galaxy type groups. Expressions describing these relations were derived using linear fits to the available data in the ESO catalog, and our tentative sample contains over 1600 galaxies estimated to be brighter than $m_B = 14.5$. However, the scatter about the mean relations is large and the sample should change when more accurate photometry becomes available for the southern galaxies.

In Table I, we list the heliocentric velocities for 228 galaxies drawn from the sample defined above. Most of the observed galaxies are expected to be brighter than 13.5, although fainter objects are also included. In column 1, we give the galaxy's name (NGC, IC, or ESO identification number), followed by the 1950.0 coordinates taken from the ESO catalog. The symbol * next to the object's name indicates observations made with the 1200-line/mm grating. In column 4, we list the value for the parameter R introduced by Tonry and Davis (1979), which is a measure of the relative prominence of the true maximum of the correlation function, and it is inversely proportional to the uncertainty in the redshift measurement. The next three columns labeled by V_c, V_e, and V_f are, respectively, the correlation, emission, and weighted average final velocity in km s^{-1}. The estimated error in the redshift determination is given in column 8. Finally, the column denoted by V gives the results of redshift measurements available in the literature, listing in column 9 the quoted velocity uncertainty whenever available. This information comes from the sources listed in the notes following Table I and are indicated in the last column. Our list contains 174 new redshifts, while most of the remaining galaxies were observed because they had either velocity uncertainties greater than our nominal accuracy of 40 km s^{-1} or no reported value for the error. Among the 54 galaxies in the main list with available redshifts, there are 11 galaxies for which our velocity differs by more than 200 km s^{-1} from the published value. The most serious cases of discrepant redshifts are for six galaxies, with velocities given by Fairall *et al.* (1983), for which the difference is of several thousands of km s^{-1}. For some galaxies, we have the results of measurements made with both gratings. In general, the redshifts are consistent and we quote only the values obtained with the 900-line/mm grating. In due course, we expect to reobserve all galaxies whose redshifts were determined using high-dispersion spectra.

TABLE I. Galaxy heliocentric velocities.

Galaxy	R.A. (1950)	Dec. (1950)	R	V_c	V_e	V_f	±	V	±	Ref.
ESO 409-G12	00 02.1	− 30 46	10.5	7 985		7 985	23			
NGC 10	00 06.0	− 34 08	8.0	6 813		6 813	27			
NGC 92*	00 19.0	− 48 54	3.4	3 356		3 356	47	3 499	45	b
NGC 98	00 20.4	− 45 33	8.6	6 158		6 158	26	6 134		a
NGC 101	00 21.4	− 32 49	4.2	3 332	3 454	3 400	30			
ESO 350-G15	00 23.0	− 33 19	6.5	14 940		14 940	31			
ESO 242-G14*	00 32.1	− 43 56	4.6	5 914		5 914	39			
ESO 242-G17	00 32.9	− 44 21	5.1	7 502		7 502	36			
ESO 79-G5	00 38.5	− 63 43	2.2	− 148	1 771	1 771	39			
NGC 312	00 54.1	− 53 03	7.5	8 026		8 026	28			
IC 1608	00 57.0	− 34 36	10.8	3 460	3 489	3 463	22			
ESO 51-G11*	00 58.1	− 68 24	3.1	6 936	7 012	6 990	30	7 015		b
NGC 360	01 00.9	− 65 53	7.4	2 242	2 324	2 264	25			
NGC 378	01 03.8	− 30 27	3.9	9 654	9 596	9 620	30			
IC 1625	01 05.5	− 47 10	7.9	6 714		6 714	27			

TABLE I. (continued).

Galaxy	R.A. 1950	Dec. 1950	R	V_c	V_e	V_f	±	V	±	Ref.
ESO 113-G14*	01 06.1	−58 43	3.0	4 969	4 932	4 944	32			
NGC 409	01 07.2	−36 04	5.6	6 550		6 550	34			
IC 1633	01 07.7	−46 12	7.9	7 233		7 233	27			
ESO 352-G18	01 09.8	−32 30	7.3	9 836		9 836	28			
NGC 439	01 11.4	−32 01	9.2	5 803		5 803	25	5 644	62	b
IC 1657	01 11.8	−32 55	5.1	3 509	3 617	3 564	27			
ESO 352-G28	01 12.7	−32 30	8.7	5 852		5 852	25			
NGC 466	01 15.3	−59 10	3.7	5 276	5 431	5 311	40			
NGC 352-G41	01 16.8	−34 22	10.6	5 612		5 612	23			
ESO 244-G17	01 18.1	−44 23	2.5	7 039	7 067	7 059	33			
ESO 352-G69	01 21.9	−34 59	6.0	5 998	6 080	6 034	26			
ESO 352-G71	01 22.3	−33 26	7.3	9 250		9 250	28			
NGC 568	01 25.7	−35 59	8.2	5 600		5 600	26			
ESO 353-G9	01 29.6	−33 23	5.2	4 984	4 957	4 970	27			
NGC 623	01 32.9	−36 45	7.5	8 955		8 955	28			
ESO 297-G6	01 33.0	−39 24	9.3	5 618	5 695	5 623	24			
ESO 297-G9	01 33.4	−39 37	9.6	5 966		5 966	24			
ESO 3-G1	01 34.8	−85 26	6.0	4 026	4 066	4 043	26			
IC 1719	01 35.3	−34 11	6.8	5 778		5 778	30			
NGC 641	01 36.5	−42 47	8.7	6 397		6 397	25			
ESO 353-G40	01 41.5	−36 20	12.8	5 304		5 304	21			
ESO 353-G45	01 44.7	−34 10	8.7	10 387		10 387	25			
NGC 692	01 46.7	−48 54	11.4	6 256		6 256	22	7 700		a
ESO 152-G26	01 47.7	−56 18	7.2	6 065		6 065	29			
ESO 354-G3	01 48.7	−36 16	7.9	5 736		5 736	27			
ESO 114-G14	01 53.1	−62 21	6.4	7 138		7 138	31			
NGC 749	01 53.4	−30 19	7.3	4 391	4 403	4 394	25			
IC 1759	01 55.7	−33 14	7.6	3 853		3 853	28			
ESO 354-G25	01 58.1	−34 33	10.5	5 034		5 034	23			
ESO 197-G18	02 00.6	−51 10	10.5	6 303		6 303	23			
ESO 3-G7	02 03.1	−84 14	5.2	3 413	3 555	3 413	35			
ESO 354-G34	02 03.6	−32 55	10.2	5 788		5 788	23			
ESO 153-G27	02 08.8	−54 04	9.6	5 693	5 801	5 704	23			
NGC 854	02 09.4	−36 04	8.6	6 204	6 298	6 218	24			
ESO 30-G11	02 11.0	−73 24	9.9	8 067		8 067	24			
NGC 862	02 11.0	−42 16	6.7	5 337		5 337	30			
ESO 298-G28	02 17.5	−38 03	9.9	5 061		5 061	24			
NGC 893	02 18.0	−41 38	7.9	4 990	5 102	5 018	24			
ESO 415-G19	02 18.9	−32 10	4.5	9 429	9 508	9 471	29			
IC 1812	02 27.6	−43 02	8.7	5 169		5 169	25			
ESO 246-G21	02 28.5	−43 15	7.0	5 451		5 451	29			
NGC 1031	02 35.1	−55 05	10.8	5 604		5 604	23			
ESO 416-G9	02 40.2	−30 32	6.0	6 518		6 518	32			
ESO 154-G10	02 43.7	−55 57	6.8	5 511	5 483	5 507	28			
NGC 1097A	02 44.0	−30 26	6.7	1 327		1 327	30			
ESO 356-G11	02 46.7	−32 33	7.0	6 753		6 753	29			
IC 1860	02 47.5	−31 24	6.1	6 959		6 959	32			
ESO 416-G34	02 48.3	−31 46	6.2	7 069		7 069	28			
IC 1864	02 51.6	−34 24	11.5	4 465		4 465	22			
NGC 1165	02 56.7	−32 18	6.0	4 869	4 945	4 893	28			
ESO 31-G5	02 58.4	−74 39	5.0	4 769	4 846	4 802	29			
NGC 1217	03 04.2	−39 14	10.8	6 236		6 236	23			
NGC 1317	03 20.8	−37 17	11.4	1 883	2 006	1 898	21	1 900	70	b
IC 1919	03 24.0	−33 04	6.0	1 187		1 187	32			
IC 1932	03 24.4	−51 31	6.7	11 960	12 005	11 970	27			
NGC 1336	03 24.6	−35 53	7.9	1 466		1 466	27			
ESO 358-G22	03 33.3	−32 46	7.2	1 192		1 192	29			
NGC 1375	03 33.3	−35 26	6.2	757		757	31	669	104	b
IC 1969	03 34.6	−45 21	5.5	20 143		20 143	34			
ESO 358-G34	03 34.8	−36 25	6.9	1 347		1 347	29			
IC 2006	03 52.6	−36 07	13.0	1 340		1 340	21	1 374	42	b
NGC 1495	03 56.7	−44 36	2.2	1 253	1 242	1 245	34			
IC 2051	03 58.4	−83 59	7.4	1 646	1 734	1 675	25			
NGC 1510	04 01.9	−43 32	3.4	937	1 035	1 004	30	968	70	b
ESO 15-G5	04 02.1	−81 12	7.3	4 831	5 028	4 831	28			

TABLE I. (continued).

Galaxy	R.A. 1950	Dec. 1950	R	V_c	V_*	V_f	±	V	±	Ref.
ESO 250-G5	04 03.0	− 46 11	2.4	1 365	1 226	1 289	34			
ESO 201-G22	04 07.6	− 48 51	3.8	3 952	4 132	4 014	37			
NGC 1537	04 11.7	− 31 46	9.1	1 371		1 371	25	1 378	45	b
NGC 1543	04 11.7	− 57 52	9.6	1 088		1 088	24	1 400	52	b
ESO 202-G1	04 15.0	− 47 58	8.0	9 987		9 987	27			
NGC 1558	04 18.7	− 45 09	6.4	4 541		4 541	31			
NGC 1567	04 19.7	− 48 22	10.1	4 538		4 538	23			
NGC 1571	04 20.5	− 43 45	10.7	4 415		4 415	23			
NGC 1572	04 21.0	− 40 43	5.7	5 988	6 076	6 012	29			
ESO 202-G15	04 22.9	− 47 38	10.4	4 570		4 570	23			
IC 2085	04 30.3	− 54 31	5.4	974	1 000	984	29			
ESO 202-G35	04 30.9	− 49 47	4.1	1 805	1 899	1 856	30			
ESO 361-G16	04 51.9	− 32 31	8.7	5 490		5 490	25			
NGC 1706	04 52.0	− 63 04	5.9	4 870		4 870	33	5 130		b
ESO 422-G10	04 53.6	− 31 53	8.2	5 683		5 683	26			
ESO 119-G25	04 58.3	− 58 44	10.4	5 916		5 916	23			
ESO 33-G4	04 58.9	− 75 30	6.7	5 192		5 192	30			
ESO 422-G23	05 00.4	− 30 31	7.4	6 340		6 340	28			
ESO 252-G10	05 04.7	− 45 07	7.3	9 821		9 821	28			
NGC 1824	05 06.2	− 59 47	2.7	1 197	1 298	1 263	35			
NGC 1796B	05 07.9	− 61 26	2.8	8 819	8 942	8 895	35			
ESO 159-G2	05 14.0	− 53 48	5.0	4 248	4 341	4 289	29			
ESO 159-G3	05 15.1	− 54 09	11.2	3 902		3 902	22			
NGC 1956	05 22.1	− 77 47	5.7	4 844		4 844	34			
NGC 1930	05 24.5	− 46 46	8.7	4 224		4 224	25			
NGC 1947	05 26.5	− 63 48	9.7	1 106	991	1 100	24	1 289	46	b
ESO 306-G9	05 30.1	− 42 12	5.4	14 536	14 520	14 531	30			
ESO 306-G17	05 38.5	− 40 52	9.1	10 734		10 734	25			
IC 4906	19 52.5	− 60 36	7.0	3 761		3 761	29			
ESO 284-G4	19 54.7	− 46 15	6.9	5 937	6 017	5 957	26			
ESO 284-G11*	19 58.7	− 45 35	3.9	10 269		10 269	43			
NGC 6848	19 58.8	− 56 14	12.0	4 379	4 489	4 392	21			
ESO 185-G54	19 59.5	− 56 05	5.0	4 348		4 348	22			
IC 4933*	19 59.5	− 55 07	3.8	4 797		4 797	44	4 990	40	b
NGC 6851	19 59.9	− 48 25	15.8	3 043		3 043	19	3 020	23	b
NGC 6855	20 02.8	− 56 32	10.1	4 331		4 331	23			
IC 4944	20 03.2	− 54 35	9.1	5 723	5 804	5 743	23			
NGC 6861*	20 03.7	− 48 31	4.2	2 769		2 769	41	2 819	24	b
NGC 6868	20 06.3	− 48 32	2.8	2 876		2 876	21	2 763	21	b
ESO 284-G23	20 08.0	− 45 44	10.6	5 188	5 286	5 205	22			
NGC 6878	20 10.4	− 44 41	9.0	5 813		5 813	25	5 845	23	b
ESO 340-G7*	20 12.1	− 37 40	2.0	25 019	6 100	6 100	35			
IC 4991	20 15.0	− 41 12	11.3	5 613		5 613	22			
ESO 340-G15	20 16.1	− 41 29	9.5	6 473		6 473	24			
IC 4998	20 18.9	− 38 28	8.4	6 662	6 636	6 656	24			
ESO 285-G7*	20 20.5	− 44 09	4.4	2 923		2 923	40	2 902	18	b
NGC 6899	20 20.7	− 50 36	9.4	5 720		5 720	24			
ESO 234-G21*	20 20.7	− 49 51	2.7	5 443		5 443	56			
NGC 6909	20 24.1	− 47 11	13.9	2 753		2 753	20	2 640	59	b
IC 5011	20 25.3	− 36 12	11.2	2 281		2 281	22			
ESO 285-G20	20 26.2	− 44 00	6.6	6 687	6 762	6 710	26			
ESO 186-IG59	20 28.3	− 53 55	1.8	17 756	3 255	3 255	34			
ESO 234-G47*	20 30.8	− 49 36	2.8	6 142	6 152	6 147	39	10 300		a
NGC 6925*	20 31.2	− 32 09	4.0	2 756		2 756	43	2 799	15	b
ESO 234-G51*	20 32.4	− 49 47	3.5	4 888		4 888	46			
NGC 6932	20 36.7	− 73 48	12.3	3 762	3 871	3 774	21			
ESO 341-IG4*	20 38.0	− 38 22	4.5	5 973		5 973	39			
NGC 6948	20 39.8	− 53 32	9.2	3 217	3 300	3 228	24			
ESO 341-G11*	20 42.3	− 38 21	3.9	6 969	7 193	7 193	47			
NGC 6958	20 45.5	− 38 11	11.7	2 627	2 623	2 627	22	2 742	150	b
IC 5063*	20 48.2	− 57 15	1.7	3 425		3 425	75	3 402	6	b
IC 5053	20 48.6	− 71 20	5.1	4 187		4 187	36			
IC 5065	20 48.7	− 30 02	5.1	9 698		9 698	36			
ESO 286-G10	20 51.0	− 44 16	9.3	5 368		5 368	25			
ESO 235-G16*	20 51.7	− 49 23	2.6	7 214	7 099	7 135	34	5 600		a

TABLE I. (continued).

Galaxy	R.A. 1950	Dec. 1950	R	V_c	V_e	V_f	±	V	±	Ref.
NGC 6984	20 54.3	− 52 04	3.8	4 686	4 690	4 689	29	4 670	23	c
IC 5071	20 56.2	− 72 50	7.9	3 129		3 129	27			
ESO 235-G33	20 57.4	− 48 48	8.6	7 301		7 301	26	4 600		a
ESO 107-G4	20 59.0	− 67 23	13.7	3 099		3 099	20			
NGC 7002	21 00.3	− 49 14	8.9	7 520		7 520	25			
ESO 235-G50	21 01.3	− 52 01	8.4	14 713		14 713	26	6 300		a
ESO 286-G41	21 01.8	− 43 37	6.3	14 641		14 641	31			
ESO 235-G55	21 02.5	− 48 24	7.3	4 990		4 990	28			
ESO 235-G58	21 03.0	− 48 19	5.1	4 342	4 267	4 308	28			
IC 5084	21 05.1	− 63 30	8.0	3 097	3 215	3 097	27			
ESO 342-G26	21 13.5	− 42 28	9.9	5 138		5 138	24			
ESO 342-G27	21 13.7	− 42 28	9.3	5 384		5 384	25			
IC 5096	21 14.3	− 63 58	8.9	3 087		3 087	25			
ESO 235-G84	21 14.5	− 48 37	3.4	6 856	6 803	6 821	31			
ESO 287-G6*	21 15.4	− 45 13	4.8	9 179		9 179	38			
ESO 287-G7*	21 16.5	− 45 20	3.7	5 139		5 139	45			
ESO 342-G35	21 17.0	− 39 59	10.2	3 750	3 796	3 760	22			
ESO 402-G26	21 19.4	− 36 54	6.4	2 817	2 759	2 796	26			
IC 5105	21 21.2	− 40 45	7.4	5 437		5 437	28	5 363	64	b
IC 5105A	21 22.4	− 40 29	8.1	5 071	5 226	5 082	26	5 012		a
NGC 7060	21 22.7	− 42 38	9.5	4 810		4 810	24			
NGC 7059*	21 23.6	− 60 14	1.7	1 749	1 696	1 704	33	1 752	16	c
ESO 287-G34	21 28.6	− 43 04	8.2	2 382		2 382	26			
NGC 7079	21 29.4	− 44 17	8.8	2 670		2 670	25	2 677	75	b
NGC 7090*	21 33.0	− 54 47	2.3	29 931	774	774	34	866	7	c
NGC 7097*	21 37.1	− 42 46	3.7	2 572		2 572	45	2 404	32	b
NGC 7118*	21 42.9	− 48 35	2.8	5 074		5 074	55			
IC 5131	21 44.4	− 35 07	9.3	2 629		2 629	25	2 610	70	b
NGC 7123	21 46.5	− 70 34	8.5	3 698		3 698	26			
ESO 75-G28	21 46.6	− 71 38	11.7	3 814		3 814	22			
IC 5139	21 47.5	− 31 14	8.7	5 362		5 362	25			
NGC 7144*	21 49.5	− 48 29	3.7	1 921		1 921	45	2 098	150	b
IC 5141	21 49.7	− 59 44	6.3	4 391	4 402	4 392	29			
NGC 7151	21 51.8	− 50 54	4.8	1 798	1 914	1 849	30			
NGC 7154	21 52.4	− 35 03	2.6	21 739	2 636	2 636	35	2 615	28	c
ESO 288-G21	21 52.7	− 43 27	4.5	7 817	7 877	7 849	29			
ESO 146-G1	21 52.8	− 59 32	2.7	22 759	4 396	4 396	36			
ESO 404-G11	21 53.8	− 36 44	2.9	5 716	5 837	5 796	34			
ESO 404-G12	21 54.1	− 34 49	5.8	2 575	2 637	2 603	26			
NGC 7187	21 59.8	− 33 03	12.5	2 670		2 670	21			
IC 5157	22 00.5	− 35 11	9.1	4 443		4 443	25			
ESO 404-G27	22 00.9	− 32 32	3.4	2 570	2 529	2 546	33			
IC 5169	22 07.2	− 36 20	5.8	3 003	3 060	3 028	26			
IC 5170	22 09.4	− 47 28	8.3	1 551	1 612	1 570	23			
NGC 7219*	22 09.5	− 65 06	3.8	2 930		2 930	44	2 933		c
IC 5176	22 11.2	− 67 06	5.6	1 735	1 733	1 734	28			
IC 5186	22 15.9	− 37 03	10.0	4 924		4 924	24			
ESO 27-G8	22 17.8	− 80 15	5.8	2 471	2 484	2 476	28			
IC 5212	22 20.6	− 38 17	7.3	8 316	8 333	8 320	26			
NGC 7267	22 21.5	− 33 57	4.8	3 321	3 370	3 346	28			
IC 5222	22 26.4	− 65 55	5.7	3 158	3 177	3 167	27	3 150		b
IC 5227	22 30.6	− 64 57	3.3	3 296	3 317	3 310	31	3 133	119	b
IC 5244	22 40.9	− 64 18	10.5	3 449		3 449	23			
NGC 7358	22 42.2	− 65 23	12.2	3 347		3 347	21			
NGC 7368	22 42.7	− 39 36	7.0	2 386	2 384	2 385	25	2 360		c
ESO 346-G3	22 46.5	− 37 44	7.2	8 595		8 595	28			
NGC 7400	22 51.4	− 45 37	4.3	2 919	3 074	2 919	41			
NGC 7404	22 51.5	− 39 35	12.3	1 891	1 964	1 899	21			
NGC 7410*	22 52.2	− 39 56	4.8	1 717	1 782	1 751	28	1 638	18	b
IC 1459*	22 54.4	− 36 44	4.1	1 748		1 748	42	1 624	17	b
NGC 7424*	22 54.5	− 41 20	2.3	28 673	944	944	37	942	4	c
NGC 7417	22 54.6	− 65 18	11.4	3 191	3 305	3 196	22	4 315		a
IC 5270	22 55.1	− 36 07	3.0	1 794	1 884	1 858	31	1 636		c
NGC 7476	23 02.2	− 43 22	3.7	2 982	2 935	2 952	29			
ESO 469-G11	23 03.1	− 30 53	2.6	8 675	8 578	8 605	32			

TABLE I. (continued).

Galaxy	R.A. 1950	Dec. 1950	R	V_c	V_e	V_f	±	V	±	Ref.
NGC 7484	23 04.3	− 36 33	12.6	2 728		2 728	21			
ESO 407-G14	23 14.9	− 35 04	3.6	2 778	2 745	2 757	30	2 755		c
NGC 7599*	23 16.6	− 42 32	1.6	27 698	1 781	1 781	35	1 692	15	b
NGC 7633	23 20.0	− 67 56	10.8	3 749		3 749	23			
IC 5323	23 24.6	− 68 05	9.8	3 965		3 965	24			
ESO 148-G17	23 27.3	− 59 44	12.1	3 099		3 099	21			
IC 5328*	23 30.6	− 45 17	4.4	3 136		3 136	40	3 049	48	b
NGC 7713A	23 34.5	− 37 59	3.5	2 980		2 980	47			
ESO 240-G11	23 35.1	− 48 00	11.4	2 817		2 817	22			
NGC 7733	23 39.8	− 66 14	7.2	10 569	10 636	10 587	26	10 285		a
NGC 7744	23 42.3	− 43 11	12.1	3 098		3 098	21	2 990		a
ESO 28-G2	23 43.3	− 75 33	7.9	6 431		6 431	27			
ESO 149-G1	23 45.1	− 57 21	1.6	19 613	1 723	1 723	44			
ESO 408-G37	23 47.3	− 35 45	9.5	12 782		12 782	24			
NGC 7793*	23 55.2	− 32 52	2.5	204	218	214	31	226	7	c
NGC 7796	23 56.4	− 55.44	9.0	3 252		3 252	25	3 358	82	b
ESO 293-G27*	23 57.9	− 40 46	2.2	30 883	3 166	3 166	34			
ESO 193-G9	23 58.3	− 47 38	9.6	5 903		5 903	24	6 200		a

*Fairall *et al.* (1983).
[b]Huchra *et al.* (1983b).
[c]Huchtmeier *et al.* (1983).
*Observation made with 1200-line/mm grating.

TABLE II. Comparison galaxies outside the survey region.

Galaxy	R.A. 1950	Dec. 1950	R	V_c	V_e	V_f	±	V	±
NGC 2207	06 14.2	− 21 21	12.3	2 746	2 832	2 754	21	2 748	13
NGC 2223	06 22.5	− 22 49	11.5	2 657		2 657	22	2 751	20
NGC 2763	09 04.5	− 15 18	8.4	1 834	1 887	1 844	24	1 889	9
NGC 3145	10 07.7	− 12 11	11.9	3 643	3 870	3 643	22	3 664	20
IC 2627	11 07.4	− 23 27	6.2	2 034	2 129	2075	26	2 075	3
NGC 3717	11 29.1	− 30 02	10.4	1 707	1 766	1 718	22	1 731	20
NGC 4030	11 57.8	− 00 48	15.5	1 431	1 410	1 429	21	1 463	15
NGC 4304	12 19.6	− 33 12	5.8	2 578	2 652	2 612	26	2 631	15
NGC 5101	13 19.0	− 27 10	17.5	1 841	1 914	1 848	18	1 858	10
NGC 5134	13 22.6	− 20 53	9.5	1 739		1 765	23	1 754	10
NGC 5135	13 22.9	− 29 34	2.2	4 047	4 072	4 067	32	4 112	20
NGC 5161	13 26.4	− 32 55	4.9	2 375	2 416	2 396	28	2 387	15
NGC 5247	13 35.4	− 17 38	5.8	1 335	1 372	1 350	27	1 360	10
NGC 5464	14 04.2	− 29 47	2.4	2 857	2 656	2 656	35	2 705	20
NGC 5483	14 07.3	− 43 05	4.2	1 747	1 769	1 760	29	1 778	4
NGC 5560	14 17.5	04 13	5.8	1 716	1 778	1 742	27	1 741	4
NGC 5577	14 18.7	03 40	3.0	20 491	1 484	1 484	40	1 490	3
NGC 5645	14 28.2	07 30	3.4	1 462	1 430	1 440	30	1 363	8
NGC 5643	14 29.5	− 43 57	3.6	1 142	1 142	1 142	30	1 202	11
NGC 5713	14 37.6	− 00 04	2.5	1 851	1 920	1 904	31	1 862	10
NGC 5740	14 41.9	01 53	5.5	1 577	1 548	1 564	27	1 567	10
NGC 5746	14 42.4	02 10	9.1	1 761		1 761	25	1 724	10
NGC 5792	14 55.8	− 00 53	6.1	1 985	2 070	2 021	26	1 930	20
NGC 5796	14 56.6	− 16 25	11.5	2 957		2 957	22	2 946	12
NGC 5806	14 57.5	02 05	12.6	1 353	1 384	1 357	20	1 369	8
NGC 5915	15 18.8	− 12 55	3.7	2 199	2 253	2 234	29	2 274	10
NGC 5921	15 19.5	05 15	13.4	1 478	1 518	1 484	20	1 478	4
NGC 6070	16 07.4	00 50	8.7	1 978	2 067	2 001	23	2 010	9
NGC 6106	16 16.4	07 32	1.9	28 236	1 470	1 470	41	1 457	20
NGC 6118	16 19.2	− 02 10	3.8	1 605	1 584	1 594	32	1 571	9
NGC 6814	19 39.9	− 10 27	4.9	1 501	1 516	1 509	28	1 564	20
NGC 6835	19 51.8	− 12 42	6.9	1 636	1 627	1 632	39	1 568	10

TABLE III. Comparison with published redshifts.

Galaxy	$V - V$(21 cm)	$V - V$(CfA)	$V - V$(SSL)
NGC 2207	+ 6	+ 18	
NGC 2223	− 94		
NGC 2763	− 45		
NGC 3145	− 21		
IC 2627	0		
NGC 3717	− 13		
NGC 4030	− 34		− 19
NGC 4304	− 19		
NGC 5101	− 10		
NGC 5134	+ 11		
NGC 5135	− 45		
NGC 5161	+ 9		
NGC 5247	− 10		
NGC 5464	− 49		
NGC 5483	− 18		
NGC 5560	+ 1		+ 24
NGC 5577	− 6		+ 56
NGC 5645	+ 77	+ 47	+ 87
NGC 5643	− 60		
NGC 5713	+ 42	+ 16	+ 23
NGC 5740	− 3		+ 2
NGC 5746	+ 37		+ 25
NGC 5792	+ 91	+ 53	+ 134
NGC 5796		− 17	
NGC 5806	− 12		+ 6
NGC 5915	− 40		
NGC 5921	+ 6		+ 34
NGC 6070	− 9		+ 30
NGC 6106	+ 13		+ 18
NGC 6118	+ 23		+ 32
NGC 6814	− 55	− 15	
NGC 6835	+ 64		
NGC 7154	+ 21		
$\langle V - V$(source)$\rangle$	− 4.4	+ 17.0	+ 34.8
σ	39.6	29.6	39.2

In order to test the accuracy for our velocities, we have also observed 32 galaxies for which there are high-quality 21-cm redshifts available (e.g., Huchtmeier *et al.* 1983). Since there are very few 21-cm observations for deep southern galaxies, some comparison galaxies were observed outside the survey region and information about them is given separately in Table II. All galaxies in this table have 21-cm redshifts except NGC 5796, which has been included because it was observed at Mount Hopkins. The velocity information for this galaxy comes from Huchra *et al.* (1983b). For 13 of these galaxies, redshifts were also measured at Las Campanas by Sheetman *et al.* (1983) utilizing a blue-sensitive photon-counting Reticon and the same data-analysis system used in our redshift analysis. From these, five galaxies have redshifts measured at Mount Hopkins and together with NGC 5796 may be used for a preliminary direct comparison between the southern and northern samples.

The results of the comparison between the different sets of observations are summarized in Table III, where we list the velocity differences between our measurements and 21-cm radial velocities and optical redshifts measured at Mount Hopkins and Las Campanas, denoted by V(CfA) and V(SSL), respectively. From the comparison of our redshifts with the 21-cm measurements, we find that our velocities are shifted by -4.4 km s^{-1} in the mean with respect to the radio data, usually taken as the velocity zero-point standard. The standard deviation in the differences is 39.6 km s^{-1}, which is consistent with the rms uncertainty of 38 km s^{-1} derived by Rood (1982) for the CfA data, and indicates that our redshifts have an accuracy similar to the redshifts measured at Mount Hopkins. The zero-point shift of our data is also very close to the -5.0 km s^{-1} found by Rood (1982) for the offset of the CfA velocities, suggesting that no zero-point correction is necessary. We note that for the six galaxies in common with the CfA sample, we get a mean difference of $+17.0$ km s^{-1} and a rms residual of 29.6 km s^{-1}. However, a much larger overlapping sample is necessary before a direct comparison between the two data sets can be made.

For the 13 galaxies in common with the Las Campanas sample, we obtain an average velocity difference of $+34.8$ km s^{-1} and a standard deviation about the average of 39.2 km s^{-1}. The average residual derived here is much larger than the 13.2 km s^{-1} difference found by Sheetman *et al.* (1983) from the comparison between the Las Campanas and CfA velocities. In fact, examining Table III, we find that our velocities are systematically larger than the velocities measured at Las Campanas, with the galaxies NGC 5645 and NGC 5792 showing the largest differences. It is interesting to note that for most of the galaxies in common, Sheetman *et al.* (1983) obtained correlation redshifts, while our velocities are the weighted averages between emission and correlation velocities. This fact may partly account for the large mean velocity difference found between our measurements and the Las Campanas redshifts, possibly reflecting the zero-point error of ~ 30 km s^{-1} in the correlation velocities found by Lewis (1983). In particular, for the galaxies NGC 5560 and NGC 5577 which were also observed by Lewis (1983), we obtained substantially smaller velocity differences than those derived using Sheetman *et al.* (1983) velocities.

The systematic trend mentioned above is not observed if our redshifts are compared with 21-cm redshifts for the same set of galaxies. In the latter case, we get a mean residual of $+17.4$ km s^{-1}, quite close to the value obtained above for the deviation with respect to the CfA sample. Furthermore, if we exclude the two most discrepant cases mentioned above, we obtain an average velocity difference of $+5.3$ km s^{-1} relative to the radio data for the remaining 11 galaxies. Clearly, a more extensive comparison with the Las Campanas velocities is necessary in order to determine whether a zero-point difference exists or if the results derived here suffer from the effects of a small sample.

IV. CONCLUSION

In this paper, we have reported new redshift measurements for 228 galaxies in the southern hemisphere. These redshifts represent the initial results of an ongoing effort to extend the CfA Redshift Survey to the southern skies. A preliminary analysis of our redshifts suggests that our velocity zero point agrees closely with that determined for the northern sample. However, additional data would be necessary for a more secure velocity calibration based on a direct comparison with the CfA sample. The uncertainty in our velocities is also very similar to the uncertainties derived for the redshifts measured at Mount Hopkins, demonstrating that the ON-CfA Redshift Survey will be as accurate as its northern counterpart.

Finally, we point out that the observed sample presented here consists primarily of galaxies with estimated magnitudes brighter than $m_B = 13.5$. We estimate that about 15%

of galaxies with $m_B < 13.5$ were not observed and consist of very low surface brightness objects which we expect to observe during the next observing season. Evidently, much more work is necessary in order to achieve the ultimate goal of extending the sample to $m_B = 14.5$. We emphasize that, in addition to redshifts, a major effort will also be required to provide reliable magnitudes for the galaxies in the region of interest.

We wish to thank Dr. J. Geary for his assistance during the construction of the detector and Dr. M. Davis for his contribution in the early phases of the project. We are also indebted to G. Madjeski and B. Wyatt for getting our computing systems off the ground. We would also like to thank all the people in Brazil who have contributed to this project, especially C. Rite, D. Nascimento, C. Gneidging, R. Laporte, and the night assistants.

REFERENCES

Aarseth, S. J., Gott, J. R., and Turner, E. L. (1979). Astrophys. J. 228, 664.
Davis, M., and Latham, D. W. (1979). SPIE Proc. 172, 71.
Davis, M., and Huchra, J. (1982). Astrophys. J. 254, 437.
Efstathiou, G. (1979). Mon. Not. R. Astron. Soc. 187, 117.
Efstathiou, G., and Eastwood, J. W. (1981). Mon. Not. R. Astron. Soc. 194, 503.
Fairall, A. P., Lowe, L., and Dobbie, P. J. K. (1983) Publ. Dep. Astron. Univ. Cape Town No. 5.
Frenk, C. S., White, S. D. M., and Davis, M. (1983). Astrophys. J. 271, 417.
Hausman, M. A., Olson, D. W., and Roth, B. D. (1983). Astrophys. J. 270, 351.
Hoffman, G. L., Salpeter, E. E., and Wasserman, I. (1983). Astrophys. J. 268, 527.
Huchra, J., Davis, M., Latham, D. W., and Tonry, J. (1983a). Astrophys. J. Suppl. 52, 89.
Huchra, J., *et al.* (1983b). Catalogue of Galaxy Radial Velocities, private communication.
Huchtmeier, W. K., Richter, O. G., Bohnenstengel, H. D., and Hauschildt, M. (1983). ESO Scientific Preprint 250.
Kirshner, R., Oemler, A., and Schechter, P. (1979). Astron. J. 84, 951.
Kirshner, R., Oemler, A., Schechter, P., and Schectman, S. (1983). Astron. J. 88, 1285.
Klypin, A. A., and Shandarin, S. F. (1983). Mon. Not. R. Astron. Soc. 204, 891.
Latham, D. W. (1982). *Instrumentation for Astronomy with Large Optical Telescopes*, IAU Colloquium 67, edited by C. M. Humphries (Reidel, Dordrecht), p. 259.
Lauberts, A. (1982). ESO/Uppsala Survey of the ESO (B) Atlas, private communication.
Lewis, B. M. (1983). Astron. J. 88, 1695.
Miller, R. H. (1983). Astrophys. J. 270, 390.
Palumbo, G. G. C., Tanzella-Nitti, G., and Vettolani, G. (1983). *Catalogue of Radial Velocities of Galaxies* (Gordon and Breach, New York).
Peebles, P. J. E. (1982). Astrophys. J. 257, 438.
Rood, H. J. (1980). A Catalog of Galaxy Redshifts, private communication.
Rood, H. J. (1982). Astrophys. J. Suppl. 49, 111.
Sandage, A., and Tamman, G. A. (1981). *A Revised Shapley-Ames Catalogue of Bright Galaxies* (Carnegie Institution of Washington, Washington, D. C.).
Sheetman, S. A., Stefanik, R. P., and Latham, D. W. (1983). Astron. J. 88, 477.
Tonry, J. (1980). Ph.D. thesis, Harvard University.
Tonry, J., and Davis, M. (1979). Astron. J. 84, 1511.

THE ON-CFA REDSHIFT SURVEY OF THE SOUTHERN HEMISPHERE

L. Nicolaci da Costa, Paulo. S. Pellegrini, C. N. A. Willmer,

R. de Carvalho, M. A. G. Maia

Departamento de Astronomia, CNPq/Observatorio Nacional

Rio de Janeiro, Brazil

and

David W. Latham and John C. Geary

Harvard-Smithsonian Center for Astrophysics

Cambridge, Massachusetts

I. INTRODUCTION

Over the past few years several redshift surveys have been conducted and have had a dramatic impact on our ideas concerning the space distribution of matter in the Universe. Although these surveys have taken different forms such as sampling individual clusters and their surroundings (e.g. Chincarini and Rood 1976, Gregory and Thompson 1978, Haynes and Giovanelli 1986), deep pencil-beam surveys (e.g. Bean et al. 1983, Kirshner et al. 1978, 1987, Shanks et al. 1984), and wide-angle surveys of nearby galaxies (Sandage and Tammmann 1981, Huchra et al. 1983, de Lapparent et al. 1986) all have shown that matter tends to form filaments and sheets, probably connected in a complex and somewhat amorphous network, with a substantial fraction of the volume devoid of luminous matter.

Unfortunately, the volumes surveyed so far have been relatively small and most of the observed structures have dimensions comparable to the size of the surveys, casting some doubt about their fairness. The observational data have, nonetheless, stimulated a considerable progress in the theoretical investigations. In particular, the evolution of structures in the non-linear regime have been studied by means of N-body simulations from initial conditions corresponding to the different scenarios proposed for the origin of large structures (e.g. Gott et al. 1979, Klypin and Shandarin 1983, Mellot et al. 1983, White et al. 1987). The results of these numerical experiments have produced distributions that can be confronted with those observed, in a program that may, eventually, provide enough information to discriminate amongst competing models.

However, to achieve this ambitious goal it is essential to sample a volume of space sufficiently large that one can confidently assume that it is a fair representation of the Universe at large.

The nearby wide-angle surveys, like that undertaken by the CfA, are of particular importance to study the properties of the three-dimensional distribution of galaxies. However, despite earlier claims about the "fairness" of the 14.5 magnitude-limited northern sample (Davis and Huchra 1982), the results from the original CfA Redshift Survey strongly suggest that it should be extended both in depth and sky coverage (Davis et al. 1983). Both such programs were started about five years ago by different groups and the first results are now becoming available. Particularly interesting is the survey of the southern hemisphere since it probes a volume of space which avoids the large concentration of galaxies associated with the Virgo cluster being, perhaps, more representative of the universe at large.

Since 1982 the ON and the CfA have been conducting a major survey of galaxy radial velocities. We have accumulated about 1500 galaxy spectra in the southern hemisphere in order to complete different well-defined samples, appropriate for statistical analysis. Here we discuss the contribution of the ON-CfA collaboration to the Southern Sky Redshift Survey (SSRS), a joint effort of the ON and CfA with other groups (Menzies et al. 1987, Davis 1987) to complete a redshift survey of a diameter-limited sample of southern galaxies. In section II we describe the sample and the observations while in section III we discuss the data quality.

II. THE SAMPLE

The original goal of the ON-CfA survey was to extend the CfA Redshift Survey to cover the southern galactic cap, observing galaxies with estimated blue magnitudes brighter than 14.5 and below galactic latitude -30°. However, a major difficulty in the southern work is to compile well-defined magnitude-limited samples due to the inexistence of a catalog such as the Catalog of Galaxies and Clusters of Galaxies (Zwicky et al. 1961-1968). The available galaxy catalogs in the south like the Revised Shapley-Ames Catalog (Sandage and Tammann 1981), the Second Reference Catalogue of Bright Galaxies (de Vaucouleurs et al. 1976, RC2), the Morphological Catalog of Galaxies (Vorontsov-Velyaminov and Arkhipova 1963-1974, MCG) and the ESO/Uppsala Survey of the ESO(B) Atlas (Lauberts 1982) are either too shallow, or too incomplete, or too inhomogeneous to be used to define a magnitude-limited sample even down to 14.5. It is now a fact that with the recent efforts, redshift surveys have considerably surpassed the available photometric data in the southern hemisphere and the creation of a well-defined and homogeneous magnitude-limited sample in this hemisphere must await a major photometric survey.

At the present time a more effective approach to define a complete and moderately deep sample in the south, for statistical studies, is to work with diameter-limited catalogs. This has been done by selecting galaxies exclusively from the ESO catalog, claimed to be complete down to major diameters of 1 arcminute, south of declination -17.5° and below galactic latitude -30°. The information on morphological types and the

values of the major and minor diameters for each galaxy were used to define a diameter-limited catalog based on a "face-on" diameter D(0) defined by the expressions (da Costa et al. 1987):

$$\log (D(0)) = \log D_1 - 0.235\, A(T) \log(D_1/D_2)$$

where

$$A(T) = 0.894 \text{ for } T \geq 0$$
$$= 0.950 \text{ for } T < 0$$

In these equations D_1 and D_2 are the major and minor diameters and T denotes the morphological type as listed in the ESO/Uppsala catalog. Adopting log (D(0))= 0.1 as our diameter limit we have selected 2028 objects over an area of 1.75 steradians, within the region defined above.

The original sample of 2028 objects selected with the above cutoff includes several multiple systems and interacting galaxies (IG's) as defined in the classification scheme adopted by Lauberts (1982). Since a single diameter has been quoted for these systems we have examined these cases individually in order to determine whether each member galaxy met the selection criterion, in which case they were assigned morphological types, diameters and an indication of their relative position. A total of 170 IG entries were examined using the ESO (B) and ESO/SRC on-film copies, including 30 multiple systems and 140 binary or perturbed galaxies. From the plate inspection, we excised from our sample all galaxies in IG systems, but with diameters below our cutoff, leaving a total of 1963

leaving a total of 1963 individual galaxies. The main drawbacks of such a sample are that it cannot be easily joined with the CfA northern sample to construct a whole-sky catalog and that it picks out a substantial number of low surface brightness galaxies, for which it is very difficult to obtain an optical redshift.

III. THE DATA

The ON-CfA Redshift Survey utilized a photon-counting Reticon detector mounted on the 60 in. telescope of the ON. The observations were made through a pair of 3 x 12-arcsec entrance apertures separated by 30 arcsec on the sky. We commonly used a 900 l/mm grating, giving a dispersion of 100 A/mm with a typical resolution of 6 A. The wavelength coverage was from about 4700 to 7100 A. Further details of the observational procedure can be found in da Costa et al. (1984). The final redshift for a galaxy was determined from a suitable combination of the redshifts obtained from the emission lines and cross correlation analysis, as originally discussed by Tonry and Davis (1979).

The accuracy of our redshifts has been tested by comparing our velocities with published 21 cm data (da Costa et al. 1984), published stellar velocities, Sadler's (1984) early-type galaxy sample, and redshifts measured at the South African Astronomical Observatory (SAAO, Menzies et al. 1987) and Las Campanas Observatory (LCO, Davis 1987). A summary of these comparisons is shown in table I where we list the source, the mean and the standard deviation in the velocity differences.

A particularly important result is the rather small mean difference of -5.2 km/s obtained between our redshifts and the radio data, usually taken as the velocity zero-point standard. Furthermore, the rms value of 39.3 km/s derived from this comparison is consistent with the uncertainty established by Rood (1982) for the CfA data, indicating that our redshifts are as accurate as those measured in the North. This is an important

result since it means that the CfA and the ON-CfA extension should form a homogenous database of high-quality radial velocities. Equally important is the result coming from the comparison between our radial velocity measurements and those in the literature for ten K and G giant stars, for which we have high signal-to-noise spectra. Although the number of objects is not large, we find a mean velocity shift of about +14.9 km/s indicating that there are no serious discrepancies between our emission and correlation velocities.

Since there are several groups observing in different regions of the southern sky, it is also important to cross-compare the results from the different groups. The comparison of the velocities for 44 galaxies in common with the early-type galaxy sample of Sadler (1984) is not very satisfactory and suggests that the quoted errors in her measurements may have been underestimated. More satisfactory are the comparisons with the LCO and SAAO measurements, for which we have 151 and 179 galaxies in common, respectively. Comparing the ON-CfA with the LCO measurements we find an average velocity difference of +8.1 km/s with all individual measurements within a +/- 200 km/s range. The standard deviation of 69.2 km/s about the mean velocity difference, corresponds to an uncertainty of 48.9 km/s in each data set, if we assume that both have similar internal errors. For the sample in common with SAAO we find a mean velocity difference of + 11.7 km/s and a standard deviation of 58.9 km/ s. Since our comparison with the radio data indicates an internal error of 39.3 km/s this implies that the mean error of the SAAO is also of the order of 40 km/s and that the internal error quoted by Menzies et al. (1987) is probably too small. In summary, the

cross-comparison of the southern surveys indicate that the internal errors of all data sets are roughly 40 km/s demonstrating the high-quality and homogeneity of the radial velocities obtained for the diameter-limited sample.

The contribution of the ON-CfA survey to the SSRS sample together with the observations made by the two other groups mentioned previously will be used to assemble a catalog of galaxy radial velocities of the southern sky. This catalog represents a major contribution to the study of the large scale distribution of galaxies probing somewhat deeper an area of sky comparable to that covered by the original CfA 14.5 sample (da Costa et al. 1988). Analyses of the SSRS catalog is in progress and will be presented in forthcoming papers.

We note that the data discussed here represent only part of the radial velocities that have been accumulated over the past few years by the ongoing ON-CfA Redshift Survey. Observations have also been made using a magnitude-limited sample in the southern galactic cap and in the Centaurus-Hydra region (da Costa et al. 1986, da Costa et al. 1987). This survey is still in progress and its short-term goals are to complete a deeper survey of the declination strip between declinations -30° and -40°, where prominent voids have been detected in the SSRS data, and to extend the coverage of the Hydra-Centaurus region using the same diameter limit cut of the SSRS. The long-term objective of our redshift survey is to complete a magnitude-limited sample in the southern galactic cap, as deep as the one been carried out in the North (e.g. Huchra and Geller 1987). For the time being, we have been using a tentative sample

combining galaxies from the ESO and MCG catalogs. South of -17.5° we use estimated magnitudes derived from mean diameter-magnitude relations obtained for different morphological type groups. North of that declination we have been observing galaxies brighter than 14.5 in the MCG catalog. This sample has a large overlap with the SSRS sample and it is our intention to complete it in due course. Hopefully, our magnitude-limited sample will not differ very much from an improved catalog to be constructed when more reliable magnitudes become available.

ACKNOWLEDGMENTS

We would like to thank all the people that have contributed directly or indirectly to this long-term effort. In particular, we would like to thank Marcos Nunes for keeping the detector running throughout these years and Charles Rite for his support to the software. We also appreciate their participation in several of the observation runs. We thank Darcy do Nascimento for his contribution with the computer systems. We would also like to thank the people at CfA: Bill Wyatt, Leslie Feldman and Charlie Hughes. We would also like to thank Greg Madjeski for his help in the early part of this project. This project had the partial support of a CNPq/NSF grant.

REFERENCES

Bean, A. J., Efstathiou, G. P., Ellis, R. S., Peterson, B. A. and Shanks, T. (1983). Mon. Not. R. Astron. Soc. 205, 605.

Chincarini, G. and Rood, H. J. (1976). Astrophys. J. 206, 30.

da Costa, L. N., Nunes, M. A., Pellegrini, P. S., Willmer, C., Chincarini, G. and Cowan, J. (1986). Astron. J. 91, 6.

da Costa, L. N., Pellegrini, P. S., Nunes, M. A., Willmer, C. and Latham, D. (1984). Astron. J. 89, 1310.

da Costa, L. N., Willmer, C., Pellegrini, P. S. and Chincarini, G. (1987). Astron. J. 93, 6.

da Costa, L. N., Pellegrini, P. S., Sargent, W. L. S., Davis, M., Meiksin, A., and Latham, D. W. (1988). Astrophys. J. 327, 544.

Davis, M. (1987). To appear in "The Proceedings of the 13th Texas Symposium on Relativistic Astrophysics".

Davis, M. and Huchra, J. (1982). Astrophys. J. 254, 437.

Davis, M., Huchra, J. and Geller, M. (1983). In Early Evolution of the Universe and its Present Structure, IAU Symposium N° 104, edited by G. O. Abell and G. Chincarini (Dordrecht, D. Reidel).

de Lapparent, V., Geller, M. and Huchra, J. P. (1986). Astrophys. J. Lett. 302, L1.

de Vaucouleurs, G., de Vaucouleurs, A. and Corwin, H. (1976). Second Reference Catalogue of Bright Galaxies (Austin, University of Texas Press).

Gott III, J. R., Turner, E. L. and Aarseth, S. J. (1979). Astrophys. J. 234, 13.

Gregory, S. A. and Thompson, L. A. (1978). Astrophys J. 222, 784.

Haynes, M. and Giovanelli, R. (1986). Astrophys. J. Lett. 306, L55.

Huchra, J. P., Davis, M., Latham, D. and Tonry,J. (1983). Astrophys. J. Suppl. 52, 89.

Huchra, J. P. and Geller, M. (1987). To appear in "The Proceedings of the 13th Texas Symposium on Relativistic Astrophysics".

Kirshner, R. P., Oemler, A. J. and Schechter, P. (1978). Astron. J., 83, 1549.

Kirshner, R. P., Oemler, A. J., Schechter, P., and Schectman, S. A. (1987). Astrophys. J., 314, 493.

Klypin, A. A. and Shandarin, S. F. (1983). Mon. Not. R. Astron. Soc. 204, 891.

Lauberts, A. 1982, The ESO/Uppsala Survey of the ESO(B) Atlas (Munchen: European Southern Observatory).

Mellot, A. L., Einasto, J. Saar, Suisalu, I., Klypin, A. A. and Shandarin, S. F. (1983). Phys. Rev. Letters, 51, 935.

Menzies, J. W., Coulson, I. M. and Sargent, W. L. W. (1986). Preprint.

Rood, H. (1982). Astrophys. J. Suppl. 49, 111.

Sadler, E. M. (1984). Astron. J. 89, 23.

Sandage, A. and Tamman, G. A. (1981). A Revised Shapley-Ames Catalogue of Bright Galaxies (Carnegie Institution of Washington, Washington, D.C.).

Shanks, T., Bean, A. J., Efstathiou, G. P., Ellis, R. S., Fong, R. and Peterson, B. A. (1984). Astrophys. J. 274, 529.

Tonry, J. and Davis, M. (1979). Astron. J. 84, 1511.

Vorontsov-Velyaminov, B. A. and Arhipova, V. P. (1963-1974). Morphological Catalogue of Galaxies (Moscow). Parts 2 to 5.

White, S. D. M., Frenk, C. S., Davis, M. and Efstathiou G. (1987)

Astrophys. J., 313, 505.

Zwicky, F., Herzog, E., Wild, P., Karpowicz, M. and Kowal, C. (1961-1968). Catalog of Galaxies and Clusters of Galaxies Vols. 1-6 (Pasadena, California Institute of Technology).

TABLE I. Comparison with other sources.

Source	Number	$\langle V_{ON\text{-}CfA} - V_{source} \rangle$ (km/s)	σ (km/s)
21 cm	32	-5.2	39.3
Stars	10	14.9	15.9
Sadler	44	12.2	82.5
LCO	151	8.1	69.2
SAAO	179	11.7	58.9

II.3 AMOSTRA LIMITADA EM MAGNITUDE

A obtenção de uma amostra de galáxias moderadamente profunda e limitada em magnitude aparente no Hemisfério Sul apresenta alguns problemas específicos que precisam ser contornados. Os catálogos de galáxias mais consagrados, contendo informaçôes precisas sobre magnitudes de galáxias no Hemisfério Sul num único e bem determinado sistema padrão (B_T) são, até agora, os compilados por de Vaucouleurs et al. (RC2, 1976) e Sandage e Tamman (RSA, 1981). Entretanto , apenas o último é considerado completo até magnitude 13.2, o que representa um limite bastante raso para o estudo das grandes estruturas no Universo. Outros catálogos mais fundos, incluindo galáxias mais fracas, apresentam também dificuldades para a seleção de uma amostra adequada. A compilação feita por Vorontsov-Velyaminov e Arhipova (1963-1968) não se extende a todo o Hemisfério Sul e apresenta magnitudes estimadas visualmente com erros que chegam a 1 mag. Várias outras compilações individuais surgidas nos últimos anos (Rood 1980, Huchtmeier et al. 1983, Palumbo et al. 1983, Huchra 1983, etc.) utilizam basicamente as magnitudes de galáxias austrais determinadas no RC2 e RSA e alguns atualizam seus dados a partir da fotometria que se torna gradativamente disponível na literatura. Desta forma, estes últimos catálogos são, em geral, muito incompletos no Hemisfério Sul devido a escassa fotometria existente neste hemisfério e carecem de uma consistência quanto ao sistema fotométrico, utilizando tanto magnitudes integradas como fotometria em diafragmas.

Entretanto, entre as compilações mais fundas existentes, o catálogo

ESO/Uppsala (Lauberts, 1982), embora não utilizando a magnitude como parâmetro de seleção, é na verdade o único no Hemisfério Sul que apresenta condições para a seleção de uma amostra como a desejada. Este catálogo é considerado completo para galáxias com diâmetros maiores $D_1 > 1'$ e, com este critério de seleção, é suposto incluir uma amostra como a que se pretende analisar. Sharp (1986), por exemplo, indica um valor para a magnitude limite neste catálogo situado no domínio $14.7 \leq B_T \leq 15.5$. Para o caso mais crítico de galáxias de imagens compactas como as elípticas e S0's, Sadler (1984) indica uma magnitude limite aproximada de 14.0 no sistema B_T, o que equivale a um limite próximo a 14.4 no sistema B(0).

A determinação de uma amostra limitada em magnitude, a partir de um catálogo limitado em diâmetro maior, apresenta alguns problemas que devem ser considerados. Esses problemas decorrem, basicamente, do fato de as galáxias apresentarem uma relação diâmetro-magnitude com grande espalhamento intrínseco. Isto significa que, a partir de um catálogo limitado em diâmetro maior D_1, uma amostra selecionada até uma magnitude limite equivalente m_{lim} será sempre incompleta pela não inclusão no catálogo original das galáxias mais brilhantes que m_{lim} mas com diâmetros maiores inferiores a D1. Por outro lado, já que a maioria dos objetos do catálogo ESO/Uppsala não possui magnitude determinada, é necessário utilizar a relação diâmetro-magnitude, mesmo com sua dispersão intrínseca, para a obtenção de estimativas de magnitudes. Embora problemático sob o ponto de vista de determinações individuais de magnitudes este procedimento é, entretanto, capaz de selecionar objetivamente uma amostra bem definida, o que no contexto apresentado,

é decisivo para a confiabilidade que se venha a ter nos resultados de uma análise estatística. Esta amostra pode, no mínimo, servir como um catálogo preliminar para futuros levantamentos fotométricos tão carentes no Sul.

Para permitir uma maior flexibilidade no tratamento da massa de dados, algumas alterações foram introduzidas numa cópia do catálogo, sempre mantido residente em disco de 80 Mby de um minicomputador Nova 3. Esta cópia foi preparada em formato adequado para realizar modificações e atualizações a medida que novos dados se tornem disponíveis, assim como foi implementado um conjunto de rotinas para análise estatística e gráfica desses dados. A seguir, para todas as galáxias sem tipo T (de Vaucouleurs et al. 1976) determinado, foram atribuidos valores assim escolhidos: galáxias N, -7; galáxias peculiares ou descritas como ..., 15; galáxias em interação, 21; galáxias anãs, 22; grupos e aglomerados de galáxias, 30. Um exame visual comparando cópias em filme dos Atlas ESO(B) e SRC(J) revelou, nesta etapa, dois problemas intrínsecos do catálogo: i)- os diâmetros pretendem representar as maiores extensões dos objetos e como a subjetividade das medidas em isofotas muito fracas é bastante grande, isto implica, em alguns casos, numa determinação de diâmetro pouco relacionada à magnitude da galáxia; ii)- êrros de classificação morfológica estão presentes principalmente no caso de algumas galáxias espirais fracas, cujos discos são confundidos com envoltórios de galáxias S0. Nenhuma tentativa, entretanto, foi feita para remedir diâmetros, para manter a homogeneidade do catálogo e não introduzir uma maior subjetividade. Apenas êrros comprovados na determinação de tipos morfológicos foram corrigidos.

A determinação das relações diâmetro-magnitude passa inicialmente pela escolha do sistema em que esses parâmetros são definidos. As magnitudes quotadas no catálogo ESO/Uppsala podem ser consideradas magnitudes totais no sistema B_T já que grande parte é proveniente dos catálogos RC2 e RSA e, sempre que possível, valores determinados por fotometria em diafragmas são convertidos para este sistema. A expectativa de se unificar os dados com aqueles do levantamento CfA1 induz, obviamente, à escolha do sistema adotado naquele trabalho, que é compatível com o sistema de magnitudes B(0) definido por de Vaucouleurs et al. (1964). Transformações corretas entre esses sistemas não são encontradas facilmente na literatura e dependem do tipo morfológico da galáxia. Entretanto, Felten (1985) e Huchra (1985) indicam tranformações médias, independentes do tipo morfológico, tendo-se adotado $B(0) = B_T + 0.4$, utilizado por Huchra.

No caso dos diâmetros, a opção por um sistema representativo da área da galáxia, limitada a uma determinada isofota, é a mais indicada, já que se deseja correlaciona-los com a magnitude. Desta forma, optou-se pelo sistema usual na isofota 25 mag/(")^2 utilizando-se as tranformações indicadas por Fouque e Paturel (1985) para o catálogo ESO/Uppsala. Estes autores fazem uma revisão das transformações usuais a partir de dados mais atualizados, mostrando a necessidade de se introduzir uma correção para normalizar os sistemas fotométricos para medidas de diâmetros. Os diâmetros foram posteriormente convertidos para o sistema "face-on", D0(25), segundo de Vaucouleurs et al. (1976) para eliminar os efeitos de inclinação.

Uma única relação média entre diâmetros D0(25) e magnitudes B(0) como mostrada na figura 1 apresenta uma dispersão de 0.8 mag para um ajuste linear da forma :

$$B(0) = a + b \log (D0(25))$$

indicando a natureza dispersa da relação entre esses dois parâmetros. Entretanto agrupando-se tipos morfológicos de modo adequado é possível reduzir esta dispersão a valores mais aceitáveis. A tabela 1 mostra os parâmetros de ajuste relativos aos agrupamentos que apresentaram as menores dispersões após várias tentativas de reagrupamentos.

A primeira coluna se refere aos tipos morfológicos utilizados para os ajustes e nas colunas 2, 3 e 4 são mostrados os valores dos parâmetros de ajuste e a dispersão encontrada. A penúltima coluna se refere aos tipos morfológicos para os quais o ajuste foi aplicado. A percentagem de galáxias com os tipos morfológicos indicados na penúltima coluna é mostrada na última coluna. A dispersão do ajuste para galáxias S0 e S0a é surpreendentemente alta para objetos compactos, sendo provável a existencia de má classificação morfológica destes tipos intermediários entre elípticas e espirais. Levando em consideraçao as populações relativas, o êrro médio cometido na associação dessas magnitudes é aproximadamente 0.6 mag. Esses ajustes são mostrados na figura 2, descartando-se pontos situados a mais de 2σ. Eles foram utilizados para determinar as magnitudes, de agora em diante denominadas $m_{B(0)}$ para todas as galáxias do catálogo ESO/Uppsala, sem fotometria (cerca de 70%), nas regiões de interesse. Para as outras galáxias com magnitudes já

determinadas no catálogo, foram mantidos os valores originais adicionados de 0.4 mag.

Para a obtenção de uma amostra similar àquela do CfA1, foram selecionadas do catálogo ESO/Uppsala as galáxias com magnitudes $m_{B(0)} \leq 14.5$ resultando numa amostra de 1401 objetos que requer, ainda, uma modificação adicional. Esse conjunto de dados contém vários sistemas múltiplos, para os quais o catálogo quota um diâmetro relativo ao conjunto de objetos e, destas forma, superestimado. Todos os objetos deste tipo foram, então, examinados nas cópias em filme dos Atlas ESO(B) e SRC(J), sendo medido o diâmetro e determinado o tipo morfológico de cada componente individual do sistema. O número final de galáxias na amostra é, então, 1371 e com os dados de velocidades radiais obtidos, encontra-se completa em 92%.

Na tabela 2 é apresentada a distribuição em tipos morfológicos e também mostrado, para comparação, a distribuição de tipos morfológicos de uma amostra muito semelhante à do CfA1 (Davis e Geller 1976). Levando-se em consideração o fato de estarmos comparando catálogos diferentes e a subjetividade presente na determinação dos tipos morfológicos e na determinação das peculiaridades dos objetos, o desacôrdo de percentagens pode não ser tão significativo quanto aparenta. Note-se que a soma das percentagens de galáxias tipo "early" é $\approx$ 26% e das galáxias tipo "late" é $\approx$ 74% para ambos os catálogos. Diferenças de classificações morfológicas, determinadas em placas Schmidt, dentro destes dois grupos principais, não são muito significativas pois variam consideravelmente entre diferentes autores. Estes resultados não são

conclusivos mas, pelo menos não demonstram de uma forma inequívoca a existência de fortes efeitos de seleção no que concerne distribuição de tipos morfológicos.

Possíveis efeitos sistemáticos presentes na determinação de magnitudes com esse sistema podem também ser avaliados examinando-se a distribuição do número de galáxias em função da magnitude. Na figura 3 é mostrada a densidade superficial (em número) de galáxias N(m) com magnitudes entre m e m+dm, em função da magnitude, para a amostra aqui determinada e a amostras do CfA1 nas calotas polares norte e sul. Para comparação é também mostrada a distribuição esperada de uma amostra homogênea, log N(m) α 0.6m, ajustada às amostras na calota sul. Como pode ser visto, o acôrdo entre os dados no sul indica que a amostra determinada com o sistema descrito acima não apresenta efeitos sistemáticos que possam superestimar ou subestimar diferencialmente o número de galáxias no domínio de magnitudes em que se está trabalhando. A discrepância dos resultados com a amostra do CfA1 na calota norte é proveninte, basicamente, da presença do superaglomerado de Virgo.

Por outro lado, a adequação da escala de magnitudes adotada neste sistema pode ser verificada de um modo independente, comparando-se funções de correlação angular determinadas para esta amostra e para diferentes amostras bem definidas no sistema B(0). Como apontado por Sadler e Sharp (1984) as magnitudes limites m_1 e m_2 de amostras com mesmo coeficiente angular para funções de correlação angular adequadamente descritas por uma lei de potência, $w(\theta)=A_1\theta^{\beta}$, estão relacionadas por:

$$5 \log (A_1/A_2) = (1 + \beta) (m_2 - m_1)$$

onde β é o coeficiente angular e A_i são as constantes de normalização. Diferentes estimativas para a magnitude limite da amostra aqui derivada são mostradas na tabela 3, provenientes da comparação com os resultados das funções de correlação obtidas para uma amostra muito similar à do CfA1 (Davis e Geller 1976) e para a região de Perseus-Pisces (Giovanelli et al. 1986). As comparações foram feitas tanto para as amostras totais quanto para subconjuntos de diferentes tipos morfológicos. A função de correlação angular para a amostra em magnitude no sul foi estimada pela contagem relativa de pares a uma dada separação angular, como descrito por Hewett (1982). Os resultados que podem ser extraídos dessa comparação são grosseiros e válidos apenas no sentido estatístico já que dependem de ajustes lineares de funções que sabidamente apresentam desvios dessa linearidade. Mesmo assim os valores apresentados na tabela 3 indicam que a escala de magnitudes está aproximadamente correta, talvez com uma pequena tendência a subestimar as magnitudes das galáxias, no máximo por 0.1 mag. Os resultados deduzidos para diferentes subgrupos de tipos morfológicos devem ser vistos também com cautela já que o número de objetos nestas subamostras é reduzido e a determinação de tipos T carece da subjetividade intrínseca dos catálogos que geraram essas amostras. Estes resultados indicam uma provável subamostragem de galáxias elípticas, o que não é surpreendente já que, como mencinado anteriormente, o limite de diâmetro do catálogo ESO-Uppsala corresponde aproximadamente à magnitude 14.4 no sistema B(0) e isto pode significar a não inclusão de algumas galáxias na própria seleção original do catálogo.

Entretanto, como visto nesta seção, nenhum destes problemas, pode ser considerado suficientemente importante para invalidar a análise qualitativa que será realizada com esta amostra nos capítulos seguintes.

As relações derivadas nesta seção foram também utilizadas para determinar uma amostra mais funda, contendo galáxias mais brilhantes que $m_{B(0)} = 15.5$, na faixa de declinação $-40° \leq \delta \leq -30°$, onde está sendo realizado uma extensão do levantamento de velocidades radiais. A amostra inicialmente selecionada nesta região é limitada a tipo $T \leq 3$, já que a observação ótica de galáxias de baixo brilho superficial é pouco eficiente devido ao excessivo tempo de integração necessário para a obtenção de uma relação sinal/ruído satisfatória. Embora os efeitos de incompleteza das galáxias elípticas se agravem para uma amostra tão funda determinada a partir do catálogo ESO-Uppsala, sua principal finalidade que é o delineamento mais preciso de algumas estruturas e "voids", não é prejudicada já que as galáxias elípticas constituem apenas 5% do número total de galáxias.

REFERÊNCIAS

Davis, M. and Geller. M. J, 1976, Ap. J., **208**, 13.

de Vaucouleurs, G. and de Vaucouleurs, A. 1964, Reference Catalogue of Bright Galaxies (Austin: University of Texas Press)

de Vaucouleurs, G., de Vaucouleurs, A. and Corwin, H. 1976, Second Reference Catalogue of Bright Galaxies (Austin, University of Texas Press).

Felten, J. E. 1985, Comments Astrophys, **11**, 53.

Fouque, P. and Paturel, G. 1985, Astron. Astrophys., **150**, 192

Giovanelli, R., Haynes, M. P. and Chincarini, G., L. 1986, Ap. J., **300**, 77.

Hewett, P. C. 1982, M. N. R. A. S., **201**, 867.

Huchra, J. P. 1985, private communication.

Huchra, J. P., Davis, M., Latham, D. and Tonry,J. (1983). Astrophys. J. Suppl. **52**, 89.

Huchtmeier, W., K., Richter, O., G., Bohnenstengel, H., D. and Hauschildt, M., 1983, ESO Scientific Preprint 250.

Lauberts, A. 1982, The ESO/Uppsala Survey of the ESO(B) Atlas (Munchen: European Southern Observatory).

Palumbo, G., G., C., Tanzella-Nitti, G. and Vettolani, G 1983, Catalogue of Radial Velocities of Galaxies (Gordon and Breach, New York).

Rood, H. J. 1980, A Catalog of Galaxy Redshifts, private communication.

Sadler, E. M. 1984, A. J., **89**, 34.

Sadler, E. M. and Sharp, N. A. 1984, Ap. J., **287**, 80.

Sandage, A. and Tamman, G. A. (1981). A Revised Shapley-Ames Catalogue of Bright Galaxies (Carnegie Institution of Washington, Washington, D.C.).

Sharp, N. A. 1986, Pub. Astr. Soc. Pacific, 98, 740.

Vorontsov-Velyaminov, B. A. and Arhipova, V. P. (1963-1974). Morphological Catalogue of Galaxies (Moscow). Parts 2 to 5.

TABELA 1.

T	a	b	σ	Tipos	%
-7 a -3	14.68	-6.23	0.49	N,E,E/S0	3
-2 a 0	15.00	-5.54	0.68	S0,S0a	17
1 a 3	15.01	-4.54	0.65	Sa,Sab,Sb	29
4 e 6	15.19	-4.89	0.58	Sbc,Sc	25
1 a 6	15.22	-4.91	0.65	S...	1
7 a 10	15.18	-4.37	0.72	S/Irr,Irr	8
22	15.73	-3.77	0.68	Anãs	7
-7 a 10	15.11	-4.99	0.70	pec,...,IG	10

TABELA 2.

Tipos	%(ON)	%(CfA)
Elípticas	5	10
Lenticulares	21	17
Espirais	64	55
Irregulares	3	5
Anãs	1	0.4
Outros	6	15

TABELA 3.

T	m_{lim}	
	ONxDG	ONxGHC
All	14.6	14.5
E,E-S0	14.3	14.2
S0,S0a	14.9	14.3
S	14.5	-

FIGURAS

Figura 1. Relação entre a magnitude no sistema B(0) e o diametro "face-on" D0 para todas as galáxias no catálogo ESO-Uppsala com fotometria, situadas na região $|b| \leq -30°$.

Figura 2a. Relação entre $m_{B(0)}$ e D0 para galáxias com tipos morfológicos entre -7 e -3 no catálogo ESO-Uppsala, situadas na região $|b| \leq -30°$. Galáxias situadas a mais de 2σ de um primeiro ajuste linear foram eliminadas. Os pontos e o reta mostrados na figura se referem a um segundo ajuste linear.

Figura 2b. O mesmo qué na figura 2a para galáxias com tipos morfológicos entre -2 e 0.

Figura 2c. O mesmo que na figura 2a para galáxias com tipos morfológicos entre 1 e 3.

Figura 2d. O mesmo que na figura 2a para galáxias com tipos morfológicos 4 e 6.

Figura 2e. O mesmo que na figura 2a para galáxias com tipos morfológicos entre 1 e 6.

Figura 2f. O mesmo que na figura 2a para galáxias com tipos morfológicos entre 7 e 10.

Figura 2g. O mesmo que na figura 2a para galáxias com tipos morfológicos entre -7 e 10.

Figura 2h. O mesmo que na figura 2a para galáxias com tipo morfológico 22.

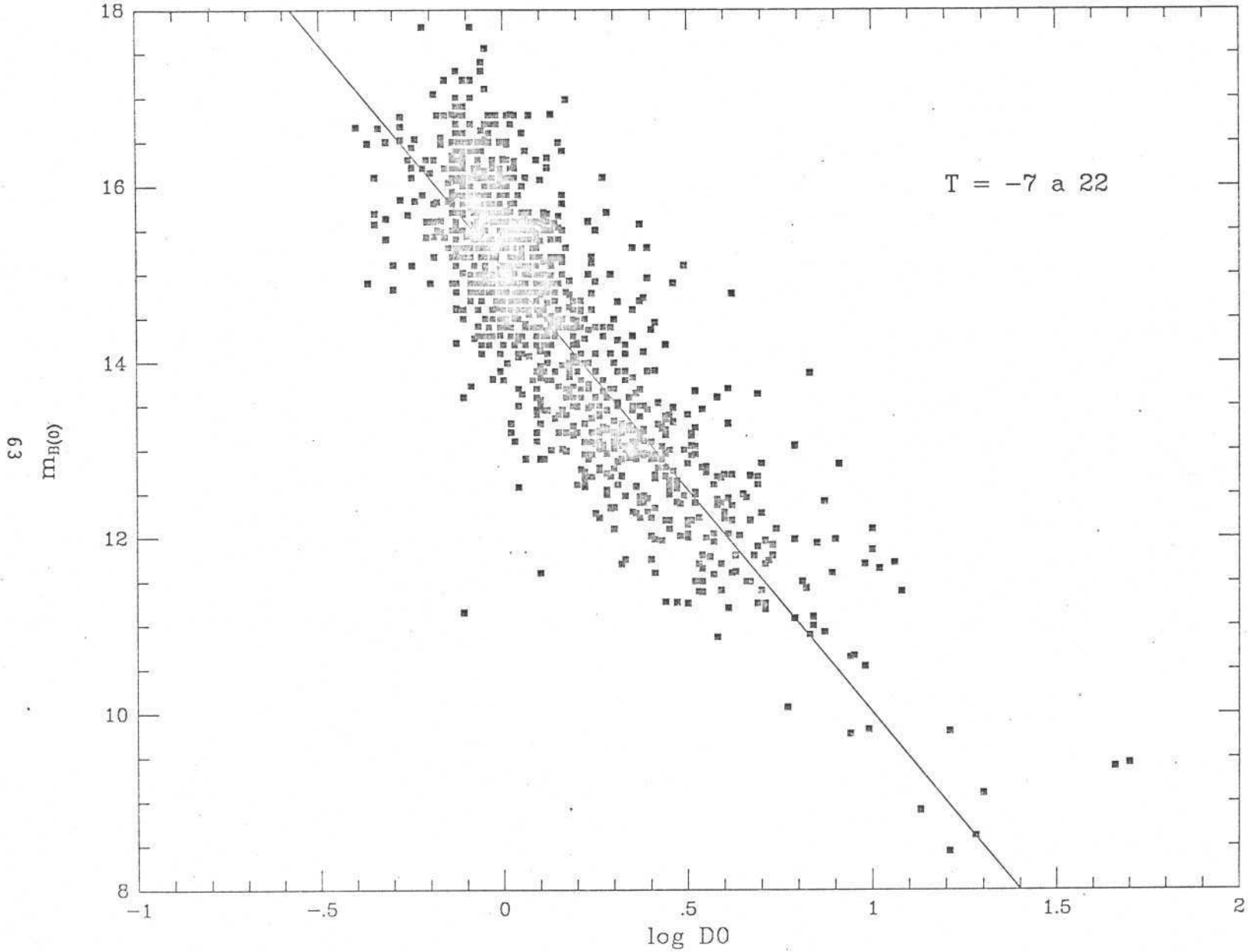

Figura 1

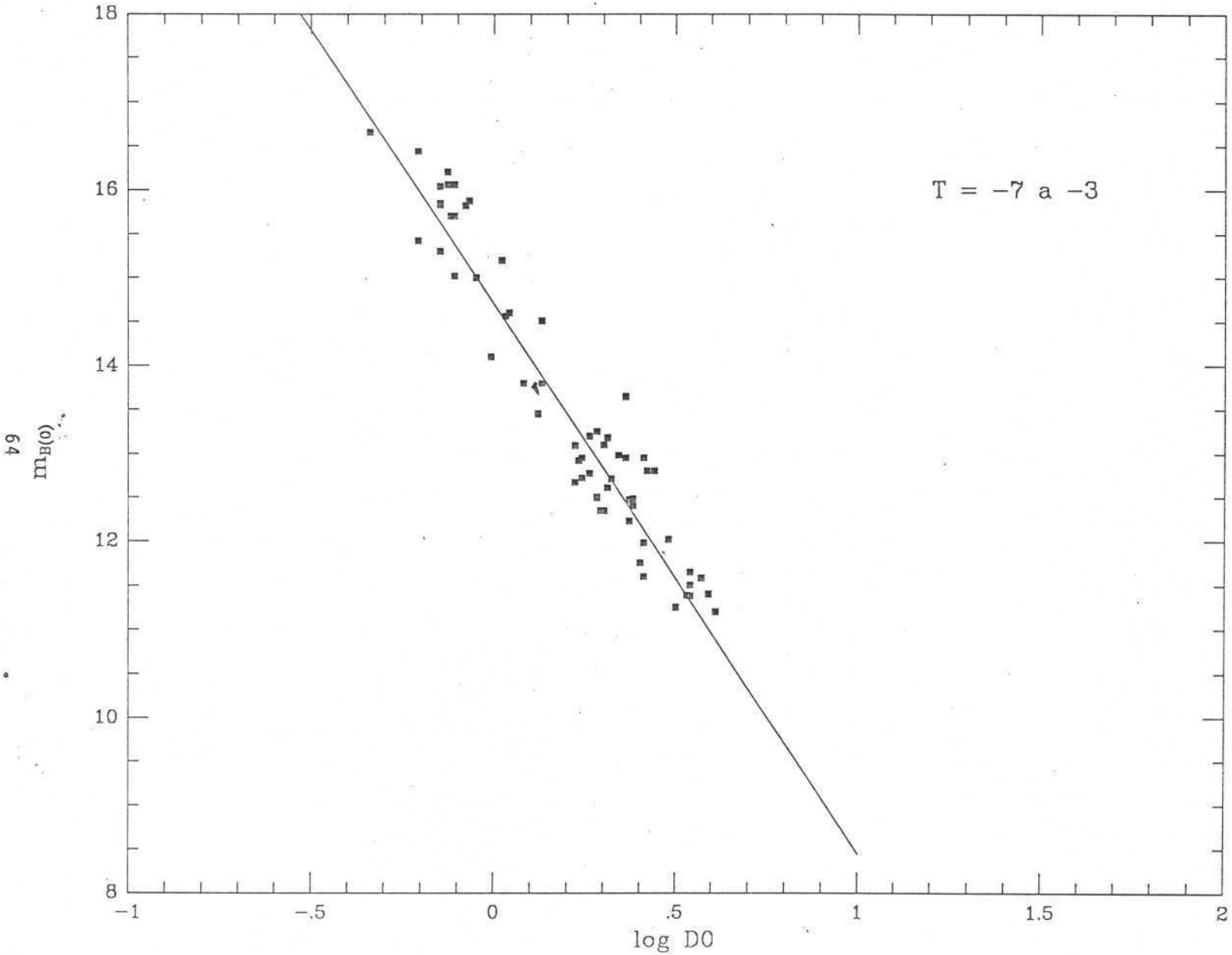

Figura 2a

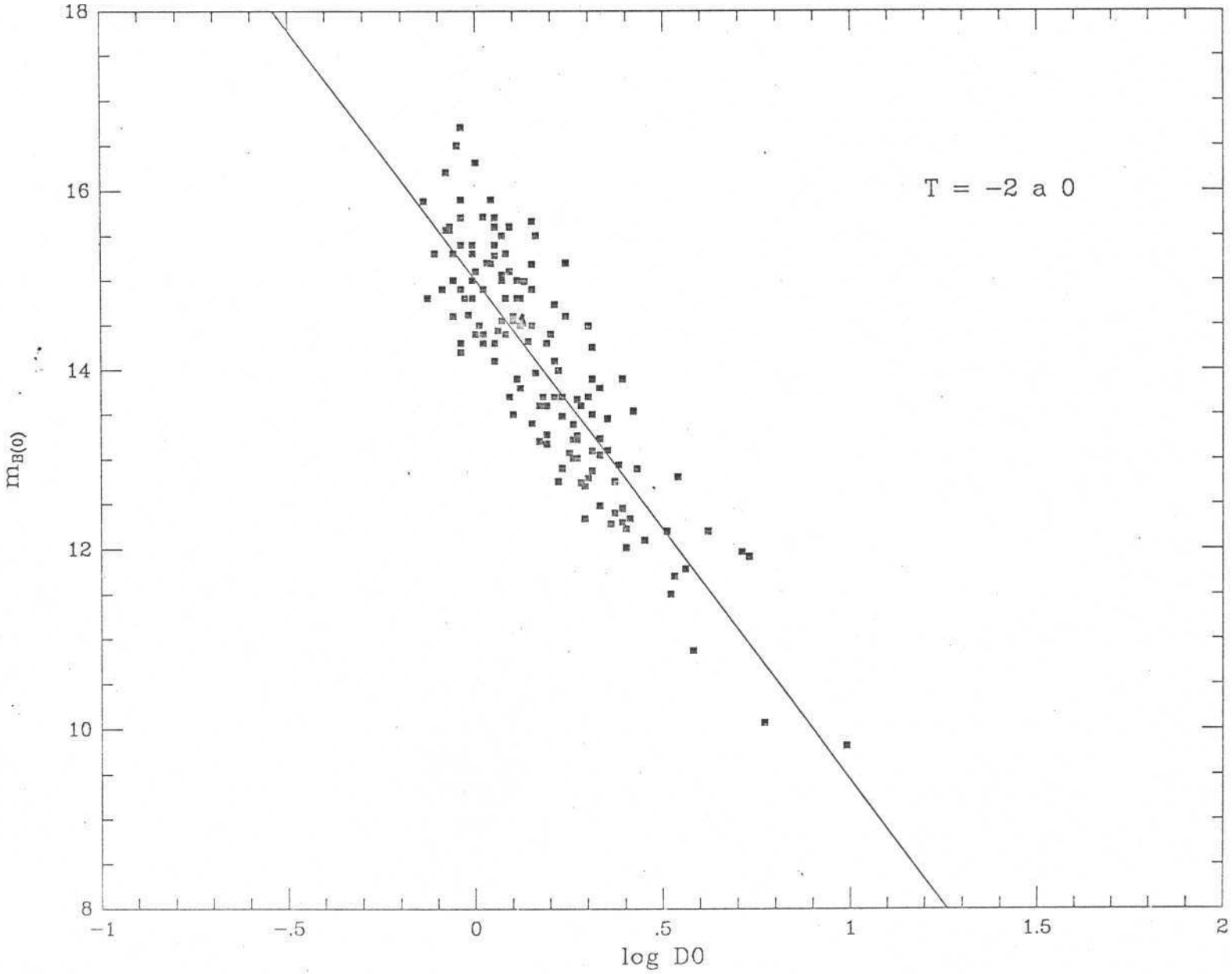

Figura 2b

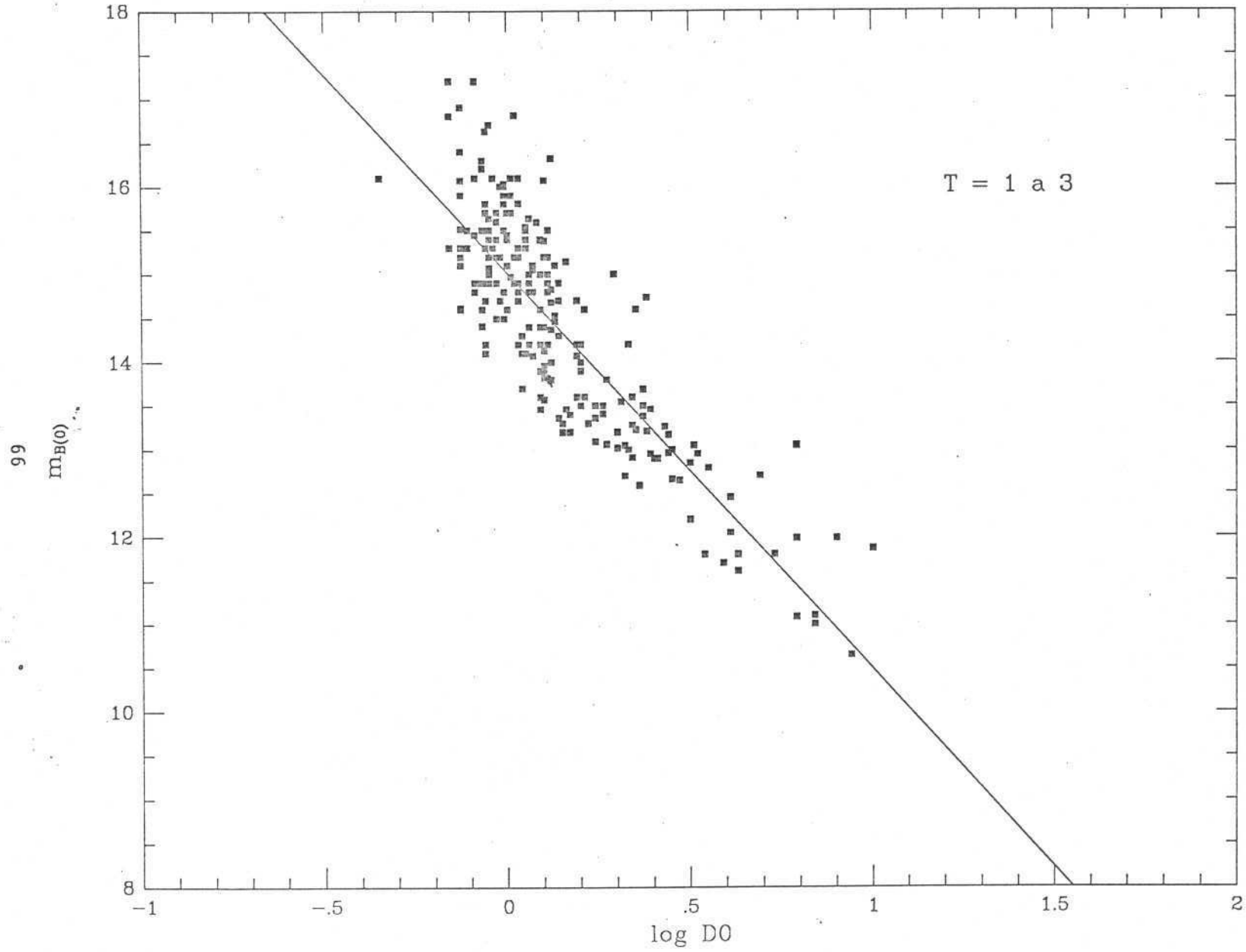

Figura 2c

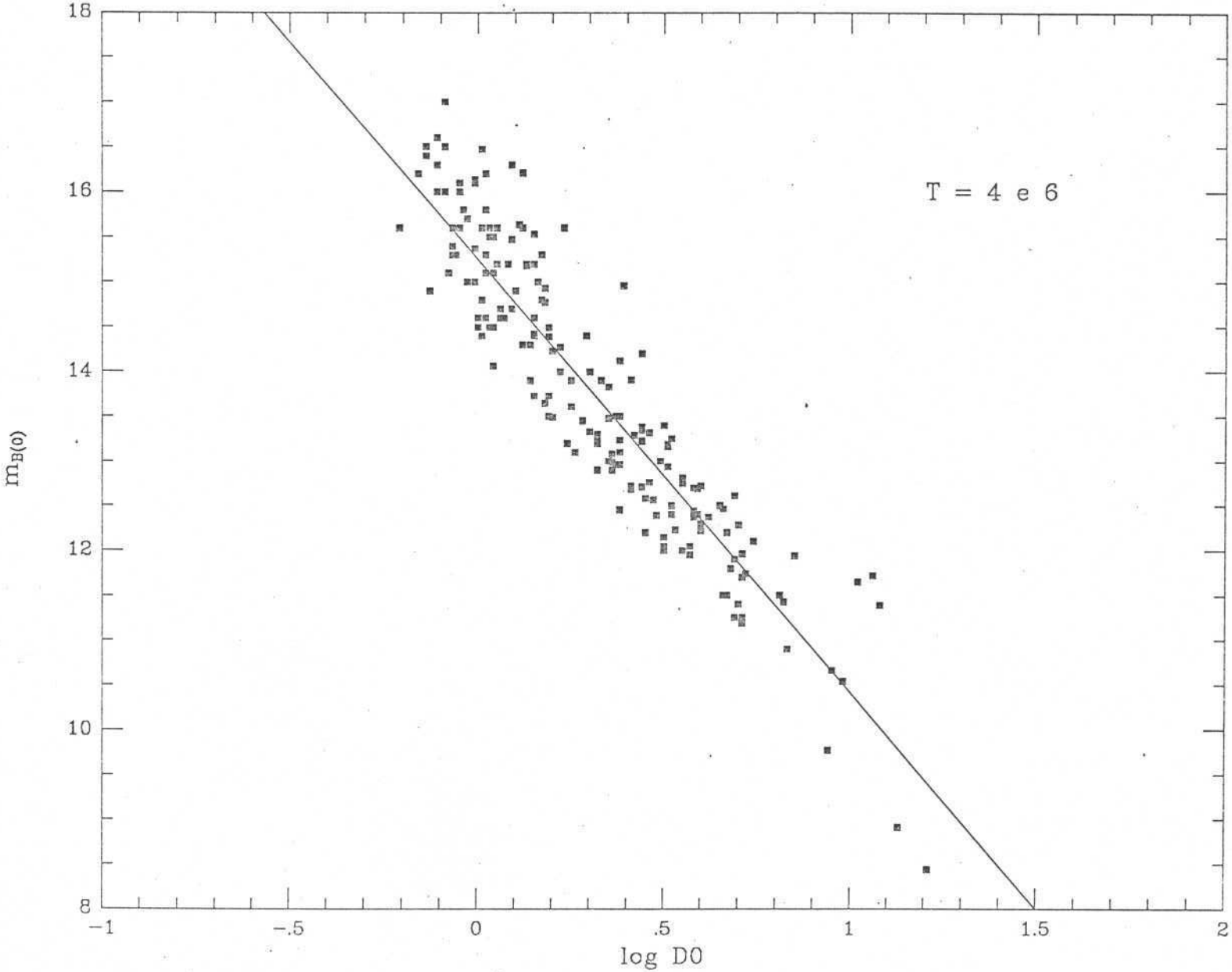

Figura 2d

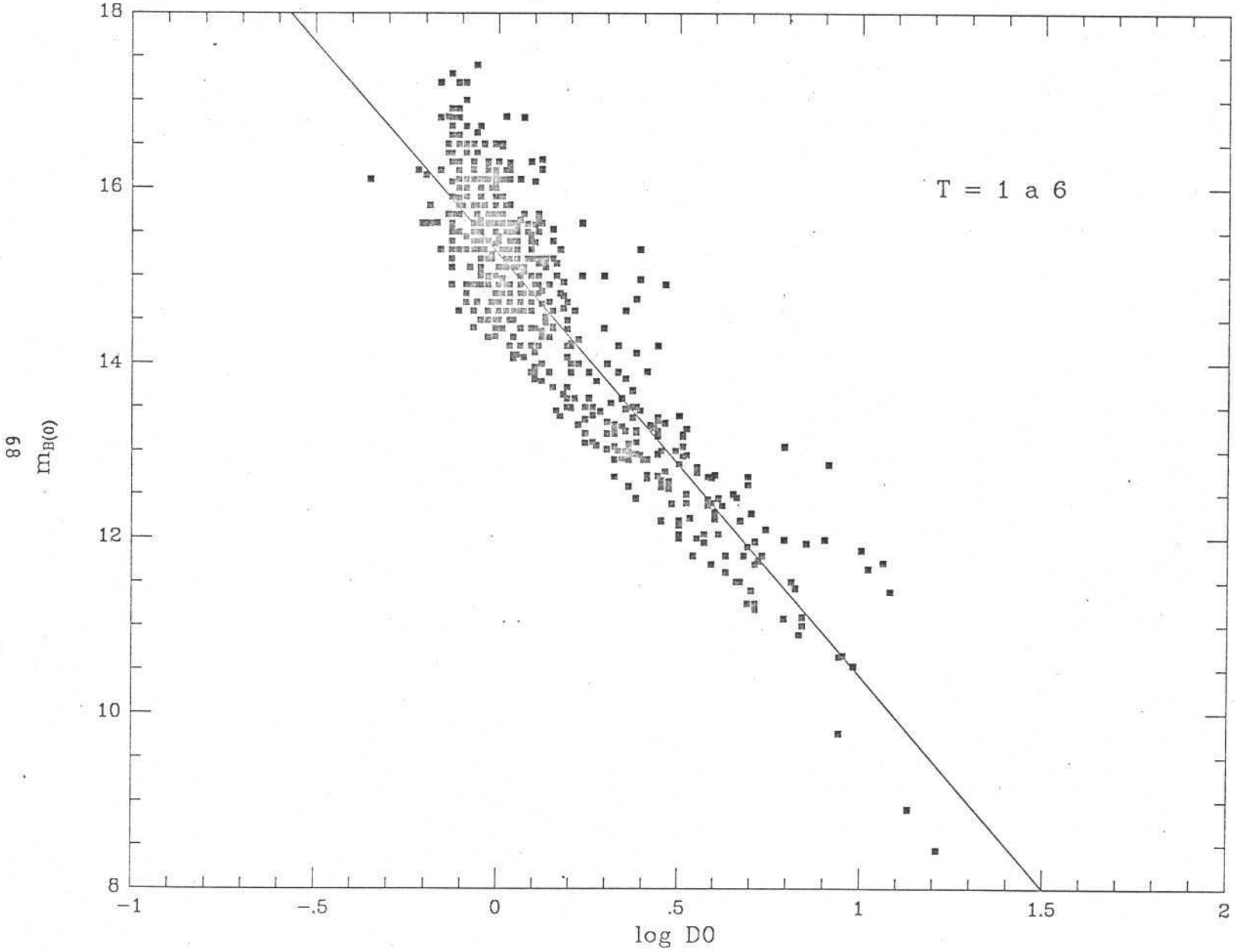

Figura 2e

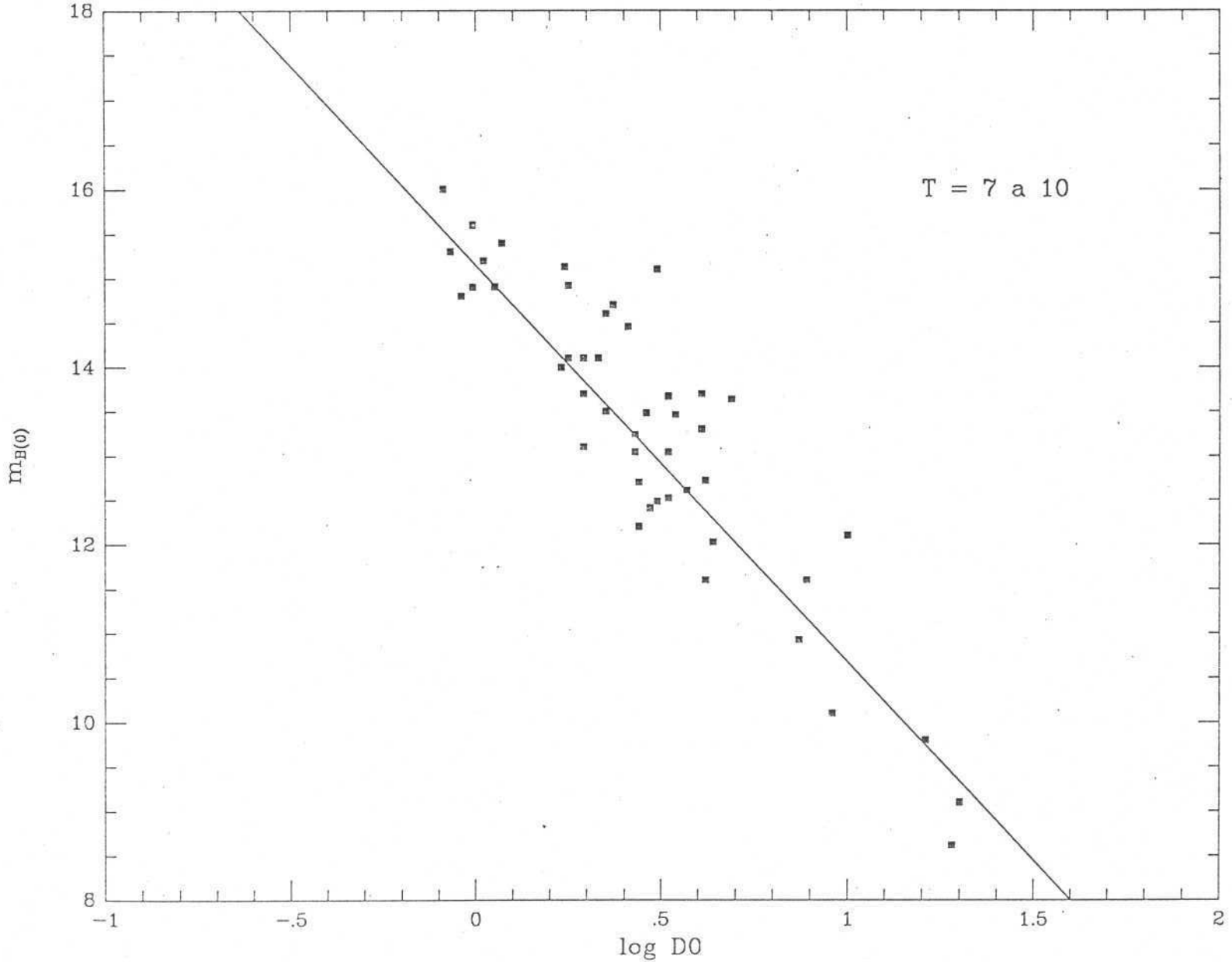

Figura 2f

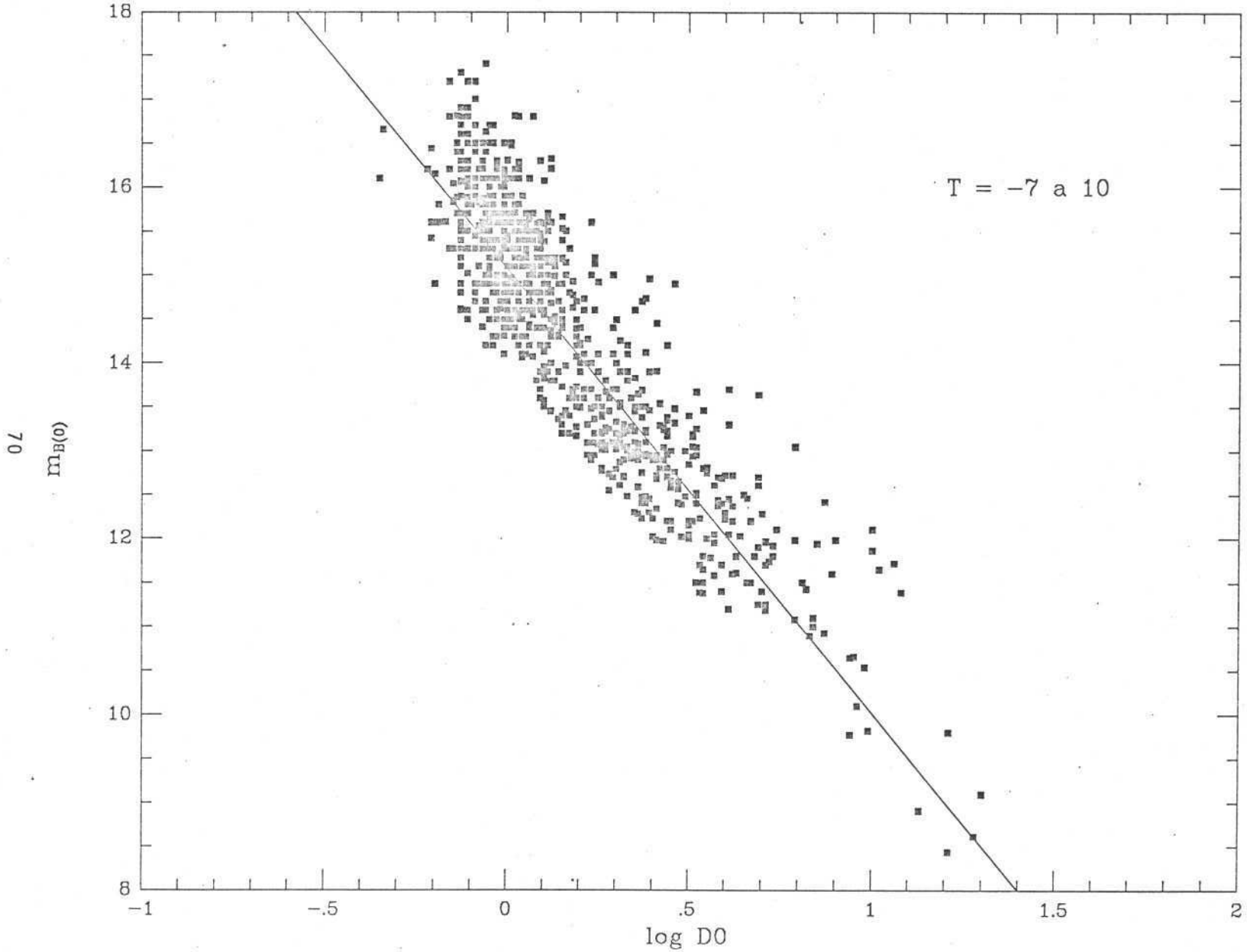

Figura 2g

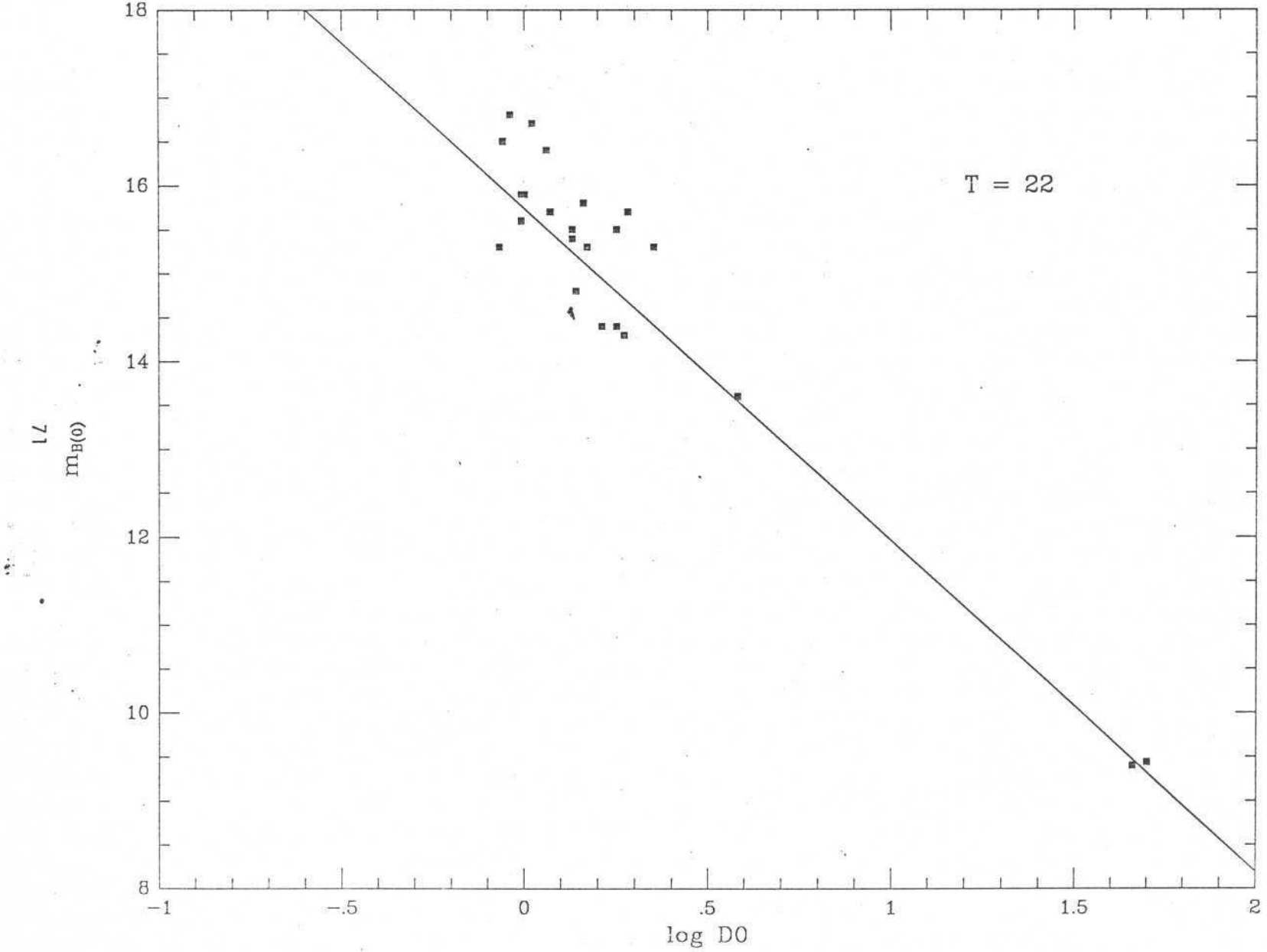

Figura 2h

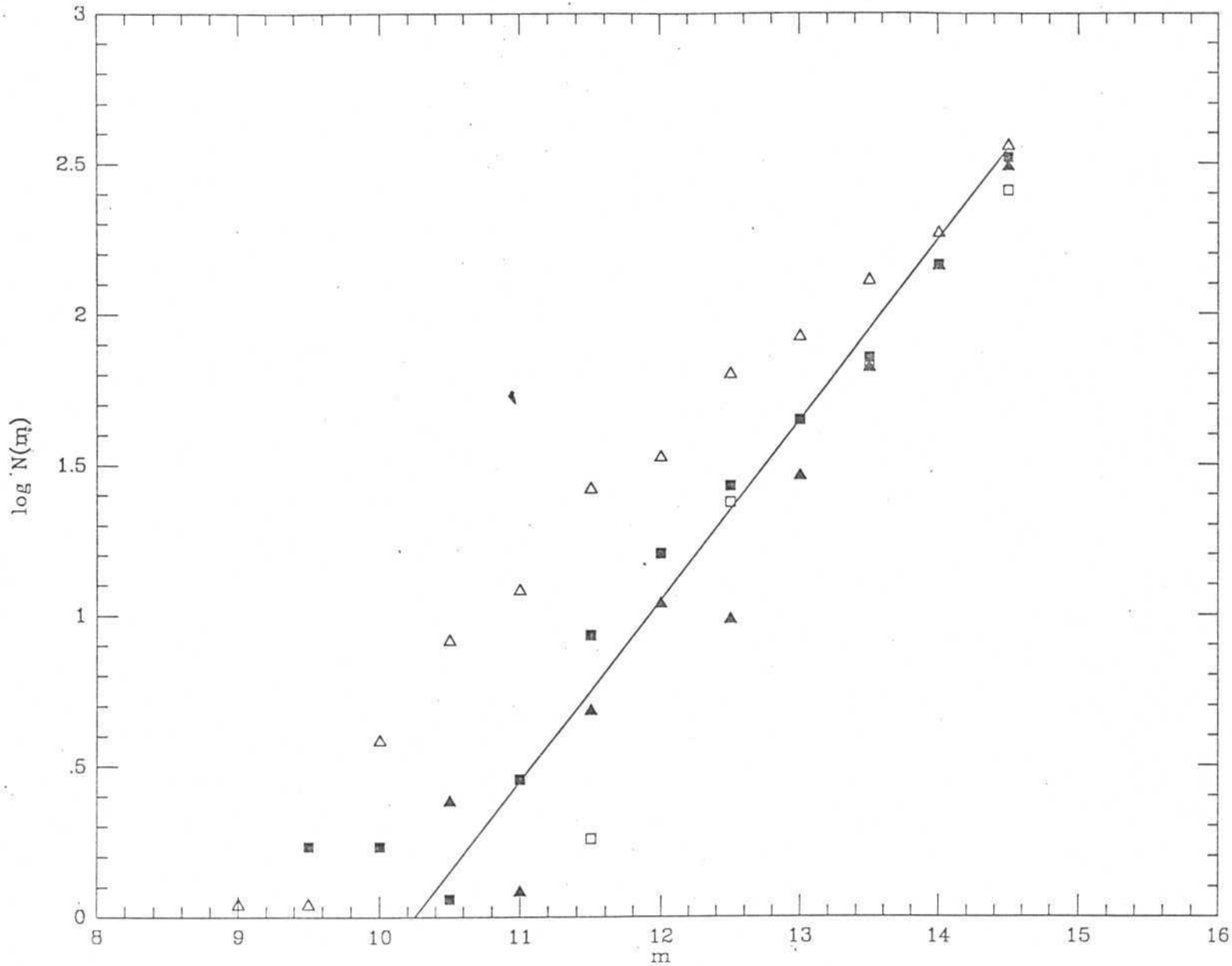

Figura 3

III. O SOUTHERN SKY REDSHIFT SURVEY (SSRS)

THE ASTROPHYSICAL JOURNAL, 327:544–560, 1988 April 15

THE SOUTHERN SKY REDSHIFT SURVEY

L. NICOLACI DA COSTA AND P. S. PELLEGRINI
Departamento de Astronomia, CNPq/Observatorio Nacional
W. L. W. SARGENT AND J. TONRY
California Institute of Technology
M. DAVIS AND A. MEIKSIN
Departments of Physics and Astronomy, UC Berkeley
DAVID W. LATHAM
Harvard-Smithsonian Center for Astrophysics
AND
J. W. MENZIES AND I. A. COULSON
South African Astronomical Observatory

ABSTRACT

We have finished a redshift survey of galaxies selected from the ESO catalog and present here maps of the resulting space distribution. The sample consists of 2028 galaxies in an area of 1.75 sr with declination south of −17°.5 and galactic latitude below −30°. The sample diameter is limited with all galaxies having log [$D(0)$] greater than 0.1 where $D(0)$ is a "face-on" diameter in arcminutes. The redshift sample is not complete at the smallest diameter, particularly for the later type galaxies, for which the surface brightness is very low; redshifts are available for 1657 of the galaxies. This survey provides useful information on large-scale structure to a depth of 120 h^{-1} Mpc ($H_0 = 100\ h$ km s^{-1} Mpc^{-1}). The galaxy distribution exhibits prominent filaments, sheets, and voids as seen in previous surveys, although there are no very rich clusters within the sample, the observed structure displays a diverse heterogeneity of morphology; some large-scale structures are highly subclustered, others are much more diffuse. Only a few of the more compact groups display conspicuous redshift space distortion. One large void in the foreground has an extent of $20 \times 30 \times 50\ h^{-1}$ Mpc and appears quite promising for future searches of material less clustered than luminous galaxies.

Subject headings: cosmology — galaxies: clustering — galaxies: redshifts

I. INTRODUCTION

In recent years considerable progress has been made in the observational study of the space distribution of galaxies. In particular, over the past decade several large-scale redshifts surveys have led to a dramatic change in our ideas of the clustering pattern of galaxies in the universe (see the review by Huchra and Geller [1987] for a summary of recent surveys). It is now recognized that the distribution of galaxies is very inhomogeneous, with galaxies tending to concentrate in high-density clusters and lower density filaments and sheetlike structures that pervade space, delineating large empty regions largely devoid of bright galaxies. Although some properties of the distribution, such as the statistics derived from the two-point correlation function, $\xi(r)$, are thought to be well determined on small scales ($r < 5\ h^{-1}$ Mpc), even the sign of $\xi(r)$ is undetermined for $r > 15\ h^{-1}$ Mpc, and the overall pattern of the galaxy distribution is still controversial. This results from the heterogeneity and complexity of the observed structure on large scale; the volumes surveyed thus far are too small to be confident that they are sufficiently representative. Some sections of the universe appear remarkably ordered, with a large fraction of the galaxies readily associated with well-defined filaments (see, e.g., de Lapparent, Geller, and Huchra 1986), while other sections appear chaotic and disordered, with no obvious clustering centers (e.g., several sections from Davis *et al.* [1982] and Haynes and Giovanelli [1986]). The study of the topology of the galaxy distribution and the geometrical properties of individual large-scale structures is further complicated by the expected distortions in the redshift maps used to represent the actual three-dimensional distribution of galaxies (Kaiser 1987).

The topological information is of great interest since different scenarios for the formation of large-scale structures probably lead to different topologies of the galaxy distribution. Both the hot dark matter and cold dark matter models are fully specified by their initial power spectra of density perturbations because the initial perturbations are expected to have had random phases, leading to Gaussian random initial fluctuations. These two models with rather different initial spectra seem to lead to virtually identical topologies as defined by Gott, Melott, and Dickinson (1986). However, the nonrandom phase models, such as the explosion models (Ostriker and Cowie 1981; Ostriker, Thompson, and Witten 1986) wherein large bubbles form hydrodynamically around isolated rare events, are likely to have somewhat different topology today. The cosmic sting model is another example where the fluctuations are initially non-Gaussian, and the present topology of structures in this model should also differ from the Gaussian models.

The largest existing complete redshift survey is the original CfA survey (Huchra *et al.* 1983) which is a wide-angle modest depth survey claimed, by at least some of its authors, to possibly represent a fair sample of the universe at large. In the past few years this sample has been used extensively in a variety of statistical analyses and to confront the results of theoretical N-body models for the formation and evolution of structures

in the universe. However, as pointed out by Davis *et al.* (1982) and by Davis and Huchra (1982, hereafter DH), the largest structures observed are comparable in size to the survey depth, casting some doubt on how representative of the universe this sample is on scales larger than $20\ h^{-1}$ Mpc. Since its completion there has been considerable interest in extending the original CfA survey both in depth and in sky coverage. For the past 5 yr, several groups have followed these two routes (da Costa *et al.* 1984; de Lapparent, Geller, and Huchra 1986; Menzies, Coulson, and Sargent 1987). The southern extension of the CfA redshift survey is of particular interest since it probes a different and, perhaps, more representative region of space that avoids the large concentration of galaxies associated with the Virgo cluster. At the same time it provides the first expanded view of our surroundings to the south. Furthermore, another large survey can be used to address the question of the statistical reproducibility of the results obtained in the original CfA survey. These considerations have motivated a cooperative effort of several groups to complete a survey of over 2000 galaxies, here referred to as the Southern Sky Redshift Survey (SSRS), covering an area of 1.75 sr of the south Galactic cap in the region south of declination -17.5 and below galactic latitude $-30°$. The goal was to obtain a complete sample down to a limiting galactic diameter given by $\log [D(0)] = 0.1$, where $D(0)$ is in arcminutes. In this paper we present redshift maps of the observed galaxy distribution and a qualitative description of the nature of the galaxy clustering. In § II we describe the properties of the selected southern sample, while in § III we show different projection maps of the galaxy distribution and describe the main features observed. Finally, in § IV the general characteristics of the three-dimensional distribution of galaxies are discussed. A future paper will discuss more quantitative aspects of the statistics of the galaxy distribution.

II. GALAXY DATA

The sample of galaxies was selected from the ESO/Uppsala catalog (Lauberts 1982) which is considered complete for galaxies south of declination -17.5 with major diameters greater than 1'. The information on morphological types and the values of the major and minor diameters for each galaxy were used to define a diameter-limited catalog based on a "face-on" diameter $D(0)$ defined by the expressions

$$\log [D(0)] = \log (D_1) - 0.235A(T) \log (D_1/D_2) , \qquad (1)$$

where

$$A(T) = 0.894 \quad T > 0$$
$$= 0.950 \quad T < 0 . \qquad (2)$$

In these equations D_1 and D_2 are the major and minor diameters and T denotes the morphological type as listed in the ESO Uppsala catalog. We note that the above definition of $D(0)$ is similar but not identical to that given by de Vaucouleurs, de Vaucouleurs, and Corwin (1976, hereafter RC2), since no correction is made for the major diameter to transform it to the isophotal system used in the RC2. In addition, the correction for the axial ratios is assumed to be similar to that determined in the RC2 for the axial ratios given by the Uppsala General Catalog (UGC, Nilson 1973). We emphasize that for the definition of a statistical sample it is not important to define an absolute system but simply to have a well-defined criterion in order to correct for selection effects, in the same way as is usually done for magnitude-limited samples. The diameter cutoff was arbitrarily chosen to be $\log [D(0)]_{\rm lim} = 0.1$. Adopting this diameter limit we have drawn 2028 objects over an area of 1.75 sr, within the region defined by galactic latitude below $-30°$ and declination south of -17.5, corresponding to a mean surface density of 1159 galaxies per steradian. This value is comparable to the mean surface density of galaxies in the magnitude-limited sample of the northern Galactic cap of the CfA survey, which includes the Virgo cluster. Therefore we find that using the diameter limit defined above we should sample at least as deep as the northern survey if not somewhat deeper.

Although a diameter-limited catalog is a perfectly valid statistical sample and in some applications may even be superior, it is important to note that it yields a quite different sample from one selected in terms of a limiting magnitude. In particular, it leads to a relative increase of low surface brightness (LSB) galaxies which makes completeness of the optical spectroscopy difficult. For example, selecting a diameter-limited sample from the Nilson UGC catalog (1973) yields 7% ellipticals, 12% lenticulars, 61% spirals, 2% irregulars, 8% dwarfs, and 8% others. In a magnitude-limited selection of the same UGC catalog, Davis and Geller (1976) found 10% ellipticals, 17% lenticulars, 55% spirals, 5% irregulars, 0.4% dwarfs, and 15% others, i.e., essentially no dwarfs. In the ESO diameter-limited sample there are 3% ellipticals, 17% lenticulars, 63% spirals, 8% irregulars, 7% dwarfs, and 2% others. Apparently the E, S0 division is not consistent between ESO and UGC, but otherwise the distributions are similar. It appears that a diameter-limited catalog yields a dramatic increase in the fraction of dwarfs, and a relative decrease in high surface brightness early-type galaxies when compared to a magnitude-limited sample. This is not unexpected.

The original sample of 2028 objects selected from the diameter cutoff chosen includes several multiple systems and interacting galaxies (IGs) as defined in the classification scheme adopted by Lauberts (1982). Since a single diameter has been quoted for these systems we have examined these cases individually in order to determine whether each member galaxy met the selection criterion, in which case they were assigned morphological types, diameters, and new coordinates. All 170 IG entries, including 30 multiple systems and 140 binary or perturbed galaxies, were examined using the ESO (B) and ESO/SRC on-film copies. From the plate inspection, all galaxies in IG systems, but with diameters below our cutoff, were excised from the list, leaving a total of 1963 individual galaxies.

Radial velocities for the galaxies in the sample were obtained in a collaborative effort with observations being made at the Observatorio Nacional (ON), Las Campanas Observatory (LCO), and South African Astronomical Observatory (SAAO). The data and a discussion of the quality of the radial velocities are presented elsewhere (da Costa *et al.* 1984; Menzies, Coulson, and Sargent 1987; Sargent *et al.* 1987). The velocities from all three groups are of high quality with an estimated error of less than 40 km s^{-1}. A substantial fraction of the sample has at least two and sometimes three redshift measurements which allows a good intercomparison among the different sets of observations. A final catalog which consolidates all the available data will be compiled in the near future (Sargent *et al.* 1987).

Combining all the observations we have radial velocities for a total of 1657 galaxies. The remaining objects had too low a surface brightness to allow the measurement of an optical redshift in the time available. This means that our completeness is not an exact step function of $D(0)$, and corrections should be made to account for this effect which is, in general, a function

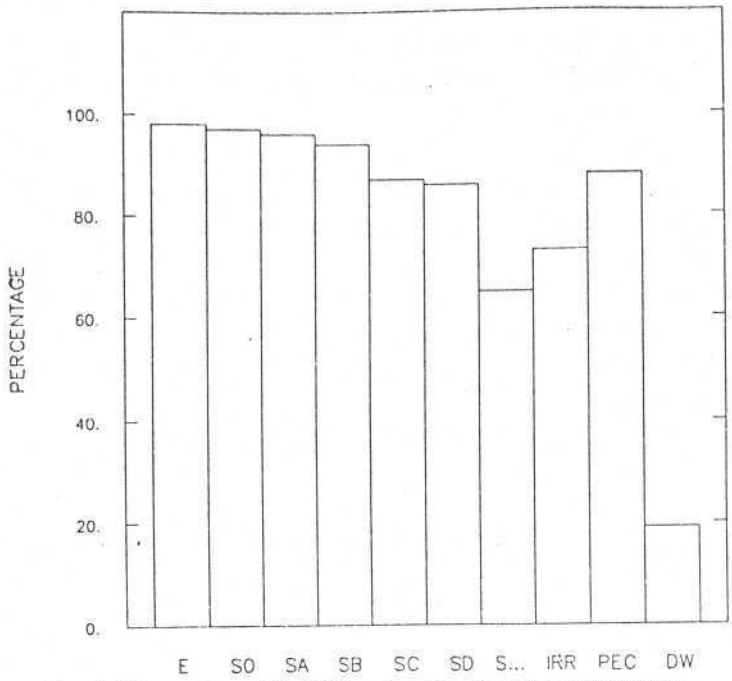

FIG. 1.—The completeness of the SSRS sample as a function of the morphological type

of the morphological type, as shown in Figure 1. Our completness rate is high up to Sc falling dramatically for later types or unclassified galaxies. The sample of dwarfs is especially incomplete since very little radio data are available in the southern hemisphere, and it is very difficult to obtain an optical redshift in reasonable integration times for low surface brightness galaxies. The incompleteness as a function of $D(0)$ for different morphological type groups is shown in Figure 2, and it is clear that the corrections amount to less than 20%, except for Sd, Irr, and dwarf galaxies. Although the plots shown below include the dwarfs, these were discarded from the quantitative analysis below, which considers a sample of 1830 galaxies with a redshift completeness of 90%.

III. GALAXY DISTRIBUTION

a) Space Density

Since we are dealing with a diameter-limited sample, at increasingly larger distances only the intrinsically larger galaxies will make it into the catalog. This introduces a selection effect that must be taken into account in any statistical analysis. In a similar fashion, when dealing with a magnitude-limited sample we may define a selection function $\phi(r)$ to be the fraction of galaxies at distance r that are sufficiently large to be included in the catalog. The derivation of this selection function is entirely analogous to that adopted by DH in the analysis of the CfA sample. It is derived from the ratio of the number of galaxies whose maximum observable distance is between r and $r + dr$ to the number of galaxies within a distance r observable to distances greater than or equal to r. The incompleteness of the present redshift sample presents only minor difficulties which are not relevant to the largely qualitative discussion below. A more detailed analysis will be presented elsewhere.

In order to minimize selection effects and to allow a comparison with the results of DH we have also defined a semivolume-limited sample, deleting galaxies that are not observable to at least a distance corresponding to 4000 km s^{-1}, resulting in a sample of about 1236 galaxies with absolute physical diameters D greater than 14.6 h^{-1} kpc. For the semivolume-limited sample the selection function is, by definition, unity for r less than 40 h^{-1} Mpc, decreasing steeply with distance beyond that, as shown in Figure 3. We recall that we do not include in our analysis the dwarf galaxies. This should not matter since most dwarf galaxies are likely to be nearby, intrinsically small galaxies and thus will be rejected from the semivolume-limited survey. For comparison Figure 3 also shows the selection function computed for the CfA northern cap sample, assuming a 250 km s^{-1} Virgocentric infall velocity. Note that, as expected, the diameter-limited sample extends somewhat deeper than the CfA sample; the maximum distance at which this sample can be considered statistically useful [$\phi(r) = 0.1$] is approximately 90 h^{-1} Mpc compared to 75 h^{-1} Mpc for the CfA sample.

The definition of the selection function allows one to determine an unbiased estimate of the mean number density of galaxies with diameters greater than 14.6 h^{-1} kpc. We have evaluated the mean density utilizing the estimator n_1 defined by DH,

$$n_1 = \frac{1}{V} \sum_{\text{shells}} \frac{N_c(r)}{\phi(r)} = 6.51 \times 10^{-3} \text{ galaxies Mpc}^{-3}, \quad (3)$$

In the above equation $N_c(r)$ is the number of observed galaxies in the radial interval dr at a distance r. The volume V and the

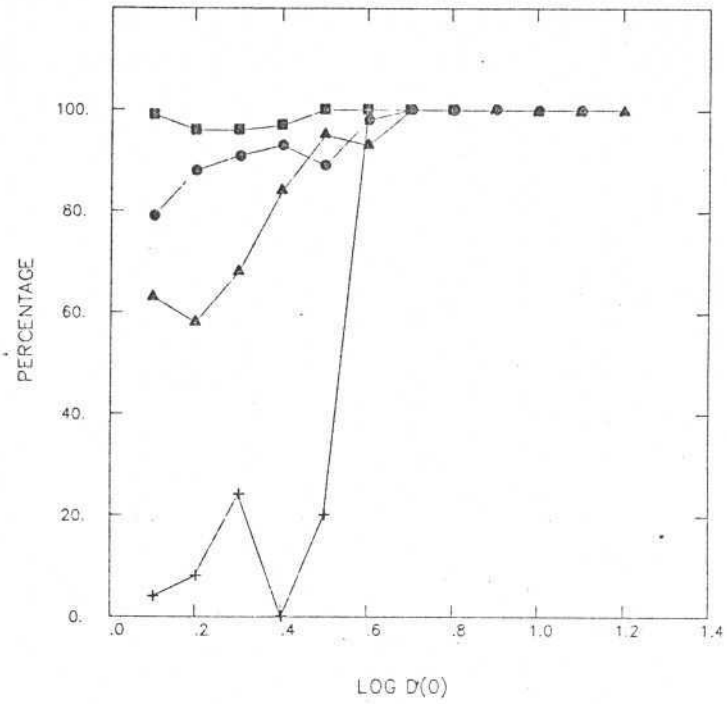

FIG. 2.—The completeness of the SSRS sample as a function of the "face-on" diameter $D(0)$, for different morphological type groups. The different symbols denote *full squares*: early-type galaxies; *open circles*: spirals; *full triangles*: Sd and Irregulars; *crosses*: dwarfs.

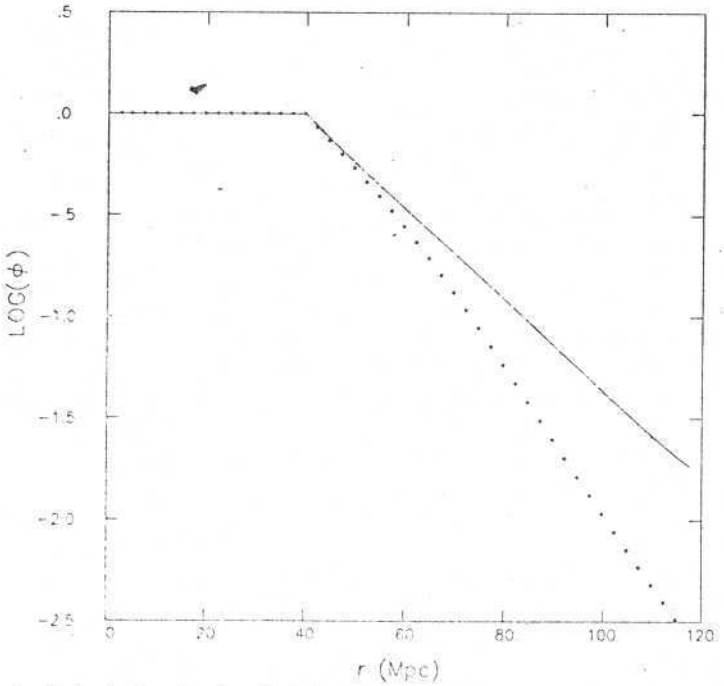

FIG. 3.—Comparison between the selection functions for volume-limited samples for the southern (*continuous line*) and northern hemispheres (*dotted line*). The southern sample is the diameter-limited sample of the SSRS, while the northern is the CfA one, both volume-limited at 4000 km s^{-1}. The curves were derived assuming a Virgocentric infall of 250 km s^{-1}.

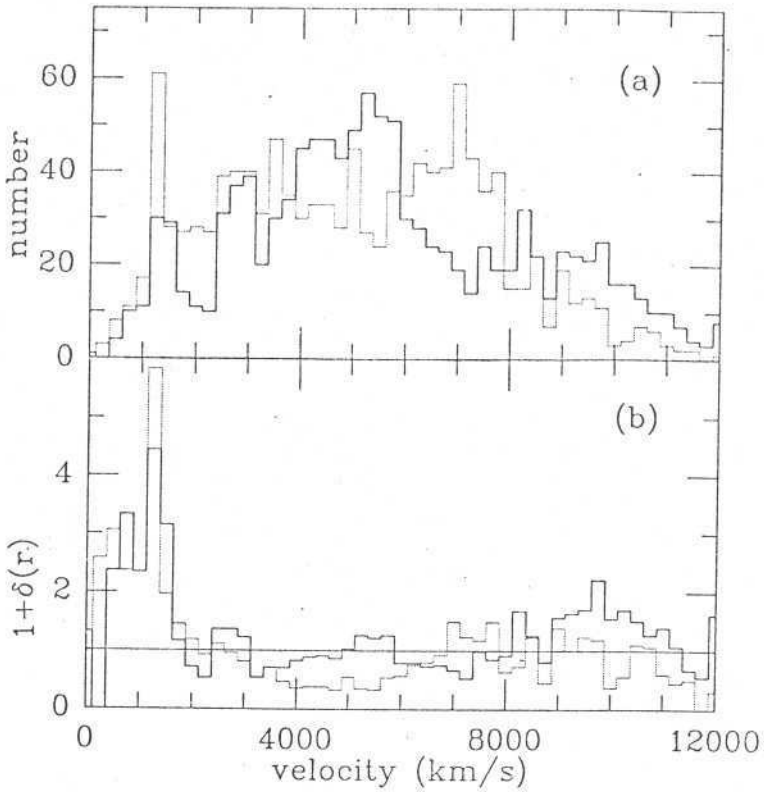

FIG. 4.—(*a*) Histogram of the observed counts of galaxies per shell of width 250 km s^{-1}, N_c, in the SSRS (*continuous line*) and the CfA north (*dotted line*) samples. Only galaxies in the semivolume-limited subset are included. (*b*) Histogram of the overdensity in shells $1 + \delta(r) = N_c/N_e$ for the two samples.

summation have been cut off at 90 h^{-1} Mpc. Velocities were corrected for a spherical infall of 250 km s^{-1} for the Local Group toward Virgo. Unfortunately, the different selection criteria between the northern and southern surveys prevents an accurate comparison of the mean densities of the two surveys, which would be the best indicator of the "fairness" of either sample. Hopefully this important comparison will be possible once magnitudes are available for the ESO catalog.

While the absolute value of n_1 cannot be directly compared with the CfA result (for galaxies brighter than $M_B = -18.5$) we may use the mean values calculated for both samples to examine the radial variation of the overdensity in the north and the south as shown in Figure 4. Figure 4*a* plots the raw distribution of counts per bin of width 250 km s^{-1}, N_c, for galaxies in the semivolume-limited distribution in the two surveys after correcting the observed velocity for Virgocentric infall. This distribution should be relatively unaffected by the incompleteness of our redshift survey because few of the missing galaxies are likely to have sufficient intrinsic size to be in the semivolume-limited subset. Figure 4*b* is the histogram of N_c divided by the number of counts per bin, N_e, expected if the galaxies were homogeneously distributed with density n_1. N_e is given simply by $N_e = \omega\phi(r)r^2\,dr$ where ω is the solid angle of the survey.

The similarities in Figure 4*b* between the two surveys are striking, including the presence of nearby clusters in both hemispheres followed by underdense regions. The mean underdensity of the hole in the region $3000 < v < 6000$ km s^{-1} is quite substantial for the northern survey, and there is nothing quite as dramatic in the south. The close agreement in overdensity contrast of foreground clusters of the north and the south is a cause for concern, as the Virgo supercluster in the north is certainly richer than Fornax plus Eridanus in the south, all of which are prominent in the magnitude-limited Shapley-Ames catalog. A complete set of magnitudes will we hope, clear up this mystery, which could be caused by nonlinearities in the ESO diameter scale.

b) Space Distribution

In Figure 5*a* we plot the distribution of all galaxies in our diameter-limited sample (1963 galaxies), including those without measured redshifts, projected onto the sky in equal area galactic coordinates. The most noticeable feature of this distribution is the enhanced structure along the north-south direction in the range $\alpha = 3^h$–4^h. A less concentrated structure runs across the sky along the east-west direction from $\alpha = 0^h$ to $\alpha = 3^h$. A V-shaped structure with sides aligned preferentially along the north-south direction occupies the region between $\alpha = 20^h$ and 22^h. Redshift information shows the filamentary appearance of these structures to be real in most cases. In Figure 5*b* we present the projected distribution of galaxies lacking redshifts. These are mostly dwarfs, which to a large

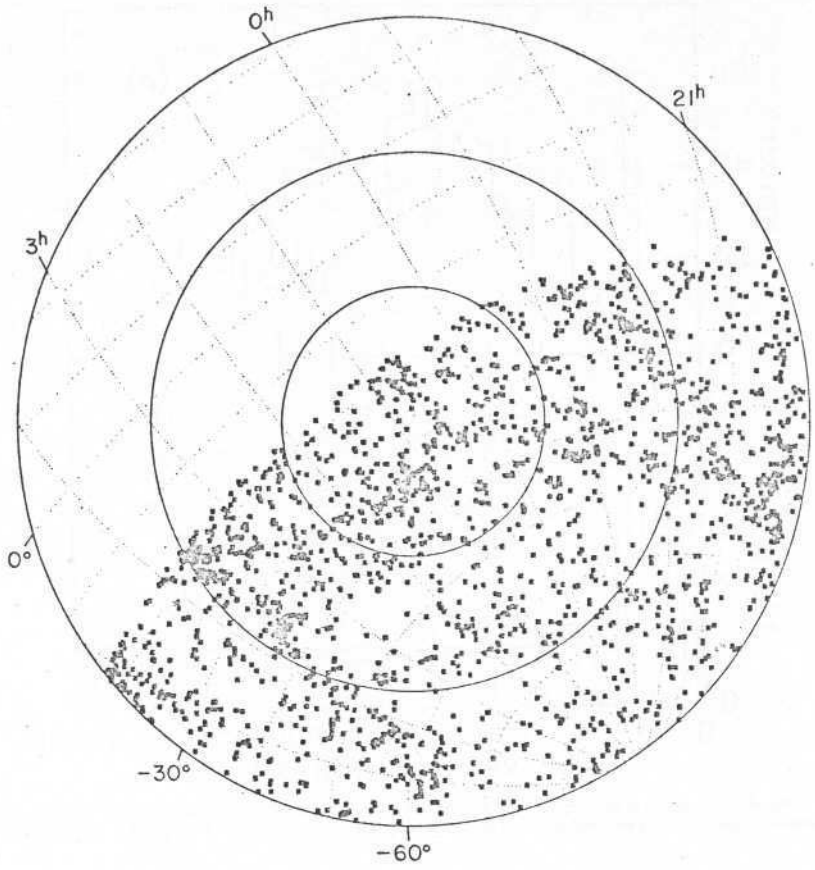

FIG. 5a

FIG. 5.—The 1963 galaxies of the SSRS sample (*a*) and the subset of 296 galaxies without measured velocities (*b*) projected onto equal area galactic coordinates. The south galactic pole is at the center and the circles denote the galactic latitudes $-70°$, $-50°$, and $-30°$. In the plot, constant declination and right ascension are indicated by dotted lines. About 200 of the galaxies without redshifts are either unclassified spirals or types later than Sc, of which 107 are dwarfs.

extent, follow the same general pattern displayed in Figure 5*a*. This indicates that the neglect of the dwarfs and other low surface brightness galaxies without measured redshifts should not hamper any future statistical analysis.

We examine the space distribution of all the observed galaxies by presenting in Figure 6 the data in distinct redshift windows. The nearest window is artificially richer than the others since it includes nearby intrinsically small galaxies. In the first window ($0 < v < 3000$ km s^{-1}) the most prominent structures are the Fornax cluster (3^h5, $-35°$, 1100 km s^{-1}) and the Eridanus group (3^h5, $-21°$, 1320 km s^{-1}) at the northern edge of the survey area. These two systems seem to form, with the looser group in Dorado (4^h5, $-58°$, 810 km s^{-1}), a connected linear structure that may extend beyond the present boundary of the survey. There are also two clearly discernible low-density regions suggesting the presence of two nearby voids: void 1 located approximately between right ascensions 0^h and 3^h and between declinations $-40°$ and $-60°$, and void 2 located around $\alpha = 21^h$ and $\delta = -25°$. Other recognizable high-density structures in this redshift window are several well-known nearby groups of galaxies like the Grus group (22^h, $-39°$, 1390 km s^{-1}), the NGC 7213 group (22^h2, $-46°$, 1800 km s^{-1}), and NGC 7144 group (21^h9, $-49°$, 1650 km s^{-1}) all listed in previous group catalogs (de Vaucouleurs 1975; Sandage 1975; Huchra and Geller 1982). This concentration of groups in the range $\alpha = 21^h$ to 23^h seems to be the front end of a large-scale structure stretching some 4000 km s^{-1} in depth. The main part of this structure, the so-called Telescopium-Pavo-Indus complex, can be seen in the second redshift window (Fig. 6*b*) which shows the velocity interval $3000 < v < 6000$ km s^{-1}. It has a well-defined filamentary appearance and extends over 40° across the sky at the western section of the surveyed area. This filament delineates a third void (void 3) centered around $\alpha = 23^h5$ and $\delta = -35°$. The other low-density region between $\alpha = 0^h$ and 4^h and $\delta < -45°$ is a continuation of void 1. In this velocity interval we also see a large structure with a nearly uniform surface density of galaxies covering an area of roughly 600 square degrees centered

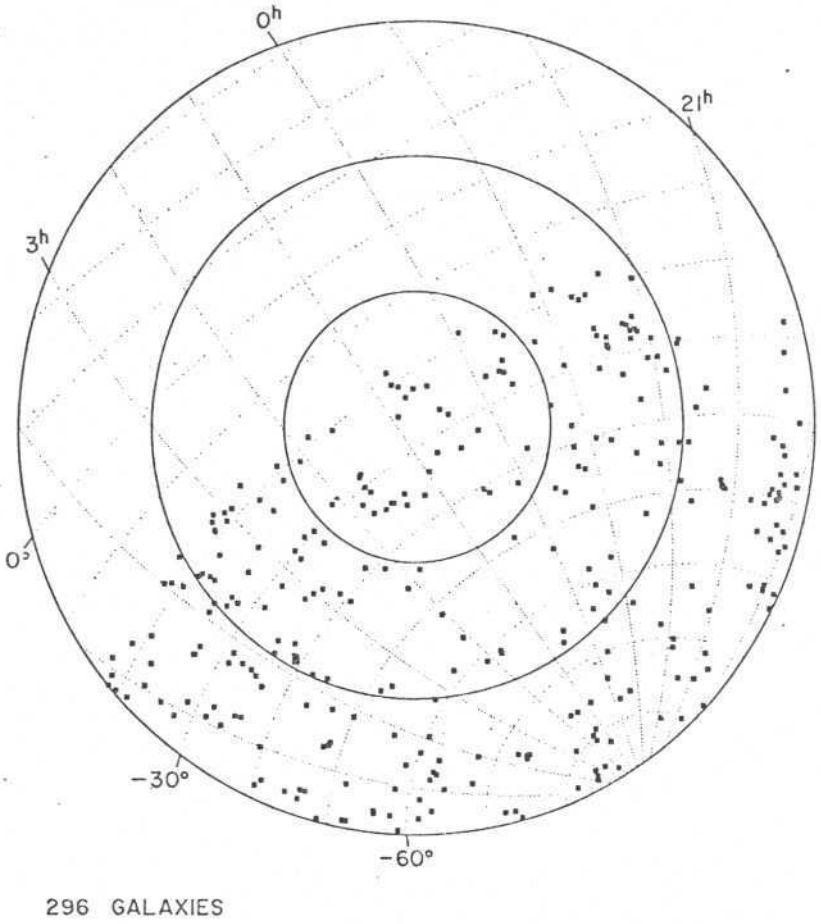

FIG. 5*b*

at $\alpha = 2^h$ and $\delta = -30°$. This loose structure is in fact a flattened distribution seen here nearly face-on. In Figures 7*a–c* below this feature is a prominent diagonal structure stretching over 50 h^{-1} Mpc, from (4^h5, 4000 km s^{-1}) to (0^h5, 9000 km s^{-1})! This feature has not been previously noted, and we shall refer to it as the "wall."

In Figure 6*c* we show the redshift window $6000 < v < 10{,}000$ km s^{-1} where the galaxies exhibit a trend to concentrate in the middle section of the plot in the range $0^h < \alpha < 2^h$ separating what appears to be two low-density regions. The westernmost, in the range $\alpha = 21^h$–0^h is the extension of void 3, while the other centered at approximately $\alpha = 4^h$ and $\delta = -40°$ and covering two hours of right ascension, is the fourth (void 4) very low density region that can be identified on the basis of these maps. Additional discussion of these empty regions is given below. Finally, Figure 6*d* shows the distribution of galaxies beyond 10,000 km s^{-1}. While a substantial number of galaxies have been observed with $v > 10{,}000$ km s^{-1}, at these large distances the distribution is severely undersampled with only the largest galaxies being surveyed, preventing any attempt to describe in a meaningful way the characteristics of the sample at these distances.

A more convenient way of showing the characteristics of the three-dimensional galaxy distribution is provided by the wedge diagrams shown in Figure 7, where we plot right ascension versus redshift, for different declination slices. We present only galaxies up to 12,000 km s^{-1} and use different symbols to denote different morphological type groups, as described in the figure captions. While a detailed description of the spatial distribution is a difficult task akin to detailing cloud formations in the sky, the basic feature of these maps that stands out immediately is the high degree of clustering exhibited by the galaxies. Large-scale linear and apparently connected structures delineate large empty regions. Although different in detail, the observed distribution clearly resembles those of previous surveys. One interesting characteristic of the present sample is the lack of prominent clusters in the surveyed volume. Redshift distortion effects are conspicuous only as mild radial elongations in the foreground groups. In general, the large-scale structures detected in the present survey cut across the line of sight and thus cannot be mistaken for "finger of god" structures due to virial motion within individual clumps.

In the foreground of Figures 7*a–c* the Fornax and Eridanus clusters are prominent; the signal-to-noise ratio on these clus-

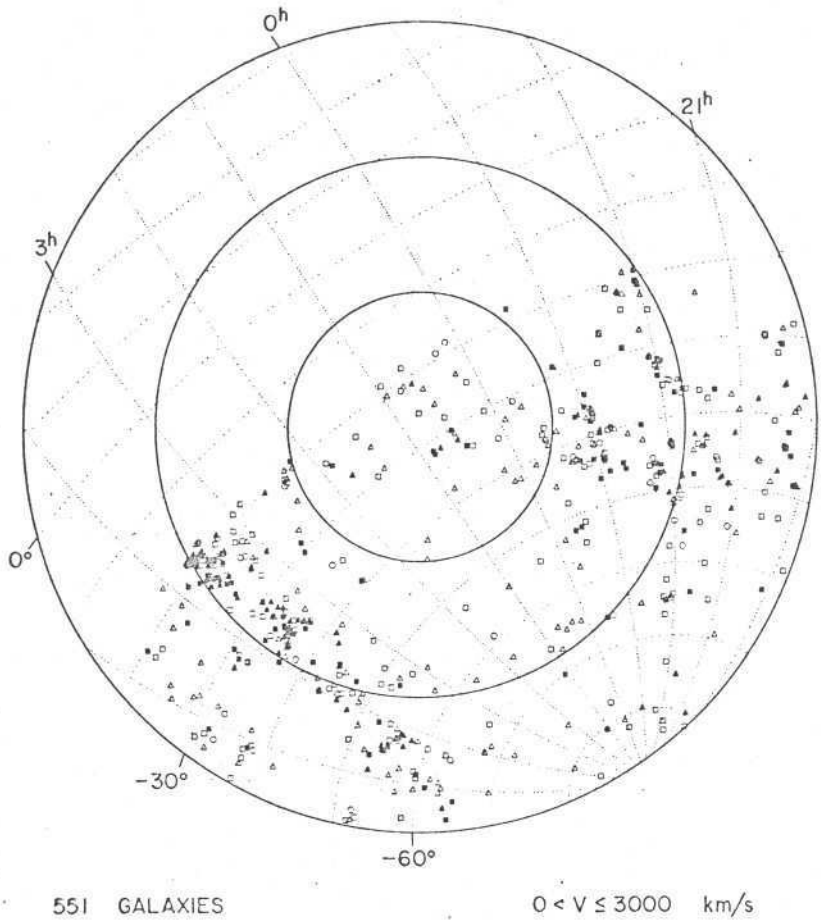

FIG. 6a

FIG. 6.—Projected distribution of galaxies, for different redshift windows, in the same coordinates as in Figure 5. The various symbols denote different morphological type groups: *full triangles*: E and S0; *full squares*: Sa and Sb; *open squares*: Sc; *open triangles*: unclassified spirals, peculiar, and irregular galaxies; *open circles*: dwarf galaxies.

ters and surrounding voids is best because the diameter function is probed most deeply. As a consequence it is possible to discern relatively sharp transitions between high- and low-density zones. In the region of 20^h–21^h the distribution is dominated by an elongated structure, the Telescopium-Pavo-Indus clouds. These must be distinct structures as there is a gap from 3000 to 4000 km s^{-1} in this complex. The most prominent structure in the middle region of the map is the long diagonal filament, the "wall" mentioned above. This structure is of low-density contrast and is approximately $50 \times 20 \times 10\ h^{-1}$ Mpc in extent. Note in all these maps that the different morphological types appear quite mixed throughout the structures; no obvious morphological segregation is apparent in the maps, an impression confirmed by correlation analysis.

Several low-density void regions are also conspicuous in the wedge diagrams. We summarize their positions and provide rough estimates of their sizes in Table 1. Perhaps the best defined void because of its proximity is void 1, located in the foreground just behind the Eridanus-Fornax-Dorado complex, with a mean redshift of approximately 3000 km s^{-1} and between $\alpha = 0^h$ to the easternmost limit of the survey. In the wedge diagrams it clearly extends through all observed slices, and is especially well defined south of $\delta = -30°$. Since it is at

TABLE 1

SSRS VOIDS

Void	Center	Dimensions (h^{-1} Mpc)
1.....	$\alpha = 1^h5$, $\delta = -50°$, $z = 3000$ km s^{-1}	$z\Delta\alpha \sim 30$, $z\Delta\delta \gtrsim 30$, $\Delta z \sim 40$
2.....	$\alpha = 21^h$, $\delta = -25°$, $z = 5000$ km s^{-1}	$z\Delta\alpha \gtrsim 30$, $z\Delta\delta \sim 30$, $\Delta z \sim 30$
3.....	$\alpha = 23^h5$, $\delta = -35°$, $z = 6000$ km s^{-1}	$z\Delta\alpha \sim 70$, $z\Delta\delta \sim 30$, $\Delta z \sim 50$
4.....	$\alpha = 4^h$, $\delta = -40°$, $z = 9000$ km s^{-1}	$z\Delta\alpha > 50$, $z\Delta\delta > 100$, $\Delta z \sim 50$

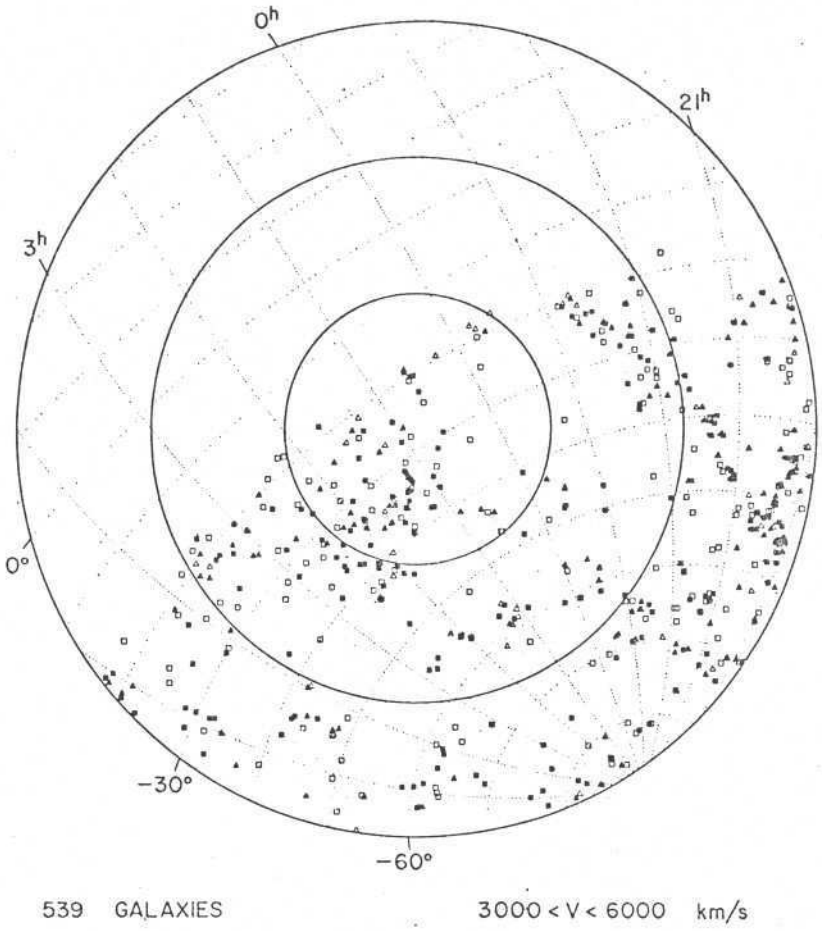

FIG. 6*b*

the edge of the survey area, however, we cannot from the present data establish its actual shape. The other nearby void mentioned earlier (void 2), in the direction $\alpha = 21^h$, is located very close to the western edge of the survey. It is seen in the declination range $-17°.5$ to $-50°$ and has a mean redshift of 5000 km s^{-1}. At large distances, there are two other important voids. One (void 3), centered at approximately 6000 km s^{-1}, is delineated by two of the structures described above. While it is especially well defined in the declination zone $-30°$ to $-40°$, it seems to extend farther south, being generally deficient of galaxies up to $\delta = -60°$. The other (void 4) is at a mean distance of 9000 km s^{-1} and spans some 4000 km s^{-1} in depth. This empty region is probably the largest in the survey volume, although its backside is undersampled and observations of a deeper sample are necessary to determine its reality and total extent.

IV. DISCUSSION

In this paper we have examined the general characteristics of the space distribution of galaxies in the SSRS sample, covering the southern Galactic cap. This sample is the largest existing survey of the southern hemisphere and probes a volume of space comparable to that of the original CfA redshift survey. Its size and the fact that it covers a distinct region of space make it of particular interest for the purpose of evaluating whether the presently available wide-angle surveys are sufficiently large to represent a fair sample volume of the universe. Comparison between the northern and southern surveys indicates that the clustering morphology of bright galaxies has a reproducible nature and can be considered as fairly well established. Galaxies tend to occupy a small fraction of the surveyed volume, with some fraction of the galaxies forming filaments and sheets which surround empty regions. However, not all galaxies can be neatly assigned to a well-defined large-scale structure; a good fraction of the galaxies are associated in loose groupings that have only the vaguest interconnection to each other.

The space distribution of galaxies described in the previous section can be summarized as consisting of several large structures which divide the survey volume into regions significantly devoid of galaxies. In order to obtain a more easily interpreted projected distribution we show in Figure 8 maps of a part of the galaxy distribution in a Cartesian coordinate system defined in the figure caption. We plot galaxies within contig-

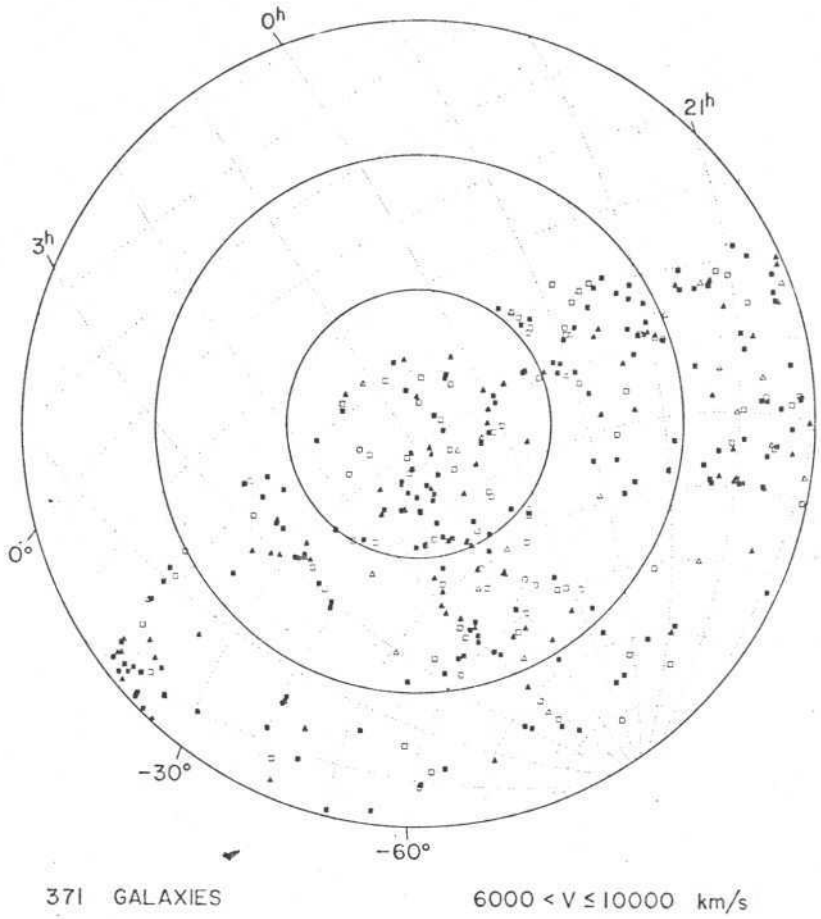

FIG. 6c

uous slabs, 10 h^{-1} Mpc thick, in the region of the survey encompassing the largest volume. The shape and extent of the main structures observed are not well-defined, because of selection and boundary effects. However, examination of the distribution in the Cartesian system suggests that the structure in the eastern side of the survey ($x < 0$), the "wall" at a mean distance of 50 h^{-1} Mpc, is primarily planar within the observed volume. It can be described by the simple expression $y = 2x + 80$, independent of z, in units of h^{-1} Mpc. It extends to the limit of the survey area for at least 50 h^{-1} Mpc in depth, 30 h^{-1} Mpc in the observed declination range and has a typical thickness of 5 h^{-1} to 10 h^{-1} Mpc. The second major component, lying in the Telescopium-Pavo-Indus (T-P-I) region, is a more complex conglomerate of condensed substructures. While it is actually formed by several small groups, it still appears to form a connected two-dimensional structure, extending as much as 60 h^{-1} Mpc in depth and with a transverse dimension of over 40 h^{-1} Mpc. The "wall," on the other hand, has much less pronounced substructure, especially as seen in the wedge plots. Inspection of the projection maps in the Cartesian system reveals that the T-P-I complex intersects another sheet at a sharp angle, which is not very well mapped since it is located at the western edge of the survey. It is interesting that in Figure 8 this branch of the Telescopium-Pavo-Indus complex appears even more prominent than that observed in the wedge diagrams. This illustrates the basic difficulty of grasping the characteristics of a three-dimensional distribution from a set of projection maps.

The wedge diagrams and the Cartesian map give clear evidence of a "bridge," at a mean distance of 30 h^{-1} Mpc and 30 h^{-1} Mpc long, connecting the "wall" and the T-P-I complex and forming the front side of void 3. A preliminary attempt to analyze the distribution taking into account the selection effects suggests that the backside edge of this void occurs within the survey volume and bridges the major structures at larger distances, but this must be confirmed by deeper samples. Besides all these structures, the maps examined also show several less prominent, sometimes curved, filaments which intersect the larger sheets often forming sharp edges. These curved structures closely resemble those described by de Lapparent, Geller, and Huchra (1986) who described the overall galaxy distribution in terms of bubbles in contact.

In the preceding section we have attempted to identify individual voids on the basis of visual inspection of the several

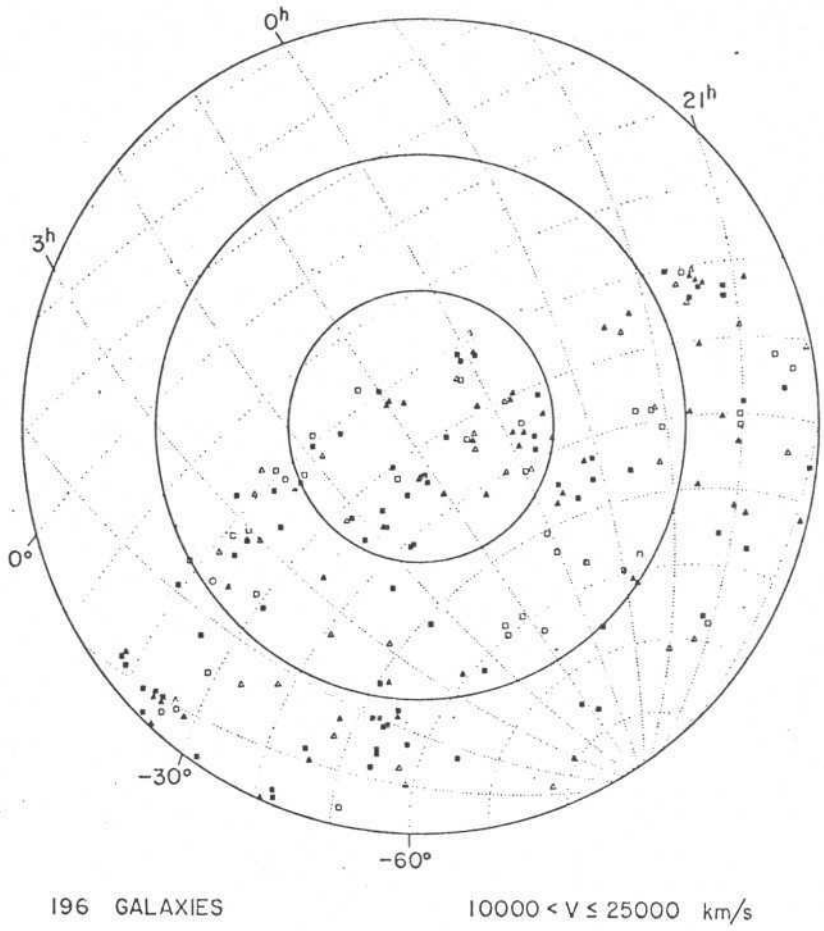

FIG. 6*d*

projection maps presented. We have called attention to at least four relative prominent empty regions, with typical sizes ranging from 10 h^{-1} to 60 h^{-1} Mpc. Although we have described them as separate entities, the voids do not seem to be completely surrounded by unbroken sheets as would a bubble, but rather they appear to be connected throughout the survey volume, giving the impression of a spongy topology as described by Gott, Melott, and Dickinson (1986). It is also significant that the voids seem to be deficient in all types of galaxies, including the dwarf galaxies. This is a qualitative statement that will be supplemented with detailed correlation analyses in a future paper. One of the voids (void 1) identified here is particularly interesting for further investigating this question due to its proximity.

The above description is rather qualitative and meant solely to highlight some of the prominent features of the observed galaxy distribution. However, the fact that the clustering pattern of bright galaxies has been confirmed to have a reproducible appearance is, by itself, already important, since it imposes stringent constraints on theoretical models. Successful models for the formation and evolution of large-scale structures must be able to reproduce at least the major features of the observed distribution described here. In this respect, it is remarkable that the observed distribution in the south looks very similar in nature to the results of the N-body simulations of White *et al.* (1987) in a flat, cold, dark matter model of the universe. For example, their Figure 10 bears a striking resemblance to our Figures 7*a–c*, especially in the nature of the long diagonal filaments. In future papers we intend to investigate the properties of the SSRS using the different quantitative methods that have been developed to analyze several recent surveys. A quantitative description of the properties of the observed distribution is essential to allow the comparison with results of White *et al.* (1987) and other numerical simulations. We hope that from this comparison we may eventually be able to discriminate among the competing models that have been proposed to account for the formation of large-scale structure in the universe.

Several people have contributed to the survey and we thank them all for their support. L. N. da Costa and P. S. Pellegrini would like to thank J. Geary and M. A. Nunes for keeping the ON detector running over the years and C. Willmer, R. de

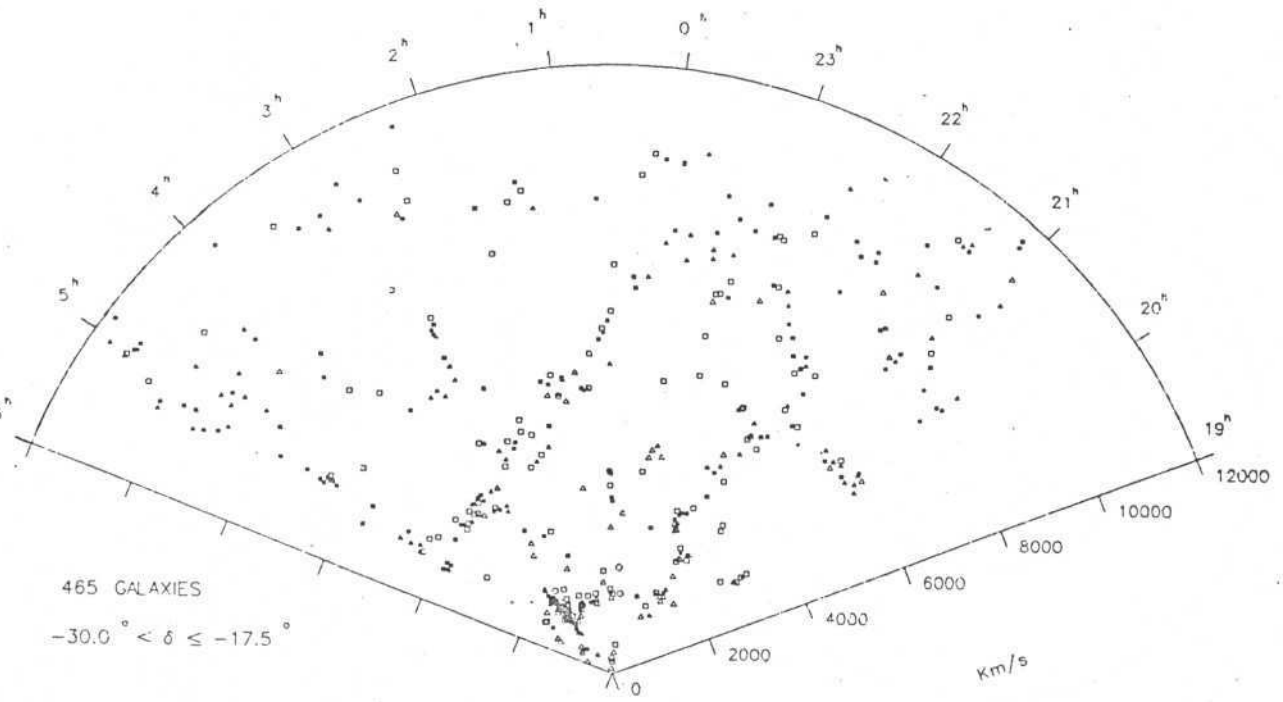

FIG. 7a

FIG. 7.—Cone diagrams of right ascension vs. redshift showing galaxies in the SSRS sample with $v < 12{,}000$ km s^{-1}. The range in declination of each wedge is indicated in the figures. The symbols are the same as in Fig. 6.

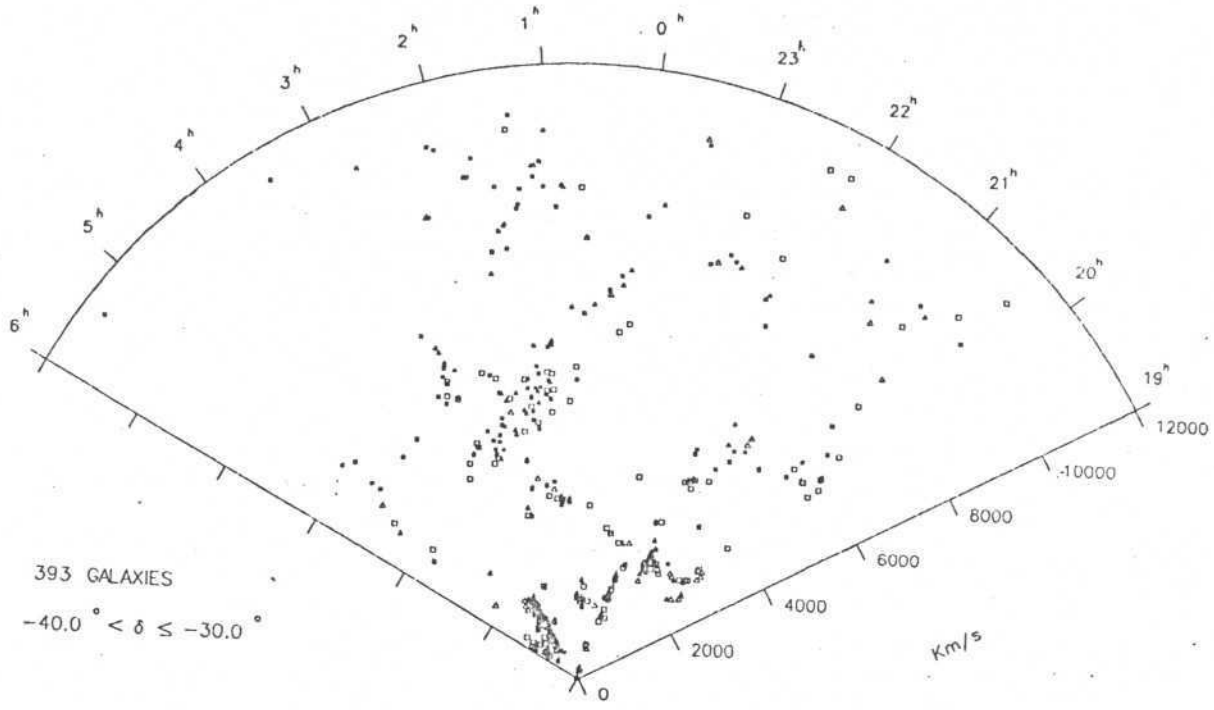
0 h
1 h
2 h
3 h
4 h
5 h
6 h
23 h
22 h
21 h
20 h
19 h
2000
4000
6000
8000
10000
12000
Km/s
0
393 GALAXIES
−40.0 ° < δ ≤ −30.0 °

Fig. 7b

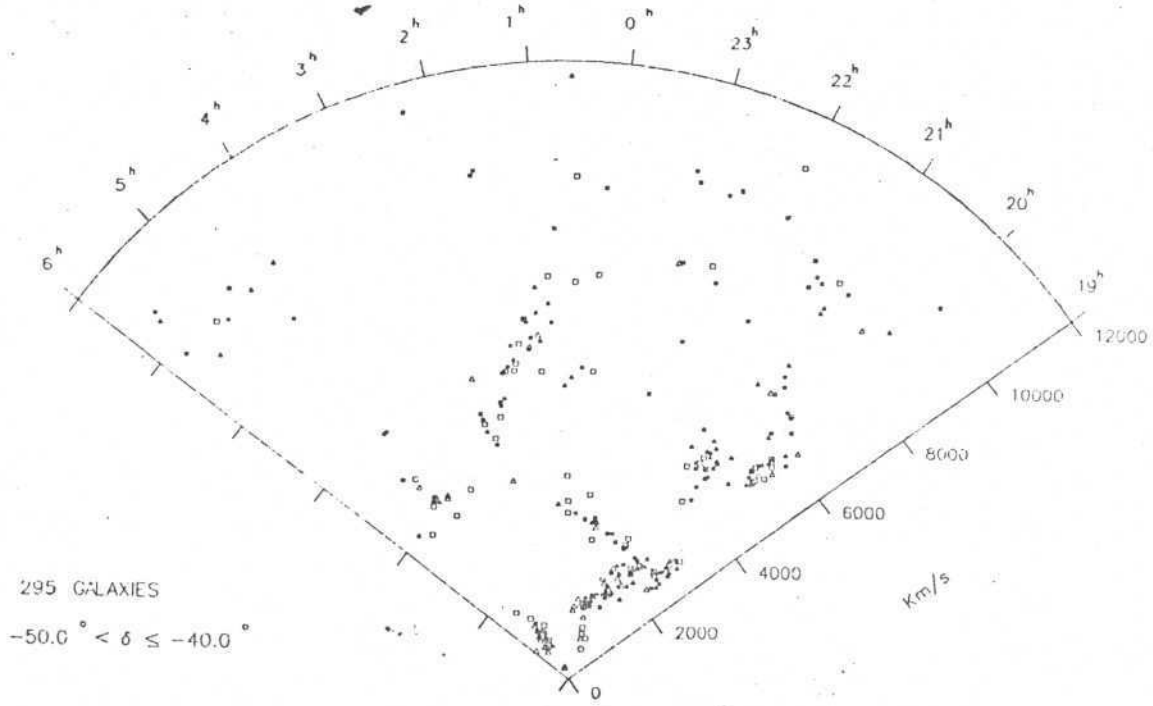
0 h
1 h
2 h
3 h
4 h
5 h
6 h
23 h
22 h
21 h
20 h
19 h
2000
4000
6000
8000
10000
12000
Km/s
0
295 GALAXIES
−50.0 ° < δ ≤ −40.0 °

Fig. 7c

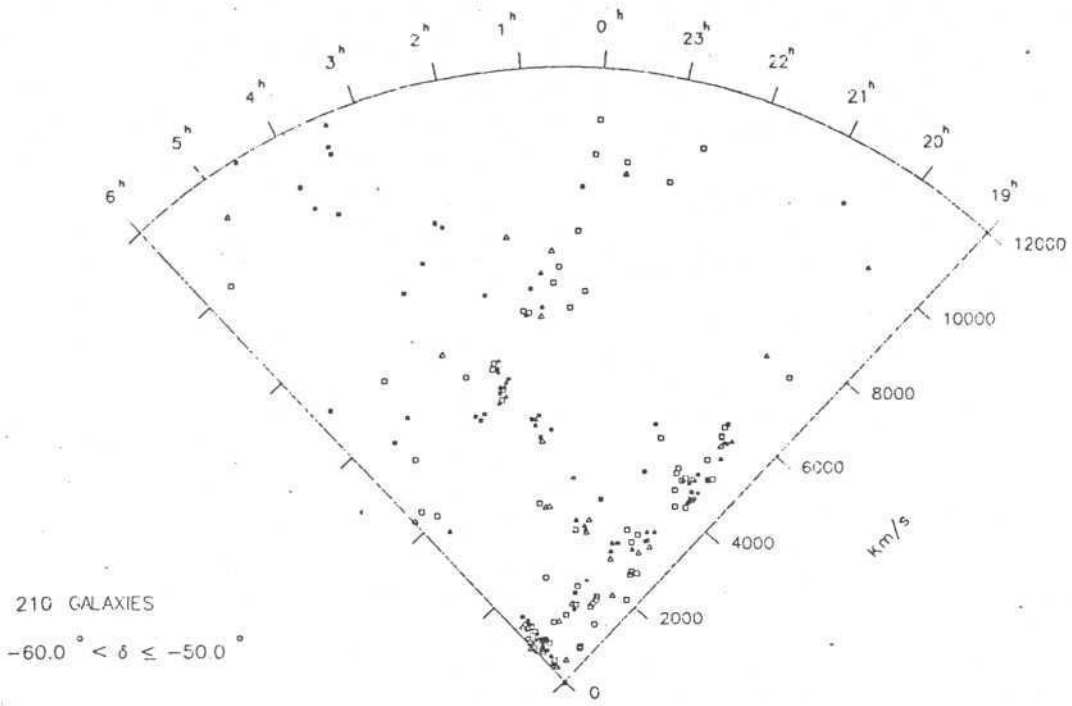
0 h
1 h
2 h
3 h
4 h
5 h
6 h
23 h
22 h
21 h
20 h
19 h
12000
10000
8000
6000
4000
2000
0
Km/s
210 GALAXIES
−60.0 ° < δ ≤ −50.0 °

FIG. 7d

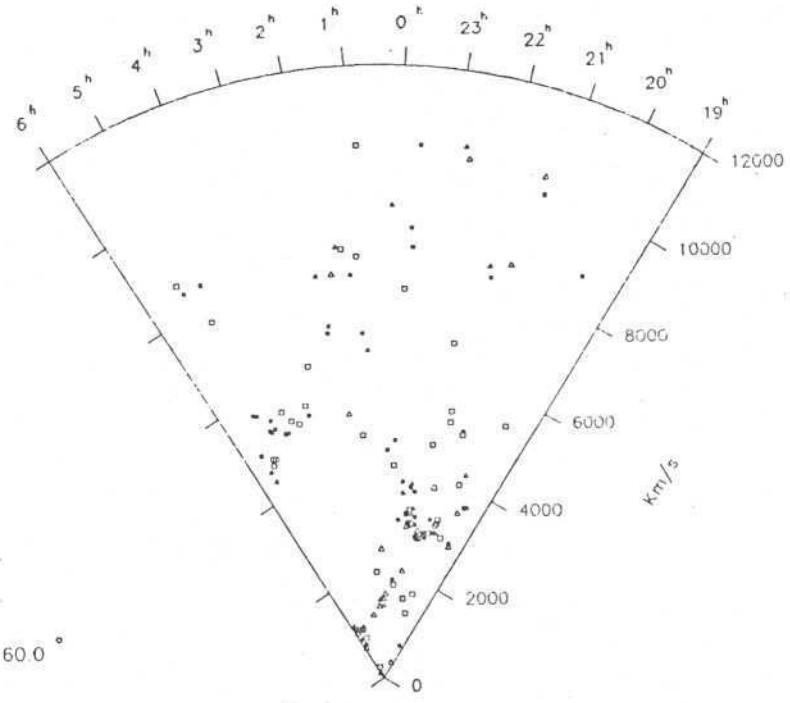
0 h
1 h
2 h
3 h
4 h
5 h
6 h
23 h
22 h
21 h
20 h
19 h
12000
10000
8000
6000
4000
2000
0
Km/s
140 GALAXIES
−70.0 ° < δ ≤ −60.0 °

FIG. 7e

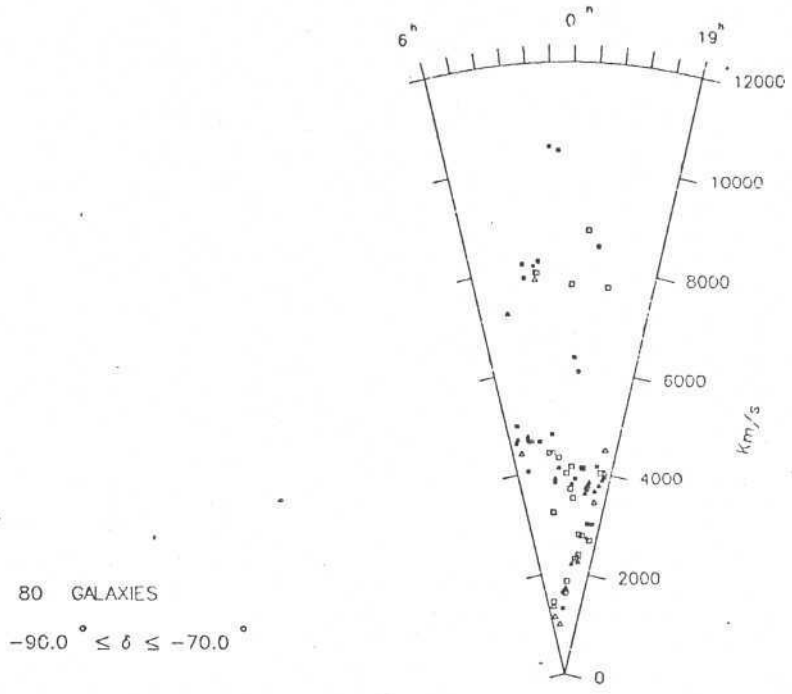

FIG. 7f

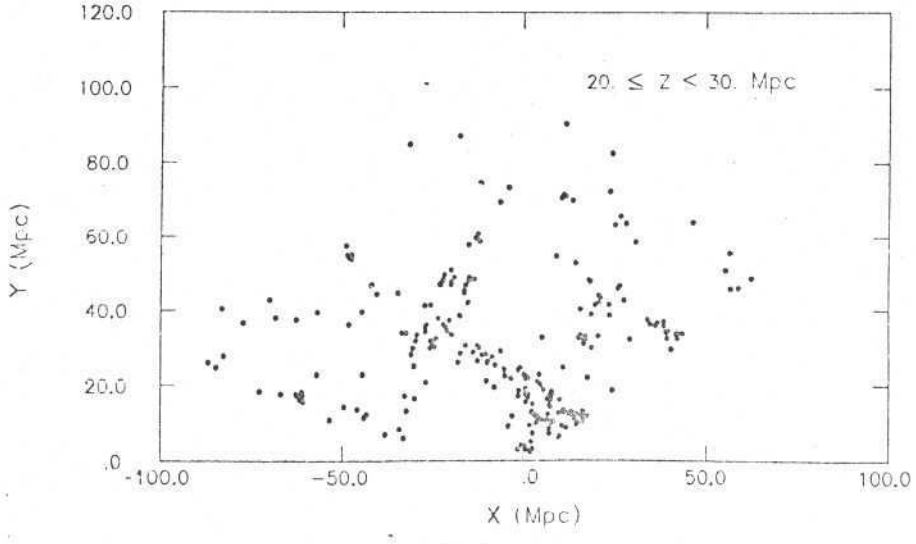

FIG. 8a

FIG. 8.—Distribution of galaxies plotted in a Cartesian coordinate system with the x and y axes lying in the equatorial plane and pointing in the directions of $\alpha = 18^h$ and $\alpha = 0^h$, respectively; the z axis toward the south celestial pole. In the figure we show the projection onto the $(x - y)$ plane of galaxies with $v < 10{,}000$ km s^{-1} covering the range $20 < z < 50\ h^{-1}$ Mpc, in $10\ h^{-1}$ Mpc intervals.

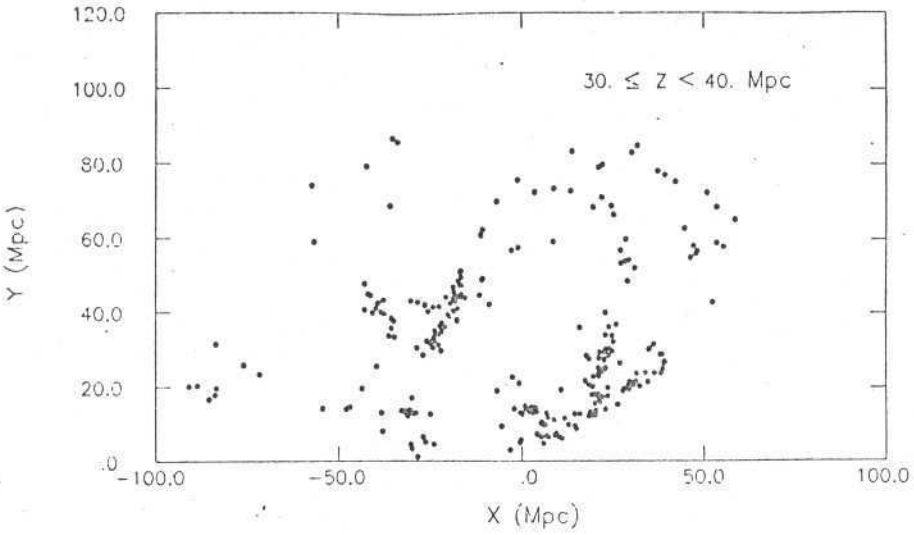
30. ≤ Z < 40. Mpc
120.0
100.0
80.0
60.0
40.0
20.0
0
Y (Mpc)
-100.0
-50.0
.0
50.0
100.0
X (Mpc)

FIG. 8*b*

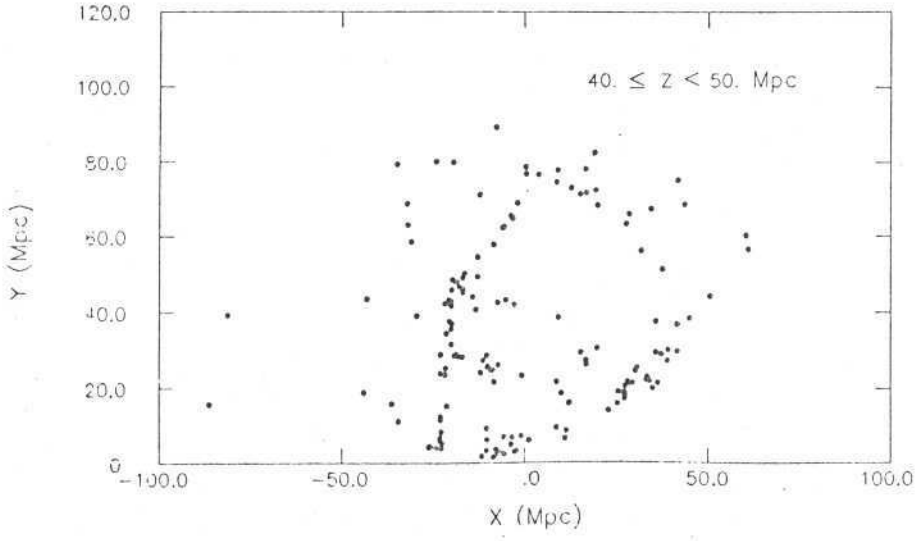
40. ≤ Z < 50. Mpc
120.0
100.0
80.0
60.0
40.0
20.0
0
Y (Mpc)
-100.0
-50.0
.0
50.0
100.0
X (Mpc)

Fig. 8*c*

Carvalho, M. Maia, C. Rite, D. Nascimento, B. Wyatt, G. Madjeski, and L. Feldman for their contribution in various stages of this project. We also acknowledge help from C. Steidel, C. Hassler, and V. Lindsay. W. L. W. Sargent and M. Davis received support from NSF under grants AST-8416704 and AST-8614552, respectively.

REFERENCES

da Costa, L. N., Pellegrini, P. S., Nunes, M. A., Willmer, C., and Latham, D. W. 1984, *A.J.*, 89, 1310.
Davis, M., and Geller, M. 1976, *Ap. J.*, 208, 13.
Davis, M., and Huchra, J. 1982, *Ap. J.*, 254, 437 (DH).
Davis, M., Huchra, J., Latham, D., and Tonry, J. 1982, *Ap. J.*, 253, 423.
de Lapparent, V., Geller, M., and Huchra, J. P. 1986, *Ap. J. (Letters)*, 302, L1.
de Vaucouleurs, G. 1975, in *Galaxies and the Universe*, ed. A. Sandage, M. Sandage, and J. Kristian (Chicago: University of Chicago Press), p. 557.
de Vaucouleurs, G., de Vaucouleurs, A., and Corwin, H. 1976, *Second Reference Catalog of Bright Galaxies* (Austin: University of Texas Press) (RC2).
Gott, J. R., Melott, A. L., and Dickinson, M. 1986, *Ap. J.*, 306, 341.
Haynes, M. P., and Giovanelli, R. 1986, *Ap. J. (Letters)*, 306, L55.
Huchra, J. P., and Geller, M. 1982, *Ap. J.*, 257, 423.
Huchra, J. P. and Geller, M. 1987, to appear in "The Proceedings of the 13th Texas Symposium on Relativistic Astrophysics", ed. M. Ulmer, (Singapore: World Scientific) p. 275.
Huchra, J. P., Davis, M., Latham, D., and Tonry, J. 1983, *Ap. J. Suppl.*, 52, 89.
Kaiser, N. 1987, *M.N.R.A.S.*, 227, 1.
Lauberts, A. 1982, *The ESO/Uppsala Survey of the ESO(B) Atlas* (Munchen: European Southern Observatory).
Menzies, J. W., Coulson, I. M., and Sargent, W. L. W. 1987, *A.J.*, in print.
Nilson, P. 1973, *Uppsala General Catalog of Galaxies* (*Uppsala Astr. Obs. Ann.* 6).
Ostriker, J. P., and Cowie, L. L. 1981, *Ap. J. (Letters)*, 243, L127.
Ostriker, J. P., Thompson, C., and Witten, E. 1986, *Phys. Letters B*, 180, 231.
Sandage, A. 1975, *Ap. J.*, 202, 563.
Sargent, W., Tonry, J., da Costa, L., Pellegrini, P. S., Davis, M., Meiksin, A., and Latham, D. 1987, in preparation.
White, S. D. M., Frenk, C. S., Davis, M., and Efstathiou, G. 1987, *Ap. J.*, 313, 505.

I. A. COULSON and J. W. MENZIES: South African Astrophysical Observatory, P.O. Box 9, Observatory 7935, South Africa

L. NICOLACI DA COSTA and P. S. PELLEGRINI: CNPq/Observatorio Nacional, Rua General Bruce 586, Sao Cristovao, 20921, Rio de Janeiro, Brasil

MARC DAVIS and AVERY MEIKSIN: Department of Astronomy, University of California at Berkeley, Berkeley, CA 94720

DAVID W. LATHAM: Center for Astrophysics, 60 Garden Street, Cambridge, MA 02138

W. L. W. SARGENT: Department of Astronomy 105-24, California Institute of Technology, Pasadena, CA 91125

JOHN L. TONRY: Department of Physics 37-521, Massachusetts Institute of Technology, Cambridge, MA 02139

IV. EXTENSÕES DO SSRS

IV.1 A CALOTA POLAR SUL

THE MCG REDSHIFT SURVEY

AND

THE SOUTHERN GALACTIC CAP

Paulo. S. Pellegrini and L. Nicolaci da Costa

Departamento de Astronomia, CNPq/Observatório Nacional

and

J. P. Huchra and D. W. Latham

Harvard-Smithsonian Center for Astrophysics

and

C. N. A. Willmer

Departamento de Astronomia, CNPq/Observatório Nacional

ABSTRACT

In this paper we discuss some results obtained with new radial velocity data obtained in the southern hemisphere in the declination range $-17.5^\circ \leq \delta \leq -2.5^\circ$, south of galactic latitude $b = -30^\circ$. These observations, when combined with those available from the southern section of the original CfA Redshift Survey and the Southern Sky Redshift Survey (SSRS) recently completed south of $\delta = -17.5^\circ$, allow us to investigate the spatial distribution of galaxies over a contiguous area of 3.13 steradians of the Southern Galactic Cap (SGC) to a magnitude limit of $m_{B(0)} = 14.5$. The large angular coverage of the sample makes it complementary to the deeper surveys being currently carried out in both hemispheres. In the SGC it is difficult to combine the three sets of survey data to create a homogeneous magnitude-limited sample, because of the lack of reliable photometric surveys of galaxies south of $\delta = -2.5^\circ$. Compared to the CfA Redshift Survey in the Northern Galactic Cap (NGC) and the SSRS, the SGC covers 1.7 times as much area of the sky, and it is not dominated by a large nearby concentration of galaxies such as the Virgo cluster in the NGC. The large-scale structure that we find in the SGC is similar to that seen in the NGC; bright galaxies are distributed on walls which intersect at sharp corners and nearly surround voids which are almost empty of galaxies. The largest voids seen in the SGC have dimensions up to $60h^{-1}$ Mpc ($H_0 = 100h$ km/s/Mpc) with the indication that some walls have an even larger extent. Some times voids are crossed by tenuous bridges of galaxies and some times the walls are

breached by large holes. In the SGC sample we cannot identify a void that is completely enclosed by walls, suggesting that voids may be interconnected in a sponge-like topology.

I. INTRODUCTION

Over the past few years major efforts have been undertaken to map out the three-dimensional distribution of galaxies in the southern hemisphere, with several groups involved in large redshift surveys. Some of the data are now becoming available, in particular, the results of the Southern Sky Redshift Survey (SSRS) of a diameter-limited sample have been recently reported by da Costa et al. (1988, hereafter paper I). This survey covers an area of 1.75 steradians of the Southern Galactic Cap (SGC) south of $\delta = -17.5°$ and below galactic latitude -30°. Together with the southern portion of the CfA Redshift Survey (CfA1, Huchra et al. 1983) it leaves an uncovered strip of 0.55 steradians in the declination range $-17.5° \leq \delta \leq -2.5°$ for which no systematic observations had been made until recently. To fill this gap we undertook redshift observations of galaxies in this strip. The goal of this paper is to combine these new data with the results of the CfA1 and SSRS to create a homogeneous magnitude-limited sample in order to provide a global view of the entire SGC over an area of 3.13 steradians, 1.7 times as much area as it is covered either in the NGC by the CfA1 Survey or in the SGC by the SSRS. The large angular coverage of such a sample is complementary to deep strip surveys now underway in both hemispheres. The deep surveys can probe more efficiently for the existence of large structures, but can see only a limited cross-section of such structures. Our shallower but much wider-angle sample can be used to investigate the full three-dimensional structure of nearby features.

In this paper we present some results derived with the new data obtained in the strip described above. In section II, we describe the sample of galaxies used in the strip, the observations, and the main features of the galaxy distribution in this region of the sky. In section III, we discuss how we construct an approximately homogeneous magnitude-limited sample of galaxies in the SGC from different catalogs and discuss the properties of the galaxy distribution in the full 3.13 steradian sample based on different projections of redshift maps. Finally, in section IV we give a brief summary of our main results.

II. THE MCG SURVEY

Galaxies in the previously uncovered region, in the declination interval $-17.5° \leq \delta \leq -2.5°$ and below galactic latitude $b = -30°$, were selected from the Morphological Catalog of Galaxies (MCG, Vorontsov-Velyaminov and Arhipova 1963-1968), even though there are several problems with this catalog, namely: non uniformity, innacurate coordinates, magnitudes estimated visually to only the nearest 0.5 mag, and a morphological classification very difficult to relate to the systems usually adopted by western authors. However, it is the only available catalog, covering the strip of interest, that extends down to a magnitude limit comparable to that adopted for the CfA1. According to Huchra (1985) the MCG magnitudes are approximately 0.5 mag brighter than their values in the B(0) system, which is equivalent to the magnitude system used to define the CfA1 sample. In order to maintain some degree of uniformity with the northern data and to guarantee that our sample includes galaxies down to $m_{B(0)} = 14.5$ magnitude limit adopted for the CfA1, we have selected from the MCG catalog galaxies down to and including MCG magnitude bin 14.5. The sample consists of 765 galaxies, of which 441 are brighter than MCG magnitude bin 14.0.

The observations were carried out with identical photon-counting Reticon detectors and similar spectrographs mounted at the Cassegrain foci of the 1.5-m telescopes of the Fred L. Whipple Observatory and the Observatório Nacional (ON). A detailed description of the observation and reduction procedures can be found in Tonry and Davis (1979) and da

Costa et al. (1984); typical errors in the velocity determinations are less than 40 km/s. The sample is 86% complete down to MCG magnitude bin 14.0 while 77% to 14.5.

In figure 1 we show plots of the observed velocity versus right ascension for all MCG galaxies down to bin 14.5 with available redshifts in the strip. A total of 574 galaxies are shown in two wedges of 7.5° in declination and out to 12000 km/s. From a comparison of these wedge diagrams with those presented for the SSRS (paper I) we find that the overall pattern of the galaxy distribution is very similar to that observed southwards. In fact, most of the structures observed in the MCG strip correlate well with the structures observed in adjacent wedges to the south, indicating that some of the most prominent features observed in the SSRS extend into the new region covered by the MCG survey. In particular the nearby void at (1^h, 3000 km/s) and the concentration of galaxies in an eloganted structure cutting the volume from about (4^h, 4000 km/s) to (0^h, 7000 km/s) appear to be extensions of features previously observed further to the south. A more detailed discussion is presented below.

III. THE SOUTHERN GALACTIC CAP (SGC)

a) A magnitude-limited sample for the SGC

As mentioned in section I the main motivation of the MCG survey was to fill the gap in the angular coverage of the existing southern surveys, allowing us to examine the distribution of galaxies in the SGC as a whole. This provides coverage of a contiguous area of 3.13 steradians, and enables the investigation of continuous structures with dimensions of more than $100h^{-1}$ Mpc even for a shallow survey limited to $m_{B(0)} = 14.5$, which has an effective depth of about $60h^{-1}$ Mpc. However, towards this end it is necessary to generate, from the different catalogs covering the southern hemisphere, a homogeneous sample of galaxies with a uniform magnitude limit. Attempts to combine data from different catalogs have also been made by Sharp (1986) and Lahav (1987), who discuss procedures for combining the available catalogs based on diameters. Here we take an alternative approach and try to combine the catalogs to define a magnitude-limited sample.

For galaxies north of -2.5° we have taken the data directly from the southern portion of the CfA1 sample. In the strip covered by the MCG we have followed a suggestion of Huchra (1985) and have added 0.5 to the magnitudes listed in the MCG catalog, to transform them to a system compatible to that utilized in the CfA1. Finally, south of -17.5° we have drawn galaxies from the ESO/Uppsala catalog (Lauberts 1982), estimating magnitudes from linear least-square fits of the relation

between diameters and magnitudes for those galaxies with magnitudes listed in the ESO/Uppsala catalog. The diameters were converted to face-on using the prescription of Fouque and Paturel (1985), and the magnitudes were converted from the B_T to the B(0) system by adding 0.4 mag (Huchra 1985). These relations were obtained for different morphological type groups, in an attempt to minimize the scatter. Nevertheless, the errors are still large with a rms dispersion of about 0.6 mag. A more detailed discussion of these magnitude versus diameter relations is given by Pellegrini (1988).

Despite the large uncertainties associated with the individual magnitudes, the sample assembled this way appears to be homogeneous and consistent with a magnitude limit of $m_{B(0)} = 14.5$. For example, angular covariance functions were calculated for the galaxies in this sample south of -17.5°, both for all morphological groups combined and also for the various individual morphological groups used to derive the mean diameter-magnitude relations. Utilizing the scaling properties of the covariance function, we can relate the amplitudes and the limiting apparent magnitude of different samples (e.g. Fall 1979, Sadler and Sharp 1984). Comparing the results with those determined by Davis and Geller (1976) and Giovanelli et al. (1986) for samples with a limiting magnitude of $m_{B(0)} = 14.5$, we find that the limiting magnitude of our sample drawn from the ESO/Uppsala catalog is within 0.1 mag of the $m_{B(0)} = 14.5$ cutoff adopted for the CfA1. When the sample is divided into early-type galaxies and spirals the limiting magnitudes are within 0.3 mag of $m_{B(0)} = 14.5$. In this context it is interesting to note that even for the

ellipticals, which as pointed out by Sadler (1984) become progressively incomplete in the ESO/Uppsala catalog at $B_T = 14.0$ ($B(0) \approx 14.4$), comparison of the covariance functions indicates that our limit corresponds to $m_{B(0)} = 14.3$.

We conclude that despite the large errors in the estimation of the magnitudes of individual galaxies, the combined catalog is, nevertheless, reasonably homogeneous with a magnitude limit near $m_{B(0)} = 14.5$. Further support for this conclusion comes from the comparison of the surface number density of galaxies as a function of magnitude for the various samples used in the generation of the final SGC catalog, shown in figure 2. We also plot the data from the CfA1 northern sample and the law $N(m) \propto 10^{0.6m}$, eye-fitted to the southern samples. As can be seen, the three components of the SGC sample agree fairly well over the entire apparent magnitude range, while the differences with the northern sample are primarily due to the contribution of the Virgo cluster, which has an influence down to apparent magnitude 13.5 or so. The final SGC sample consists of 2372 galaxies; we emphasize that although it may be adequate for a qualitative description of the galaxy distribution, it should be used with caution for quantitative analyses.

b) Galaxy Distribution

In figure 3 we present a plot of all galaxies brighter than $m_{B(0)} = 14.5$ in the SGC projected onto galactic coordinates, followed by a sequence of redshift windows showing the distribution of galaxies in

different velocity intervals. In these plots we include velocity data from the CfA1, the present survey and the SSRS; redshifts are available for 92% of the galaxies in our SGC sample. We note that, south of δ =-17.5°, these plots are not significantly different from those presented by da Costa et al. (1988) for a diameter-limited sample. With these plots it is possible for the first time to have a global view of the spatial galaxy distribution in the SGC, without serious problems due to incomplete sky coverage or inhomogeneous sampling.

In figure 3a, there are some indications for patches of obscuration, especially in the region west of 22^h and north of -20°, and the region east of 3^h and north of 0°. In figure 3b, the connected linear structure running from Dorado (5^h, -60°) through Fornax (3.5^h, -35°) to Eridanus (3.5^h, -20°) was already apparent in the SSRS. In our extended SGC sample, it can now be seen that this feature extends as a somewhat diffuse structure to the northwest. We also call attention to a very long filament that stretches more than 100° across the sky, starting from the near side of the Pavo-Indus complex (22^h, -50°) and running to at least (1.5^h, +10°) where it joins the Dorado-Fornax-Eridanus structure in a low-density and amorphous connection near (0^h, 0°). Almost the entire upper left section of figure 3c, covering an area of roughly 60° x 60° on the sky, is a region more heavily populated by galaxies. The lower right (or southwest) corner of this region of enhanced galaxy number density was already noted to be a very large flat structure in the SSRS, and was named the "wall". As is described below, the SGC sample allow us to see that the wall extends to the northwest where it meets another feature

composed of galaxies from the top left of figure 3c. Finally, in figure 3d we show the more distant redshift window, where there are hints of the presence of large underdense regions and of several elongated linear structures, with dimensions over $50h^{-1}$ Mpc.

To give a better idea of the three-dimensional distribution of galaxies in the south we present in figure 4 a set of wedge diagrams, where we plot the observed redshift versus right ascension for our magnitude-limited SGC sample. We show declination slices 10° thick in the range $-70° \leq \delta \leq +20°$. Examination of these diagrams shows that the overall pattern of the galaxy distribution has the same general nature in all the declination slices. Many of the galaxies fall in elongated, often thin, structures that intersect at sharp corners and mark the boundaries of regions which are nearly empty of galaxies.

The wider angular coverage of the wedges in declination allows us to explore further the main structures identified in the SSRS, to see how far they extend to the north. One striking feature identified in the SSRS (paper I) was the wall, which can be seen, for instance, in our $-30° < \delta < -20°$ wedge as a concentration of galaxies running from (4^h, 4000 km/s) to about (0^h, 9000 km/s). This same feature can be identified in all the wedges southward to -70° and northward to about -10°. Further to the north the wall becomes less coherent, but the central part can still be seen prominently as a concentration centered near (1 to 2^h, 5000 km/s) that extends all the way to at least +10°. The central spine of the wall makes a continuous structure that runs north and south nearly

perpendicular to the line of sight for more than $70h^{-1}$ Mpc. There are no obvious virial fingers in this wall that can be identified with clusters residing on the wall.

Four voids were specifically pointed out in the SSRS (paper I). The structure of void 2, located at the western edge of the SSRS, is not clarified particularly by our larger SGC sample. On the other hand, some interesting topology is revealed as voids 1, 3 and 4 are followed to the north, out os the SSRS and into the MCG and CfA1 regions. These two voids are well outlined in the $-40° < \delta < -30°$ wedge, with void 1 being closer at about (1.5^h, 3000 km/s) and void 3 being larger at about (23.5^h, 6000 km/s). As was noted in paper I, both voids can be seen in the successive wedges to the south, down to -70° at least. North of about -30°, void 1 is split by a bridge that runs in the direction of 2.5^h, and north of about -10° the eastern half of void 1 has been closed over. At about the same declination, the more distant half of void 3 is also closed over and the two remaining adjacent open halves of voids 1 and 3 merge into a single void that worms its way up to +30 in a sort of chimney. This example suggests to us that the idea of a bubble-like topology in which galaxies lie on thin surfaces which completely enclose voids is not entirely adequate. Here we see an example of a topology that is more sponge-like, in which there are breaches in the walls between voids and there is a connectivity between neighbooring voids. Indeed, in all the redshift maps that we have inspected, we can find no example of a void where it is unambiguous that the surrounding walls are not breached.

To present a different view of the large walls andd voids in the SGC, we plot our sample using the same cartesian coordinates defined in paper I. In figure 5 we show projections onto the (x,y) plane for slabs that are $10h^{-1}$ Mpc thick. The main wall and its central spine can be seen rather clearly in these plots because they are aligned nearly perpendicular to the (x,y) plane, with the wall extending between about (-40, 10) and (10, 80). Voids 1 and 3 also run nearly perpendicular to the (x,y) plane, and their progress can be traced from the $40 < z < 50h^{-1}$ Mpc slab northward until they merge into a single smaller void in the $0 < z < 10h^{-1}$ Mpc slab. In these plots we again see that the walls of the voids intersect at sharp corners and that there are breaches in the walls between neighbooring voids. It remains to be seen whether these breaches will be closed by deeper surveys.

IV. SUMMARY

In this paper we have presented the results of a redshift survey which fills the gap in the SGC between the original CfA1 which ended at $\delta = -2.5°$ and the recently completed SSRS, which gives wide-angle coverage south of $\delta = -17.5°$. We have also made a preliminary attempt to construct from the available catalogs a reasonably homogeneous magnitude-limited sample down to $m_{B(0)} = 14.5$, enabling us: a) to investigate the properties of the spatial distribution of galaxies in a region of the sky which is not dominated by a large nearby concentration of galaxies as is the case with the Virgo cluster in the NGC; b) to examine the nature of this distribution over a contiguous area of the sky, covering roughly 25% of the celestial sphere. This area is about the maximum one can expect to cover in the south using data from optical surveys, without encountering problems of severe obscuration.

Three of the major features noted in paper I, namely the main wall and voids 1 and 3, are seen to extend to the north, gradually evolving their forms as they go. They form connected structures which stretch across the line of sight for distances as large as $70h^{-1}$ Mpc and suggest a sponge-like topology.

The general pattern of the large-scale structure is similar to that seen in the NGC. Bright galaxies are distributed on walls which intersect at sharp corners and nearly surround voids which are almost empty of galaxies.

We emphasize the pressing need for a complete photometric survey of the southern sky in order to create a well-defined, homogeneous magnitude-limited sample appropriate for statistical analyses. In contrast to the past, a wealth of radial velocity information is now becoming available in the south from various large redshift surveys. However, the lack of photometric data precludes a more quantitative analysis of the properties of the galaxy distribution, essential for a direct comparison with the results of numerical simulations of the most popular scenarios for the origin and evolution of large-scale structures in the Universe.

ACKNOWLEDGMENTS

We would like to thank all the people involved in the redshift effort. From the CfA we would like to thank Ed Horine and Jim Peters for making most of the observations at the Whipple Observatory and Susan Tokars for handling the data reductions. From the ON we would like to thank R. de Carvalho and M. Maia for their help in the observations, and M. Nunes, D. Nascimento and C. Rite for their technical support.

REFERENCES

da Costa, L. N., Pellegrini, P. S., Nunes, M. A., Willmer, C. and Latham, D. W. 1984, A. J., **89**, 1310.

da Costa, L. N., Pellegrini, P. S., Sargent, W. L. W., Tonry, J., Davis, M., Meiksin, A. and Latham, D. 1988, Ap. J. **327**, 544.

Davis, M. and Geller, M. J. 1976, Ap. J., **208**, 13.

Davis, M., Huchra, J., Latham, D. and Tonry, J. 1982, Ap. J., **253**, 423.

Fall, S. M. 1979, Rev. Mod. Phys, **51**, 21.

Fouque, P. and Paturel, G. 1985, Astron. Astrophys., **150**, 192

Geller, M. J., Huchra, J. P. and de Lapparent, V. 1987, IAU Symp. 124, Observational Cosmology, ed. A. Hewitt, G. Burbidge and L. Z. Fang (Dordrecht: Reidel) p. 301.

Geller, M. J. 1987, 17th Advanced Course in Astrophysics

Giovanelli, R., Haynes, M. and Chincarini, G. L. 1986, Ap. J., **300**, 77.

Huchra, J. 1985, private communication.

Huchra, J., Davis, M., Latham, D. and Tonry, J. 1983, Ap. J. Suppl., **52**,89.

Lahav, O. 1987, M.N.R.A.S., **225**, 213.

de Lapparent, V., Geller, M. and Huchra, J. P. 1986, Ap. J. (Letters), **302**, L1.

Lauberts, A. 1982, The ESO/Uppsala Survey of the ESO(B) Atlas (Munchen: European Southern Observatory).

Pellegrini. P. S. 1988, Ph. D. thesis, Observatório Nacional.

Sadler, E. M. 1984, A. J., **89**, 34.

Sadler, E. M. and Sharp, N. A. 1984, Ap. J., **287**, 80.

Sharp, N. A. 1986, Pub. A. S. P., **98**, 740.

Tonry, J. and Davis, M. 1979, A. J., **84**, 1511.

Vorontsov-Velyamnov, B. A. and Arhipova, V. P. 1963-68, Morphological Catalogue of Galaxies (Moscow) Parts 2 to 4.

FIGURE CAPTIONS

Figure 1- Plots of the observed velocity versus right ascension showing galaxies in the MCG survey with $v < 12000$ km/s. The range in declination of each wedge is indicated in the figures.

Figure 2- Galaxy counts per steradian for the following samples: CfA sample in the northern galactic cap (open triangles); CfA sample in the southern galactic cap (solid triangles); MCG strip (open squares); SSRS magnitude-limited sample below $\delta = -17.5°$ (solid squares). The line is an eye-fit of a homogeneous distribution to the SGC samples.

Figure 3- Projected distribution of galaxies in the SGC sample onto equal area galactic coordinates. The south galactic pole is at the center and the circles denote galactic latitudes -70°, -50° and -30°. Panel (a) shows the whole sample, while panels (b) to (d) show different redshift windows.

Figure 4- Plots of observed velocity versus right ascension of galaxies in the SGC sample with $v < 12000$ km/s, for 10° declination wedges in the range $-70° < \delta < 20°$. The limits of each wedge are indicated in the figures.

Figure 5- Distribution of galaxies plotted in a Cartesian coordinate system with the x and y axes lying in the equatorial plane and

pointing to $\alpha = 18^h$ and 0^h, respectively; the z axis points to south celestial pole. We show galaxies with $v < 10000$ km/s projected onto the x-y plane in consecutive slices of $10h^{-1}$ Mpc from $z = -10$ to $z = 50h^{-1}$ Mpc.

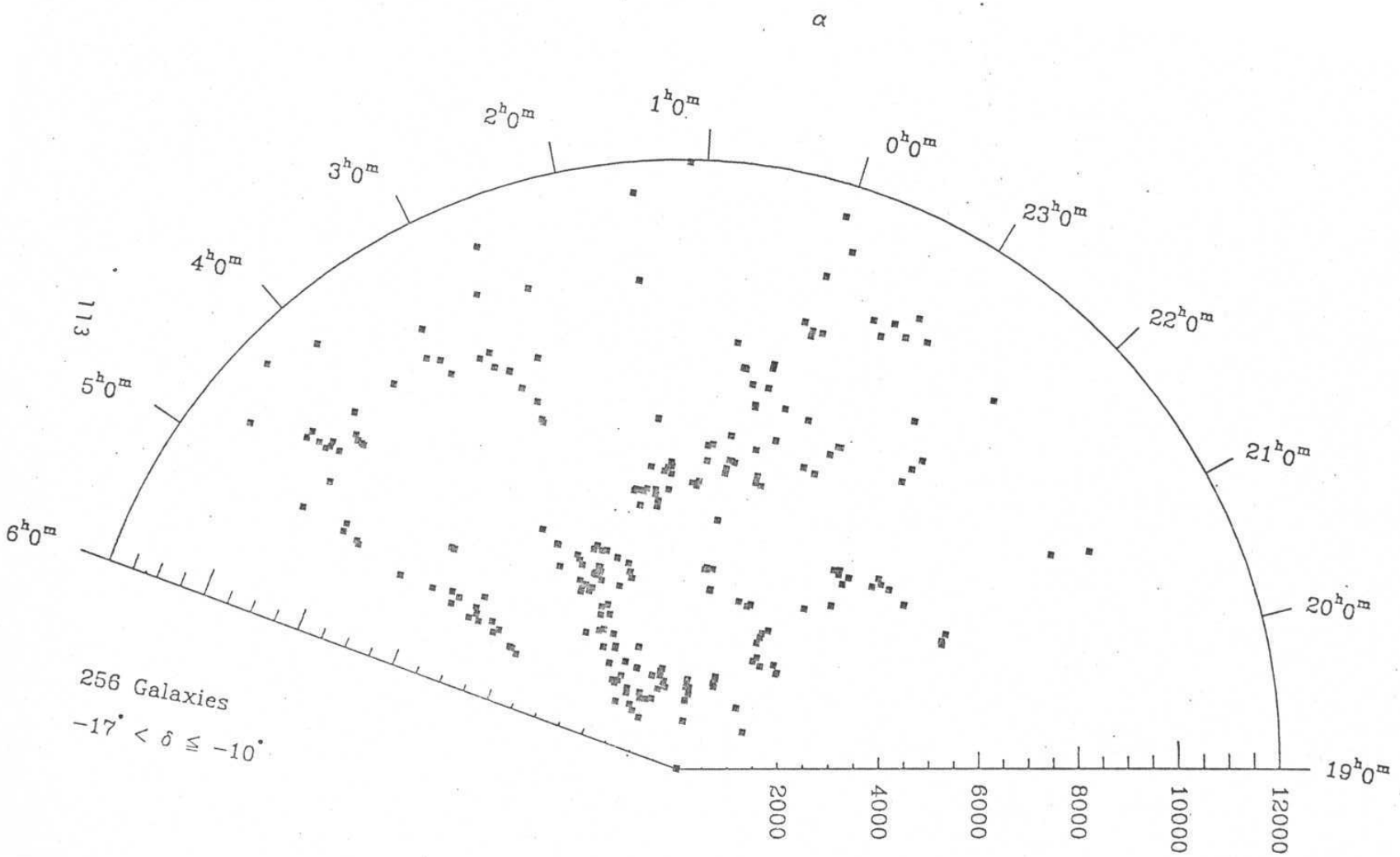
α
1^h0^m
2^h0^m
3^h0^m
4^h0^m
5^h0^m
6^h0^m
0^h0^m
23^h0^m
22^h0^m
21^h0^m
20^h0^m
19^h0^m
113
256 Galaxies
−17° < δ ≤ −10°
2000
4000
6000
8000
10000
12000
V (km/s)

Figure 1a

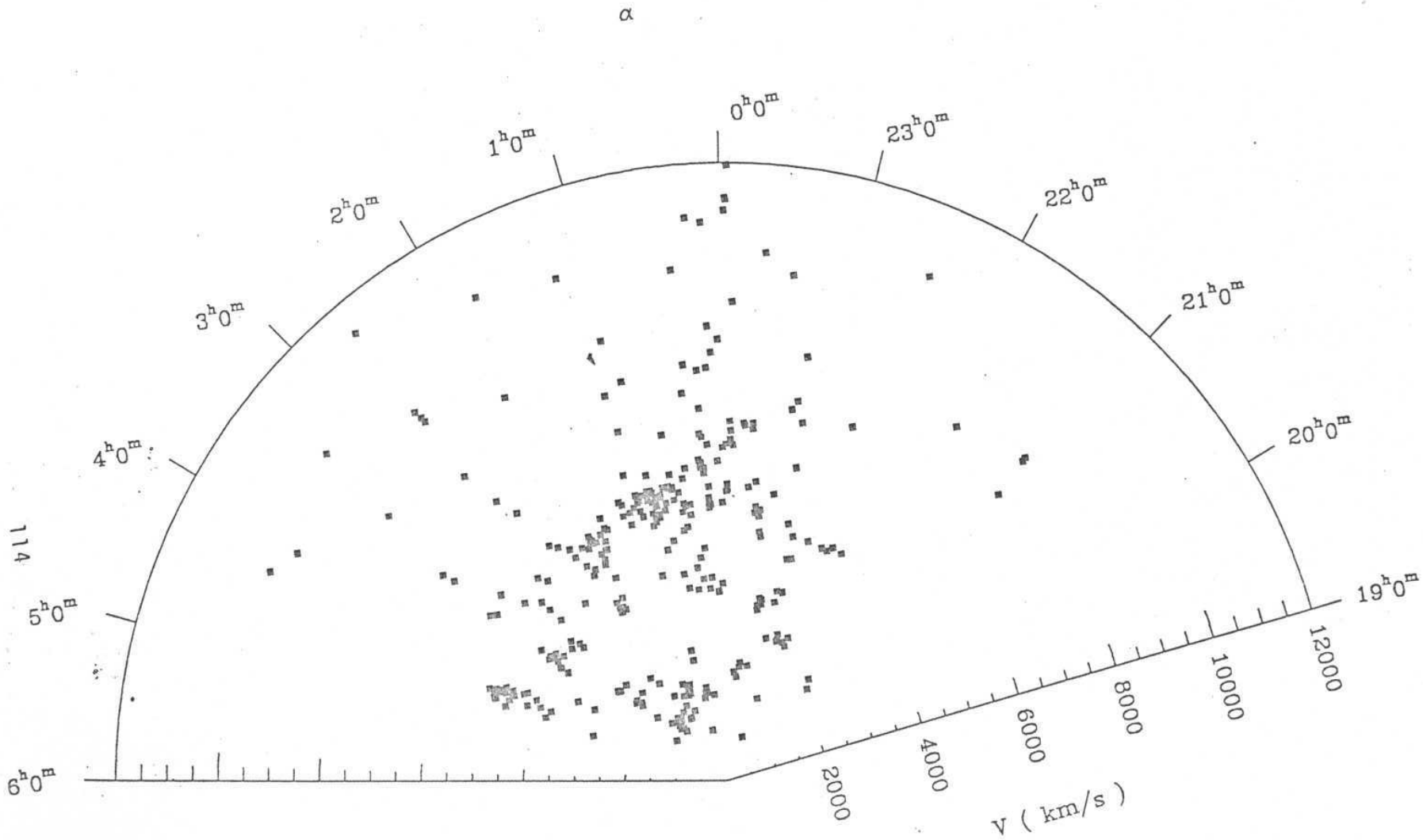

319 Galaxies

$-10^{\circ} < \delta \leq -2^{\circ}$

Figure 1b

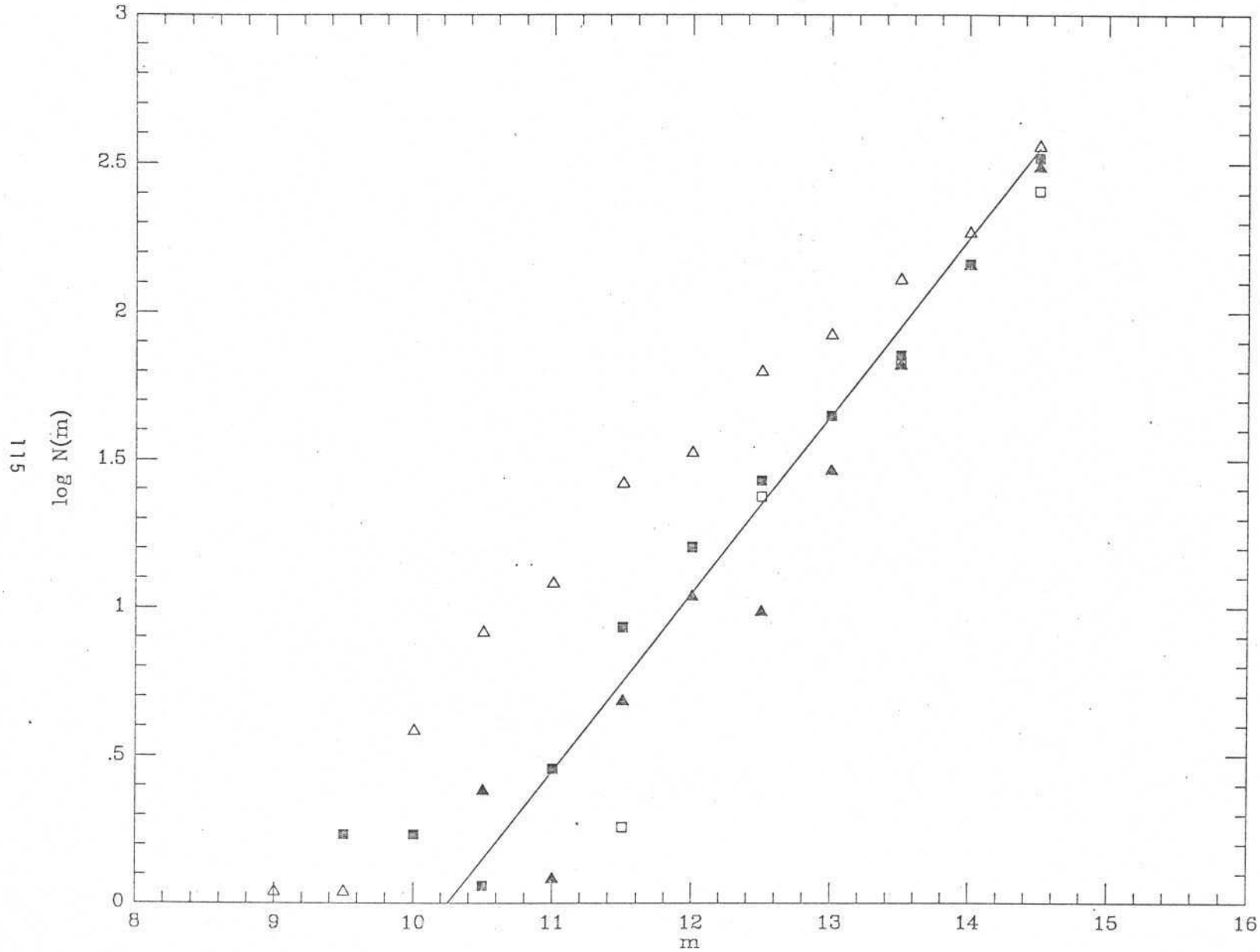

Figure 2

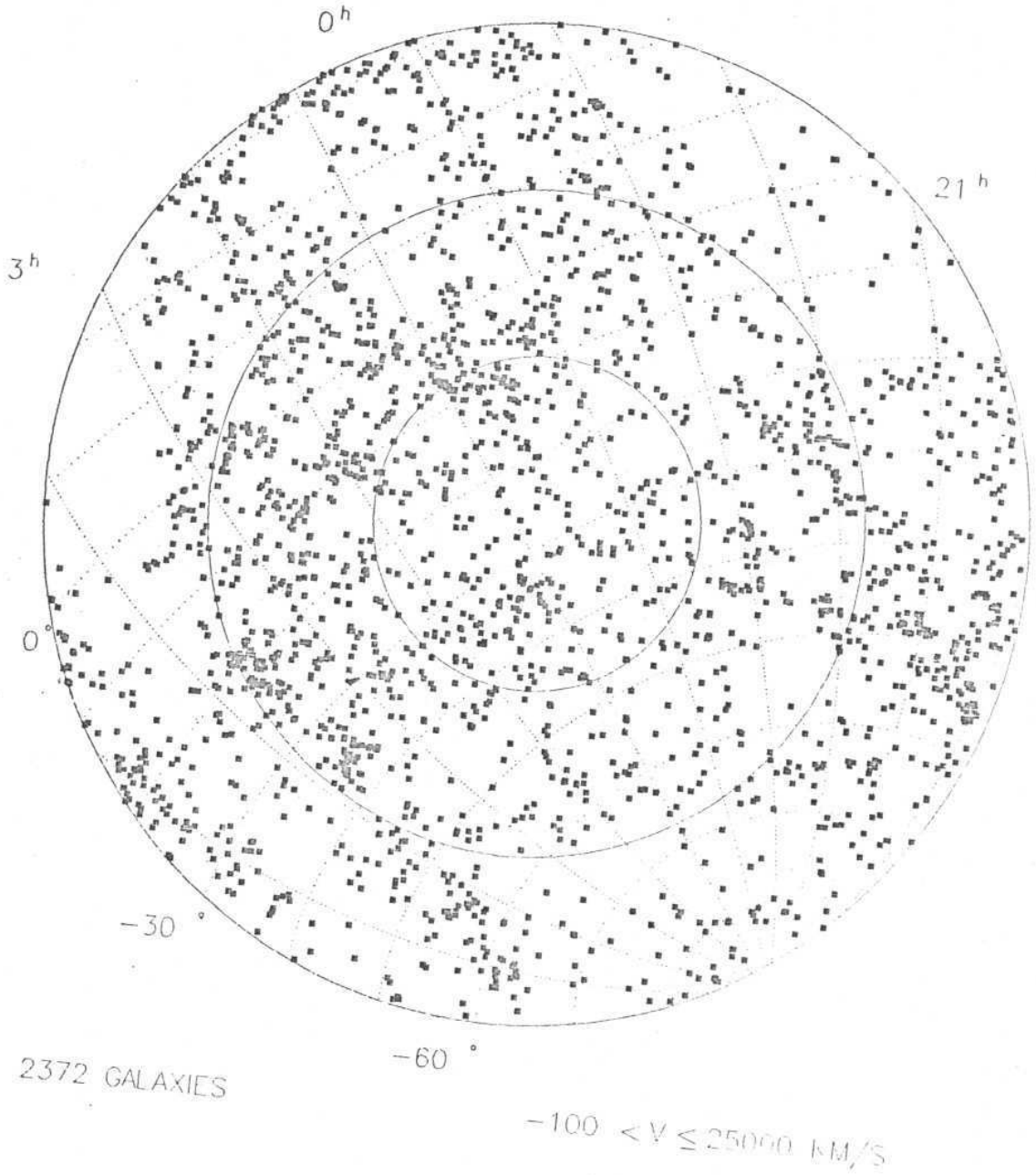

Figure 3a

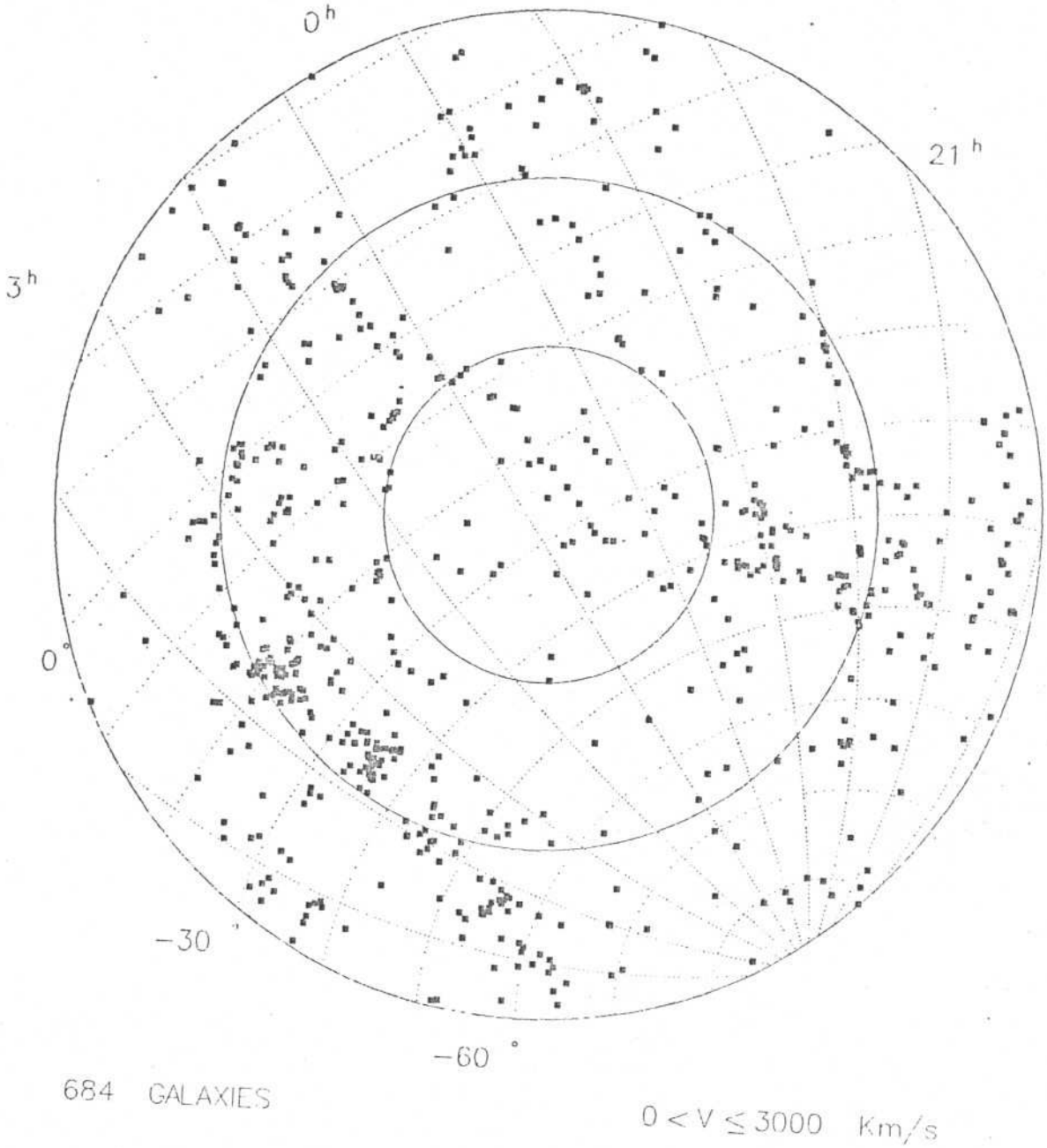

Figure 3b

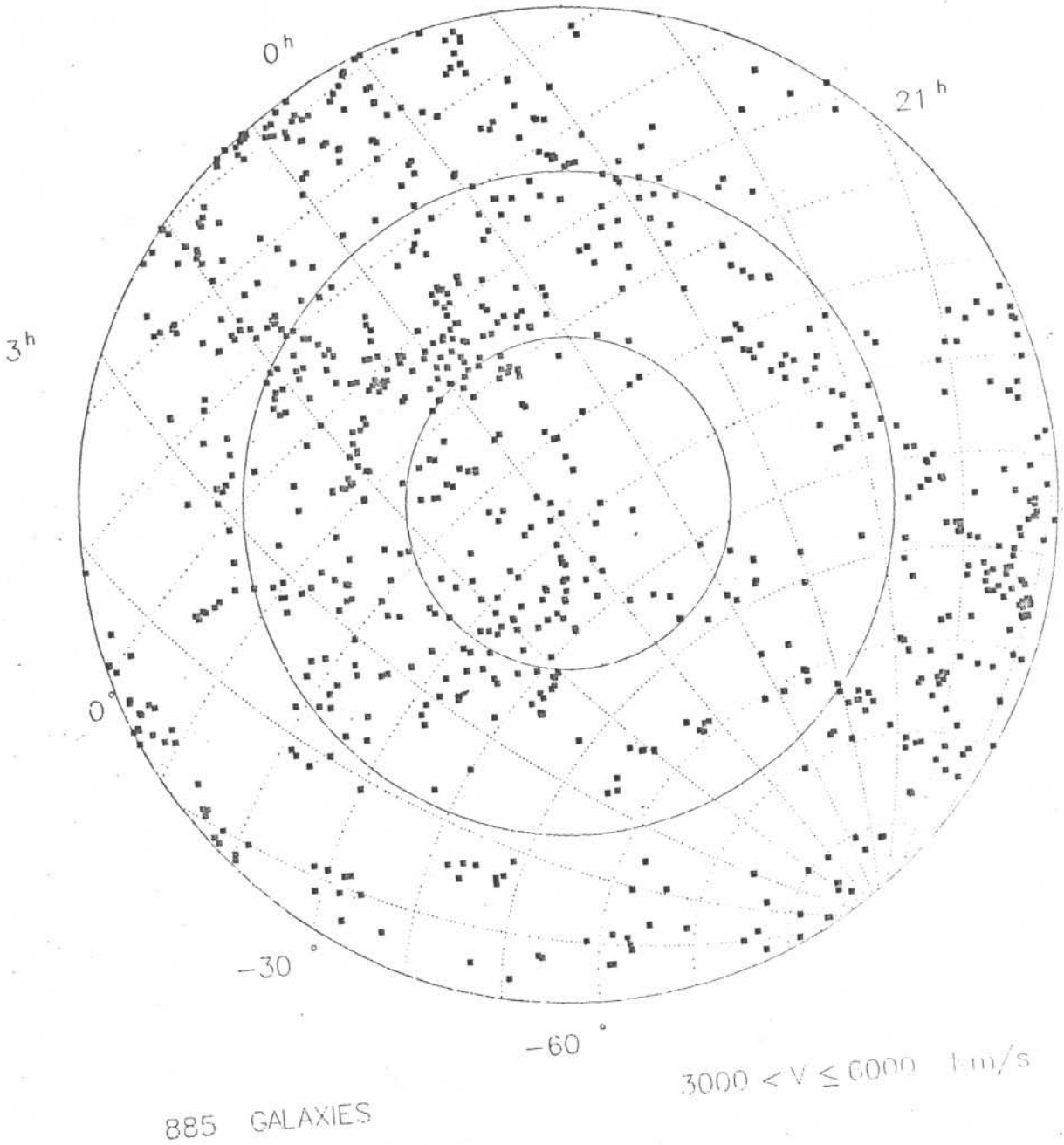

Figure 3c

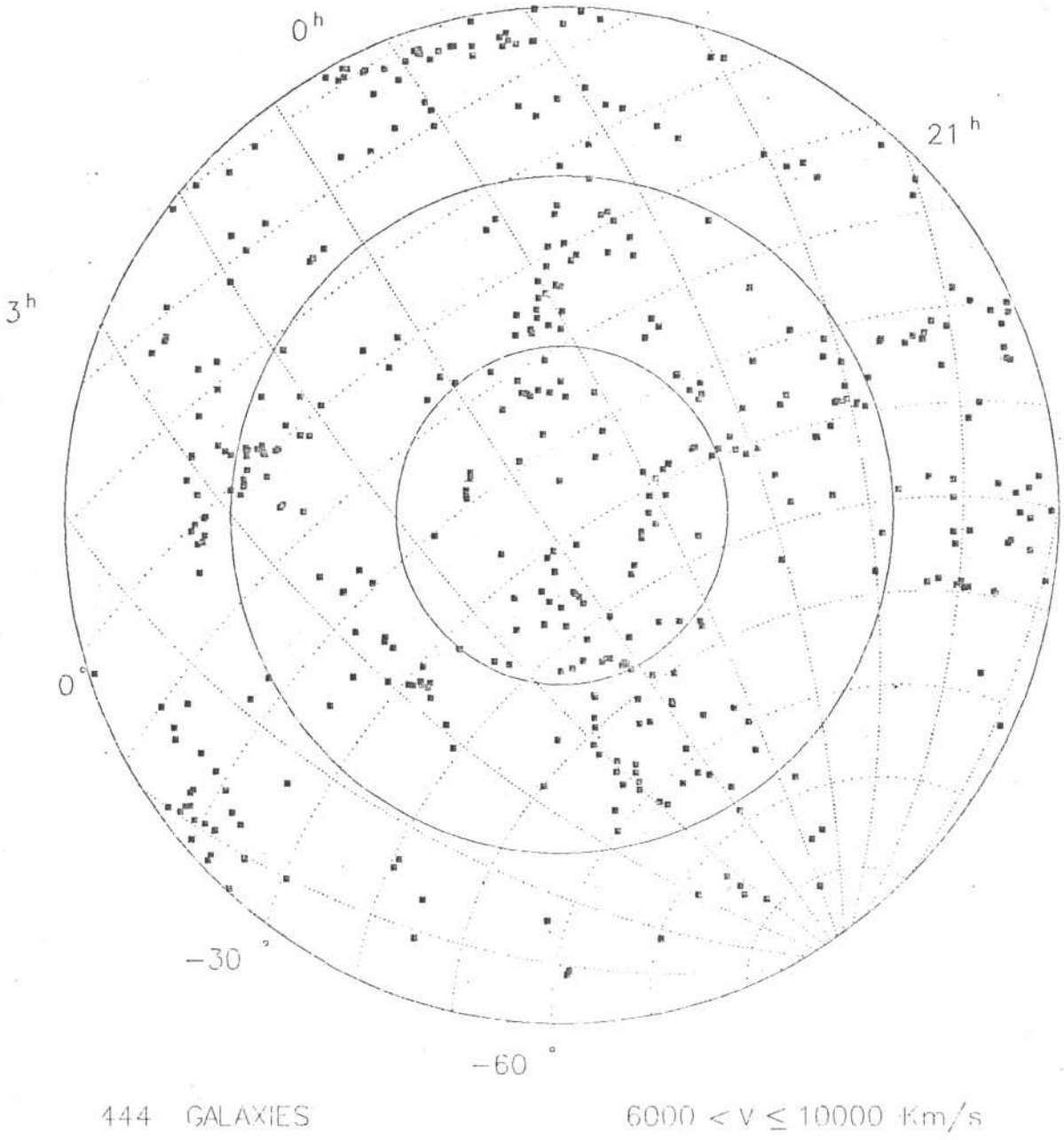

Figure 3d

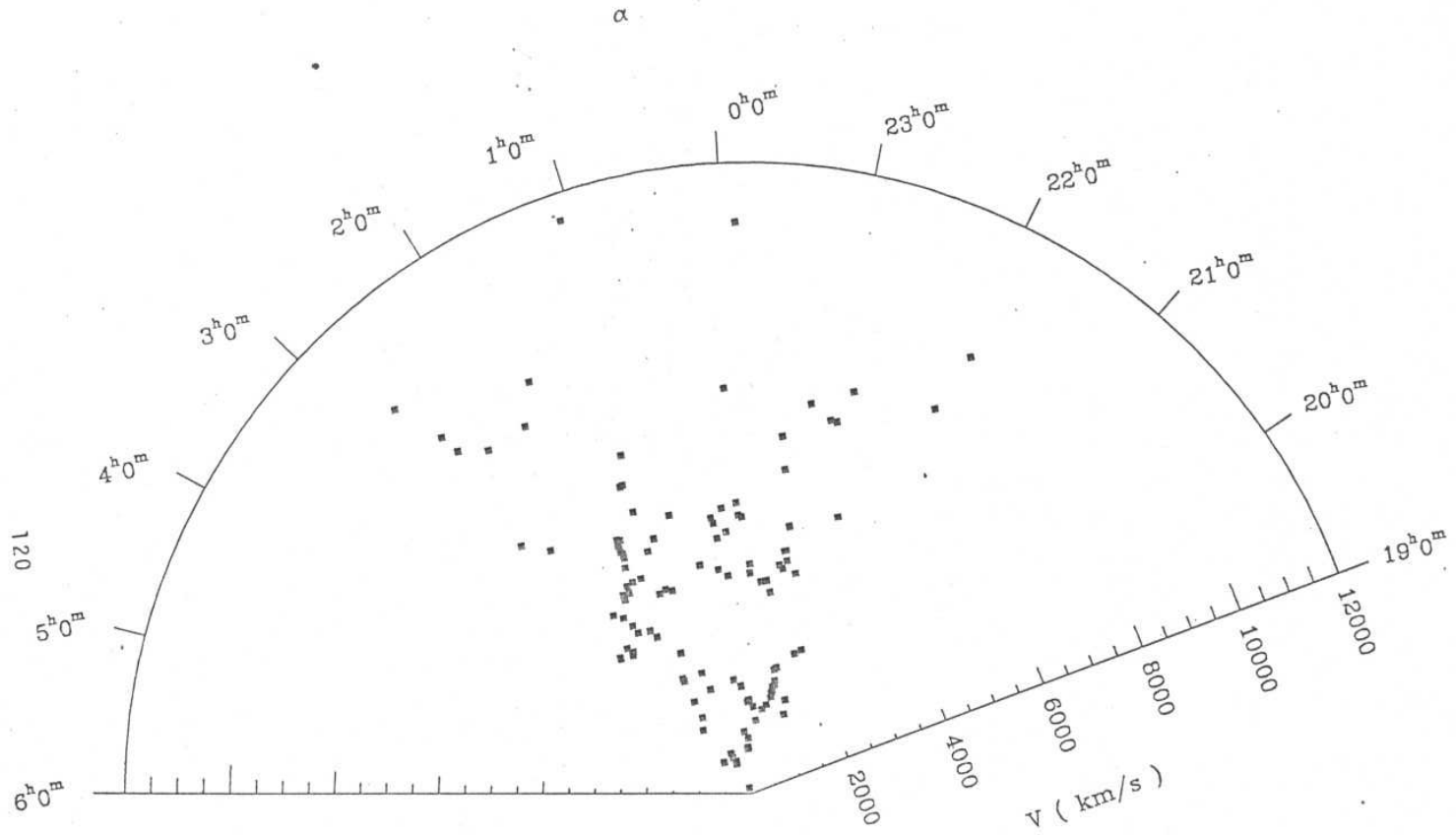

122 Galaxies

$10^{\circ} < \delta \leqq 20^{\circ}$

Figure 4a

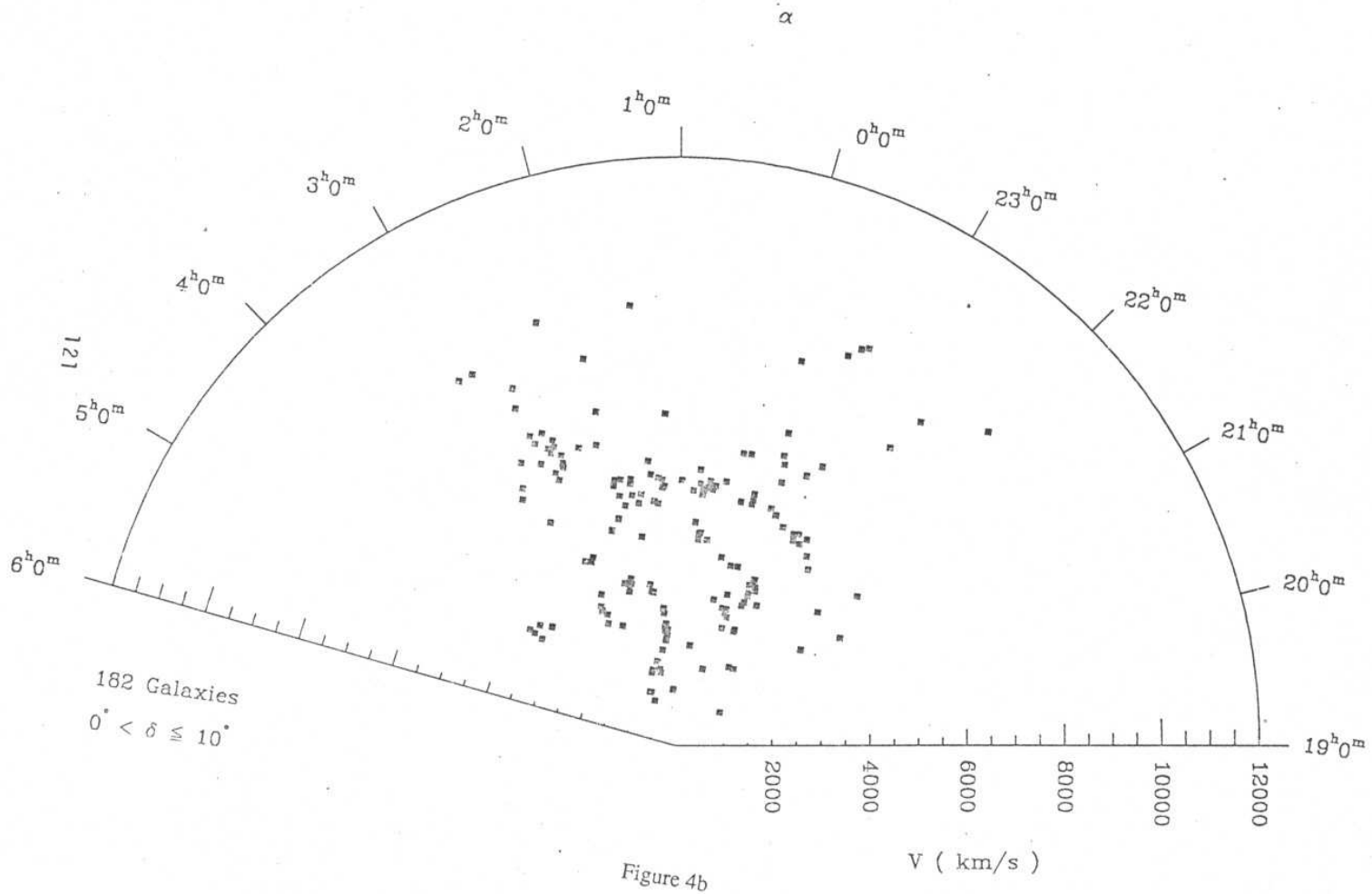
α
1h0m
2h0m
3h0m
4h0m
5h0m
6h0m
0h0m
23h0m
22h0m
21h0m
20h0m
19h0m
121
182 Galaxies
0° < δ ≤ 10°
2000
4000
6000
8000
10000
12000
V (km/s)

Figure 4b

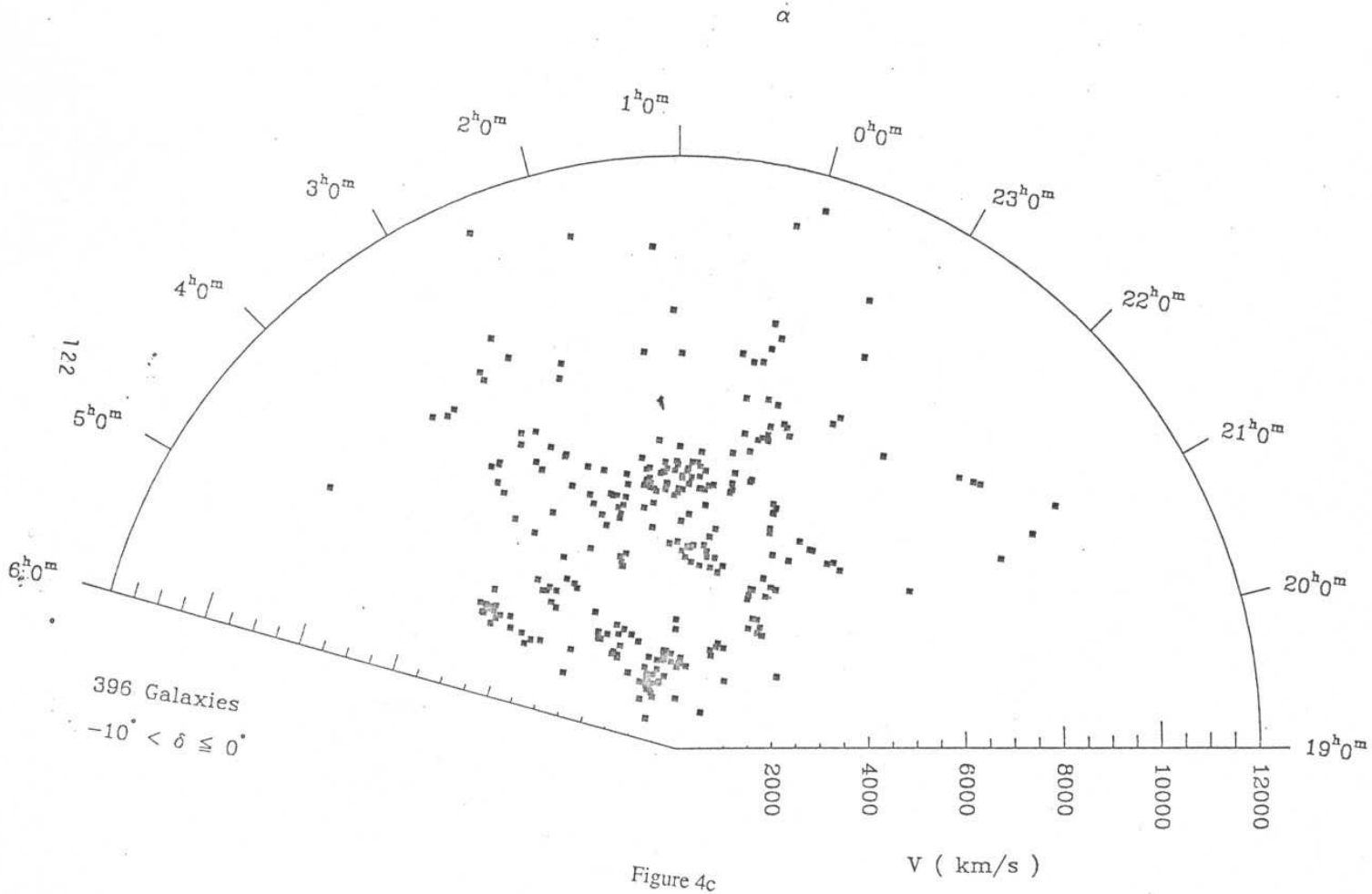
α
1h0m
2h0m
0h0m
3h0m
23h0m
4h0m
22h0m
5h0m
21h0m
6h0m
20h0m
19h0m
396 Galaxies
−10° < δ ≤ 0°
2000
4000
6000
8000
10000
12000
V (km/s)

Figure 4c

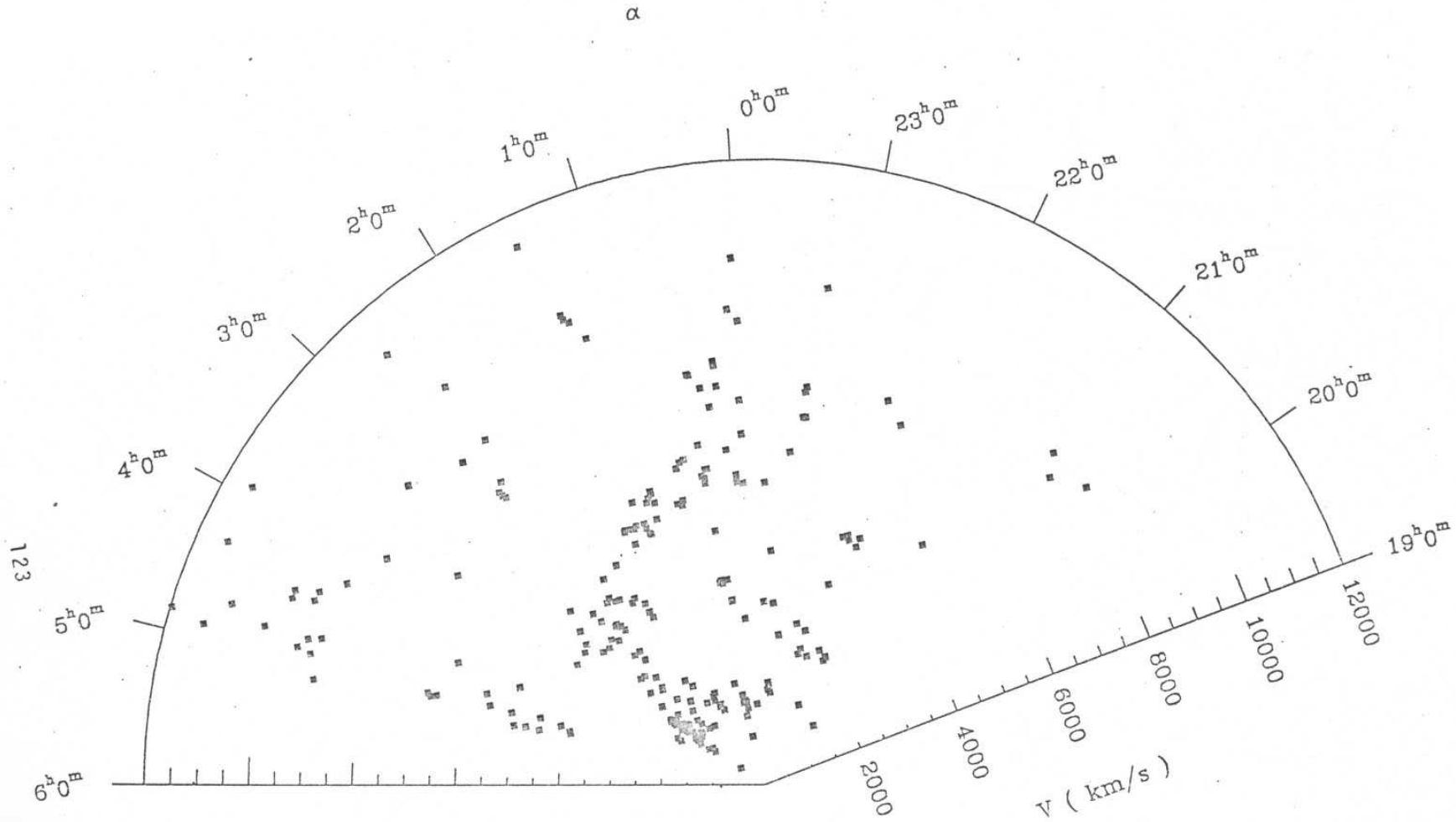

249 Galaxies

$-20^{\circ} < \delta \leq -10^{\circ}$

Figure 4d

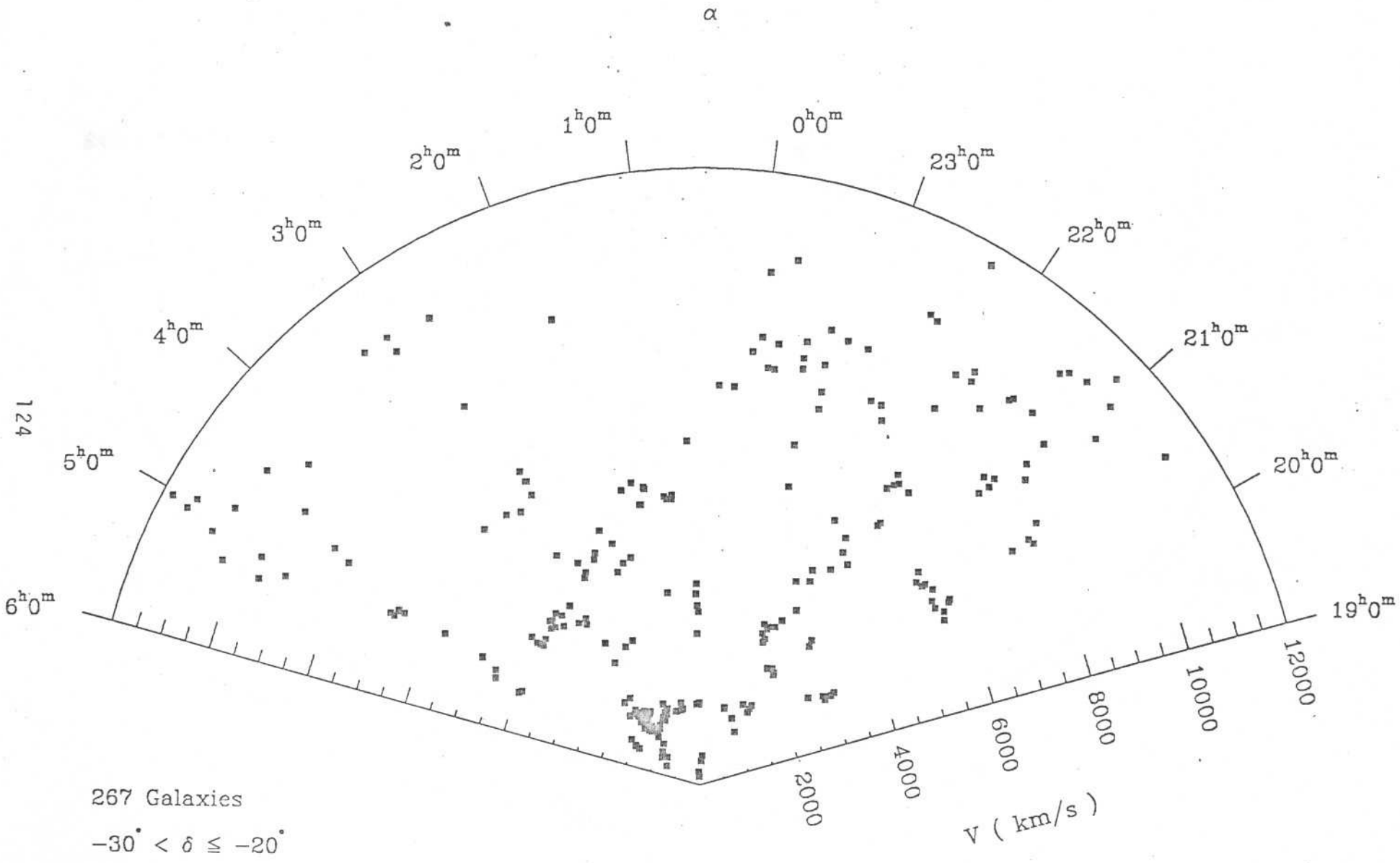
α
1h0m
0h0m
2h0m
23h0m
3h0m
22h0m
4h0m
21h0m
5h0m
20h0m
6h0m
19h0m
124
2000
4000
6000
8000
10000
12000
V (km/s)
267 Galaxies
−30° < δ ≦ −20°

Figure 4e

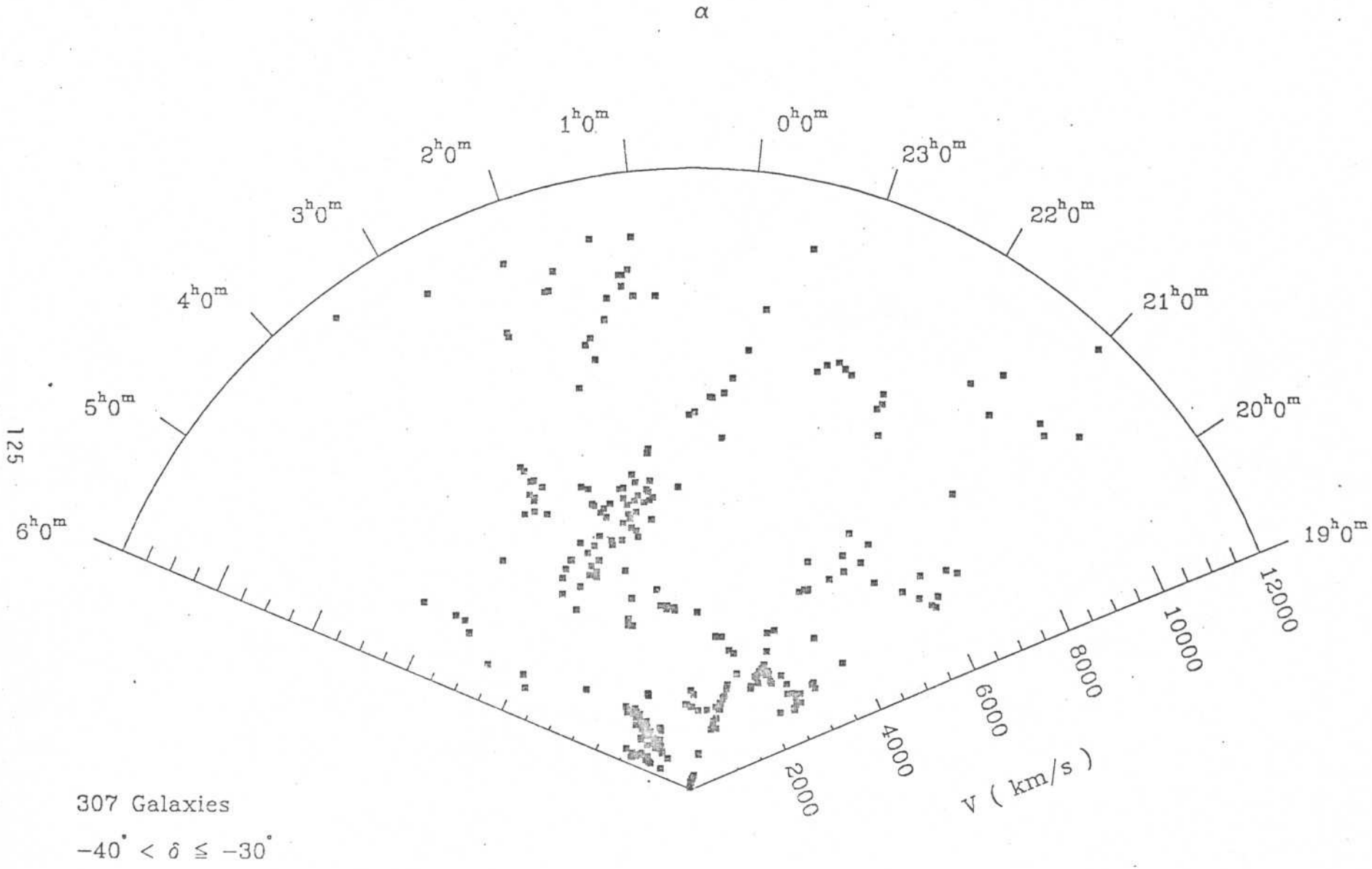
α
1h0m
0h0m
2h0m
23h0m
3h0m
22h0m
4h0m
21h0m
5h0m
20h0m
6h0m
19h0m
125
2000
4000
6000
8000
10000
12000
V (km/s)
307 Galaxies
−40° < δ ≤ −30°

Figure 4f

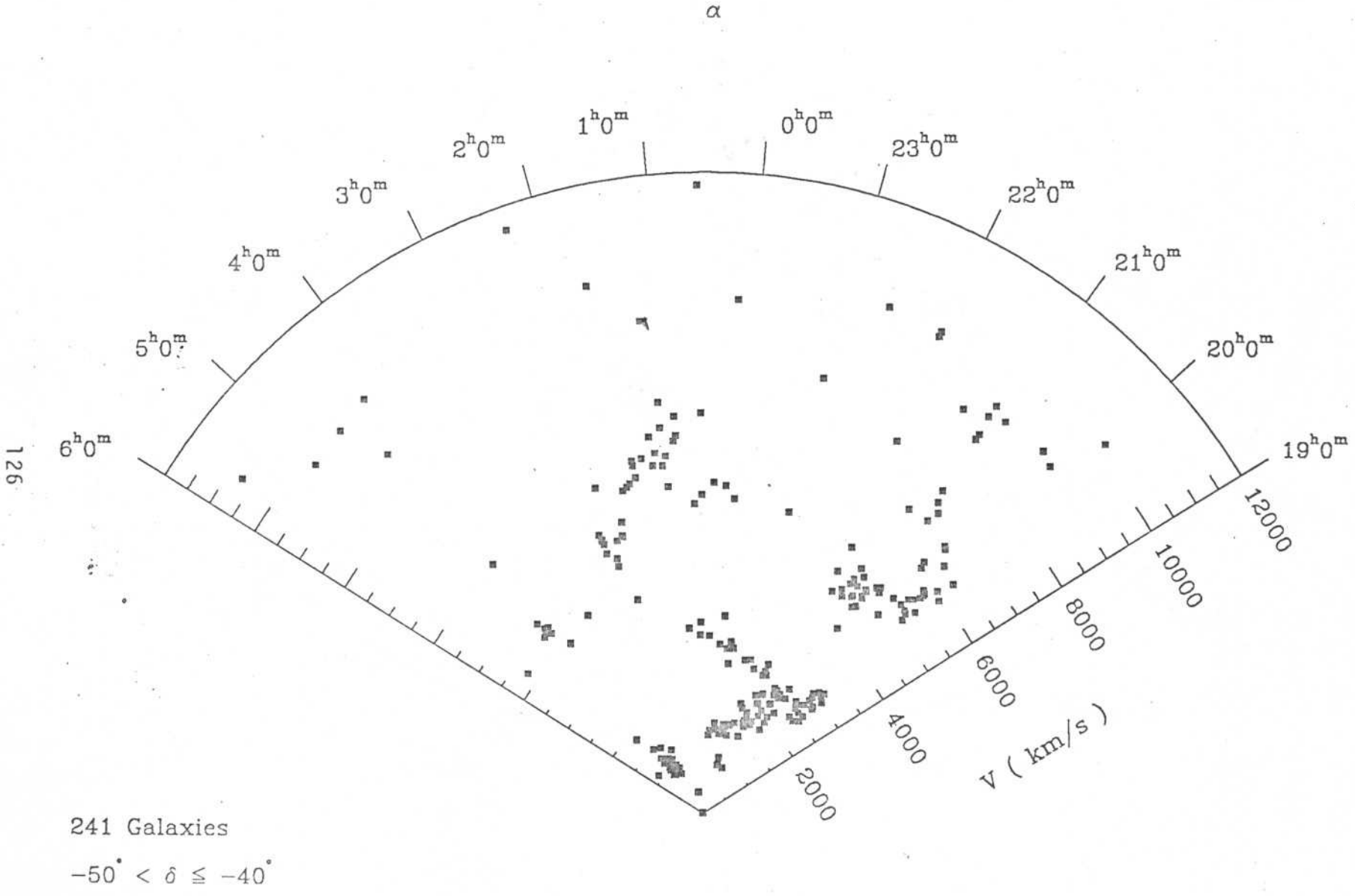
α
0h0m
1h0m
2h0m
3h0m
4h0m
5h0m
6h0m
23h0m
22h0m
21h0m
20h0m
19h0m
2000
4000
6000
8000
10000
12000
V (km/s)
241 Galaxies
−50° < δ ≦ −40°

Figure 4g

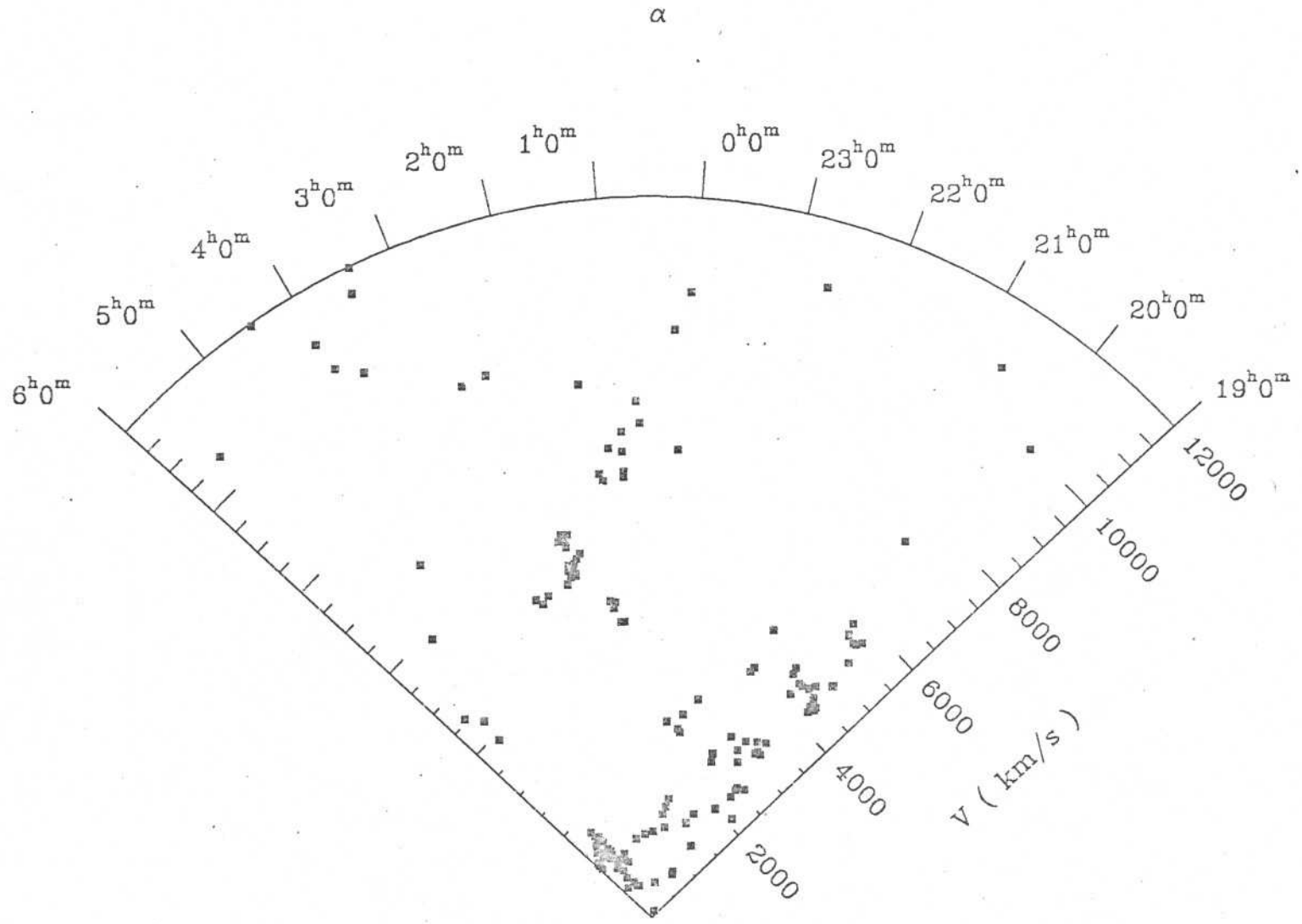

158 Galaxies

$-60^{\circ} < \delta \leq -50^{\circ}$

Figure 4h

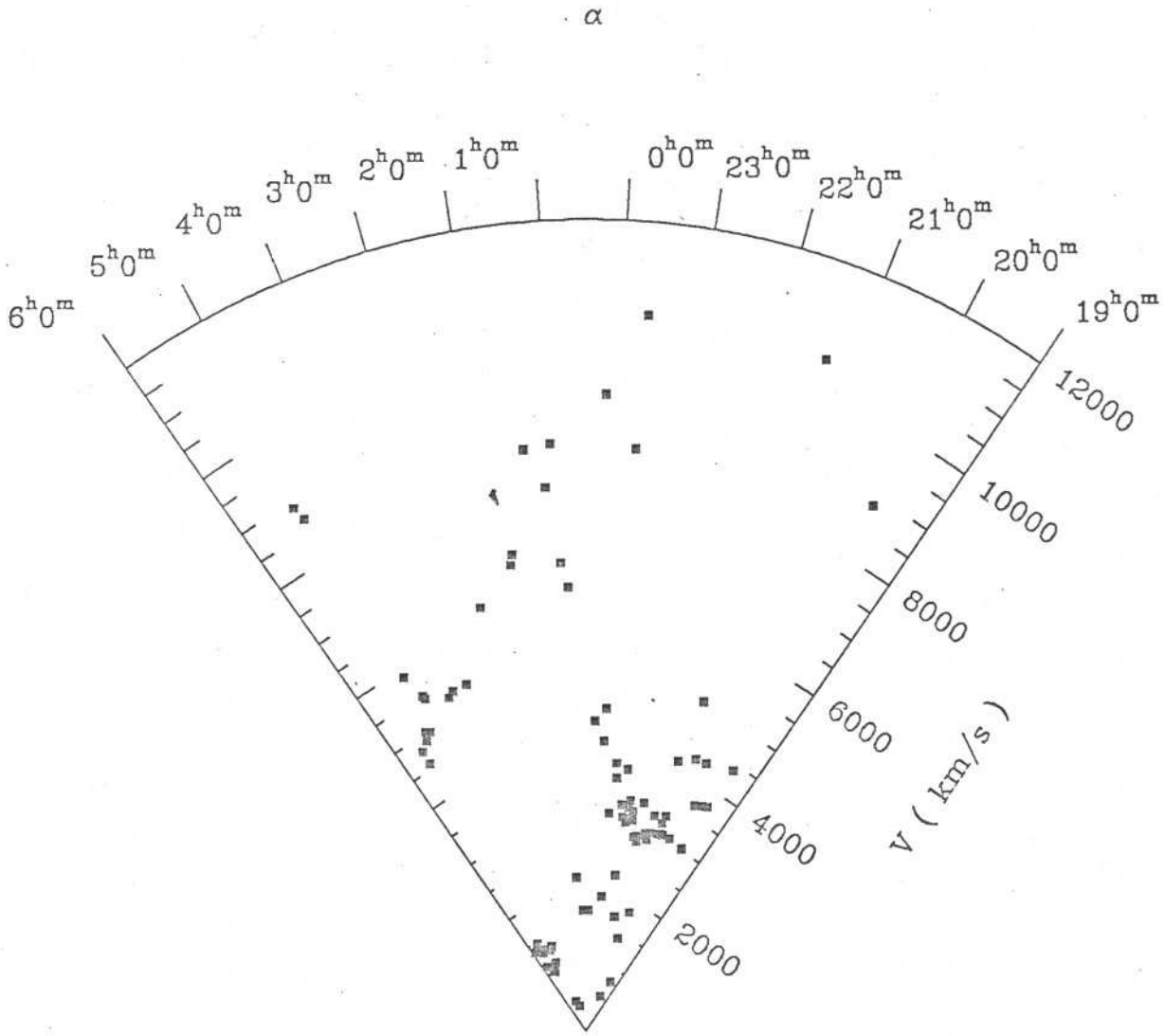

96 Galaxies

$-70^{\circ} < \delta \leq -60^{\circ}$

Figure 4i

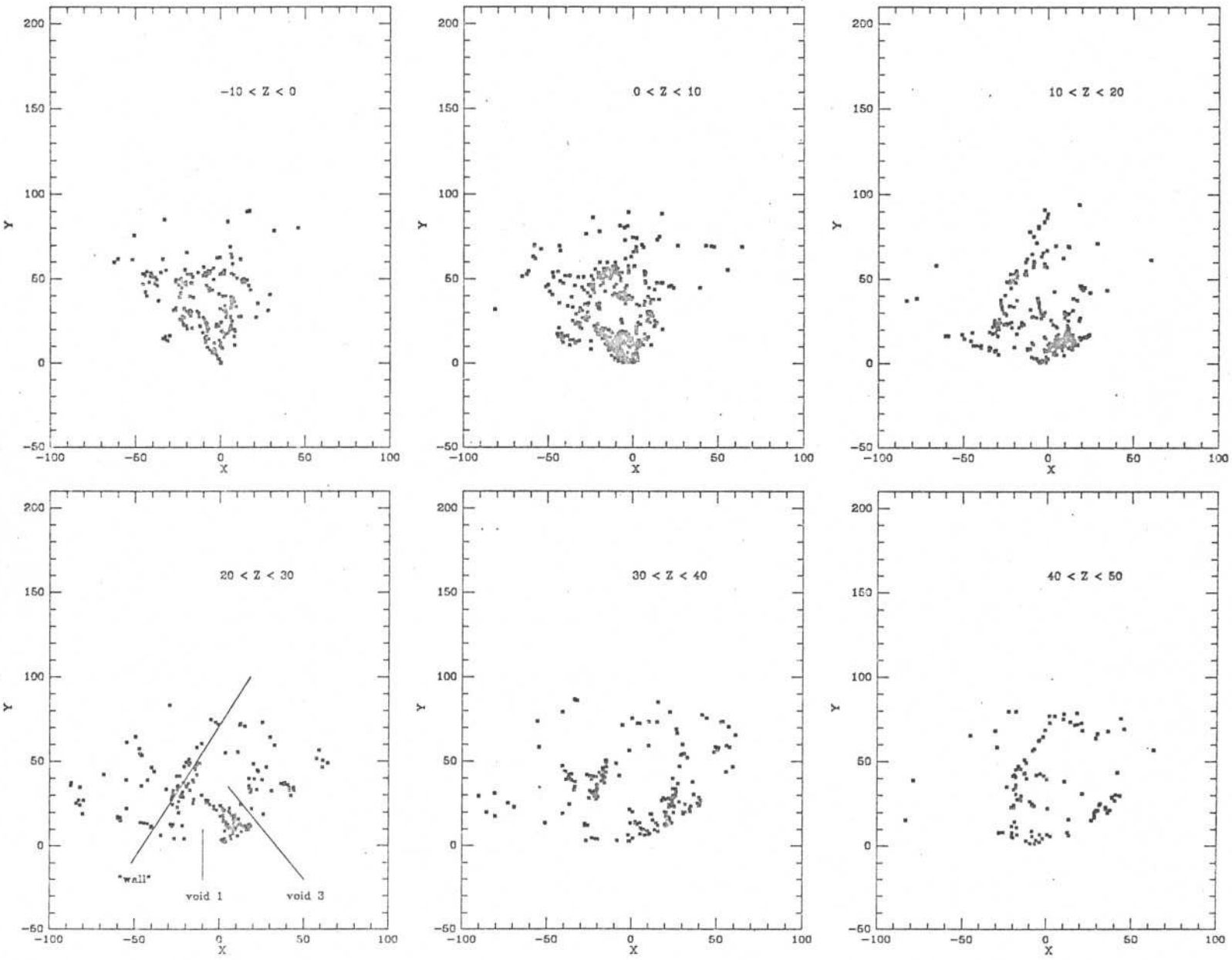
−10 < Z < 0
0 < Z < 10
10 < Z < 20
20 < Z < 30
30 < Z < 40
40 < Z < 50
"wall"
void 1
void 3
X
Y

IV.2 LEVANTAMENTO MAIS FUNDO NA REGIÃO

$-40^\circ < \delta < -30^\circ$

A FIRST GLIMPSE OF A SOUTHERN REDSHIFT SLICE

L. Nicolaci da Costa, Paulo S. Pellegrini and C. N. A. Willmer

Departamento de Astronomia, CNPq/Observatório Nacional

and

David W. Latham

Harvard-Smithsonian Center for Astrophysics

ABSTRACT

In this paper we present the first results from an effort to extend in depth the recently completed Southern Sky Redshift Survey. We have measured redshifts for a complete sample of galaxies with morphological types earlier than Sbc in a declination strip of ≈ 135° x 10°, down to a magnitude limit of $m_{B(0)} \approx 15.1$. We confirm the general pattern seen in the north that galaxies are distributed on relatively thin wall-like structures that surround vast voids, some as large as $60h^{-1}$ Mpc (H_0 = 100h km/s/Mpc). The presence of two large voids immediately adjacent to each other in our slice supports earlier suggestions that such large voids may be a common feature. Our sample also contains two elongated structures with linear dimensions ranging from at least $60h^{-1}$ Mpc to over $100h^{-1}$ Mpc.

I. INTRODUCTION

In the past few years there have been several attempts to study the nature of the three-dimensional galaxy distribution either qualitatively, from the inspection of redshift maps available from a host of redshift surveys, or quantitatively by determining the parameters that describe the topology of isodensity surfaces (see the recent review by Geller (1988)). However, these attempts have been hampered by the fact that the volumes sampled so far are relatively small and their fairness is questionable since, in all of the currently available nearby wide-angle redshift surveys, the largest structures identified have dimensions comparable to their depths. This is the case, for instance, in both of the large-angle surveys of the nearby Universe, namely the CfA Redshift Survey (CfA1, Huchra et al. 1983), the first major effort to map the spatial distribution of galaxies beyond the Local Supercluster, and the recently completed Southern Sky Redshift Survey (SSRS), which probes a somewhat deeper volume in the direction opposite of the Virgo cluster (da Costa et al. 1988, hereafter paper I). Moreover, this remains true when deeper samples are considered such as those recently completed as part of the CfA Redshift Survey Extension (CfA2, e.g. Geller et al. 1987, hereafter GHL).

The results of these previous surveys have demonstrated the pressing need to extend them to fainter magnitude limits for the purpose of establishing the characteristic size of the largest features of the galaxy distribution. One such effort is the CfA2, recently described by GHL, whose ultimate goal is to measure redshifts for all galaxies in the

northern hemisphere down to a magnitude limit of 15.5, completing 6° slices in declination. Some preliminary results have already been reported (de Lapparent et al. 1986, hereafter LGH, GHL, Geller 1988), showing the dramatic increase in information gained by these deeper surveys. A particularly remarkable result of this work was the finding "that bright galaxies are distributed on thin sheets which surround (or nearly surround) vast voids" (GHL), the size of these voids being as large as $60h^{-1}$ Mpc. When fainter galaxies are observed, they simply enhance the boundaries of the empty regions identified by shallower surveys, with only a few falling inside the voids, giving further support to the idea that these regions are almost completely empty of galaxies. The nearly circular appearance of some of these voids, in the first slice completed, led LGH to interpret the galaxy distribution as consisting of bubble-like features in contact with each other, with galaxies residing on the surface of shells. As pointed by these authors, a possible implication of this picture is that the large-scale structures could have originated from explosions at some earlier epoch.

We are presently undertaking a long-term project to extend the SSRS deeper, following the same strategy as adopted by GHL, of slice surveys. Our first goals are to examine whether patterns similar to those found by LGH are present in a statistically independent sample and to have a clearer picture of the structures observed in the southern hemisphere by the SSRS. We have started this program observing a 10° slice in the declination interval $-40° \leq \delta \leq -30°$ where some of the main features of the SSRS are prominent.

In this work we present a preliminary report of the SSRS extension, a joint effort of the Observatório Nacional (ON) and the CfA. In section II we discuss the galaxy sample and briefly describe the observations. In section III we show redshift maps for the surveyed region and discuss the characteristics of the observed galaxy distribution. Finally, in section IV we summarize our results and future goals.

II. THE DATA

A serious drawback for carrying out a deep redshift survey in the southern hemisphere is the lack of a homogenous photometric catalog of galaxies. The only existing catalog in the region is the ESO/Uppsala compilation (Lauberts 1982) which is diameter limited, and magnitudes are available for only a small fraction of the objects. Therefore, in order to define a magnitude-limited sample for the SSRS extension it was necessary to estimate magnitudes for the rest of the catalog. This was done using mean relations that approximately describe the observed correlation between corrected face-on diameters and magnitudes, for different morphological type groups. A more detailed description of the method is given by Pellegrini (1988), who shows that despite the large errors in the estimates, the magnitudes obtained are at least statistically compatible with the B(0) system used in the CfA1. However, since the errors are large one should consider the present sample as tentative, and it will need to be refined as more accurate magnitudes become available for ESO/Uppsala galaxies (e.g. Lauberts and Sadler 1984, Lauberts and Valentijn 1987), or ideally, from a photometric survey of the southern sky to a well-defined magnitude limit (e.g. Geller and Kurtz 1988).

In this paper we examine the distribution of galaxies brighter than $m_{B(0)} = 15.1$, located in the declination range $-40° \leq \delta \leq -30°$, south of $b \leq -30°$, covering a strip of $\approx 135° \times 10°$. In order to be more efficient in our optical redshift observing, we limited our sample to galaxies with morphological types earlier than Sbc ($T \leq 3$ in the notation used by Lauberts 1982). This restriction is not severe when investigating the

general pattern of the galaxy distribution since the morphological types considered delineate fairly well the structures of interest (paper I). Furthermore, Bothun et al. (1986) and Thuan et al. (1987) have found evidence that dwarf galaxies are also located in the structures delineated by the brighter galaxies. It is our intention to extend the survey to later types only when a well-defined magnitude-limited sample down to 15.5 becomes available in the region.

We should note that a potential source of incompleteness in our sample is the lack of compact high surface-brightness galaxies near our magnitude limit, since as one goes to fainter magnitudes these galaxies tend to drop out gradually from the ESO/Uppsala catalog because of its diameter limit. This is particularly true for ellipticals which, as first pointed out by Sadler (1984), become incomplete fainter than about B_T = 14.0 (B(0) ≈ 14.4), since at this magnitude the ellipticals have a diameter comparable to the ESO/Uppsala diameter cut. The problems with the present sample will only be resolved when an object list generated from the analysis of plate scans and/or CCD surveys becomes available, yielding more accurate magnitudes and including galaxies not listed in the ESO/Uppsala catalog (e.g. Geller and Kurtz 1988).

Most of our redshift observations were carried out at the 1.5-m telescope of the ON using an intensified Reticon detector described by da Costa et al. (1984), who also discuss the reduction procedures. The spectral range covered was from 4700A to 7100A, with a 6A mean resolution and 100 A/mm dispersion. More recently, observations were also made with the same detector system on the Boller and Chivens

spectrograph at the 2.15-m telescope of the Complejo Astronomico El Leoncito (CASLEO) in Argentina, with a slightly larger spectral coverage. The mean external errors of the ON-CfA redshifts have been determined from comparisons with various sources to be less than 40 km/s (da Costa et al. 1984, 1988). The data obtained in this work will be published elsewhere.

In figure 1 we show in the upper panel the projected distribution of all 1564 galaxies listed in the ESO/Uppsala catalog within the strip considered, for which there are 816 with measured redshifts. In the lower panel we plot the 788 galaxies with magnitudes brighter than 15.1, for which 674 radial velocities are available. In panel (b) squares denote galaxies in our sample (489 galaxies), while triangles denote late-spirals (299 galaxies); solid symbols indicate objects with measured redshifts. Our sample is essentially complete, with only four galaxies without a redshift, two because of superposed stars. It contains 250 galaxies with $T \leq 3$ not included in the SSRS sample, for which we have measured 222 new redshifts, another 6 were observed by Fairall (1988) and 7 were provided by Davis (1987). Comparison of the panels indicates that the galaxies in our sample trace fairly well the main features observed in the projected distribution of all galaxies in the ESO/Uppsala catalog within the surveyed strip.

III. RESULTS

In figure 2 we compare the SSRS and our present sample showing the distribution of galaxies in redshift space using wedge diagrams; in panel 2a galaxies from the diameter-limited sample of the SSRS are plotted, while in panel 2b we show the distribution of the galaxies which comprise the sample used in the present work. The most striking result when comparing these figures is the fact that with the new sample all structures already detected in the SSRS are enhanced, especially the more distant ones at about 10000 km/s, while very few galaxies fall inside the empty regions observed in the SSRS. The effect of limiting our sample by morphological type is also visible in the foreground, where the nearby structures are being less densely sampled when compared to the SSRS maps (paper I).

The void centered at (23.5^h, 6000 km/s), void 3 of paper I, is a particularly good example of a significantly empty region detected in the SSRS, to which no galaxies were added by the deeper survey. The new observations delineate more clearly the far side of this void, allowing us to estimate its depth and transverse dimension to be roughly $60h^{-1}$ and $40h^{-1}$ Mpc, comparable to the estimated diameter of the void in Bootes (e.g. Kirshner et al. 1987). Void 3 appears to be the most depopulated void in the region and, as outlined by the galaxies in our sample and is as prominent as the voids observed in the northern slices (LGH, GHL). In contrast to LGH, who described the largest void in the first slice completed in the north as delineated by boundaries that look nearly circular, void 3 is perhaps better described as being bounded by relatively

thin structures that intersect at a variety of angles, some of them making sharp corners. We note that similar irregular shapes are also visible in some voids of the northern slices (cf. GHL).

On the other hand, a few galaxies have been detected by our deeper survey within the original volume of voids 1 and 4 of paper I; the former centered in the slice considered here at (3^h, 3000 km/s), immediately behind Fornax, and the latter at (4^h, 9000 km/s). In both cases there is a suggestion that we have detected a tenuous structure crossing them, a feature which seems to occur some times in voids. Although the deeper survey has slightly enhanced the far side of void 4, thought to be the largest in the SSRS, it is still undersampled because it lies beyond 10000 km/s and at these large distances only the bright end of luminosity function is observed. In paper I we estimated its depth to be of about $40h^{-1}$ Mpc but the absence of a sharp edge makes this value uncertain. In addition, the appearance of a few galaxies in the middle of the original volume raises the question of whether we are, perhaps, seeing two (or more) smaller voids, one centered at (3.5^h, 9000 km/s) and the other near the eastern border of the survey. Regardless of the details of the structure in void 4, this is a large underdense region, with a long dimension at least comparable to that of void 3. These findings support the suggestion of Postman et al. (1986) that large empty regions with long dimensions comparable to the diameter of the void in Bootes may be quite common.

In order to estimate the underdensity of void 3, the most prominent in our slice, we plot in figure 3 the observed and expected distribution of

galaxies between 22.5^h and 0.5^h, in bins of 500 km/s. In the calculation of the expected distribution we assume a Schechter luminosity function and use the parameters $M_* = -19.4$ and $\alpha = -1.30$, given by Davis and Huchra (1982). We note that these parameters are valid when all morphological types are considered, but here we ignore any possible effects associated with morphology and normalize this curve by the total number of observed objects in the region considered. It can be seen that there is a significant deficiency of galaxies between 2000 and 7500 km/s, where there are 12 galaxies observed whereas 58 would be expected. This corresponds to a density contrast of roughly 0.20, similar to that found in other underdense regions (Kirshner et al. 1987, LGH). However, as can be seen in figure 3 the density contrast is in fact more pronounced and the value of 0.20 should be considered only as an upper limit. Note that there are no galaxies between 3000 and 6500 km/s. The excesses observed in the histogram for radial velocities greater than 12000 km/s are associated with a real structure discussed below.

A remarkable feature revealed by the present extension is the presence of a linear structure at about 9000 km/s extending roughly from about 21^h to 2^h, corresponding to a linear dimension of at least $100h^{-1}$ Mpc, comparable to one of the elongated structures observed by GHL. Parts of this structure were already seen in the shallower survey, but the better sampling obtained here shows more convincing evidence for the presence of a long connected structure. In the right ascension interval $21^h < \alpha < 23.5^h$ this structure forms the far side of void 3. This elongated thin structure cuts across the survey volume almost perpendicular to the line of sight and intersects the main wall defined in

paper I at an angle of about 90°. At about 1.5^h it intersects another small linear feature which runs almost parallel to the main wall. This structure ends abruptly, thus opening a connection between void 4 and a large adjacent empty region at (1^h, 8000 km/s).

One of the main features noted in paper I was the prominent wall near 0^h, running from about 4000 km/s to 9000 km/s. This wall seems to be extended by our new observations out to almost 20000 km/s. Although sampling effects become severe at these large distances, this structure exhibits sufficient contrast with the surroundings to suggest that it may prove to be real, thus forming a connected structure extending over $150h^{-1}$ Mpc in length. Beyond about 12000 km/s the regions on either side of the wall appear to be underdense, especially to the west at about 14000 km/s. However, poor sampling and the possibility that the distant linear structure may consist of an alignment of a few relatively distant clusters, for which we are seeing the effects of virial motion on the brightest galaxies, precludes a more conclusive statement.

We have attempted to identify possible Abell-like clusters in the surveyed strip beyond 5000 km/s, using the catalogs of clusters compiled by Dressler (1980) and Abell, Olowin and Corwin (1987). The only secure identification is of the cluster DC 0247-33 at a mean redshift of about 7000 km/s. Based on innacurate redshift estimates there are six other clusters from Abell et al.'s list within the survey volume, all with richness class ≤ 2. We note that the identification of these systems in our wedge diagram is not simple since for most clusters the redshifts were estimated using the relation m_{10}-redshift given by Leir and van der

Bergh (1977), with the exception of two clusters recently observed by Colless and Hewett (1987): one at $\alpha = 00^h\ 00.7^m$ and $\delta = -36°\ 14'$ at a mean redshift of 14764 km/s and the other at $\alpha = 23^h\ 49.5^m$ and $\delta = -34°\ 40'$ at 17527 km/s (cf. Fairall and Jones 1988). However, we find no evidence for virial distortions in our map at the positions of these six clusters, indicating that if we are picking out member galaxies at all, they comprise only a very small number of objects. This is a further indication that the feature stretching out to 20000 km/s may indeed form a real connected structure rather than just an alignment of distant clusters. Another point that should be stressed, is that in the slice presented here, there are no prominent clusters of galaxies such as Coma. Therefore, in order to identify clusters of galaxies it will be necessary to probe deeper, producing a larger overlap between galaxy and cluster samples. We note that mild virial distortions, similar to that observed for the cluster DC 0247-33, are detected at approximately ($23^h\ 55^m$, 9200 km/s) and ($00^h\ 02^m$, 8200 km/s).

IV. DISCUSSION

In this paper we have presented a preliminary report of an ongoing effort to extend the SSRS in selected slices of the southern hemisphere. The main purposes of the present paper are: a) to inform about the present status of this effort; b) to show what can be learned about some of the structures observed in the SSRS as we go to fainter magnitudes; c) to demonstrate the pressing need for a large photometric survey of galaxies in the southern sky.

Inspection of the redshift maps lead us to the following tentative conclusions:

1) The general pattern of the galaxy distribution that we find in our southern slice is similar to that found in the first slices of the CfA2 (GHL). The galaxies in our sample are distributed on relatively thin structures which delineate voids with sizes up to at least $60h^{-1}$ Mpc. The fainter galaxies enhance the boundaries of the voids found by the shallower SSRS, while very few fall in the empty regions. However, deeper samples, including all morphological types, are required to establish whether the sizes and density contrasts estimated here can depend on effects such as morphology and/or luminosity. These samples should also allow us to determine how frequently such large voids occur and whether even larger voids exist.

2) In the strip there are two long structures: one that extends at least $60h^{-1}$ Mpc (the main wall), with a hint that it may extend for as much as

$150h^{-1}$ Mpc; the other, perpendicular to the former, has a long dimension over $100h^{-1}$ Mpc.

3) No evidence is found for the occurrence of galaxy clusters at the intersections, in contrast to what would be expected in some scenarios for the formation of large-scale structures (e.g. Mellot 1983).

4) The presence of a second large void $40h^{-1}$ Mpc across and immediately adjacent to our largest void, supports previous suggestions that such large voids are common (e.g. Postman et al. 1986).

The first results of our slice survey are encouraging. We are currently completing a sample in a smaller 5° strip in the declination interval $-37.5° \leq \delta \leq -32.5°$ down to $m_{B(0)} \approx 15.5$, for which we have about 100 additional redshifts obtained in collaboration with Fairall (1988). However, much of our future work will require a more homogenous magnitude-limited sample down to 15.5.

ACKNOWLEDGMENTS

We would like to thank all the people involved in the Redshift Survey effort both at the ON and the CfA, in particular M. Nunes, D. Nascimento and D. Gilmore for their dedication in making the Reticon operational at the Complejo Astronomico El Leoncito (CASLEO) in Argentina, where some of the data were obtained. We would also like to thank the director of CASLEO, Dr. O. H. Levato and all his staff.

Finally, we thank Dr. A. Fairall for providing some redshifts before publication and Dr. R. Olowin for providing us with the southern cluster catalog. We also thank M. J. Geller and J. P. Huchra for their interest in the extension of this project.

REFERENCES

Abell, G., Olowin, R. P. and Corwin, H. G., 1987, private communication.

Bothun, G. D., Beers, T. C., Mould, J. R. and Huchra, J. P. 1986, Ap. J., **308**, 510.

Colless, M. and Hewett, P. 1987, M.N.R.A.S., **224**, 453.

da Costa, L. N., Pellegrini, P. S., Nunes, M. A., Willmer, C. and Latham, D. W. 1984, A. J., **89**, 1310.

da Costa, L. N., Pellegrini, P. S., Sargent, W. L. W., Tonry, J., Davis, M., Meiksin, A. and Latham, D. W. 1988, Ap. J., **327**, 544 (Paper I).

Davis, M. and Huchra, J. 1982, Ap. J., **254**, 437.

Davis, M. 1987, private communication.

Dressler, A. 1980, Ap. J. Suppl., **42**, 565.

Fairall, A. P. 1988, private communication.

Fairall, A. P. and Jones, A. 1988, Pub. Dep. Astron. University of Cape Town, N° 10.

Geller, M. J. 1988, "17th Advanced Course in Astronomy and Astrophysics, Saas-Fee, Switzerland, in press.

Geller, M. J., Huchra, J. P. and de Lapparent, V. 1987, IAU Symp. 124, Observational Cosmology, ed. A. Hewitt, G. Burbidge and L. Z. Fang (Dordrecht: Reidel), p. 301.

Geller, M. J. and Kurtz, M. J. 1988, private communication.

Gott, J. R., Melott, A. L. and Dickinson, M. 1986, Ap. J., **306**, 341.

Huchra, J. P., Davis, M., Latham, D. and Tonry, J. 1983, Ap. J. Suppl., **52**, 89.

Kirshner, R. P., Oemler, A., Schechter, P. L. and Shectman, S. A. 1987, Ap. J., **314**, 493.

de Lapparent, V., Geller, M. and Huchra, J. P. 1986, Ap. J. (Letters), **302**, L1 (LGH).

Lauberts, A. 1982, The ESO/Uppsala Survey of the ESO(B) Atlas (Munchen: European Southern Observatory).

Lauberts, A. and Sadler, E. 1984, ESO Scientific Report 3.

Lauberts, A. and Valetijn, E. A. 1987, in Astronomy from Large DataBases (Munchen: European Southern Observatory)

Leir, A. A. and van den Bergh 1977, Ap. J. Suppl., **34**, 381.

Melott, A. L. 1983, M. N. R. A. S., **202**, 595.

Pellegrini, P. S. 1988, Ph D. thesis, Observatório Nacional.

Postman, M., Huchra, J. P. and Geller, M. J. 1986, A. J. **92**, 1238.

Sadler, E. M. 1984, A. J., **89**, 34.

Thuan T. X., Gott, J. R. and Schneider, S. E. 1987, Ap. J. (Letters), **315**, L93.

FIGURE CAPTIONS

Figure 1- Projected distribution of galaxies in the strip $-40° < \delta < -30°$ onto equatorial coordinates: (a) all galaxies in the ESO-Uppsala catalog; (b) galaxies brighter than $m_{B(0)} = 15.1$. In (b) squares represent galaxies with $T \leq 3$ and triangles later types. Full (open) symbols denote galaxies with (without) velocities.

Figure 2- Diagrams showing observed velocity versus right ascension for galaxies with $v < 20000$ km/s in the strip: (a) the SSRS (including all morphological types); (b) the SSRS extension ($T \leq 3$).

Figure 3- Histogram of redshifts in 500 km/s intervals for galaxies in the right ascension domain of the strip containing void 3; between $22^h\ 30^m$ and $0^h\ 30^m$. The solid curve is a Schechter luminosity function normalized to the number of galaxies in the same region.

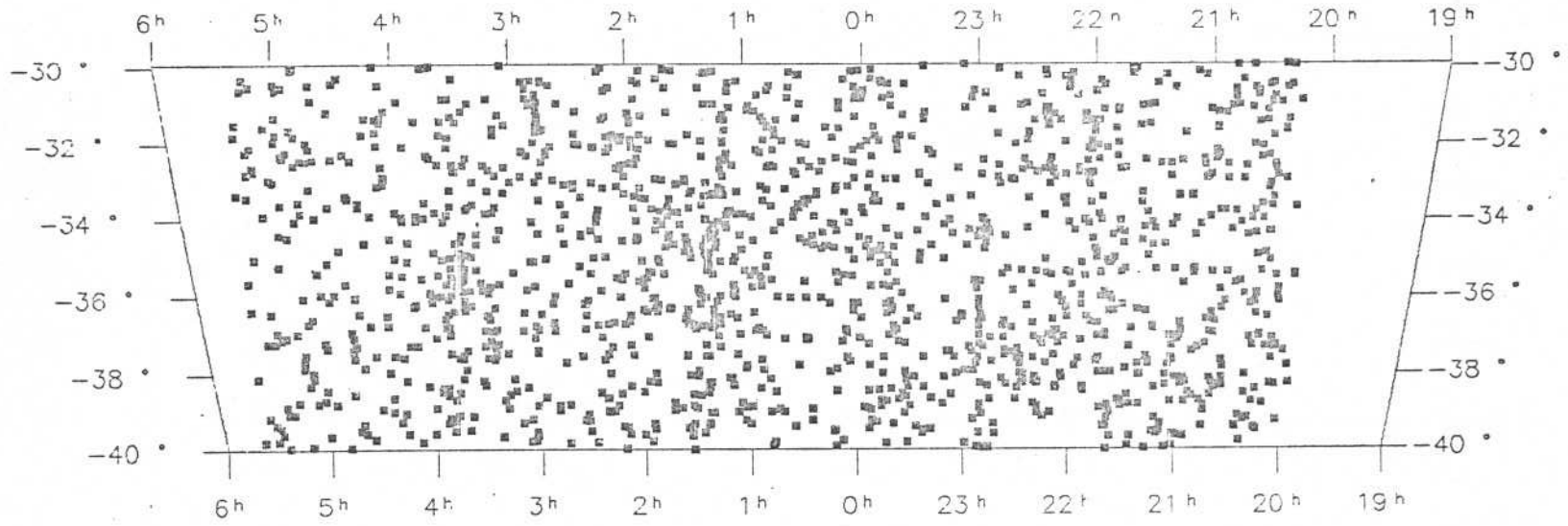

Figure 1a

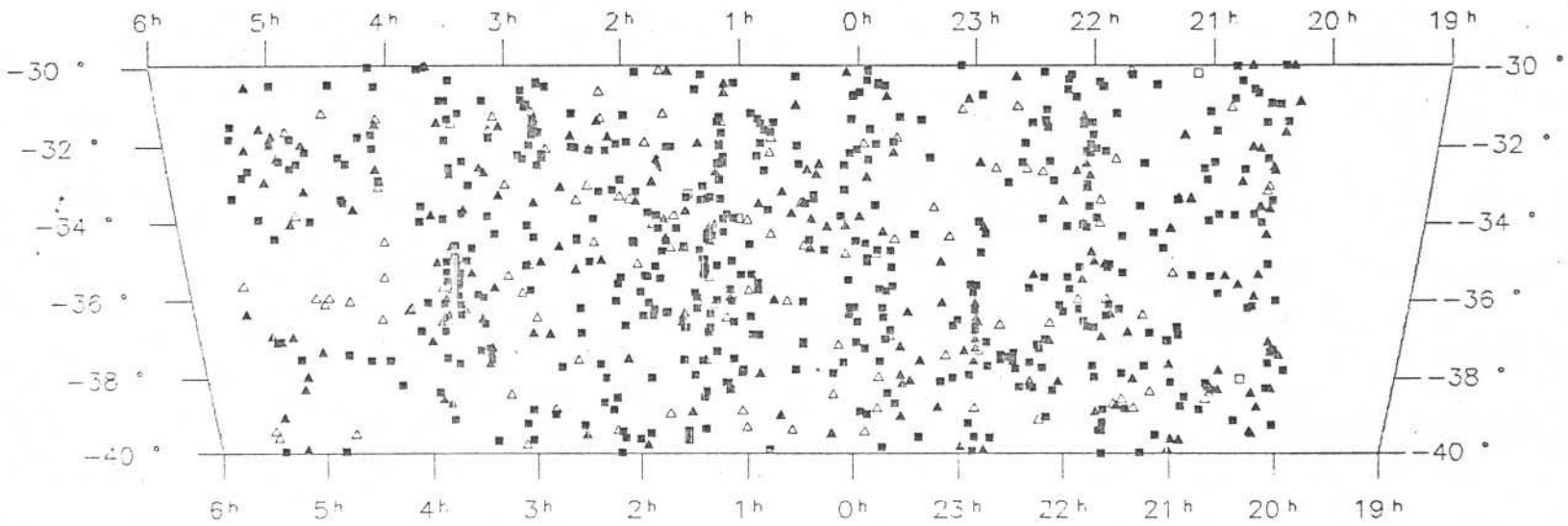

Figure 1b

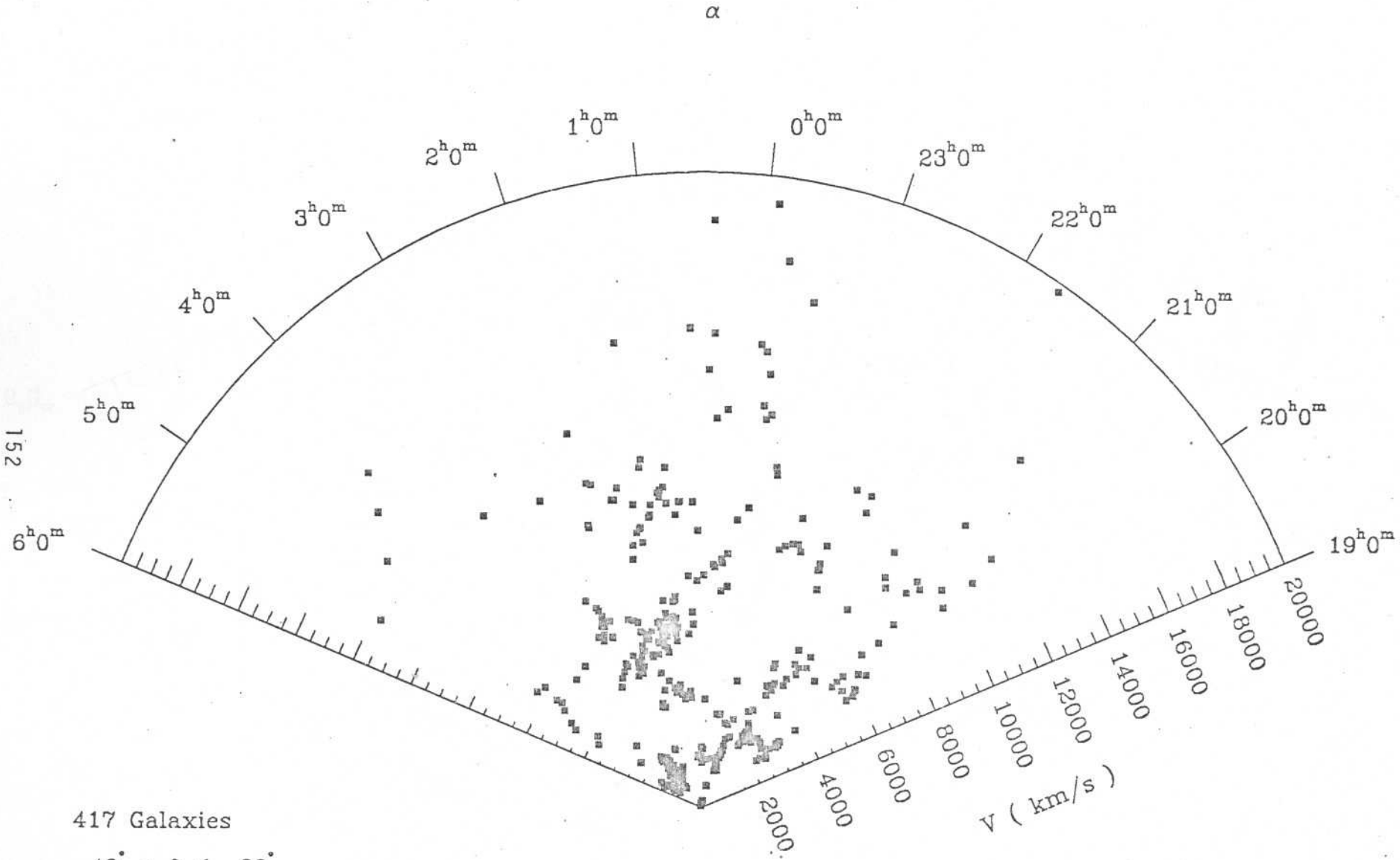
α
1h0m
0h0m
2h0m
23h0m
3h0m
22h0m
4h0m
21h0m
5h0m
20h0m
6h0m
19h0m
2000
4000
6000
8000
10000
12000
14000
16000
18000
20000
V (km/s)
417 Galaxies
−40° < δ ≦ −30°

Figure 2a

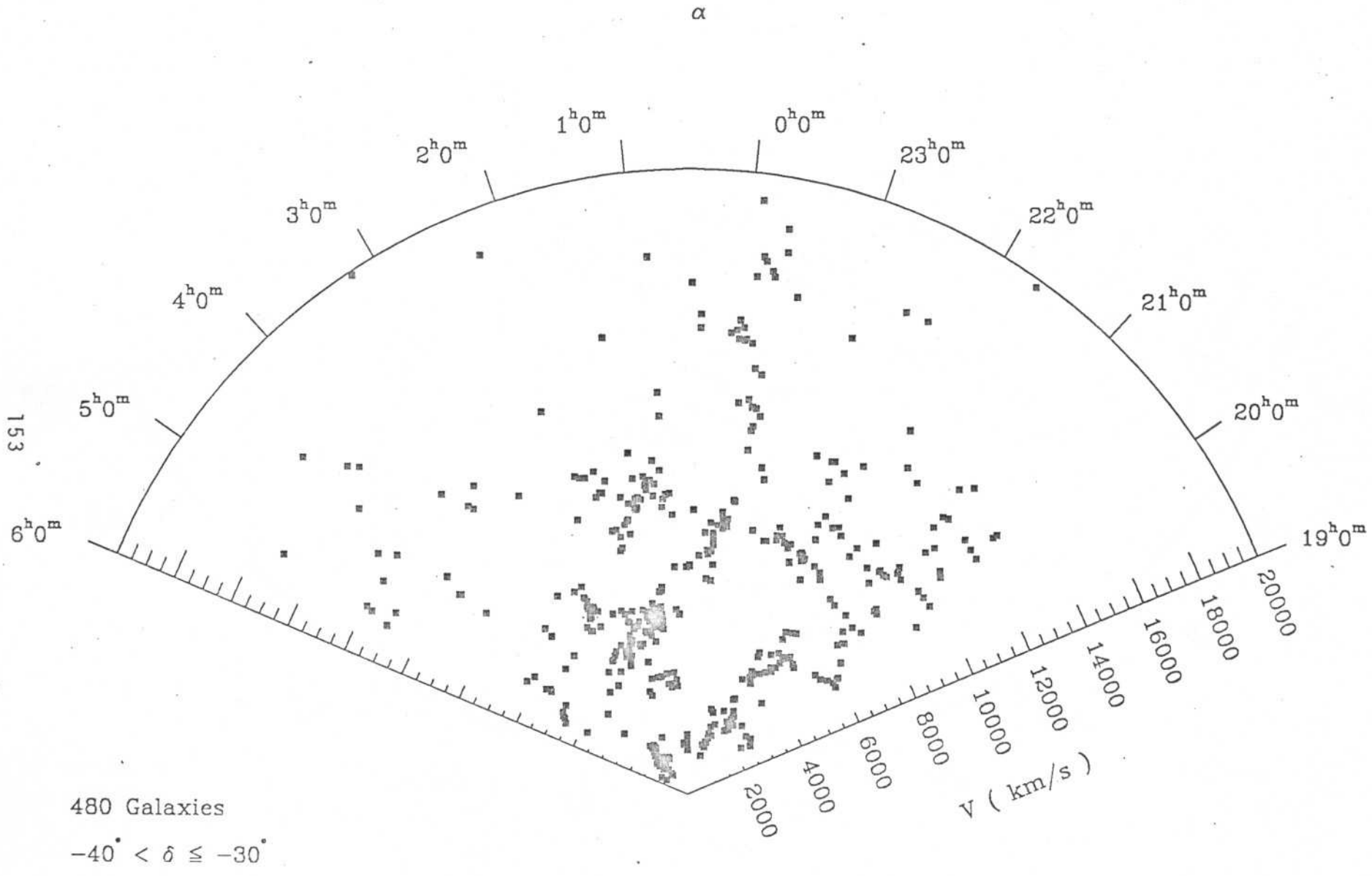
α
1h0m
0h0m
2h0m
23h0m
3h0m
22h0m
4h0m
21h0m
5h0m
20h0m
6h0m
19h0m
153
2000
4000
6000
8000
10000
12000
14000
16000
18000
20000
V (km/s)
480 Galaxies
−40° < δ ≦ −30°

Figure 2b

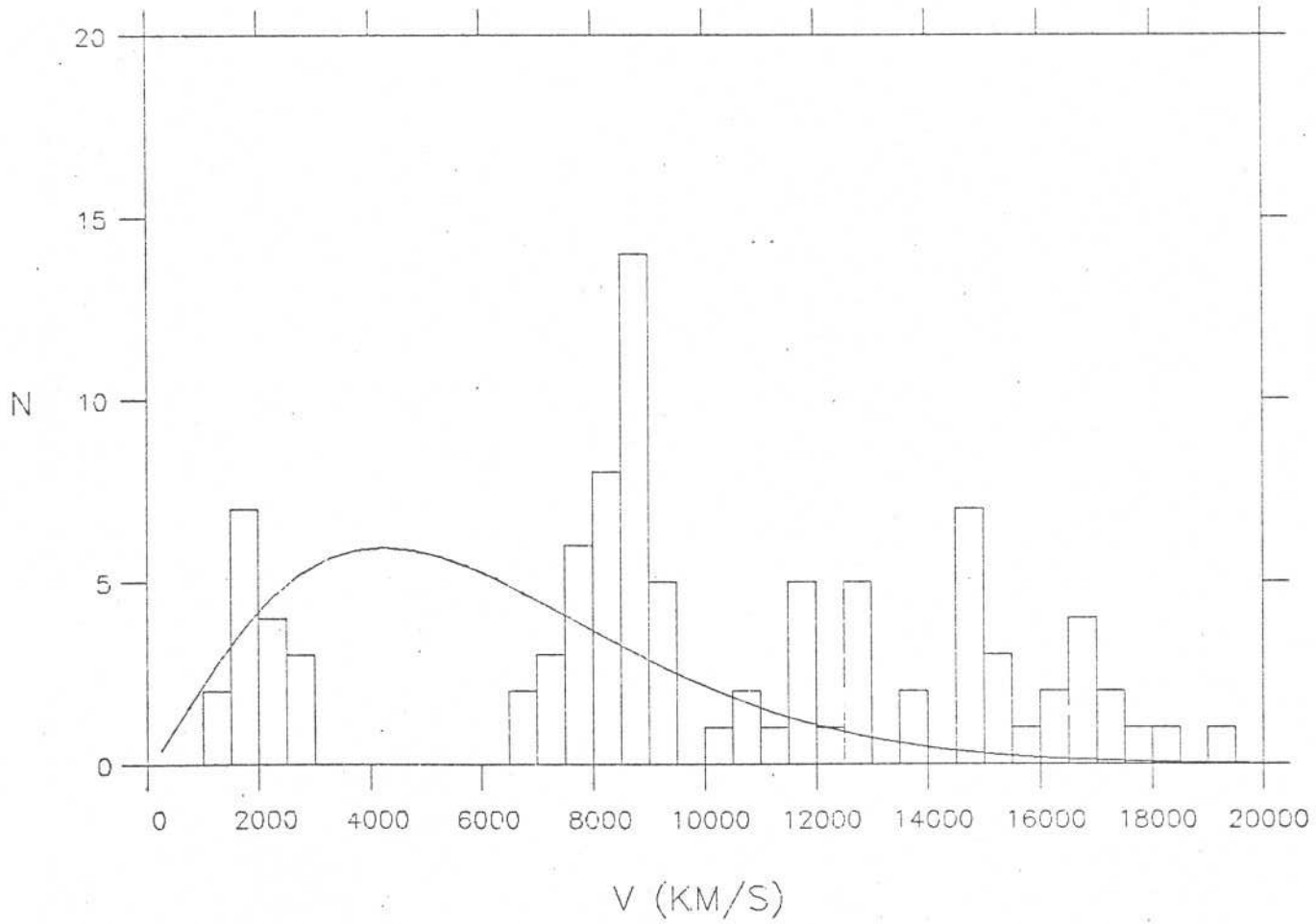
20
15
10
5
0
N
0
2000
4000
6000
8000
10000
12000
14000
16000
18000
20000
V (KM/S)

Figure 3

V. ALGUMAS PROPRIEDADES DA DISTRIBUIÇÃO DE GALÁXIAS

V.1 PROPRIEDADES ESTATÍSTICAS DO SSRS

SOME STATISTICAL PROPERTIES OF THE SSRS

Paulo. S. Pellegrini, C. N. A. Willmer and L. Nicolaci da Costa

Departamento de Astronomia, Observatorio Nacional

ABSTRACT

In this paper we compare the statistical properties of the distribution of galaxies in the northern and southern hemispheres, using the redshift catalogs of the CfA Redshift Survey and the Southern Sky Redshift Survey (SSRS). These surveys probe comparable volumes of space, allowing us to examine whether the spatial distributions of galaxies have the same general characteristics. The results obtained from the analyses of several statistical indicators suggest that either these indicators are not sufficiently sensitive to be useful in discriminating different structural characteristics or the present samples have the same statistical properties. If the latter interpretation is correct then our results suggest that a fair sample volume of the universe has already been reached.

I. INTRODUCTION

The recently completed wide-angle redshift surveys have provided a wealth of information for studying the large-scale distribution of galaxies and have contributed to our understanding of the nature of the three-dimensional distribution of galaxies. A general impression obtained from redshift maps is the existence of conspicuous voids nearly surrounded by sheet-like structures. However, in order to make full use of this information it is essential to devise quantitative techniques to analyze the data, especially to confront model distributions obtained in N-body simulations with the observational data.

Over the years several statistics have been proposed to analyze galaxy distributions; among the most widely used are the correlation analysis, which measures the properties of the two- and three-point correlation functions (Peebles and collaborators), and the cluster analysis (e.g. Zel'dovich et al. 1982, Einasto et al. 1984) from which one can derive the multiplicity function and some other properties of galaxy clustering. These methods are relatively simple to apply to a discrete distribution of points like a galaxy catalog and are thought to give complementary information about the large-scale structures. An alternative method has been recently considered by Einasto and Saar (1987), who construct a continuous density function to describe the underlying galaxy distribution, by counting galaxies in cells. These methods, except the cell-method, are only suitable to describe the properties of high density regions. However, an outstanding feature of the galaxy distribution is the existence of large empty regions and to

quantify their properties statistical methods like the nearest neighbor distribution (e.g. Ryden and Turner 1984) and the void probability function (e.g. White 1979, Schaeffer 1984, Maurogordato and Lachieze-Rey 1987) have been used. More recently, Goit et al. (1986) have introduced a more powerful method which treats the high- and low- density regions on an equal footing, analyzing the topology of equal density surfaces and showing how different cosmogonic scenarios may be distinguished (Weinberg et al. 1987).

In this paper we apply some of the statistics mentioned above to the sample of galaxies of the recently completed Southern Sky Redshift Survey (SSRS, da Costa et al. 1988). These results are compared with those obtained from the analysis of the CfA Redshift survey (Huchra et al. 1983, hereafter CfA1) in order to verify whether both data sets approach a fair sample volume of the universe. A potential problem in this comparison is the different morphological composition of both samples (da Costa et al. 1988), which reflects the fact that the CfA1 sample is magnitude-limited, while the SSRS is diameter-limited, favoring the inclusion of late-type galaxies. Here we consider some of the classical methods described above, excepting the correlation analysis which will be discussed elsewhere (Davis et al. 1988). All of these methods have been previously applied to various subsets of the CfA1 catalog. In section II we describe the samples considered in the present study, while in section III we compare the results obtained in both hemispheres. Finally, in section IV we summarize our main results.

II. THE SAMPLES

The SSRS sample covers 1.75 steradians of the southern galactic cap, below galactic latitude -30° and south of δ = -17.5° and includes some 2000 galaxies from the ESO catalog (Lauberts 1982), with "face-on" diameters greater than 1.26 arcminutes (see da Costa et al. 1988 for a precise definition). Radial velocities are available for 1657 galaxies (Sargent et al. 1988) and the sample is essentially complete for galaxies earlier than Sc. Velocities were corrected for galactic rotation and for an infall velocity of 250 km/s towards the Virgo cluster, assuming a spherical flowfield model. Galaxies within 6° of the center of the Virgo cluster and redshifts less than 2500 km/s are assumed to be at the position of Virgo. In the analyses below we consider samples that are volume-limited at 4000 km/s (S4), 6000 km/s (S6) and 8000 km/s (S8), deleting galaxies with absolute physical diameters smaller than $14.6h^{-1}$, $21.9h^{-1}$ and $29.2h^{-1}$ Kpc (H_0 = 100h km/s/Mpc), respectively. Samples S4, S6 and S8 comprise 300, 343 and 224 galaxies. We note that for these diameters most dwarfs are naturally eliminated so each of the subsamples can be considered as nearly complete.

For comparison we define volume-limited samples at the same depths using the northern portion of CfA1, which covers an area of 1.83 steradians of the northern galactic cap ($b \geq 40°$, $\delta \geq 0°$). At 4000 km/s the sample includes 431 galaxies brighter than absolute magnitude M_B =-18.5 (N4), at 6000 km/s 266 galaxies with $M_B \leq -19.4$ (N6) and 213 galaxies with $M_B \leq -20.0$ (N8). We note that the sampling should still be adequate since the absolute magnitude cut is comparable to the knee of

the luminosity function derived by Davis and Huchra (1982).

In table I we list the parameters that characterize each sample, giving the number of galaxies N_g, the volume V, the mean interparticle distance $r_o = (N_g/V)^{1/3}$ and the characteristic size of the volume $L_c = (V)^{1/3}$. For completeness we also include the fraction of early and late type galaxies. Note that the percentage of early-type galaxies is relatively higher in the North, reflecting the different criteria used in defining the samples of CfA1, which is magnitude-limited, and the SSRS, diameter-limited. This difference should be kept in mind when interpreting the results presented below.

III. STATISTICAL ANALYSES

a) Cluster Analysis

Cluster analysis is a generic name given to the method of studying the properties of individual systems identified on the basis of the spatial separation of galaxies. The systems are identified using the usual "friends of friends" algorithm, drawing spheres of radius r around each galaxy and considering two galaxies to be associated whenever their separation is less than r. A system consists of those galaxies that are associated to each other by at least one neighbor closer than r. The clustering properties of two different samples such as their multiplicity function, critical percolation and shapes of the systems can be analyzed and compared for different values of the normalized neighborhood radius $s = r/r_o$, where r_o is, as before, the mean interparticle distance.

i) Multiplicity function

Multiplicity functions have been used to quantify the distribution of cluster or group sizes and it is thought to provide information on the initial fluctuation spectrum (e.g. Gott and Turner 1977, Bhavsar et al. 1981). Following Einasto et al. (1984), we examine the multiplicity function in its differential form, defining the function f(m) to be the fraction of galaxies in systems of multiplicity between m and m+dm, where the multiplicity is expressed as $m = \log_2 N$, where N is the number

of galaxies in the group. We have computed the multiplicity function for all subsamples with the dimensionless radius s varying in the range 0.2 to 1.2. Figure 1 compares the results for the different volume-limited samples extracted from SSRS and CfA1.

Apart from the differences in the definition of the dimensionless radius, these plots can be compared with those presented by Einasto et al. (1984) in their analysis of a volume-limited subsample of CfA1. The behavior of the multiplicity function of N4 is essentially the same as theirs, as expected since we are dealing with very similar samples. The similarity of the multiplicity function derived from the various samples is striking, regardless of the adopted cutoff limit. Although there are some localized differences, such as seen comparing N4 with S4 at s = 0.2, reflecting presence of the Virgo cluster in the northern hemisphere, they can generally be attributed to statistical fluctuations. To help visualizing the behavior of f(m) as a function of s we show in figure 2 the parameters α, β, γ which represent the fraction of galaxies associated to small, intermediate and large groups, respectively. These parameters were obtained dividing the multiplicity interval of figure 1 into three equal parts. For comparison we also show realizations of Poissonian distributions within the same volume and the same number of points as each volume-limited southern sample. As expected the real galaxy distribution behaves quite differently from a catalog of random points. On the other hand, there are only minor differences in the multiplicity function derived from the various samples. For instance, we can see in figure 2a that N4 seems to have in average a larger fraction of intermediate size systems as compared to S4. The situation is reversed

for the samples limited at 6000 km/s, where S6 shows a large peak at s = 0.6 (figure 2b). However, these, as well as other differences which can be seen in a closer inspection of the plots, are not very significant, and indicate that the general clustering properties of the samples are very similar. The variations are probably just reflecting the way that the structures grow in each volume.

Finally, in figure 3 we show the variation of the fraction, f_{iso}, of "isolated" galaxies for the various samples as a function of s. As can be seen, at large s "isolated" galaxies comprise less than 5% of the galaxy population.

ii) Percolation

Percolation analysis was introduced by Zel'dovich et al. (1982) and Shandarin (1983) who argued that it would be a good indicator for filamentary, or more generally, connected structures. As a matter of fact, the early comparisons of the percolation properties of adiabatic models with a Poisson distribution and a non-dynamical hierarchical model (Soneira and Peebles 1978) suggested that this statistic could adequately differentiate between the patterns expected for the galaxy distribution in these different scenarios for the formation of large-scale structures (Einasto et al. 1984). This expectation motivated further studies by Bhavsar and Barrow (1983) of the percolation properties of the CfA1 sample. These authors concluded, in contrast to Einasto et al. (1984), that dynamical models of hierarchical scenarios were also consistent with the data and that the test was not sufficiently sensitive to be useful.

This opinion was corroborated by the critical analysis of the percolation test made by Dekel and West (1985) who showed that the percolation test is not only insensitive to differences in realistic models of different scenarios but also, its behavior depends on sampling parameters such as the mean number density and volume of the sample, to the extent that any possible intrinsic difference can be washed out.

Despite these objections, we apply the percolation test to the samples defined above. Our argument for using this test is that even though similar percolation properties for the CfA1 and SSRS do not guarantee that the galaxy distributions are statistically similar, significant differences would be, in principle, evident. The test consists of comparing the maximum length of the largest system, L_{max}, identified from the cluster analysis for a given neighborhood radius, with the characteristic size of each volume considered. Critical percolation occurs when the normalized parameter $l_p = L_{max}/L_c$ is of the order of 1, and a single connected structure spans the whole volume. Since the shapes of the volumes encompassed by the samples do not have a simple geometry, we adopt the quantity L_c, defined in section II, as the characteristic scale of the volume. In figure 4 we compare the percolation properties of the northern and southern samples showing l_p as a function of the dimensionless radius s. For reference we also show curves corresponding to random distributions. The similarity between the volume-limited samples at 4000 km/s in both hemispheres is noticeable. Critical percolation occurs roughly at s = 0.70 for S4 and s = 0.75 for N4, comparable to the value found by Einasto et al. (1984), while for the Poisson distribution it occurs at s = 0.86, indicating that our choice of L_c

to characterize the volume is adequate. Although it seems that the percolation in the south is somewhat easier, we do not think that the observed difference is significant. From panels a and b of figure 4 we can see that the percolation curves of N6 and N4 are very similar, while S6 percolates significantly slower. This result is somewhat surprising, since one would expect that the sheets observed in the south would ease percolation. One possible explanation could be that in making a volume-limited sample at $60h^{-1}$ Mpc, we could be picking out only large and more dispersed late-type spirals making percolation harder. In this case the effect would reflect some degree of morphological segregation. However, inspection of table I shows that although there is a slight relative increase in the fraction of late-type galaxies, it is too small to account by itself for the behavior observed in $l_p(s)$. In fact, the curve derived for S8 is very similar to N8 and to N4 and S4. Therefore, we are led to conclude that the behavior of the curve for S6 is not due to morphological effects. A more likely explanation was found by looking at the way the structures grow as a function of neighborhood radius. From this inspection we saw that two of the walls that were observed in the south (da Costa et al. 1988) grow until s = 0.6, when the growth of these dominant structures slows down, preventing percolation. Critical percolation only occurs when a few galaxies lying in between allow them to become connected. This effect is similar to the volume-effect discussed at some length by Dekel and West (1985). Further support to this interpretation comes from figure 4d where we show the curves obtained for subsets of the N6 and S6 samples consisting of galaxies with radial velocities less than 4000 km/s. In this case the percolation properties of the northern and southern samples are very similar between

themselves and to the curves obtained for N4 and S4.

iii) Shape Properties

Another aspect of the galaxy distribution that has been debated over the years is whether galaxies are distributed primarily along filamentary or two-dimensional structures. Examples of both kinds of structures have been given in the literature (e.g. Chincarini et al. 1983, de Lapparent et al. 1986, da Costa et al. 1988) and it is thought that this information may contribute to elucidate the most likely scenario for the formation of large-scale structures. As shown by Einasto et al. (1984), in their study of the Local Supercluster, cluster analysis provides information that can be used to address this issue. In particular, the axial ratios of the largest structure can be examined as a function of the radius s. A severe limitation of this method is that it depends on the properties of a single structure and thus subject to large statistical fluctuations. It is nevertheless instructive to examine how the shapes of the largest structures in the CfA1 and SSRS compare.

The shapes of structures were examined by computing the principal moments $I_1 > I_2 > I_3$ of the distribution of galaxies associated to the largest structure, and the axial ratios $e_1 = I_2/I_1$ and $e_2 = I_3/I_2$. The comparison between the different volume-limited samples of the CfA1 and SSRS is shown in figure 5. We also show in these figures the random samples. These are an useful reference since, at large s, they should reflect the shape of the surveyed volume. On the other hand, at small s the random sample provides little information since it evolves rapidly to

singles or groups with a small number of particles for which the principal moments are not meaningful and subject to large statistical fluctuations. In real distributions the range of s where we can hope to get useful information is also restricted. At small s we may pick out the nearly round cores of dense systems while at large s the axial ratios of the largest structure should approach the values of the random distribution since they are probably cut by the borders of the survey region. These words of caution clearly show that the information one can expect to get from this test is limited and subject to large uncertainties. Nevertheless, it is interesting to find that despite localized fluctuations the general behavior of the axial ratios is very similar for all samples. From these plots we find at least some evidence that galaxies are preferentially in flat structures not in filaments, giving some quantitative support to the visual impression obtained examining the data; while e_1 is typically greater than 0.8, e_2 is in general less than 0.4 for $s < 1$. As expected, for larger values of s the axial ratios of the largest structures approach those obtained in the random distribution of points. Also interesting is the fact that even for the smallest s no significantly round systems are detected. In the N4 sample, there is a slight increase in e_2 for $s = 0.2$, but the system is still significantly flat, despite the presence of the Virgo cluster. This possibly reflects the fact that for this sample $s = 0.2$ corresponds to a scale of $1h^{-1}$ Mpc and we are still seeing the flatness of the Local Supercluster well illustrated in the plots of Einasto et al. (1984). The weakness of the method is illustrated by the large fluctuations observed in the southern sample for instance with large peaks at $s = 0.4$ for S4 and at $s = 0.6$ for S6.

Although the interpretation of the preceding plots is not as straightforward as one would wish for a statistical indicator, we believe that the curves presented reflect, within a limited range of s, the intrinsic geometry of the systems. This result is at least indicative of the presence of flat systems where the two longest axes are significantly larger than the shortest. As mentioned above this is consistent with the visual impression when following the growth of the structures. In particular, in the SSRS sample we can clearly identify for $s > 0.3$ the "walls" mentioned in da Costa et al. (1988). The largest structure of the CfA1 sample seems to have a similar shape as shown by Einasto et al. (1984).

b) Cell Method

Complementary information about the properties of the galaxy distribution can be obtained using a continuous density function instead of the discrete point distribution. A density function, ρ, is constructed by counting galaxies in cubic cells, centered at points which define a lattice that is superposed onto the survey region, and applying a smoothing process. For a given threshold density ρ_c, adjacent cells with densities $\rho \geq \rho_c$ are taken to be part of the same system and by varying ρ_c we can perform the same kind of analysis described in the preceding section. The main advantage of using this method is that high-and low-density regions can be treated on an equivalent basis, and it is more suitable for computing quantities such as filling factor and volumes and studying the properties of voids. Furthermore, the results as a function of a threshold density ρ_c, can be expressed in terms of a more

meaningful quantity than the neighborhood radius, namely the density contrast, $\delta = \rho_c/\rho_m$, where $\rho_m = (\Sigma\ \rho_i\ \Delta V_i)/V$ is the mean density and ΔV_i is the volume of a cell. This method of analysis has been recently applied by Einasto and Saar (1987) to reexamine the vicinity of the Local Supercluster.

From the maps of the galaxy distribution of the southern survey we estimate that the large-scale structures are typically $5h^{-1}$ Mpc wide and various tests showed that these structures can be well described with a grid resolution (cells) of $2h^{-1}$ Mpc, which is comparable to the scale of the distortions associated with virial motions in small groups. However, to avoid large fluctuations we have smoothed the density function by calculating the density associated to a cell from counts of galaxies in boxes with sizes $4h^{-1}$ Mpc, centered in each cell.

In order to illustrate some of the properties that can be derived from the application of the method, in the present analysis we only consider the samples N4 and S4, which give better statistics since the number of galaxies decreases rapidly with the depth. In figure 6 we compare the variation of the following quantities as a function of the density contrast: in panel (a) the ratio l_p of the length of the largest system to the characteristic length of the survey volume, defined above; in panel (b) the fraction f_v of the total volume occupied by the largest system; in panels (c) and (d) the axial ratios e_1 and e_2, defined as in the preceding section. Like the cluster analysis, the cell-method leads us to the conclusion that the properties of the galaxy distribution in both hemispheres are essentially the same. Both samples percolate roughly at

the same density contrast (figure 6a), which in our case occurs at log δ of about 0.6, consistent with that determined by Einasto and Saar (1987). The largest systems occupy roughly the same fraction of the total volume $\approx$ 5% (figure 6b) at percolation. This fraction is nearly equal to the filling factor of the whole sample, indicating the high degree of connectedness of the structures. These are primarily flat as measured by their axial ratios (figure 6c,d). Only for density contrasts greater than 16 do the structures become somewhat rounder. Complementing this information we plot in figure 7 e_1 x e_2 for structures with more than 5 cells right before critical percolation at log δ = 0.8. As can be seen at this density contrast most structures, in both hemispheres, have $e_1 > e_2$ showing some tendency of being oblate figures.

c) Nearest-Neighbor Distance Distribution

A full understanding of the galaxy distribution must necessarily address the properties of voids which are undoubtedly a fundamental characteristic of the galaxy distribution. Large empty regions with long dimensions up to $60h^{-1}$ Mpc have been identified in different regions of space by several authors underscoring the fact that they may be quite common (Kirshner et al. 1981, de Lapparent et al. 1986, Postman et al. 1987, da Costa et al. 1988a,b, Pellegrini et al. 1988). In order to investigate how the properties of voids compare in both hemispheres we use the nearest neighbor distribution test described by Ryden and Turner (1984), applying it to our volume-limited samples. To use this test we first define a three-dimensional grid filling the volumes considered, with

a cell size given by the mean interparticle distance of each sample; next we calculate for each grid point the distance to the nearest neighboring galaxy, constructing in the process the nearest neighbor distribution which measures the probability that the nearest galaxy to a grid point is at some distance r. The shape of this distribution is an indication of the size of the voids in the galaxy distribution.

Here we use the normalized nearest neighbor distribution to compare the characteristics of voids in the northern and southern samples. This comparison is shown in figure 8. We note that our results for the northern samples are not identical to those presented by Ryden and Turner (1984) because of small differences in the definition of the volume -limited sample. From figure 8a we find that the distributions obtained for the S4 and N4 samples are almost identical. The only difference, probably not significant, is that the size of the largest void in the southern volume is roughly $11h^{-1}$ Mpc slightly smaller than that found in the North with a size of about $12h^{-1}$ Mpc. We note that the latter value is comparable to that determined by Soltan (1985) for the CfA1 sample using a different method. The same is not true when the samples S6 and N6 are compared (figure 8b), with S6 showing a more extended tail than that observed in the curve for N6. This more extended tail suggests that the frequency of large voids in the south is higher than in the north. It is interesting that this difference occurs for samples defined in the same volume for which we have already noticed a peculiar behavior in the percolation properties. Note that this effect is not present for the samples limited at 8000 km/s; in this case the distributions for S8 and N8 have almost identical shapes, as can be seen in figure 8c.

Again we examine the behavior of subsets of S6 and N6 for galaxies with radial velocities less than 4000 km/s. The corresponding distributions are plotted in figure 8d, where we find that the extended tail has essentially disappeared, indicating that this effect is not associated to luminosity or morphology. A tentative explanation for this effect is given in section IV.

IV. CONCLUSIONS

In this paper we have attempted to address the important question of whether the available wide-angle redshift surveys like the CfA1 and the SSRS probe a sufficiently large volume of space to be considered a fair sample of the universe. Towards this goal we have compared the results of the application of various statistics to these samples. These tests have been frequently used in the past to analyze the clustering properties of real and model distributions. The question of reproducibility is fundamental since the available galaxy catalogs have been extensively used in recent years to confront the results of N-body simulations with observations. In order to be confident about the conclusions drawn in these various works one must have some indication that we are already approaching a fair sample with the present surveys. The availability of the SSRS, probing a volume comparable to the CfA1, enables us to attempt to answer this question for the first time.

Based on the results presented in the previous sections two very different conclusions can be drawn: either the statistical indicators used are insensitive and should be discarded in future analyses, or else, the properties of the distribution of galaxies in both hemispheres are remarkably similar out to $80h^{-1}$ Mpc, despite the known differences in appearance that were discussed by da Costa et al. (1988). This conclusion is based on the fact that all tests utilized in this paper when applied to the northern and southern samples yield very similar results. Some differences were detected when considering volume-limited samples to $60h^{-1}$ Mpc. For this samples we have found that the southern sample

percolates slower and has a larger frequency of large voids as compared to a similar sample in the northern hemisphere. Two possibilities should be considered; either it reflects the uncertainties associated to the methods of analysis or it is a real physical effect. Note that these differences are measured by to complementary statistical indicators like percolation and nearest-neighbor distribution which are sensitive to high and low densities regions, respectively. If the effect is real it could be revealing a dependence of the properties of the galaxy distribution with luminosity (if diameters correlate with luminosity) or morphology. However, as discussed in the previous sections this does not seem to be the case since when limiting the galaxies in the S6 and N6 samples to the volume of N4 and S4 the effect disappears. Nor it is present when the samples N8 and S8 are considered. An alternative explanation is that these differences are reflecting the existence of a characteristic scale of the galaxy distribution. This would be the case if the galaxy distribution consisted of a network of cells, with a characteristic scale of about $60h^{-1}$ Mpc, with galaxy sheets surrounding empty regions. In this case, when analyzing a volume with a diameter comparable to that scale, the statistical indicators would depend critically on the position of the sample volume relative to the network. If the sample volume contains a vertex near its center, percolation will be easy and the voids will tend to be smaller than when the volume contains the center of a cell. This model would account for the differences encountered since the Virgo supercluster is conspicuous in the northern sample, while large voids are the dominant structures in the south. However, it is somewhat premature to draw definite conclusions on the basis of the present data. Other explanations may be possible and whether indeed we have proved

that the available data give a fair picture of the universe at large scale must be confirmed by deeper surveys.

ACKNOWLEDGMENTS

We thank our several collaborators in the SSRS for allowing us to use the data before publication and M. Davis and J. Huchra for providing us with a copy of the CfA1 data.

REFERENCES

Bhavsar, S. P., Gott, J. R. and Aarseth, S. J. 1981, Ap. J. **246**, 656.

Bhavsar, S. P. and Barrow, J. D. 1983, M. N. R. A. S., **205**, 61P.

Chincarini, G. L., Giovanelli, R. and Haynes M. P. 1983, Astr. Ap., **121**, 5.

da Costa, L. N., Pellegrini, P. S., Sargent, W. L. W., Tonry, J., Davis, M., Meiksin, A. and Latham, D. 1988, Ap. J. **327**, 544.

Davis, M., Meiksin, A, Strauss, M., A., da Costa, L. N., and Yahil, A. 1988, preprint.

Davis, M. and Huchra, J. 1982, Ap. J., **254**, 437.

Dekel, A. and West, M. J. 1985, Ap. J., **288**, 411.

de Lapparent, V., Geller, M. and Huchra, J. P. 1986, Ap. J. (Letters), **302**, L1 (LGH).

Einasto, J. and Saar, E. 1987, IAU Symp. 124, Observational Cosmology, ed. A. Hewett, G. Burbidge and L. Z. Fang (Dordrecht: Reidel), p. 349.

Einasto, J., Klypin, A. A., Saar, E. and Shandarin S. F. 1984, M. N. R. A. S., **206**, 529.

Gott, J. R., Melott, A. and Dickinson, M. 1986, Ap. J. **306**, 341.

Gott, J. R. and Turner, E. L. 1977, Ap. J., **216**, 357.

Huchra, J. P., Davis, M., Latham, D. and Tonry, J. 1983, Ap. J. Suppl., **52**, 89.

Kirshner, R. P., Oemler, A., Schechter, P. L. and Shectman, S. A. 1981, Ap. J. (Letteres), **248**, 493.

Lauberts, A. 1982, The ESO/Uppsala Survey of the ESO(B) Atlas (Munchen: European Southern Observatory).

Maurogordato, S. and Lachieze-Rey, M. 1987, Ap. J., **320**, 13.

Pellegrini, P. S., da Costa, L. N., Huchra, J. P., Latham, D. W. and Willmer, C. N. A. 1988, in preparation.

Postman, M., Huchra, J. P. and Geller, M. J. 1986, A. J. **92**, 1238.

Ryden, B. S. and Turner, E. L. 1984, Ap. J. (Letters) **287**, L59.

Sargent W. L. W., Tonry, J., da Costa, L. N., Pellegrini, P. S., Davis, M., Meiksin, A. and Latham, D. W. 1988, in preparation.

Schaeffer, R. 1984, Astr. Ap., **134**, L15.

Shandarin, S. F. 1983, Pis'ma Astr. Zh., **9**, 195.

Soltan, A. 1985, M. N. R. A. S., **216**, 537.

Soneira, R. M. and Peebles, P. J. E. 1978, Astron J., **83**, 845

Weinberg, D., Gott, R. and Melott, A. 1987, Ap. J. **321**, 2.

White, S. D. M. 1979, M. N. R. A. S., **186**, 145.

Zel'dovich Ya. B., Einasto, J. and Shandarin, S. F. 1982, Nature, **300**, 407.

TABLE I

	S4	N4	S6	N6	S8	N8
N_g	300	431	343	266	224	213
$V(10^4 Mpc^3)$	3.7	3.9	12.8	13.1	29.8	31.6
r_0	5.0	4.5	7.2	7.9	11.0	11.4
L_c(Mpc)	33.3	33.9	50.4	50.8	66.8	68.1
% early	21	30	23	33	18	46
% late	79	70	77	67	82	54

FIGURE CAPTIONS

Figure 1. Multiplicity functions for the samples volume-limited at 4000 km/s (a), 6000 km/s (b) and 8000 km/s (c) for six values of the neigborhood radius s. Continuous histograms represent the subsamples of the SSRS, while dashed histograms those of the CfA northern sample.

Figure 2. Fraction of galaxies associated to small (α), intermediate (β) and large (γ) groups as a function of the neigborhood radius s for the samples S4 and N4 (a), S6 and N6 (b) and S8 and N8 (c). Subsamples of the SSRS are represented by continuous curves, those of the CfA northern sample by dashed curves and a Poisson distribution by dotted curves.

Figure 3. Fraction of "isolated galaxies" for the samples S4 and N4 (triangles), S6 and N6 (squares) and S8 and N8 (pentagons), as a function of the neigborhood radius. SSRS subsamples are represented by full symbols and continuous curves while CfA subsamples are represented by empty symbols and dashed curves.

Figure 4. Variation of the percolation parameter l_p for the largest system identified in the samples S4 and N4 (a), S6 and N6 (b), S8 and N8 (c) and S6 and N6 volume-limited at 4000 km/s (d), as a function of the neigborhood radius. Simbols and curves are as in figure 3. Results for a Poissonian distribution are shown as dotted curves.

Figure 5. Variation of the axial ratios e_1 and e_2 of the largest system identified in the samples S4 and N4 (a), S6 and N6 (b) and S8 and N8 (c) as a function of neigborhood radius. Symbols and curves are as in figure 3.

Figure 6. Percolation parameter (a), fractional volume (b) and axial ratios e_1 (c) and e_2 (d) for the largest structure identified in samples S4 (full symbols, continuous curve) and N4 (empty symbols, dashed curve) as a function of the logarithm of the density contrast. The dotted curves show the results for a Poisson distribution.

Figure 7. Location in a plane defined by the axial ratios e_1 and e_2 of structures with more than 5 cells identified at log δ = 0.8. Full symbols denote the results for S4 and empty symbols, those for N4.

Figure 8. Histogram of the fraction of points at a normalized distance s from galaxies in the samples S4 and N4 (a), S6 and N6 (b), S8 and N8 (c) and S6 and N6 volume-limited at 4000 km/s (d). Continuous histograms denote subsamples of the SSRS and dashed histograms subsamples of the CfA northern sample.

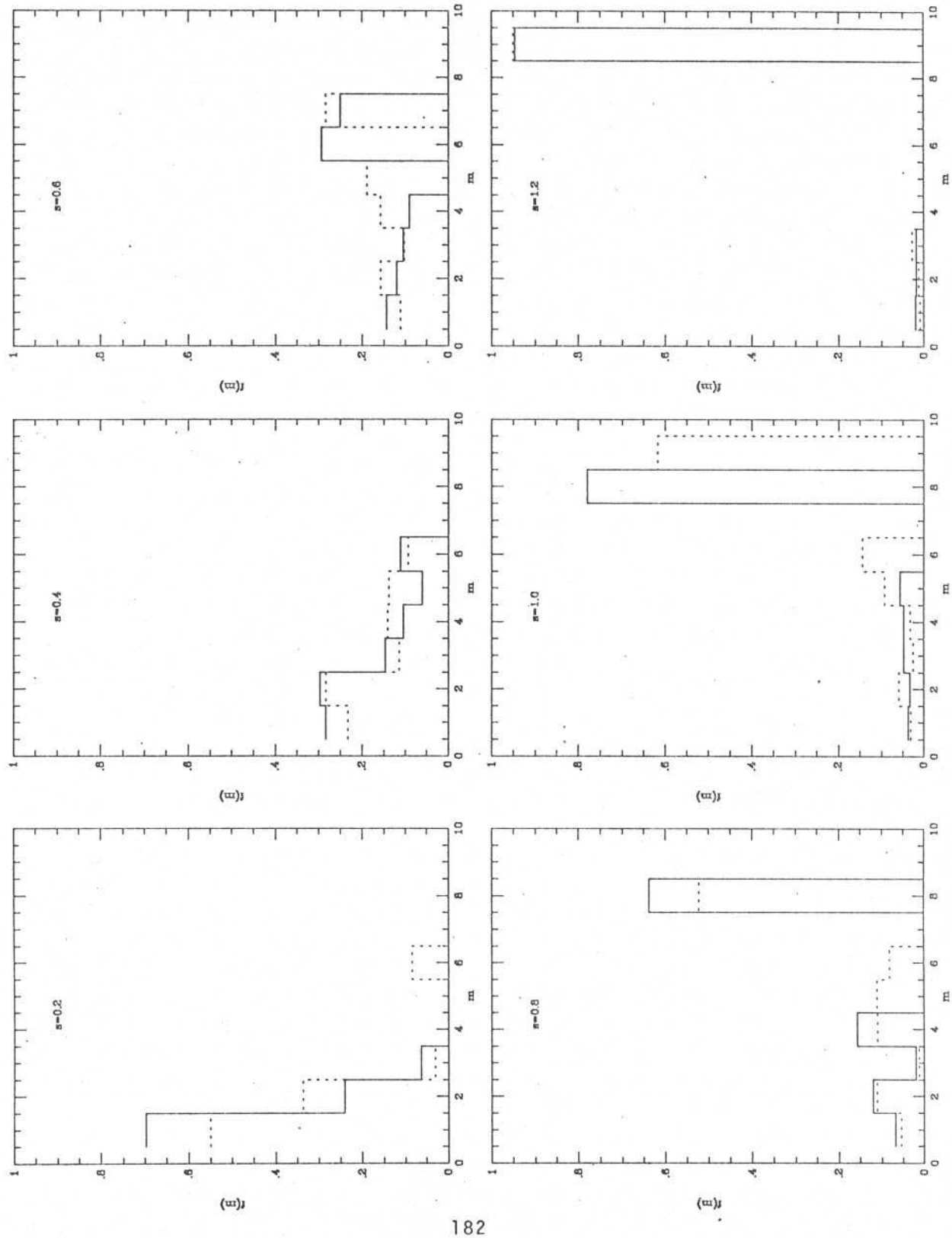

Figure 1a

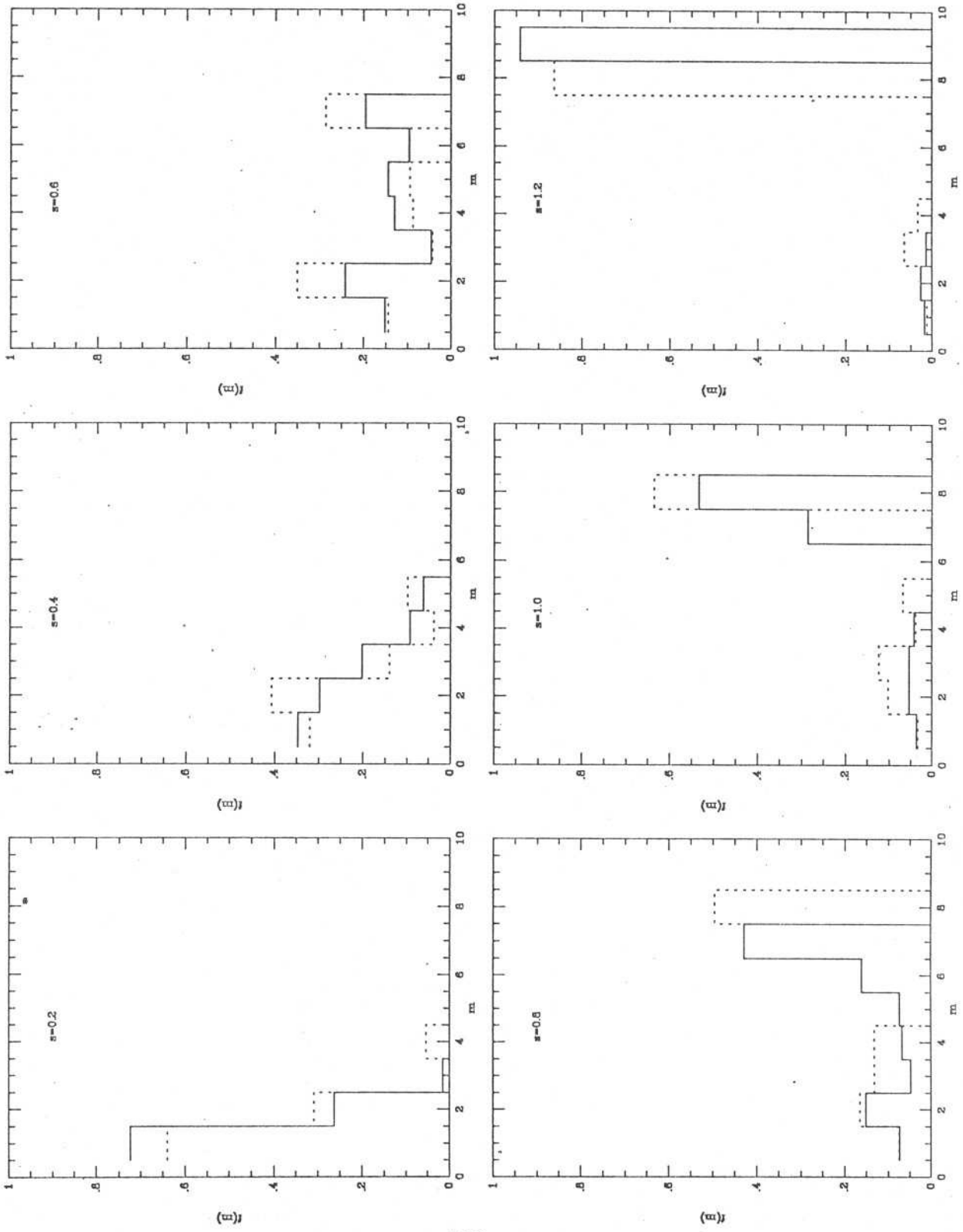

Figure 1b

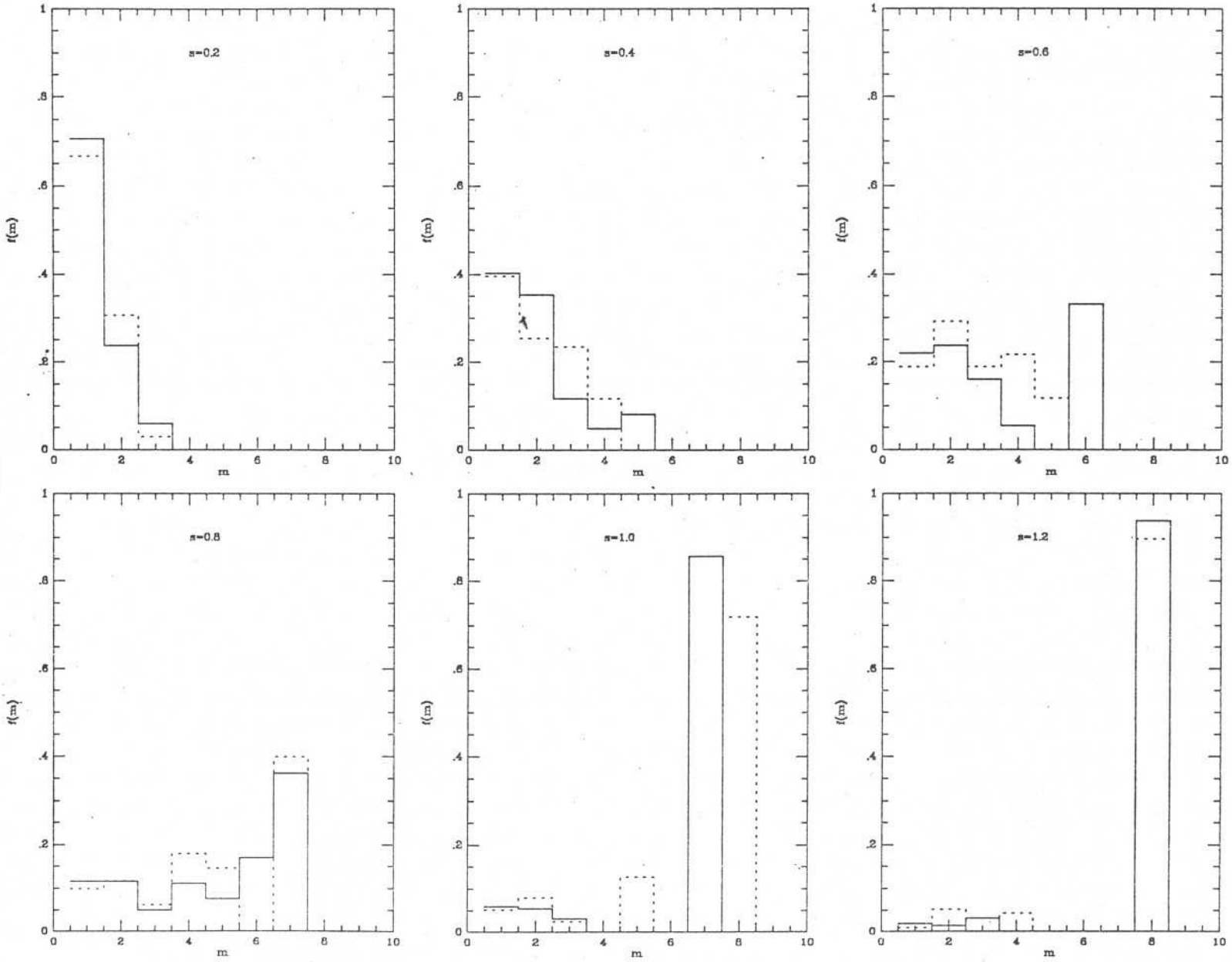

Figure 1c

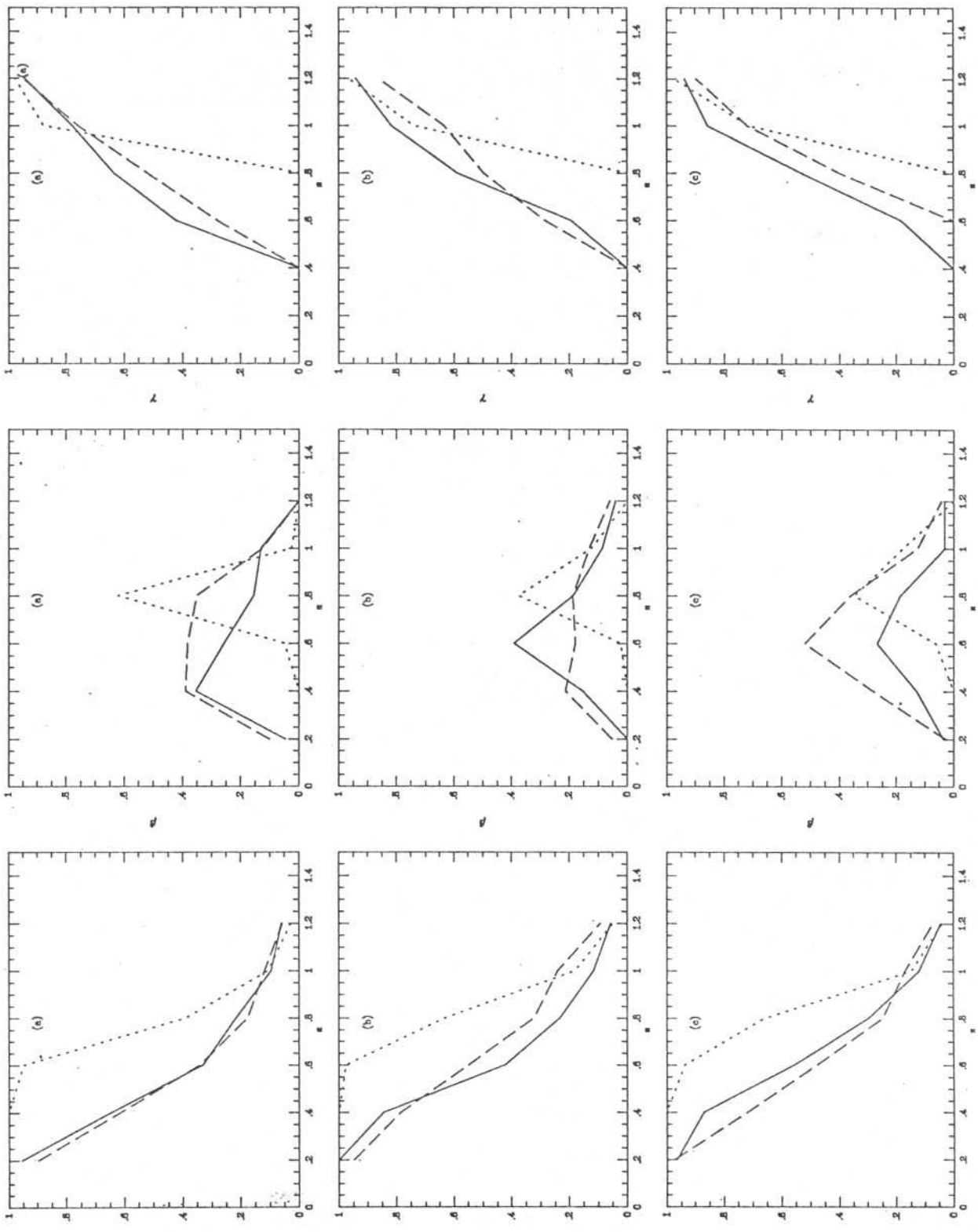

Figure 2

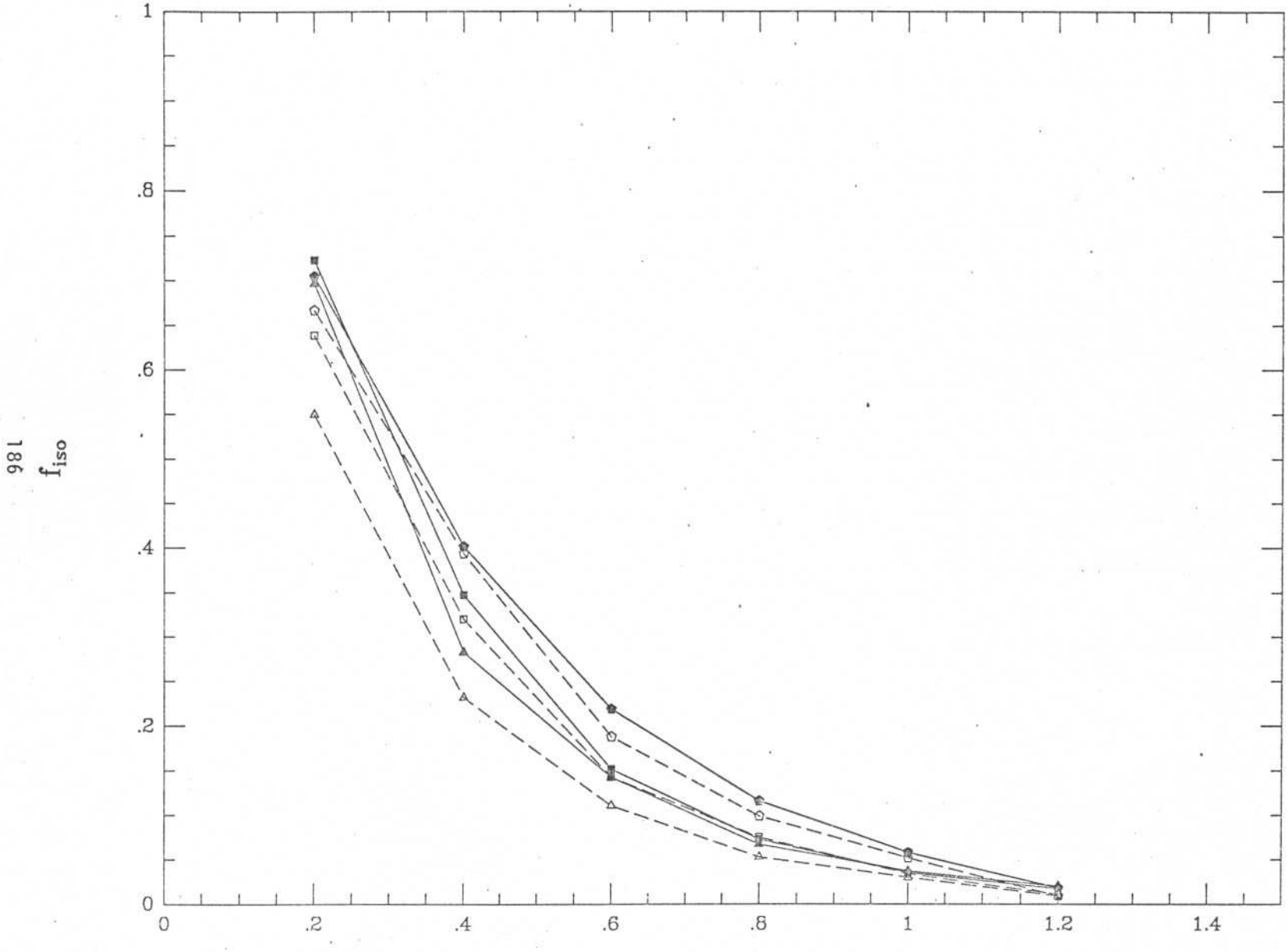

Figure.3

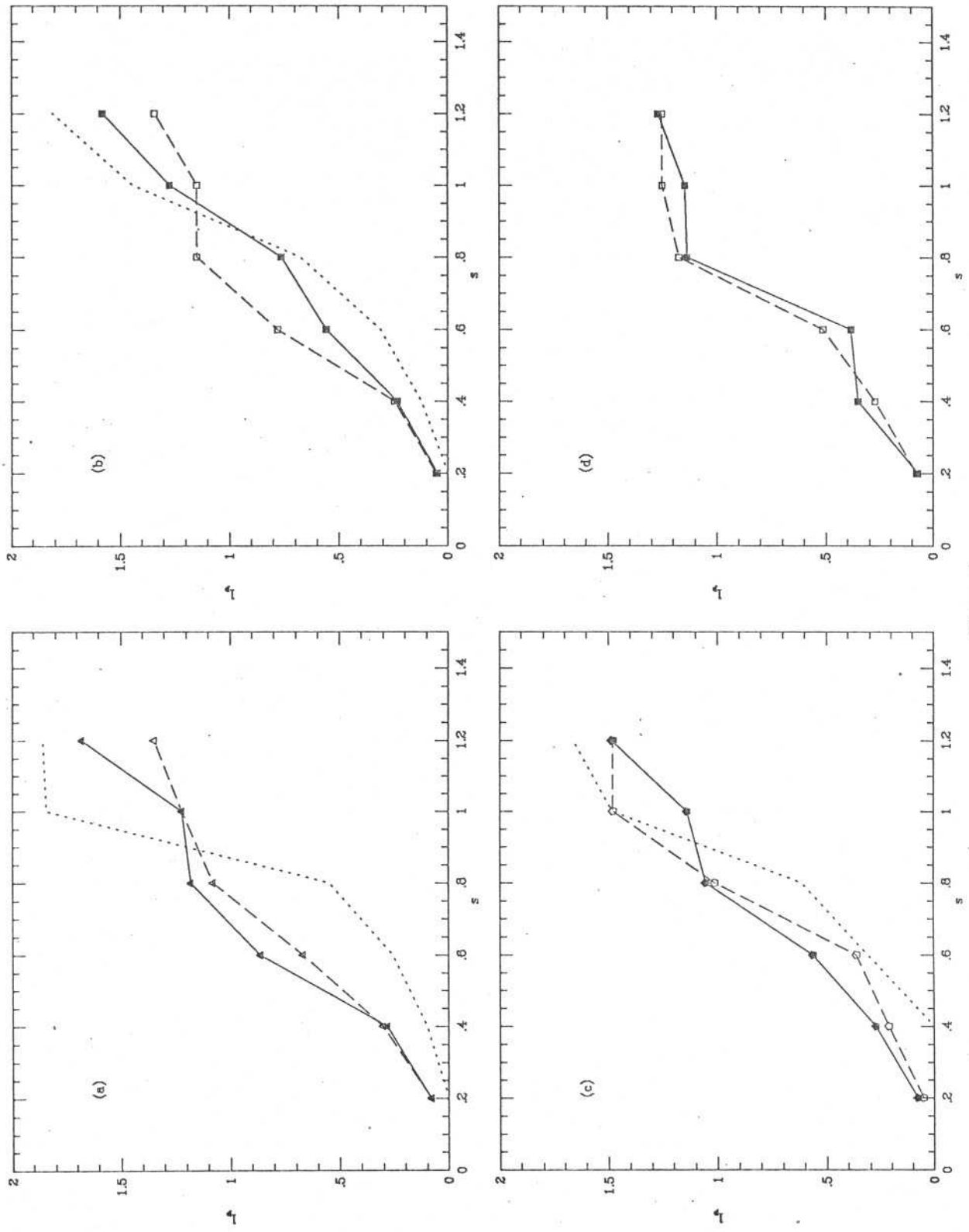

Figure 4

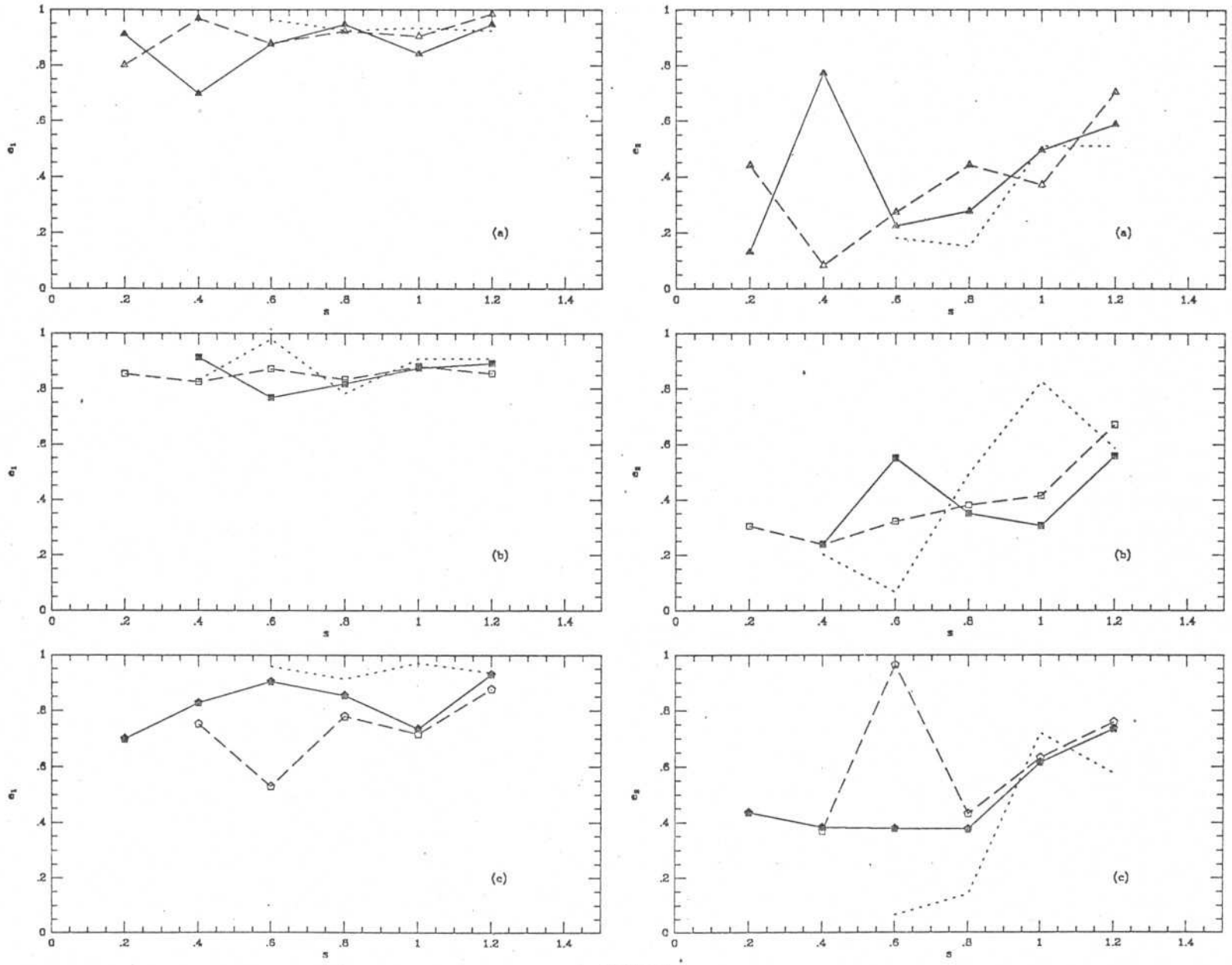

Figure 5

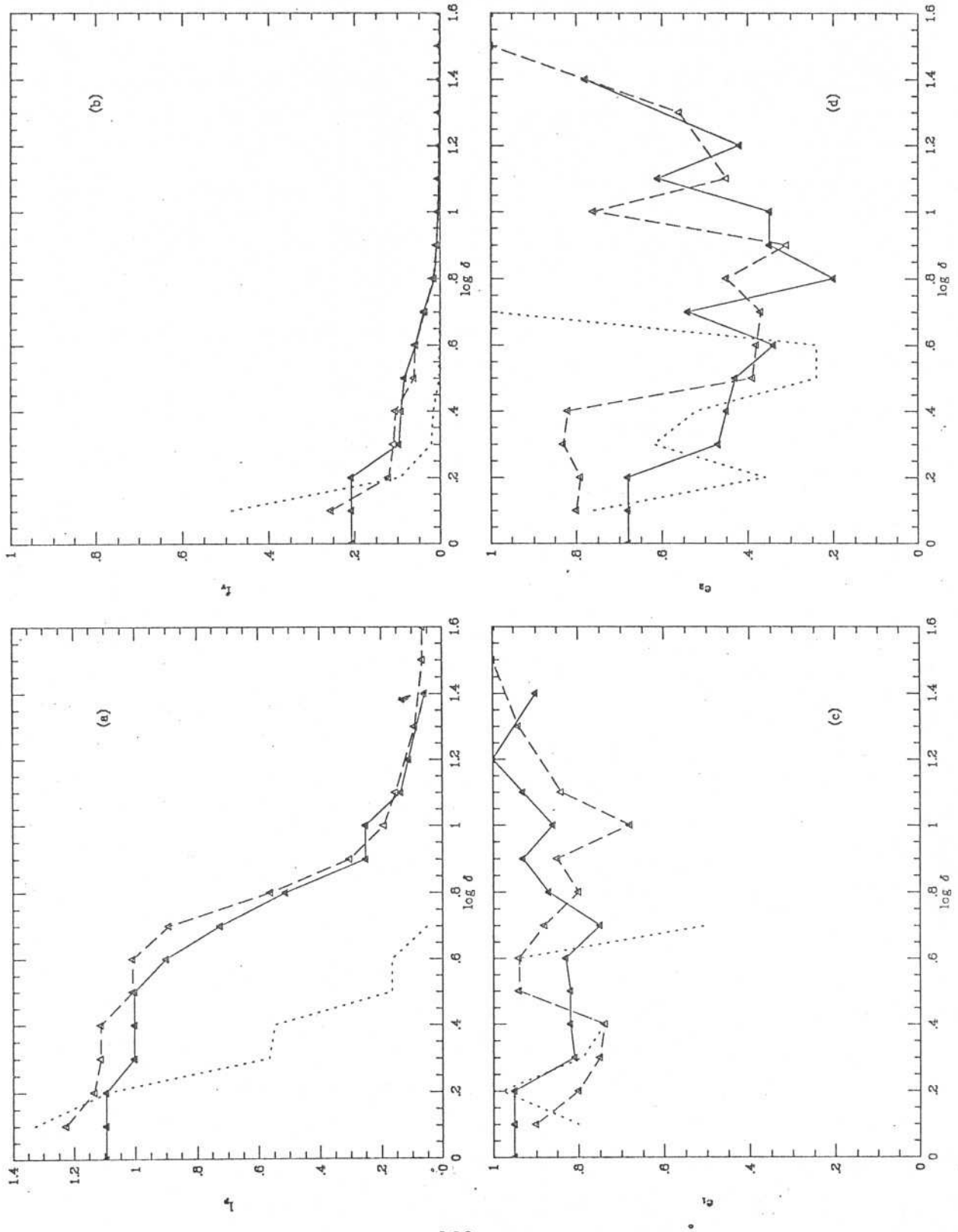

Figure 6

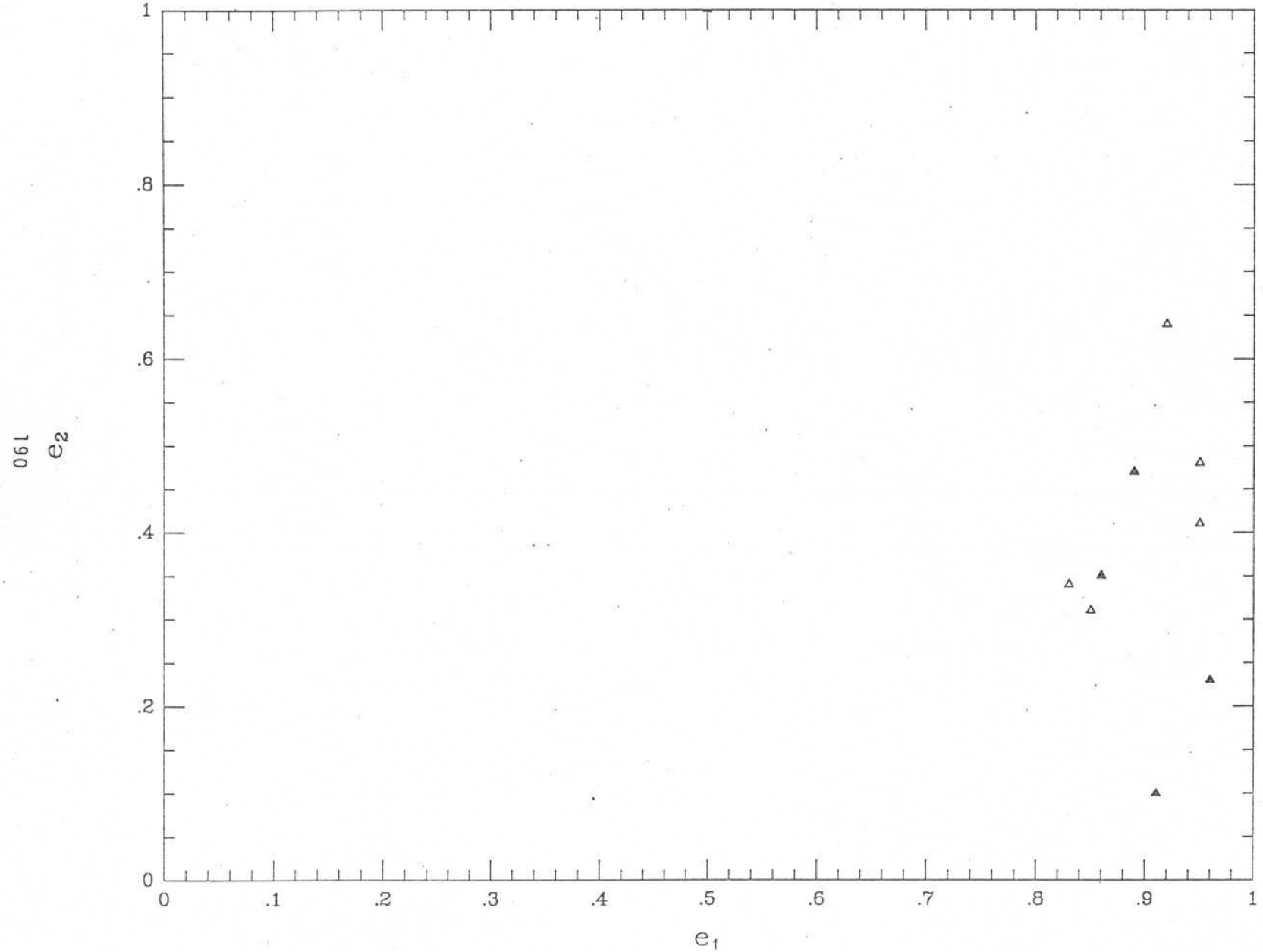

Figure 7

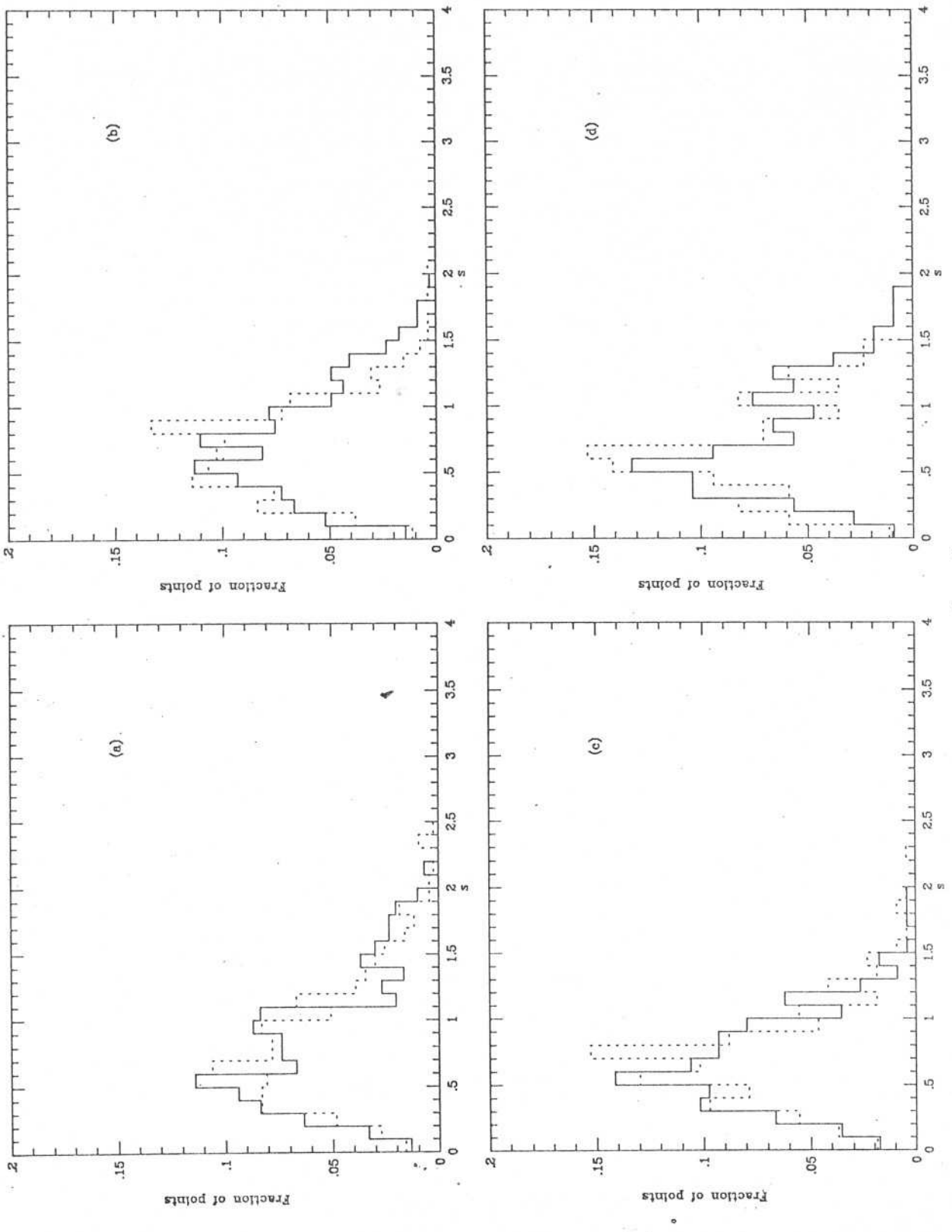

Figure 8

V.2 PROPRIEDADES DOS VOIDS DO SSRS

VOIDS IN THE SOUTHERN SKY REDSHIFT SURVEY

Paulo. S. Pellegrini, L. Nicolaci da Costa and R. R. de Carvalho

Departamento de Astronomia, CNPq/Observatório Nacional

ABSTRACT

In this paper we present a quantitative method for searching voids in a three-dimensional galaxy distribution. The method is based on the analysis of a smoothed density function, constructed from the original discrete galaxy distribution. The main advantage of the method is that it allows the investigation of the geometrical properties of underdense regions as a function of the density threshold. We illustrate our method by applying it to the recently completed Southern Sky Redshift Survey (SSRS), where conspicuous regions devoid of galaxies are noticeable from a visual inspection of the redshift maps. In fact, we find from our quantitative analysis that these voids have volumes comparable to that of Bootes, indicating that large voids may be a common feature of the galaxy distribution.

I. INTRODUCTION

Studies of the large-scale structure of the universe have revealed that galaxies tend to concentrate in high-density clusters and lower density filaments or sheet-like structures that delineate large regions devoid of bright galaxies (e.g. Davis and Huchra 1982, Haynes and Giovanelli 1986, de Lapparent et al. 1986, da Costa et al. 1988). Recently, voids have received a great deal of attention, especially after the discovery of the large empty region in Bootes with an estimated diameter that could be as large as $60h^{-1}$ Mpc (H_0 = 100 km/s/Mpc) (Kirshner et al. 1981). The interest in the properties of voids comes from the fact that their existence may place additional constraints on theories for the formation and evolution of large-scale structures. For instance, it has been pointed out that the existence of very large voids would argue against scenarios in which large scale structures develop from smaller ones via hierarchical clustering (e.g. Davis et al. 1985). On the other hand, explosive models (Ostriker and Cowie 1981) leading to the formation of bubbles, would be strongly favored if voids completely enclosed by galaxies were discovered (cf. de Lapparent et al. 1986).

The possibility of drawing important clues about the origin of structures in the universe, from the low density regions, have led several authors to examine in more detail the statistical and geometrical properties of voids detected in real galaxy catalogs, comparing these results with those obtained from a variety of models of galaxy clustering. For instance, statistical studies carried out by Vettolani et al. (1985) and

Soltan (1985) indicate that the hierarchical model cannot be ruled out on the basis of the available data. On the other hand, using the distribution of nearest neighbor distances, Ryden and Turner (1984) have found that voids observed in the magnitude-limited sample of the CfA Redshift Survey (Huchra et al. 1983), are significantly larger than those detected in some numerical simulations. Recently, the same statistics has been applied by Saarinen et al. (1987) to show that the large-scale distribution of galaxies attained in a N-body simulation of an explosive model is at least consistent with the observational data.

The task of extracting information about the nature of primordial perturbations, from the properties of the present day galaxy distribution, has also been considered from a different point of view by Gott et al. (1986). Instead of focusing attention on the characteristics of low and high-density regions separately, they have examined the galaxy distribution in terms of its topology, considering for that purpose a smoothed density function to represent the discrete distribution of data points. In particular, they argued that the median density surface of the CfA catalog has a sponge-like topology with the high- and low-density regions being equivalent and interlocking. This result has been verified by Weinberg et al. (1988) who studied the topology of the CfA sample measuring the genus of constant density surfaces at different threshold densities. Comparison of these measurements with the analytical formula derived by Hamilton et al. (1986) indicates that the observed galaxy distribution is consistent with models that invoke random phase primordial density fluctuations for the origin of structures in the universe.

Although the observational sample used in these studies is small, they demonstrate the power and the usefulness of the topology statistics. Therefore it would be very interesting to extend this analysis to the sample of the recently completed Southern Sky Redshift Survey (SSRS) (da Costa et al. 1988). In the present paper, however, we have a more modest goal and follow the suggestion of Gott and collaborators, of looking at the galaxy distribution as a smoothed density function, to make a quantitative study of the properties of the low-density regions.

We recall that an outstanding feature of the redshift maps presented by da Costa et al. (1988) of the region sampled by the SSRS, is the existence of prominent nearby underdense regions. The advantage of the method employed here, over those used in the past (Vettolani et al. 1985, Soltan 1985), is that this can be done as a function of the density contrast relative to the mean. In section II we describe the method of analysis used here, applying it in section III to the diameter-limited sample of the southern galactic cap. A summary of our results is presented in section IV.

II. METHOD OF ANALYSIS

In order to search for voids in the galaxy catalog, we take a similar approach to that of Gott et al. (1986), and consider a smooth, continuous, density fuction, instead of the actual discrete galaxy distribution. Since we are primarily interested in detecting voids, the smoothing scale should be of the order of the mean interparticle distance of a random distribution with the same number of points as the galaxy distribution being analyzed. Furthermore, for a sample with a well-defined selection criterion we may consider the whole galaxy distribution in the analysis, if the observational selection effects introduced by the magnitude or diameter cut are properly taken into account.

In the present analysis we have adopted the following procedure. First, we consider the galaxy distribution in a Cartesian coordinate system and superimpose a cubic lattice with a specified grid spacing. Next, we calculate the appropriate selection function, which measures the fractional loss of galaxies as a function of the radial distance (e.g. Davis and Huchra 1982), for the catalog being investigated and generate a random catalog with the same number of points and satisfying the same selection function. We then count the random points within a so-called search box centered at each cell but with a size that scales inversely as the cubic root of the selection function. We choose a value for the search box at some fiducial distance r_f and vary it until the full cells percolate, filling all the space. This value for the search box at r_f is then used to analyze the galaxy distribution. For each cell a local

density is defined as the total number of galaxies within the local search box divided by its volume, interior to the boundary of the survey, and the local value of the selection function, to account for the galaxies missed in the catalog. The sampling correction adopted here is the same as that used by Huchra and Geller (1982) and Maia et al. (1988) in their group analyses algorithm and by Vetollani et al. (1986) for locating voids, in magnitude- and diameter-limited surveys. This correction creates geometrical distortions in the distribution of galaxies but, as discussed below, they should not affect our main results.

The important point of analyzing a smooth density function is that the geometrical properties of the underdense regions can be investigated as a function of the density contrast relative to the mean density defined as

$$<\rho> = \sum \rho_i \, dV_i / V$$

where V is the total volume of the region being considered, dV_i the volume of the ith cell box and ρ_i its density. Since the typical galactic density of underpopulated regions in the universe is not known, we use the word void to denote the ensemble of contiguous cells with densities below a given threshold. We consider two cells to be contiguous if they are in contact either through their faces, edges or vertices. The algorithm used to keep track of the connected cells is just an extension to three-dimensions of a routine previously used for automatic-detection of images on photographic plates (Chan et al. 1985). Once a void is

identified, we calculate its mean position, total volume, unweighted and density weighted principal moments ($I_1 > I_2 > I_3$) and the ratios $e_1=I_2/I_1$ and $e_2=I_3/I_2$ which can give, in principle, some useful information about its shape. For an oblate system $e_1 \approx 1$, while for a prolate $e_2 \approx 1$.

III. RESULTS

The method described above was used to search for voids in the southern galactic cap where we have recently completed a redshift survey of a diameter-limited sample. The sample consists of all galaxies from the ESO catalog (Lauberts 1982) in the region $b \leq -30°$ and declination south of -17.5°, satisfying the condition $\log D(0) > 0.1$, where $D(0)$ is a "face-on" diameter defined by da Costa et al. (1988). The sample contains 1930 galaxies out of which 1657 redshifts are available in the SSRS. The remaining are low-surface brightness objects for which we could not obtain an optical redshift. In the present analysis we only consider galaxies with radial velocities less than 10000 km/s.

The analysis was performed considering a cubic lattice superimposed to the galaxy distribution represented in a Cartesian coordinate system with the x and y-axes lying in the equatorial plane and in the directions $\alpha = 18^h$ and $\alpha = 0^h$, respectively, and the z-axis pointing towards the south celestial pole. In figure 1 we show the x-y projection of the galaxies between $20 < z < 60h^{-1}$ Mpc, in intervals of $10h^{-1}$ Mpc in z. In this figure we show the slices that are the least affected by the boundary of the survey and encompass the largest volume. The presence of intersecting sheets which separate large empty regions is quite obvious and dominate the clustering pattern of the galaxies. We note that in this coordinate system voids 1, 3 and 4 described in da Costa et al. (1988) are easily seen in figure 1a at (-15, 10), in figure 1b at (10, 40) and in figure 1c at (-55, 40), respectively; the x and y coordinates are expressed in h^{-1}

Mpc units.

The smooth density function associated with the galaxy distribution was constructed using grid cells of 2.5, 5 and $10h^{-1}$ Mpc. For each lattice, we varied the size of the search box at $r_f = 40h^{-1}$ Mpc, until all cells were full for a Poisson distribution with the same number of points and selection function as the galaxy sample. This procedure yielded a value of $10h^{-1}$ Mpc for the size of the search box, which was then used to calculate the density function for each cubic lattice. Figure 2 illustrates the smoothed density distribution, for a grid spacing of $5h^{-1}$ Mpc, showing density contrast maps for the same slabs of figure 1. In this figure one can have a good idea of how the survey volume looks in the Cartesian coordinate system used. Examination of these figures also show that the density function reproduces fairly well the main features of the observed galaxy distribution. In particular, voids 1, 3 and 4 described above are easily recognizable. Note that the smoothing gives a broader appearance to the dense structures, mainly those at large distances which are less well-sampled and consequently more affected by the bias correction.

In table I we compare the results obtained for the different grid spacing considered. In column 1 we give the size of the cell used; in column 2 the number of voids detected; in columns 3-5 the Cartesian coordinates of the center of the two largest voids, followed, in column 6, by their respective volumes. The voids which appear in table I were defined as regions occupied by empty cells ($\rho = 0$). From this table we

can see that the resolution of the underlying cubic lattice has little effect in the definition of the largest voids. Basically, increasing the resolution simply increases the total number of voids since smaller voids can be detected. However, the parameters characterizing the large voids are stable, except at the highest resolution considered, when the two largest voids in the sample merge. Since this connection occurs only locally and involves a small number of cells, in the analysis presented below we have used a grid spacing of $5h^{-1}$ Mpc, which leaves the two large voids as separate entities and seems to give a more realistic description of the underlying galaxy distribution.

In table II we summarize the properties derived for the empty voids detected in our sample with more than three cells. In column 1 we list the number of the void; in column 2, 3 and 4 the equatorial coordinates and the radial distance of their centers; in columns 5 and 6 their volumes and corresponding equivalent radii, $r_{eq} = (3V/4\pi)^{1/3}$; in columns 7 and 8 the shape parameters e_1 and e_2, calculated from the unweighted principal moments. A total of eight voids were identified with volumes ranging from 3×10^2 to $3 \times 10^4 h^{-3}$ Mpc^{-3}. Voids 6 and 8 are the largest and have approximately the same volume, corresponding to an equivalent radius of $20h^{-1}$ Mpc, and located at mean distances of 82 and $65h^{-1}$ Mpc, respectively. Visual inspection of the largest voids indicate that they do not have a well-defined shape and extend to the limit of our survey. The shape parameters suggest that, in general, the voids are triaxial showing some tendency of being oblate ($e_1 > e_2$). However, one must be careful interpreting these parameters since they are meaningful as long as

the voids are not too irregular and boundary effects are not important.

We have also examined the consequences of relaxing the criterion adopted in the definition of a void, setting the threshold at a density level of about 25% of the mean density. The results are shown in table III, where we list the same parameters described in table II, again for voids with more than three cells. As expected, all voids grow in size with some merging, reducing the total number of voids to 4. In particular, voids 6 and 8 of table II become connected, increasing the total volume to 1.3 x $10^5 h^{-3}$ Mpc^{-3}, comparable to that estimated for Bootes. In figures 3 and 4 we illustrate the effect of varying the threshold density, showing the cells belonging to the largest voids detected, for the same slabs of the previous figures; in figure 3 we show voids 6 and 8 of table II, while in figure 4 we plot void 4 of table III.

We should emphasize that the method described above yields a conservative estimate for the size and number of voids, since the smoothing tends to increase the size of the high-density regions. While the method described is not suitable for studying the properties of dense regions, it is useful for our purposes because it picks out only statistically significant voids since the scale for the smoothing process is set from a direct comparison with a random distribution. We should also mention that even working with a smooth density distribution it is hard to decide whether the big voids found in the survey should be considered connected; while they form separate entities for $\rho = 0$, they become connected for $\rho = 0.25 \langle\rho\rangle$.

IV. SUMMARY

The most interesting result of the present work is that we confirm from a quantitative analysis that in the region of space covered by the SSRS there are at least two underpopulated regions ($\rho < 0.25 \langle\rho\rangle$) with a total volume comparable to Bootes. The voids identified in the present analysis have rather irregular shapes, with the several separate low-density regions identified with $\rho = 0$, forming a connected structure at $\rho = 0.25 \langle\rho\rangle$ that extends to the boundaries of the survey volume, suggestive of a spongy topology. In the SSRS volume we find eight empty regions, completely devoid of bright galaxies ($\rho = 0$), with equivalent radii ranging from 4 to $20h^{-1}$ Mpc; while for the 25% density contrast relative to the mean, there are four voids with equivalent radii ranging from 5 to over $30h^{-1}$ Mpc. However, these estimates should be considered as lower limits since the method employed in the analysis tends to broaden the high-density regions. Our results give further support to the suggestion of Postman et al. (1986) that large voids may be a common feature of the galaxy distribution, placing stringent constraints on theories for the origin of large scale structures in the Universe.

The voids found in the region of the SSRS are of particular interest because they are close, with mean distances of 6500 and 8200 km/s, with their front edges reaching as close as 1000 km/s. Their proximity makes them good targets for future deeper optical surveys and 21-cm measurements of low surface brightness galaxies, to address the question

of whether voids are deficient of all types of galaxies (e.g. de Lapparent et al. 1986, Bothun et al. 1986, Thuan et al. 1986). Towards this end, we are presently extending the SSRS to fainter magnitudes, concentrating our observations in the declination range -30° to -40° where these voids are more conspicuous. Some preliminary results of this ongoing survey will be forthcoming.

ACKNOWLEDGMENTS

We thank all the people involved in the SSRS effort. L. N. da Costa thanks M. Geller for useful discussions.

REFERENCES

Bothun, G. D., Beers, T. C., Mould, J. R. and, Huchra, J. P. 1986, Ap. J., 308, 510.

Chan, R., Pellegrini, P. S., and da Costa, L., N. 1986, Rev. Mex. Astr. y Astrof., 12, 393.

da Costa, L. N., Pellegrini, P. S., Sargent, W. L., Tonry, J., Davis, M., Meiksin, A. and, Latham, D. 1988. Ap. J., 327, 544.

Davis, M. and Huchra, J. P. 1982, Ap. J., 254, 425.

Davis, M., Efstathiou, G., Frenk, C. S., and White, S. D. M., 1985, Ap. J., 292, 371.

de Lapparent, V., Geller, M. J. and, Huchra, J. P., 1986, Ap. J. (Letters), 302, L1.

Geller, M. J. 1988, "17th Advanced Course in Astronomy and Astrophysics, Saas-Fee, Switzerland, in press.

Gott, J. R., Mellot, A. L., and, Dickinson, M. 1986. Ap. J. 306, 341.

Hamilton, A. J. S., Gott, J. R., and Weinberg, D., 1986, Ap. J., 309, 1.

Haynes, M. and Giovanelli, R. 1986, Ap. J. (Letters), 306, L55.

Huchra, J., Davis, M., Latham, D., and Tonry, J. 1983, Ap. J. Suppl., 52, 89.

Huchra, J. P. and Geller, M. J. 1982, Ap. J., 257, 423.

Kirshner, R. P., Oemler, A., Schechter, P.L., and Schectman, S. A. 1981, Ap. J. (Letters), 248, L57.

Lauberts, A., 1982, The ESO/Uppsala Survey of the ESO (B) Atlas (Munchen: European Southern Observatory)

Postman, M., Huchra, J. P. and Geller, M. J. 1986, A. J. 92, 1238.

Ryden, B. S., and Turner, E. L. 1984, Ap. J. (Letters), 287, L59.

Saarinen, S., Dekel, A., and Carr, B. J. 1987. Nature 325, 598.

Soltan, A. 1985. M.N.R.A.S., 216, 537.

Thuan, T. X., Gott, J. R., and, Schneder, S. E. 1987. Ap. J. (Letters) 315, L93.

Ostriker, J. P., and Cowie, L. L. 1981, Ap. J. (Letters) 243, L 127.

Vettolani, G., de Souza, R., Marano, B., and Chincarini, G., 1985, Astron. Astrophys., 144, 506.

Weinberg, D., Gott, J. R., and Mellot, A. L., 1988, submitted to Ap. J.

Table I- Characteristics of voids for different cubic lattices.

Cell size (Mpc)	# Voids	x	y	z	Vol (Mpc^{-3})
			(Mpc)		
2.5	34	125	25	52	6×10^4
		129	63	29	3×10^3
5.0	19	154	33	51	3×10^4
		100	22	61	3×10^4
10.0	10	152	32	51	3×10^4
		102	22	39	3×10^4

Table II- Properties of Voids with $\rho = 0$.

Void	α 1950	δ	<v> (km/s)	V (Mpc^{-3})	r_{eq} (Mpc)	e_1	e_2
1	03 43.0	-18 47.9	5430	$8.0x10^2$	5.7	0.88	0.14
2	21 12.6	-18 48.0	6981	$3.7x10^2$	4.4	0.75	0.33
3	20 54.6	-24 38.9	4435	$1.9x10^3$	7.6	0.83	0.55
4	01 41.4	-21 41.0	7442	$3.2x10^3$	9.1	0.89	0.56
5	03 22.6	-44 01.6	3177	$7.6x10^3$	12.2	0.92	0.80
6	03 52.3	-39 01.6	8183	$3.0x10^4$	19.2	0.77	0.64
7	20 14.2	-54 01.1	9700	$6.2x10^2$	5.2	0.97	0.21
8	23 55.7	-69 52.0	6501	$3.0x10^4$	19.2	0.90	0.33

Table III- Properties of Voids with $\rho = 0.25 \langle\rho\rangle$

Void	α 1950	δ	$\langle v \rangle$ (km/s)	V (Mpc^{-3})	r_{eq} (Mpc)	e_1	e_2
1	21 15.1	-20 01.4	6863	6.2×10^2	5.3	0.87	0.62
2	20 56.1	-25 45.3	4356	2.6×10^3	8.5	0.85	0.63
3	03 39.4	-63 46.1	9336	5.0×10^2	4.9	0.63	1.00
4	02 24.4	-54 44.5	6321	1.3×10^5	31.3	0.85	0.58

Figure Captions

Figure 1- Distribution of galaxies with v < 10000 km/s in the Cartesian coordinate system defined in the text. In the figure we show the projection onto the x-y plane of galaxies in the range 20 < z < $50h^{-1}$ Mpc, in $10h^{-1}$ Mpc intervals.

Figure 2- Contrast map representing the column density of the smoothed galaxy distribution for the same slabs shown in figure 1.

Figure 3- Projection onto the x-y plane of the empty cells defining the two largest voids in the surveyed region. The slices shown are the same as those in the previous figures. Note that all the cells shown form a single connected structure.

Figure 4- Same as in figure 3, showing cells with density less than 25% of the mean. Only cells of the largest void are shown.

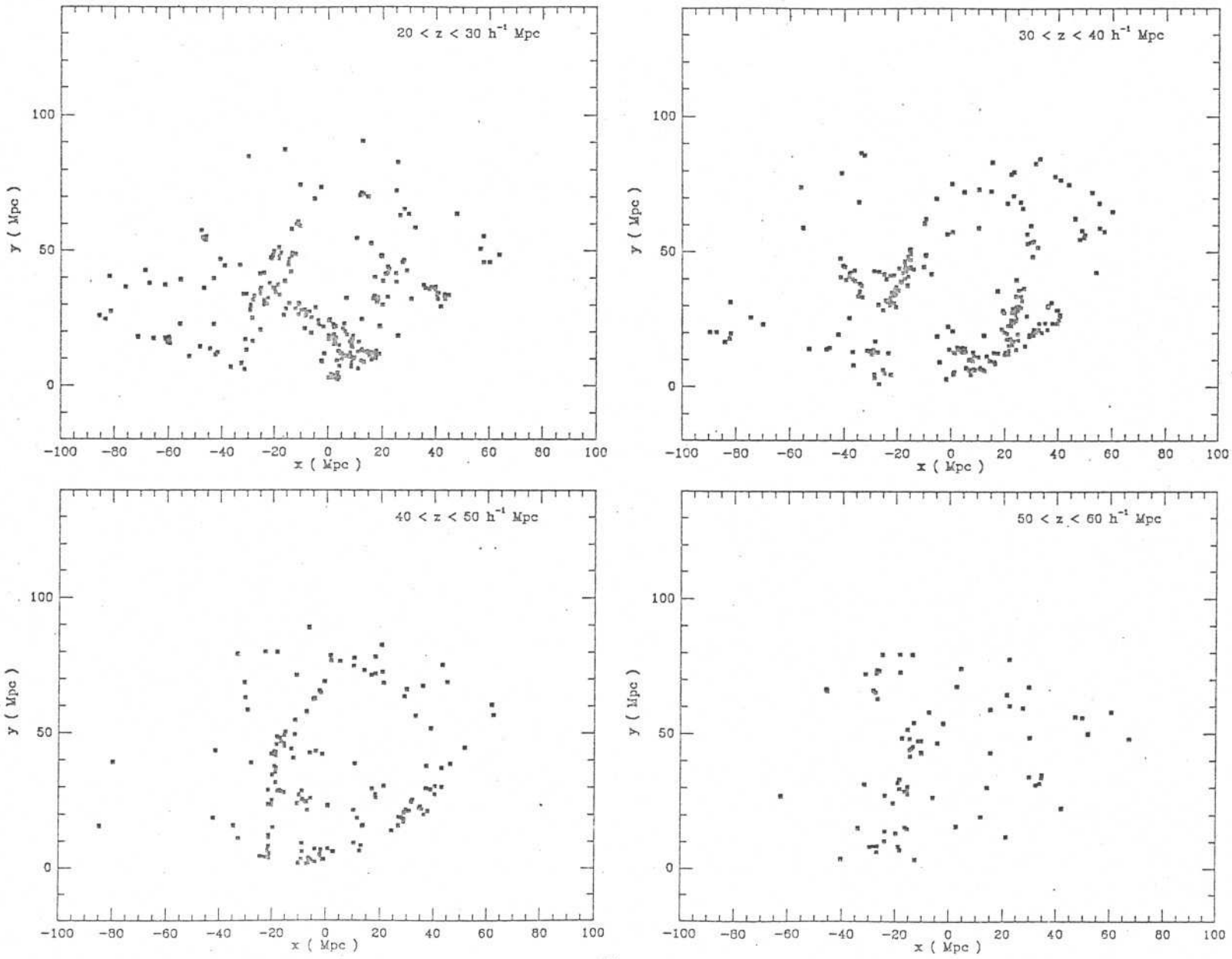
20 < z < 30 h⁻¹ Mpc
30 < z < 40 h⁻¹ Mpc
40 < z < 50 h⁻¹ Mpc
50 < z < 60 h⁻¹ Mpc
x (Mpc)
y (Mpc)
−100 −80 −60 −40 −20 0 20 40 60 80 100
0 50 100

Figure 1

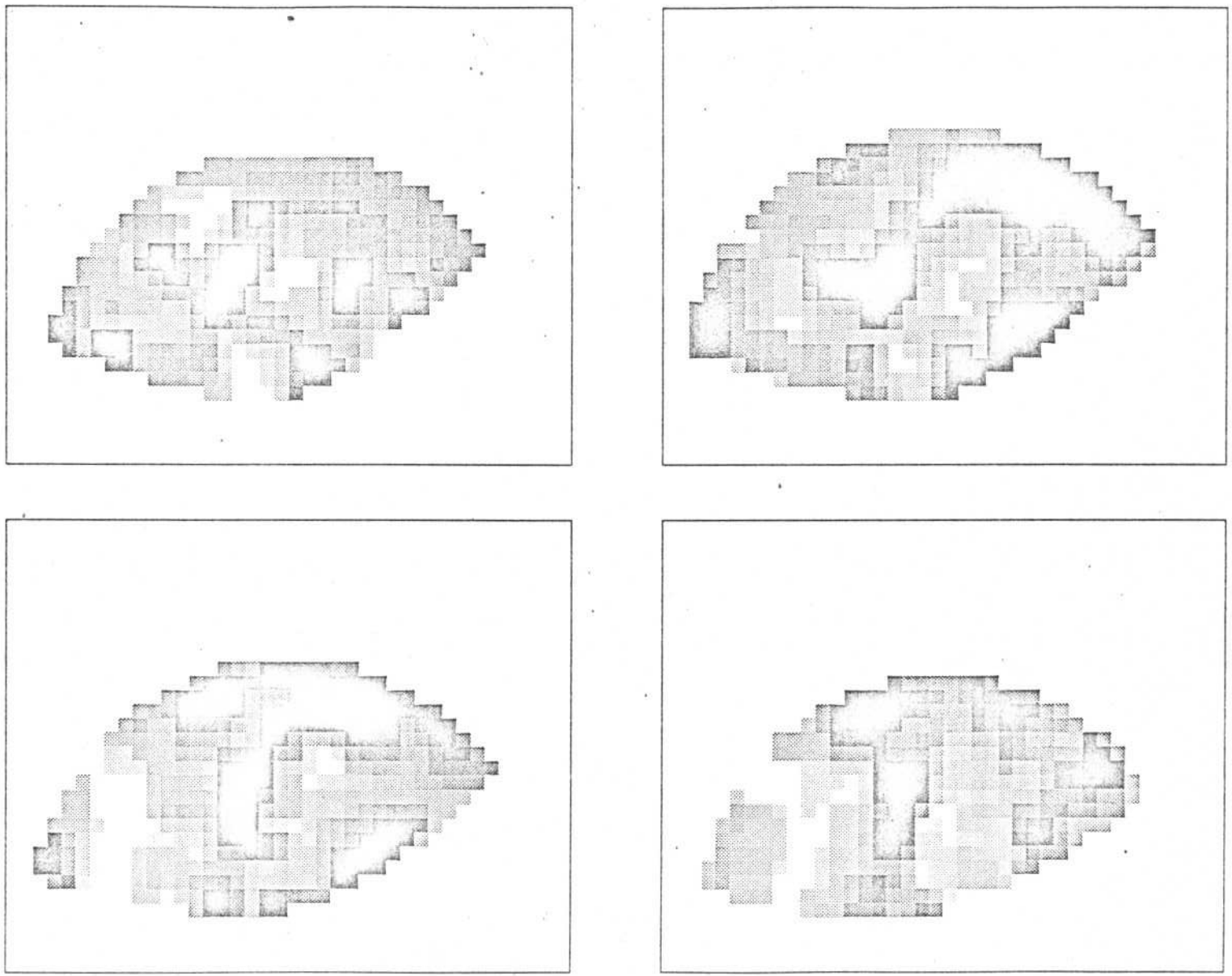

Figure 2

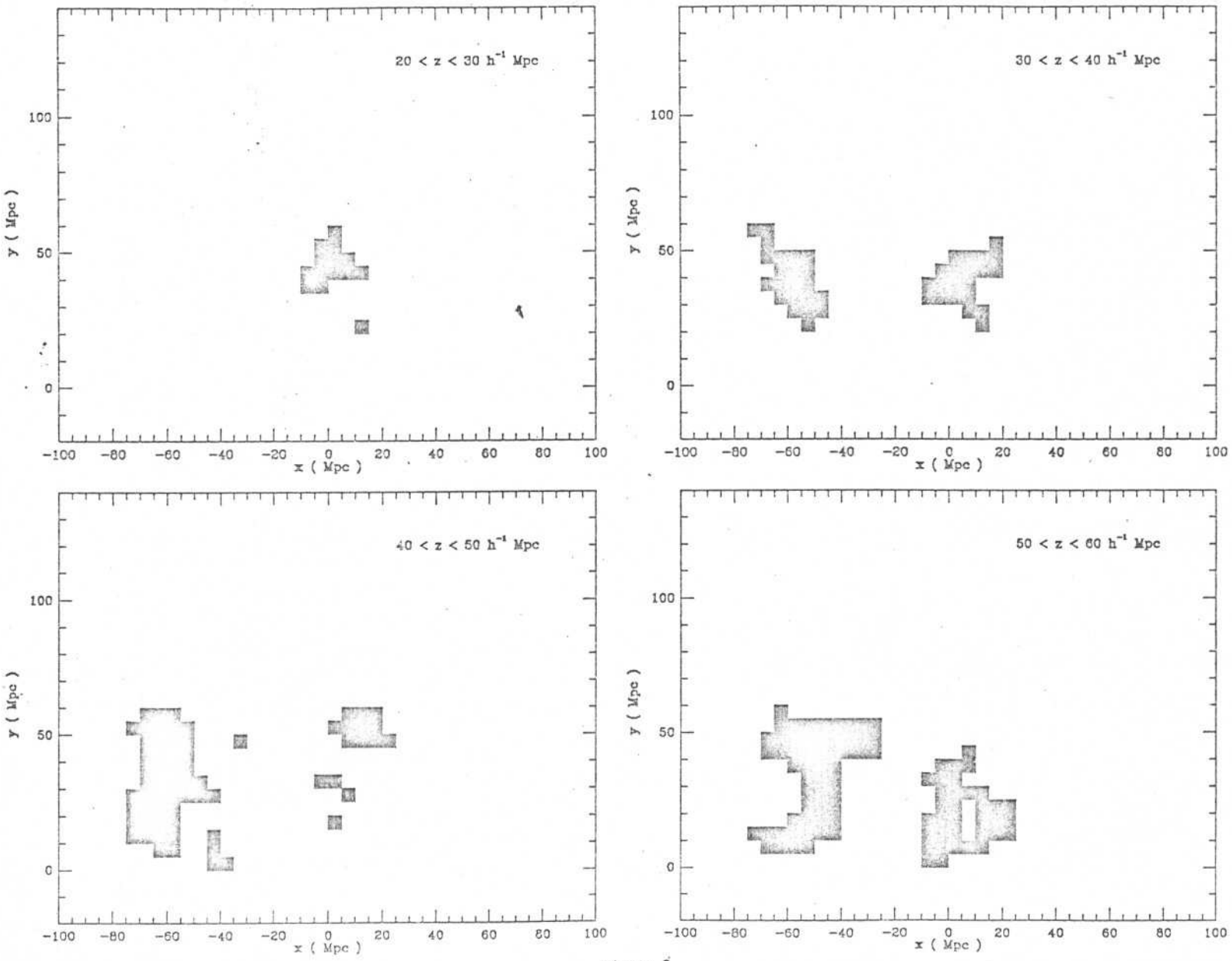
20 < z < 30 h⁻¹ Mpc
30 < z < 40 h⁻¹ Mpc
40 < z < 50 h⁻¹ Mpc
50 < z < 60 h⁻¹ Mpc
y (Mpc)
x (Mpc)
100
50
0
−100 −80 −60 −40 −20 0 20 40 60 80 100

Figure 3

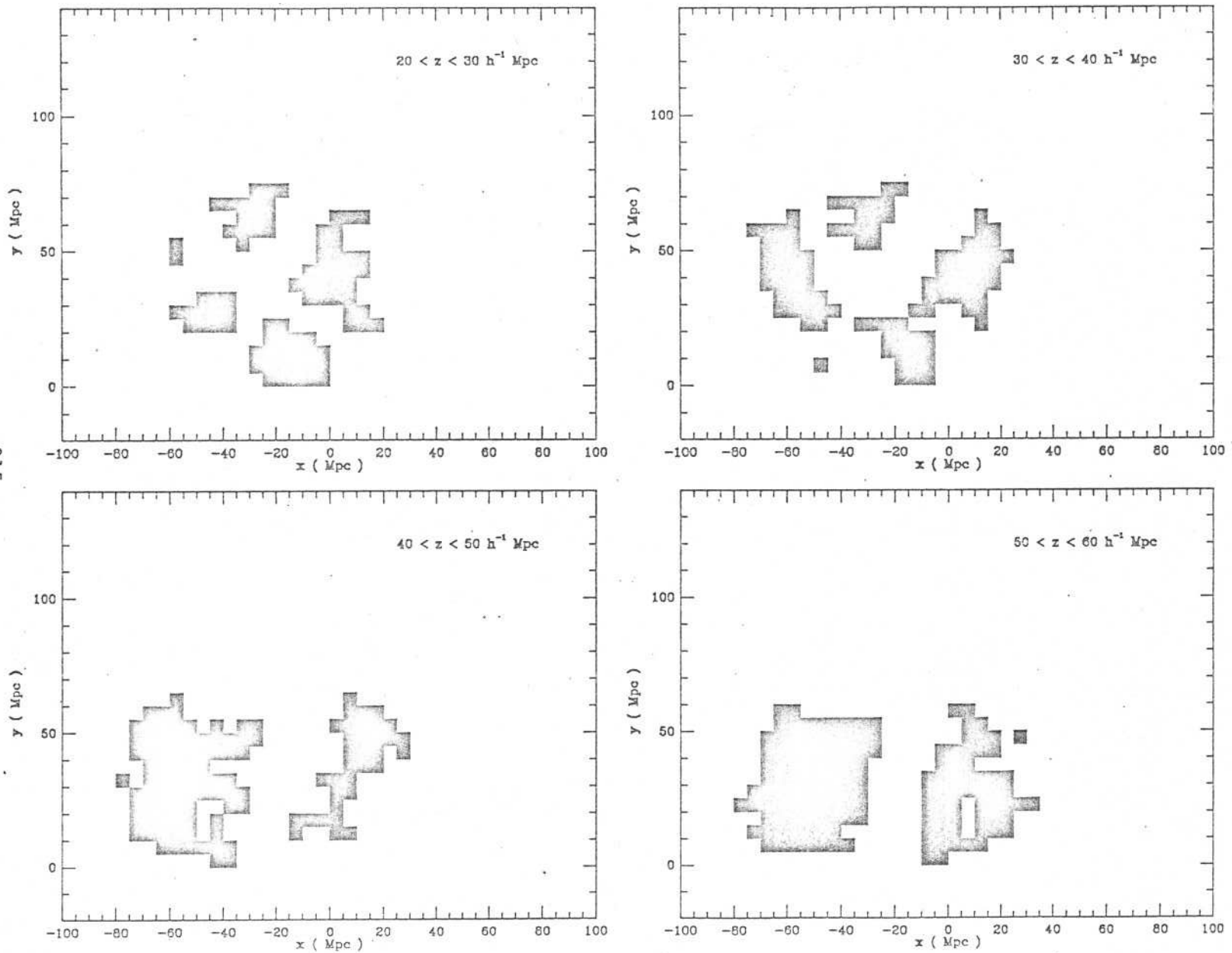
20 < z < 30 h⁻¹ Mpc
30 < z < 40 h⁻¹ Mpc
40 < z < 50 h⁻¹ Mpc
50 < z < 60 h⁻¹ Mpc
y (Mpc)
x (Mpc)
100
50
0
-100 -80 -60 -40 -20 0 20 40 60 80 100

Figure 4

V.3 VELOCIDADE PECULIAR INDUZIDA SOBRE O GRUPO LOCAL

PECULIAR VELOCITY OF THE LOCAL GROUP

Paulo. S. Pellegrini and L. Nicolaci da Costa

Departamento de Astronomia, CNPq/Observatorio Nacional

ABSTRACT

In this paper we calculate the peculiar velocity induced on the Local Group by the gravitational field of density fluctuations in the galaxy distribution. The present paper complements the earlier work of Davis and Huchra (1982), using for the southern galactic cap a much deeper sample with a slightly increased angular coverage. This allows an improved determination of the mean density of galaxies, avoiding the large concentration of objects associated to the Virgo cluster. Here we calculate the peculiar gravity produced by the material within the surveyed solid angle which covers 40% of the sky. We confirm that the dominant contribution of the southern galactic cap to the peculiar acceleration arises from low density regions, producing a net motion towards the northern hemisphere. This effect is even stronger at larger distances, because of a large void at about 6000 km/s. Within the framework of a spherical infall model we derive values of Ω from the component of the induced peculiar velocity in the direction of Virgo. We find that Ω lies in the range 0.09-0.56 for infall velocities of 100 to 500 km/s. These values are comparable to those derived by Davis and Huchra (1982) using a shallower southern sample.

I. INTRODUCTION

The dipole pattern observed in the microwave background radiation (hereafter MWB) has been interpreted as the result of a Local Group motion of ≈ 600 km/s towards l = 268°, b = 27° (e.g. Lubin et al. 1983). Over the years, much effort has been devoted to explain this motion as the result of the peculiar velocity of the Local Group induced by the gravitational field of local inhomogeneities of the galaxy distribution. A major contributor to this motion is thought to be the Virgo cluster and several works have attempted to determine the infall velocity of the Local Group towards this system using a variety of methods. As reviewed by Davis and Peebles (1983), current estimates for this velocity span the range of 200 to 400 km/s and accounts for only part of the total motion of the Local Group relative to the rest frame of the MWB. Tammann and Sandage (1985) pointed out that, if the infall velocity is of about 220 km/s, the unexplained component of the motion lies in the general direction of the Hydra-Centaurus supercluster. Although this system is apparently not as prominent as Virgo, the suggestion that it could be responsible for the additional acceleration of the Local Group, has motivated the several redshift surveys being carried out in the region (e.g. da Costa et al. 1986, 1987, Fairall and Jones 1988).

The picture above has changed recently due to the work of Dressler et al. (1987) on the motion of the Local Group with respect to a sample of elliptical galaxies distributed over the whole sky. In particular, these authors have shown that the Hydra-Centaurus supercluster may partake of a large bulk motion together with all galaxies that lie within a sphere of

about 10000 km/s from the Local Group, streaming in the direction roughly defined by the intersection of the galactic and supergalactic planes. More recently, detailed analysis of the elliptical sample carried out by Lynden-Bell et al. (1988), indicates that a better fit to the data can be obtained by postulating the existence of a concentration of mass, hidden by the obscuration zone, in the direction l = 207°, b = 9°, at a distance of 4350 km/s. Preliminary evidence in support to this large concentration of mass has been reported by Dressler (1988). However, as pointed out by Lynden-Bell et al. (1988), the great attractor model does not fully account for the observed motion of the Local Group relative to the MWB.

If the peculiar velocity of the Local Group has a gravitational origin and only the effects of large scales are considered, the peculiar velocity is proportional to the peculiar gravity (Peebles 1980). Moreover, the peculiar acceleration can be directly computed if the density field of the material in our surroundings is known, from redshift surveys of luminous galaxies, and light roughly traces the matter distribution. Evidences that this is the case come from the works of Lahav (1987) and Meiksin and Davis (1986), who have demonstrated that the dipole moments calculated from the projected distribution of an all-sky optical sample and the IRAS sample, respectively, are consistent with the direction of the microwave dipole anisotropy. However, until very recently, there was no redshift survey with adequate sky coverage and depth to allow the direct computation of peculiar motion of the Local Group. The first attempts were made by Yahil et al. (1980) using the shallow Revised Shapley-Ames Catalog of Bright Galaxies (Sandage and Tammann 1981) and by Davis and

Huchra (1982, hereafter DH), who considered the optically-selected catalog of the CfA Redshift Survey for the north. From the comparison of the computed component of the induced peculiar velocity in the direction of Virgo with assumed values for the virgocentric infall velocity, estimates for the density parameter Ω were derived.

We complement these previous works calculating the peculiar velocity generated on the Local Group using the redshift data from the CfA Redshift Survey and from a catalog recently compiled for the southern galactic cap (SGC) (Pellegrini et al. 1988). While the sky coverage of the present sample is still limited it is the largest optical sample presently available, covering 40% of the sky to comparable depths in the northern and southern hemisphere. The new data represent a great improvement over those available in DH and motivates a reexamination of their results.

In section II we describe the optical sample considered in the present work and describe the method of computing the peculiar velocity generated on the Local Group. In section III we discuss the determination of the mean density of galaxies and the contribution from shells at different distances to the peculiar velocity. A summary of our results is presented in section IV.

II. THE METHOD

In the present study of the peculiar velocity we use optically-selected samples in both galactic caps. For the northern galactic cap we use the magnitude-limited sample of the CfA Redshift Survey north of $\delta = 0°$ and $b \geq 40°$. The sample consists of 1857 galaxies covering an area of 1.83 steradians and radial velocities were taken from Huchra et al. (1983). For the southern galactic cap we use the magnitude-limited sample defined in an earlier paper (Pellegrini et al. 1988), which combines galaxies drawn from the Catalog of Galaxies and Cluster of Galaxies (Zwicky et al. 1961-68), the Morphological Catalogue of Galaxies (MCG, Vorontsov-Velyaminov and Arhipova 1963-68) and the ESO/Uppsala Catalog of the ESO (B) Atlas (Lauberts 1982). The procedure adopted for generating this magnitude-limited sample is discussed in detail by Pellegrini (1988). The resulting southern sample consists of 2372 galaxies south of $b = -30°$, covering an area of 3.13 steradians. Radial velocities in the southern hemisphere were drawn from the redshift catalog compiled by the Southern Sky Redshift Survey (SSRS) and its extension in the range $-17.5° < \delta < -2.5°$ (e.g. Sargent et al. 1988, da Costa et al. 1988b). The velocities were corrected for galactic rotation and for a virgocentric infall assuming a spherical model. Galaxies within 6° of the center of the Virgo cluster and with redshifts less than 2500 km/s were positioned at the distance of Virgo. In the analysis below two semi-volume limited samples were extracted from the complete data set, keeping only objects which are observable to at least 4000 km/s.

According to Peebles (1980) the peculiar velocity induced by

inhomogeneities in the galaxy distribution is, in the linear approximation, proportional to the peculiar acceleration and given by

$$\mathbf{v}_p = (2/3)\, f\, (H_0\Omega)^{-1}\, \mathbf{g}, \quad f \approx \Omega^{0.6} \tag{1}$$

where

$$\mathbf{g} = G\, \rho_c\, \Omega \int dV\, (n_1)^{-1}\, [\, n(\mathbf{r})/\varphi(r) - n_1\,]\, \mathbf{r}/r^3 \tag{2}$$

In the above expression $n(\mathbf{r})$ is the number density of observed galaxies at position $\mathbf{r}$, $\varphi(r)$ is the selection function and n_1 is the unbiased estimate of the mean density which can be written as

$$n_1 = (1/V) \sum_{shells} N(r)/\varphi(r) \tag{3}$$

where $N(r)$ is the number of observed galaxies in a shell from r to $r+\Delta r$. Following the notation of DH, we express the peculiar velocity as a function of the direction weighted shell density $\mathbf{n}$ and vector $\mathbf{p}$:

$$\mathbf{v}_p = (H_0\, \Delta r)\, \Omega^{0.6}\, (\omega/4\pi) \sum_{shells} (\mathbf{n}(r_s)/n_1 - \mathbf{p}) \tag{4}$$

where

$$\mathbf{n}(r_s) = (\omega'\, \varphi(r_s)\, r_s^2\, \Delta r)^{-1} \int d\omega\, \Sigma_i\, \delta(\mathbf{r}_s - \mathbf{r}_i)\, (\mathbf{r}_i/r_s) \tag{5}$$

and

$$\mathbf{p} = (1 / \omega') \int d\omega \, (\mathbf{r} / r) \qquad (6)$$

In the expressions above r_s is the radius of a shell, the sum over i includes galaxies within that shell, $d\omega$ is the element of solid angle and ω' is the solid angle encompassed by the surveyed regions. The contributions of the northern and southern galactic caps are calculated separately and the final vectors added.

The vector p depends only on the geometry of the samples considered. In the analysis below we adopt a Cartesian system with the z axis pointing towards the North Galactic pole and the x-axis towards l = 0°, b = 0° and the y-axis towards l = 90°, b = 0°. For the northern sample we derive p = (-0.07, 0.11, 0.84), in disagreement with that quoted by DH; the implications of this difference are discussed below. For the south we obtain p = (0., 0., -0.75). We note that p only enters the calculation because of the limited sky coverage of the optical sample. As in DH we assume, to a first approximation, that there is no contribution to the peculiar velocity coming from outside the solid angle considered or beyond the cutoff distance of the integrals that appear in the expressions above. In our standard calculations we have adopted a cutoff distance $r_c = 80h^{-1}$ Mpc, where φ (r) has dropped to about 0.1. The influence on the peculiar acceleration from material outside our solid angle was examined by assuming that it is dominated by a single mass concentration, like that expected in the kinematic model of Lynden-Bell et al. (1988).

III. THE MEAN DENSITY AND PECULIAR VELOCITY

A critical quantity in the calculation of the peculiar acceleration is the density estimator n_1, which affects the amplitude of the inhomogeneities and consequently their contribution to the gravitational field. Its definition is uncertain since, as has been discussed in the past, the scale of the inhomogeneities is comparable to the depth of the existing surveys, making average quantities ill-defined.

To examine how sensitive the value of n_1 is to the radial cutoff r_c and to the region of space we considered, we plot in figure 1 n_1 x r_c, showing, separately, the behavior of the northern and southern samples. As a comparison we also show the behavior of n_1 as determined from the diameter-limited sample of the SSRS. As can be seen in panel (a) n_1 is not well-defined in the North; for small radial distances the effect of Virgo is very pronounced giving rise to high values of n_1 ($\approx 12\times10^{-3}$ Mpc^{-3}). Thereafter, it rapidly drops to about 7×10^{-3} Mpc^{-3}, rising again at larger distances. The important point is that over the entire region there is no evidence that n_1 has reached a representative value and that the choice made by DH ($n_1 \approx 11.6\times10^{-3}$ Mpc^{-3}), evaluating n_1 at $r = 80h^{-1}$ Mpc does not appear to be particularly meaningful. In the south (panel b), the situation is somewhat different; n_1 is rather low for $r < 60h^{-1}$ Mpc, rising to about 8×10^{-3} Mpc^{-3} where it remains constant out to $r = 80h^{-1}$ Mpc, which is the limit of reliability of $\varphi(r)$. The influence of the selection function can be evaluated comparing the previous curves with that shown in panel (c), computed from the SSRS sample (da Costa et al. 1988a). Since this sample is somewhat deeper, we expect a better

determination of n_1 from this sample within the same volume. Indeed, we find from figure 1 (c) that despite small fluctuations, of the order of 15%, the estimate is nearly constant out to $100h^{-1}$ Mpc. The amplitude of the fluctuations is consistent with that derived by de Lapparent et al. (1988), taking into account the size of the largest empty region relative to the size of the survey.

Based on these considerations we believe that the value of the density estimator at $r_c = 80h^{-1}$ Mpc in the SGC sample ($n_1 = 7.8 \times 10^{-3}$ Mpc^{-3}) is a better estimate, and it is hereafter used as our standard value. The consequences of employing this lower value are discussed below.

In our standard calculation of the peculiar velocity we have adopted a virgocentric infall velocity of 250 km/s. The cumulative peculiar velocity is shown in figure 2, where we plot the total z-component of $v_p \Omega^{-0.6}$ and the contributions from the northern and southern samples, separately. The curve representing the northern contribution cannot be directly compared with that obtained by DH since the parameters are not the same. In addition, the lower value adopted here for the mean density makes the inhomogeneities in the north more prominent. Nevertheless, the general shape of the curve resembles those presented by DH and Strauss and Davis (1988a), rising rapidly due to Virgo, reaching a nearly constant value of about 600 km/s at $20h^{-1}$ Mpc. Thereafter, it decreases slightly until $r = 40h^{-1}$ Mpc, turning up again at larger distances. This rise is more pronounced than in the original curve computed by DH with the value of the z-component reaching a higher

value than that attained near Virgo. This raises the question of whether the radius of convergence has in fact been reached, as implicitly assumed in the calculation. It partly reflects the presence of a real fluctuation in the northern hemisphere, associated with the complex of Coma-A1367. The amplitude of this fluctuation is, however, rather uncertain because at these large distances only a small fraction of the galaxies is observed. We note that this feature remains when the southern contribution to the peculiar velocity is added.

The peculiar velocity induced by the southern sample is markedly different from the north. In the south the low-density regions predominate, producing a net positive peculiar velocity which reaches a maximum of 250 km/s at about $50h^{-1}$ Mpc. Since the peculiar velocity remains essentially constant thereafter, it suggests that this radial distance can be taken as the radius of convergence. The peaks at about 10 and $45h^{-1}$ Mpc are associated with the large voids detected in the SSRS (da Costa et al. 1988a), while the Fornax cluster is responsible for the depression at $15h^{-1}$ Mpc. From the figure we see that the southern cap contributes with about 1/3 of the total velocity, the large void in the south significantly affecting the shape of the curve that describes the total peculiar velocity. The total peculiar velocity vector in this calculation points to $l = 191°$, $b = 75°$; it is insensitive to the value used for the virgocentric infall velocity and it is only about 11° away from the direction obtained by DH, reflecting the prominence of Virgo.

Finally, we should mention that the discrepancy in the components of **p** affects the results only slightly. In figure 3 we plot the variation

of the z-component of the peculiar velocity as a function of the radial distance, calculated from the northern sample. The two lower curves were obtained using n_1 as derived from the northern sample itself but with the components of **p** given by DH (dotted curve) and as in section II (dashed curve). As can be seen, the effect is not very large at nearby distances, with the peak velocity at about $15h^{-1}$ Mpc decreasing roughly 50 km/s. The discrepancy is more dramatic at large distances where the velocity difference reaches about 200 km/s. In the figure we also illustrate the effect of using a different n_1, as obtained from the southern sample (continuous curve). In this case the effect is dramatic and the velocity difference reaches as much as 550 km/s. We also note that the use of a lower mean density is responsible for the more pronounced rise of the z-component amplitude at large distances.

In order to examine the role of the SGC to the peculiar velocity we plot in figure 4 the following curves: a) the contribution from a southern sample magnitude-limited at 13.0, $b < -40°$ and $r_c = 40h^{-1}$ Mpc, with a mean density as determined by DH for the northern sample (dotted curve); b) the contribution of the SGC sample, but again using the higher value of the mean density adopted in (a) (dashed curve); c) the same as (b) but with our value of n_1 (continuous curve). From these curves we find that the inclusion of the outer shells and the increase of the solid angle coverage in the SGC makes no difference within $40h^{-1}$ Mpc. However, if the higher value of n_1, as determined from the northern sample is adopted, the peculiar velocity increases monotonically with no hint of convergence out to $80h^{-1}$ Mpc. On the other hand, using n_1 derived from the south, the shape of the curve is very different.

Besides decreasing the overall amplitude, it reduces dramatically the influence of the outer shells with the z-component converging roughly at $50h^{-1}$ Mpc, as discussed previously.

The results above indicate the importance of adopting a lower value of n_1 and have prompted us to reevaluate the density parameter Ω estimated by DH, equating the calculated component of the peculiar velocity towards Virgo to the assumed infall velocity. The results are presented in table 1 for different infall velocities. We find that Ω lies in the range 0.09-0.38 for infall velocities in the interval 220-440 km/s. These values are somewhat lower than those deduced by DH due primarily to the lower mean density assumed. This is illustrated in figure 5 where we plot the z-component of the total peculiar velocity for two values of the mean density n_1. It is interesting to note that despite the difference in the value of n_1 the two curves have rather similar shapes and at $80h^{-1}$ Mpc differ by only 150 km/s.

Because of our limited sky coverage, we cannot adequately compute the transverse components of the peculiar velocity and examine the total motion induced to the Local Group. However, if the great attractor model of Lynden-Bell et al. (1988) is correct, the dominant contribution to the peculiar motion from the unsurveyed region must be due to this large concentration of mass. Therefore, we can examine its influence in the density field, correcting distances for the peculiar velocities in the direction of Virgo and the great attractor. We assume a spherical flow model for both systems and place a mass concentration at a distance of 4350 km/s and in the direction of $l = 307°$, $b = 9°$, inducing a velocity of

570 km/s at the location of the Local Group, as suggested by Lynden-Bell et al. (1988). In figure 6 we show the z-component of the peculiar velocity adopting the parameters given above for the great attractor model and a virgocentric infall velocity of 250 km/s. The resulting curve is quite similar to that obtained in figure 2, except at large radial distances, where the inclusion of the great attractor decreases the velocity slightly. This result suggests that the volume of space not covered by the optical redshift surveys is probably not the dominant source of error in our estimates of Ω. As discussed by Villumsen and Davis (1986) a more serious problem is probably the assumption of spherical models for the flowfield around Virgo and the great attractor. The last two entries of table 1 show the effect of including the great attractor in the calculation of Ω.

Using a value of 250 km/s for the virgocentric infall velocity and including the effects of the great attractor, we derive $\Omega = 0.13$, This value of Ω yields a total peculiar velocity of 267 km/s, considering galaxies within the observed solid angle. This vector points in the direction of $l = 195°$ and $b = 72°$, 23° away from the Virgo cluster. The vector sum of this total peculiar velocity with the 570 km/s velocity vector induced by the assumed mass concentration near galactic plane, gives a vector with an amplitude of 637 km/s, in the direction of $l = 299°$, $b = 32°$, which is 27° away from the MWB dipole anisotropy as measured by Lubin et al. (1983). This result shows that the great attractor model adopted here gives a reasonable description of the gravitational field outside the solid angle of our survey and supports the idea that the MWB anisotropy is gravitationally induced by material

within $50h^{-1}$ Mpc.

IV. CONCLUSIONS

We have used the data recently available from redshift surveys of the southern hemisphere to study the peculiar velocity induced on the Local Group by the material in our surroundings. The importance of the new southern data is two-fold: first, the deeper sample available for the southern galactic cap provides an improved estimate of the mean density of galaxies since in that region of the sky there are no large concentration of galaxies, such as Virgo in the north; second, it suggests that the contribution to the peculiar velocity arising in the SGC comes primarily from the material within $50h^{-1}$ Mpc of the Local Group. In particular, there is a slight increase of the total peculiar velocity calculated by DH, because of the large void detected by the SSRS at about 6000 km/s, which contributes to the northwards motion of the Local Group. These two factors imply in a significant reduction of the computed density parameter as compared to the values originally derived by DH, especially for smaller infall velocities in which case it is reduced by as much as a factor of 2.

We have also examined the possible influence of material outside our survey region, assuming that the dominant contribution to the peculiar acceleration comes from a large concentration of mass, as originally proposed by Lynden-Bell et al. (1988). We have shown that the presence of the great attractor has essentially no effect on the component of the peculiar velocity arising from the material within the observed region and, consequently, on our estimates of the density parameter. In addition, we have also seen that our simplistic model to account for the

transverse components of the Local Group motion yields a final peculiar velocity vector that is at least roughly consistent with the microwave dipole anisotropy. Of course, this is no proof for the existence of the great attractor.

The analysis presented here is admittedly crude because of our limited sky coverage and the assumption of spherical infall models for both Virgo and the great attractor. Progress in this area will certainly come from the analysis of the IRAS sample of galaxies which presently provides a 76% sky coverage and in the near future is expected to cover 87% of the celestial sphere (Yahil 1988). This sample will also allow for a self-consistent computation of the peculiar velocity field as recently reported by Strauss and Davis (1988b) and Yahil (1988). Although the IRAS sky coverage will be unmatched by optical surveys, the latter are important because they probe space more densely and represent the high-density regions better, since the IRAS sample is dominated by late-spirals. Therefore, a detailed comparison between the results obtained from the optical samples and the IRAS sample will help us understand the limitations of the latter and may give hints on how to overcome the bias against high-density regions. Some preliminary results have already been obtained for the northern hemisphere by Strauss and Davis (1988a), and the southern data will further contribute to this effort.

ACKNOWLEDGMENTS

We thank our collaborators in the SSRS for allowing us to use the data before publication. We thank M. Strauss and M. Davis for providing us their IRAS results before publication.

REFERENCES

da Costa, L. N., Nunes, M. A., Pellegrini, P. S., Willmer, C., Chincarini, G. and Cowan, J. 1986, Astron. J. **91**, 6.

da Costa, L. N., Willmer, C., Pellegrini, P. S. and Chincarini, G. 1987, Astron. J. **93**, 1338.

da Costa, L. N., Pellegrini, P. S., Sargent, W. L. W., Tonry, J., Davis, M., Meiksin, A. and Latham, D. 1988, Ap. J. **327**, 544.

de Lapparent, V., Geller, M. and Huchra, J. P. 1986, Ap. J. (Letters), **302**, L1 (LGH).

Davis, M. and Huchra, J. 1982, Ap. J., **254**, 437.

Davis, M. and Peebles,P. J. E. 1983, Ap. J., **267**, 465

Dressler, A., Lynden-Bell, D., Burstein, D, Davies, R. L., Faber, S. M., Terlevich, R. J. and Wegner, G. 1987, Ap. J. (Letters), **313**, 137.

Dressler, A. 1988, preprint

Fairall, A. P. and Jones A. 1988, Pub. Dep. Astron. Univ. Cape Town, Nº 10.

Huchra, J. P., Davis, M., Latham, D. and Tonry, J. 1983, Ap. J. Suppl., **52**, 89.

Lahav, O. 1987, M. N. R. A. S., **225**, 213.

Lauberts, A. 1982, The ESO/Uppsala Survey of the ESO(B) Atlas (Munchen: European Southern Observatory).

Lubin, P. M., Epstein, G. L. and Smooth, G. F. 1983, Phys. Rev. Lett., **50**, 616.

Meiksin, A. and Davis, M. 1986, Astron. J. **91**, 191.

Peebles, P. J. E. 1980, The Large-Scale Structure of the Universe (Princeton University Press)

Pellegrini, P. S., da Costa, L. N., Huchra, J. P., Latham, D. W. and

Willmer, C. N. A. 1988, in preparation.

Pellegrini, P. S. 1988, PhD. thesis, Observatório Nacional.

Lynden-Bell, D., Faber, S. M., Burstein, D., Davies, R. L., Dressler, A., Terlevich, R. J. and Wegner, G. 1988, Ap. J., in press.

Sandage, A. and Tamman, G. A. (1981). A Revised Shapley-Ames Catalogue of Bright Galaxies (Carnegie Institution of Washington, Washington, D.C.).

Sargent W. L. W., Tonry, J., da Costa, L. N., Pellegrini, P. S., Davis, M., Meiksin, A. and Latham, D. W. 1988, in preparation.

Strauss, M. and Davis, M. 1988a, IAU Symp. 130, Large Scale Structure of the Universe, eds J. Audouze and A. Szalay (Dordrecht: Reidel), in press.

Strauss, M. and Davis, M. 1988b, to be publised in the proceedings of the Vatican Study Week on Large-Scale Motions in the Universe.

Tammann, G. A. and Sandage, A. 1985, Astron. J., **294**, 81.

Villumsen, J. V. and Davis, M. 1987, Ap. J., **308**, 499.

Vorontsov-Velyaminov, B. A. and Arhipova, V. P. (1963-1974). Morphological Catalogue of Galaxies (Moscow). Parts 2 to 5.

Yahil A., Sandage, A. and Tamman, G. A. 1980, Ap. J., **242**, 448.

Yahil, A. 1988, to be publised in the proceedings of the Vatican Study Week on Large-Scale Motions in the Universe.

Zwicky, F., Herzog, E., Wild, P., Karpowicz, M. and Kowal, C. (1961-1968). Catalog of Galaxies and Clusters of Galaxies Vols. 1-6 (Pasadena, California Institute of Technology).

TABLE 1

V_V	V_{ga}	Ω_{ON}	Ω_{DH}
220	-	0.09	0.2
440	-	0.38	0.5
100	570	0.02	-
500	570	0.56	-

FIGURE CAPTIONS

Figure 1. Variation of the density estimator n_1 as a functionof the radial cutoff r_c for the CfA northern sample (a), the SGC sample (b) and the SSRS (c).

Figure 2. Cumulative z-component of the peculiar velocity as a function of the radial distance, induced by: the SGC sample (dotted curve), the CfA northern sample (dashed curve) and the total sample (continuous curve). An infall velocity of 250 km/s towards Virgo is adopted.

Figure 3. Cumulative z-component of the peculiar velocity from the CfA northern sample as a function of the radial distance. Lower curves were derived using n_1 from the northern sample and p given by DH (dotted curve) and derived in section II (dashed curve). The continuous curve was derived with n_1 from the southern sample and p derived in section II.

Figure 4. Cumulative z-component of the peculiar velocity for southern samples as a function of radial distance. Upper curves were obtained from a sample limited to m = 13.0 and $r_c = 40h^{-1}$ Mpc (dotted curve) and the SGC sample (dashed curve) using n_1 from the northern data. The lower curve was derived from the SGC sample using n_1 derived in section II.

Figure 5. Cumulative z-component of the total peculiar velocity as a

function of the radial distance for n_1 calculated from the northern sample (dashed curve) and from the southern sample (continuous curve).

Figure 6. Cumulative z-component of the peculiar velocity induced by the SGC sample (dotted curve), CfA northern sample (dashed curve) and the total sample (continuous curve) as a function of the radial distance. A motion of 570 km/s in the direction of the great attractor and an infall velocity of 250 km/s towards Virgo is adopted.

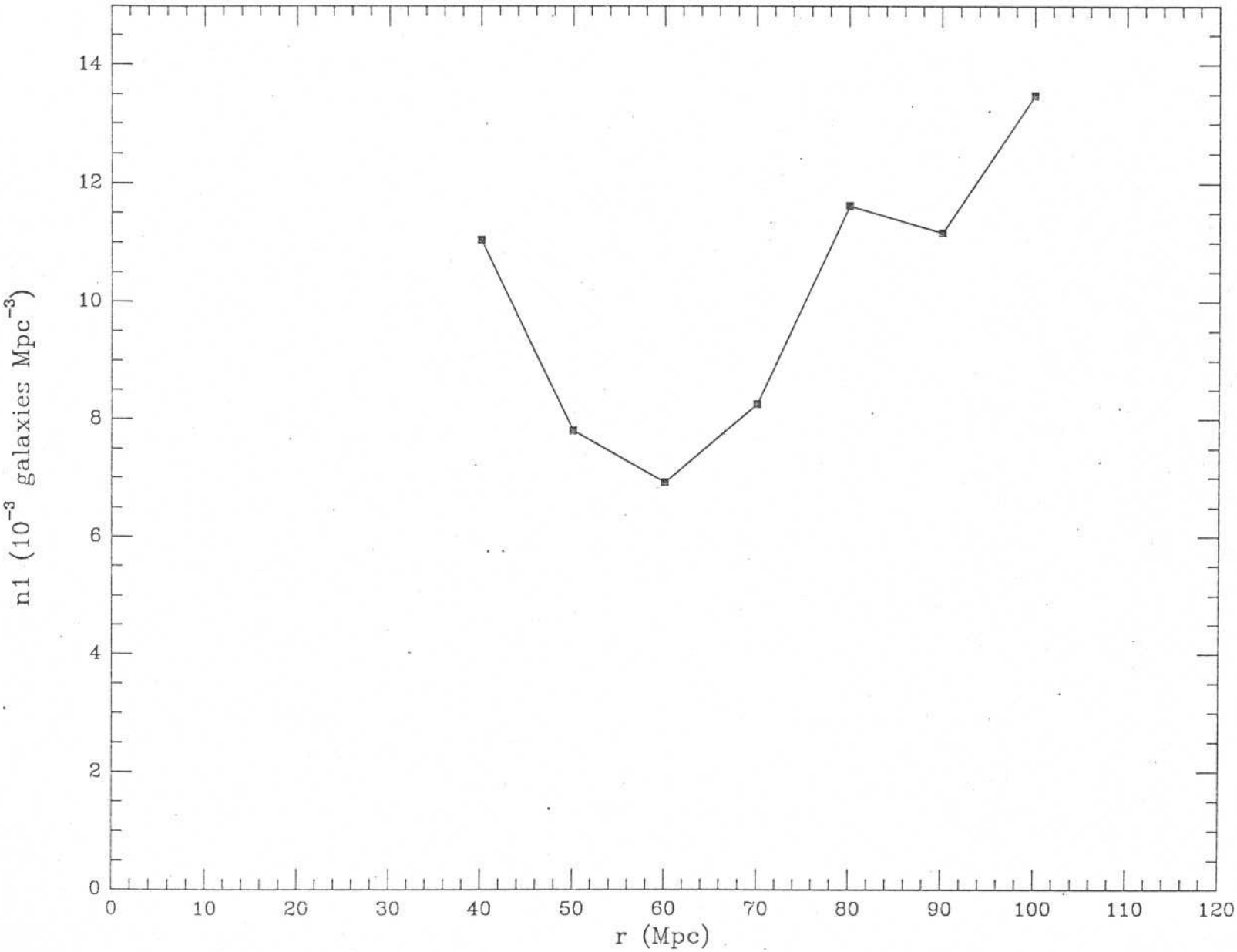
n1 (10^{-3} galaxies Mpc^{-3})
r (Mpc)
0
2
4
6
8
10
12
14
0
10
20
30
40
50
60
70
80
90
100
110
120

Figure 1a

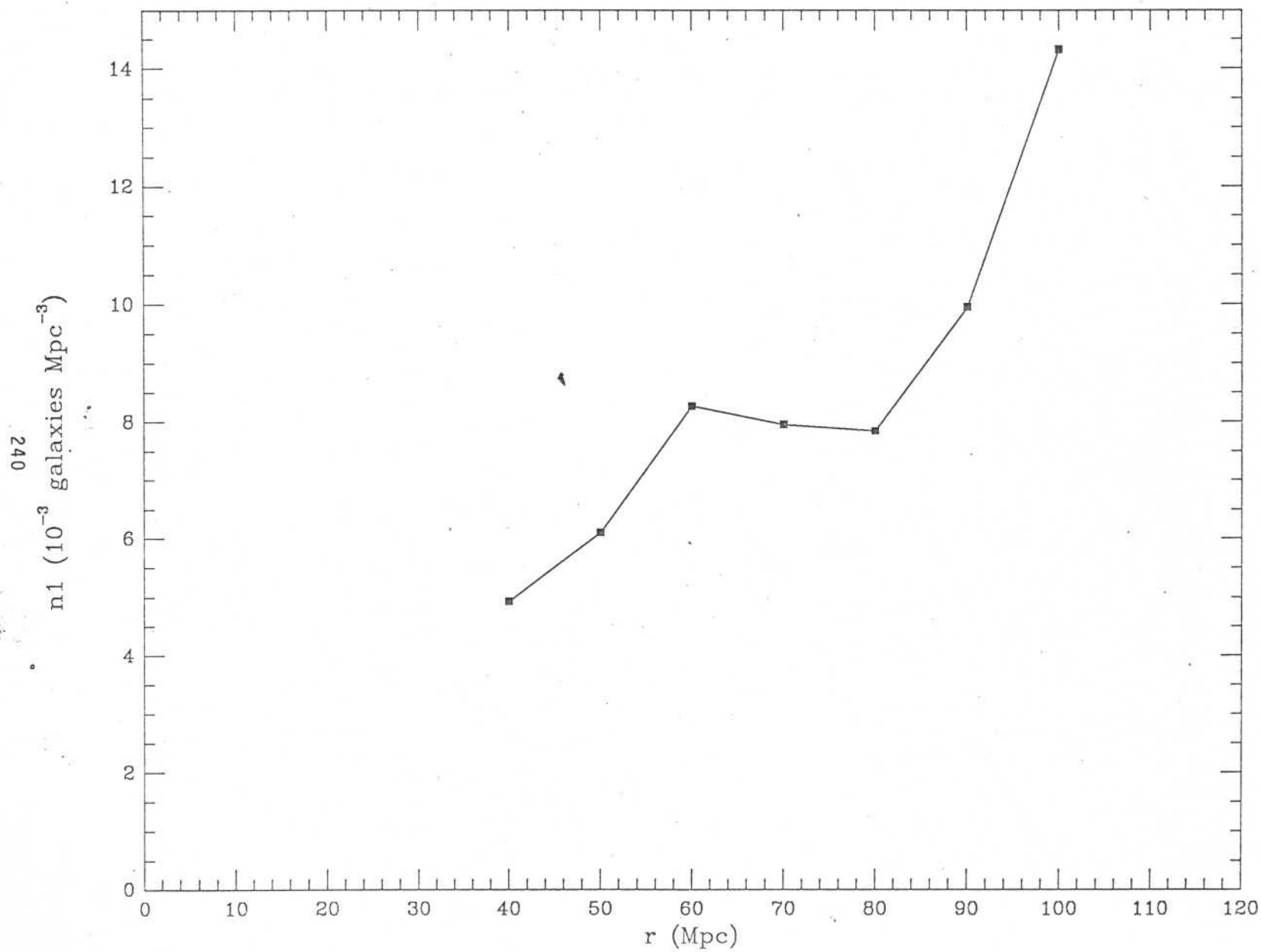
240
n1 (10^{-3} galaxies Mpc^{-3})
0
2
4
6
8
10
12
14
0
10
20
30
40
50
60
70
80
90
100
110
120
r (Mpc)

Figure 1b

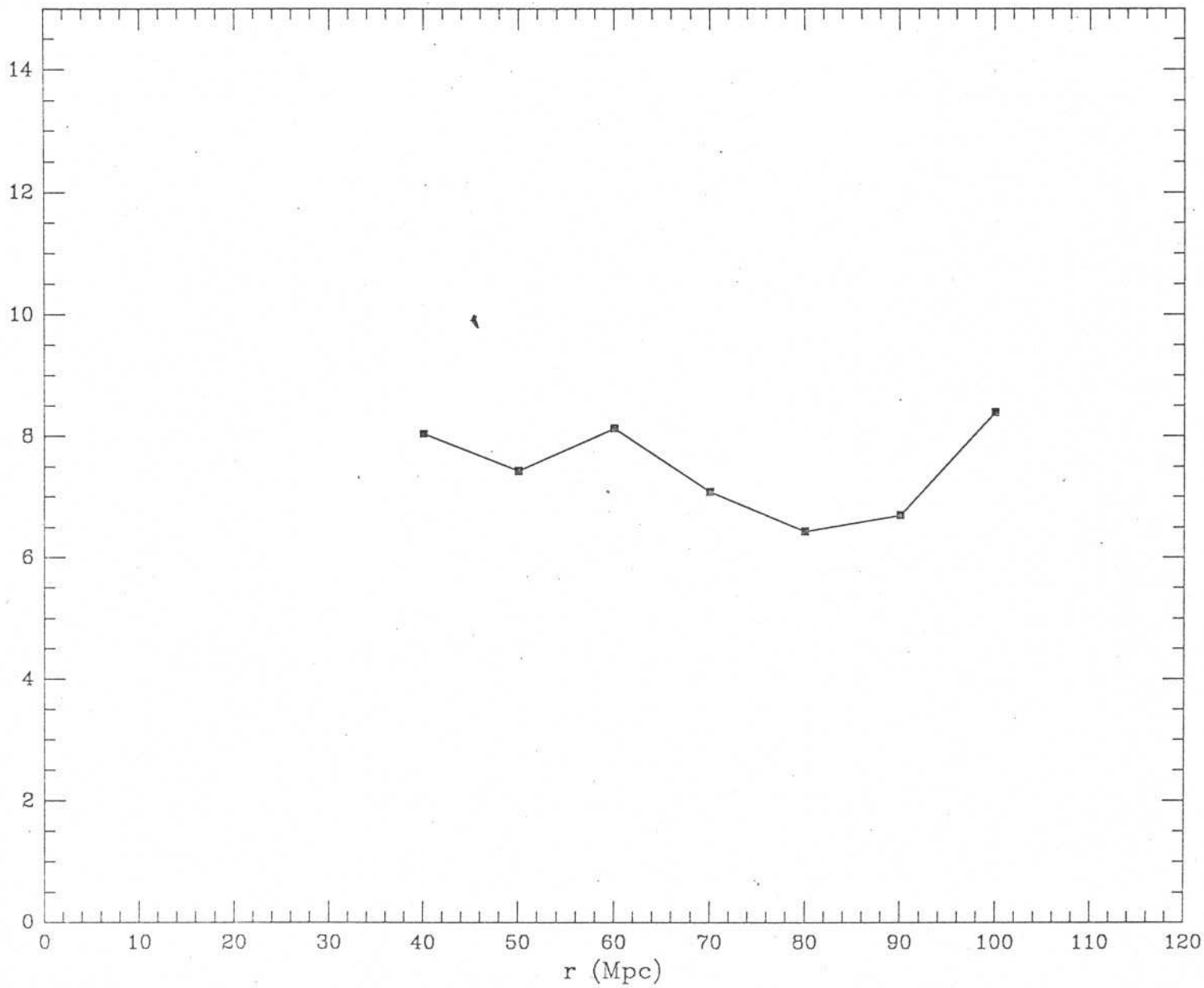
241
n1 (10^{-3} galaxies Mpc^{-3})
0
2
4
6
8
10
12
14
0
10
20
30
40
50
60
70
80
90
100
110
120
r (Mpc)

Figure 1c

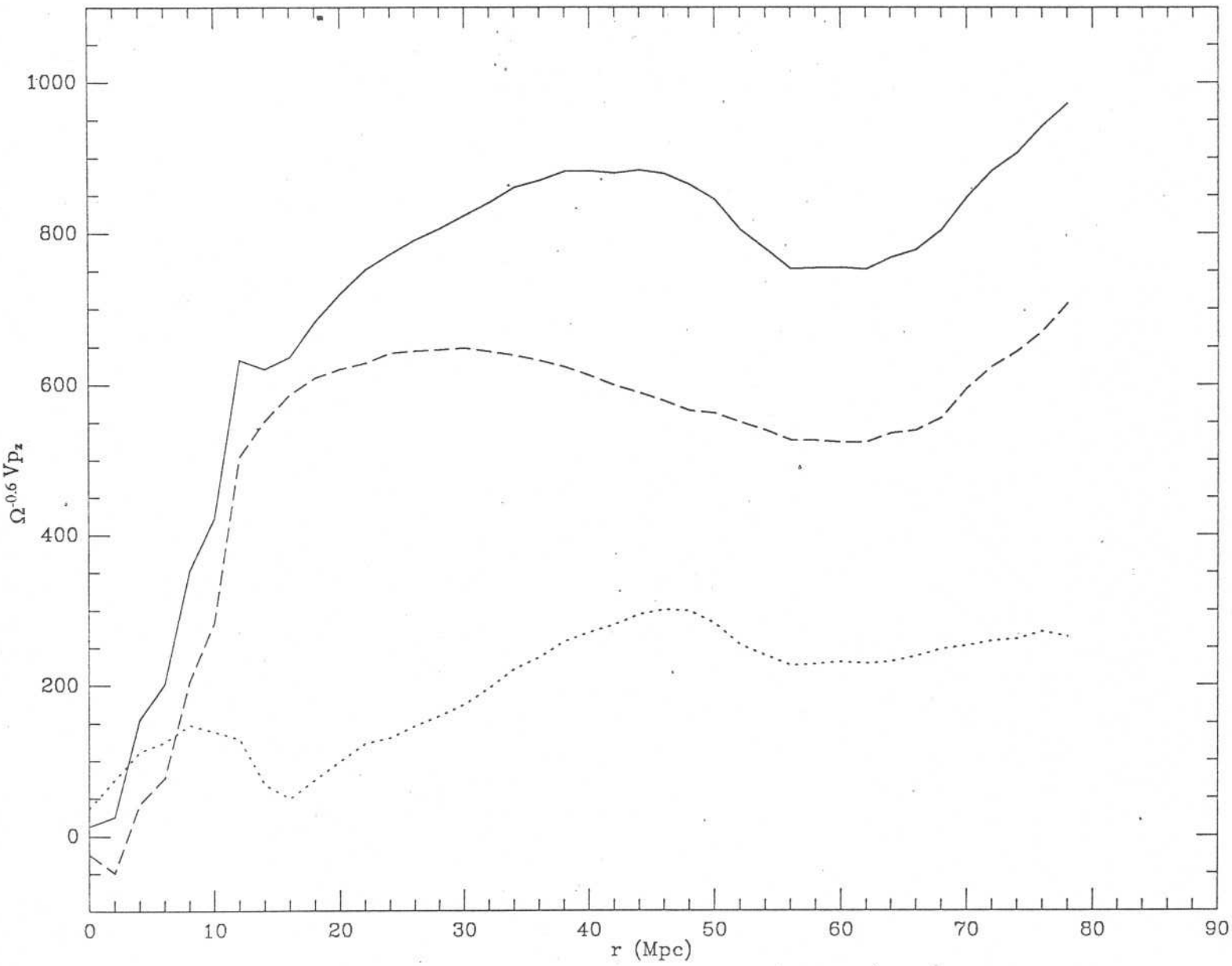
1000
800
600
400
200
0
$\Omega^{-0.6}$ Vp$_z$
0
10
20
30
40
50
60
70
80
90
r (Mpc)

Figure 2

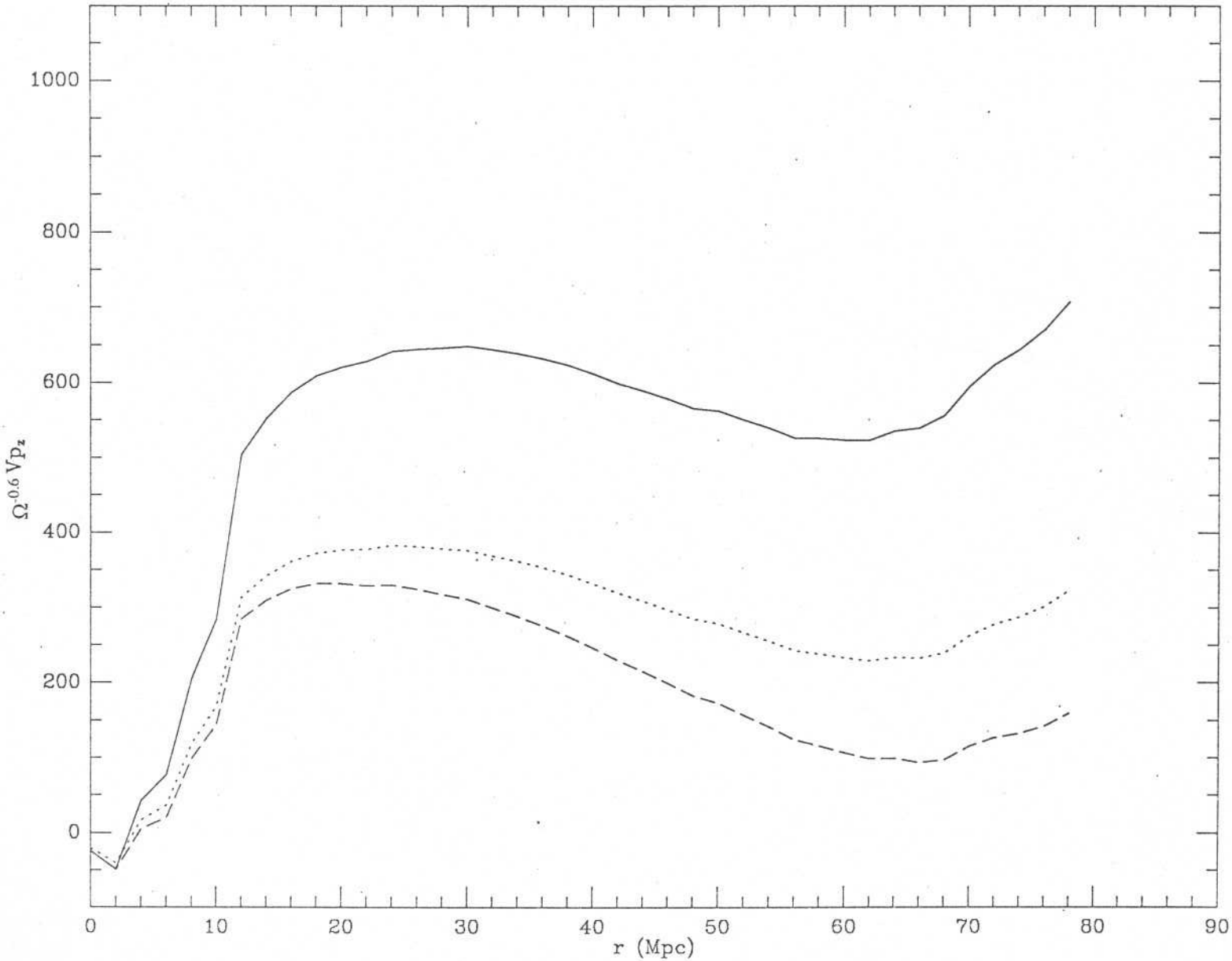

Figure 3

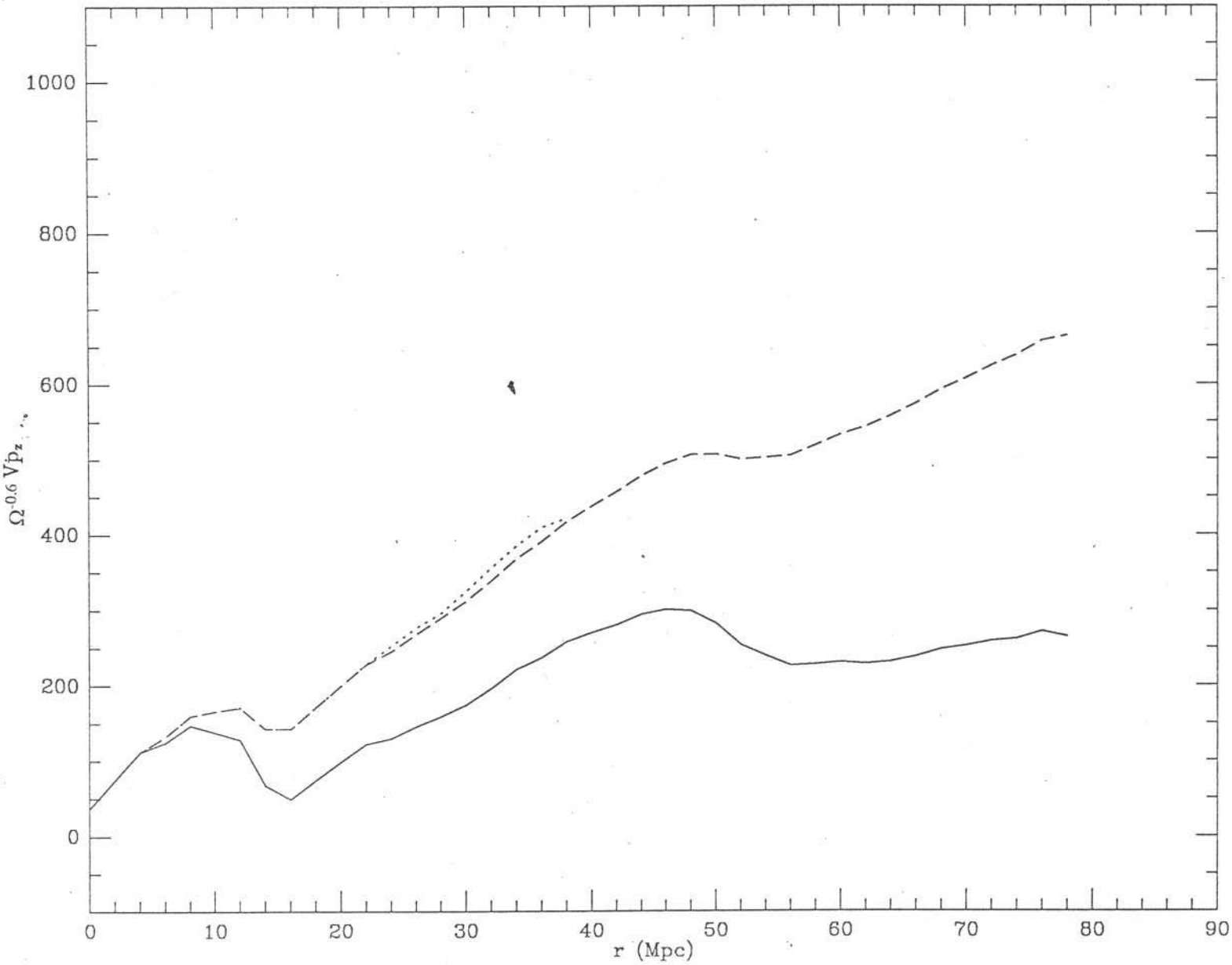
1000
800
600
400
200
0
$\Omega^{0.6} V_{pz}$
0
10
20
30
40
50
60
70
80
90
r (Mpc)

Figure 4

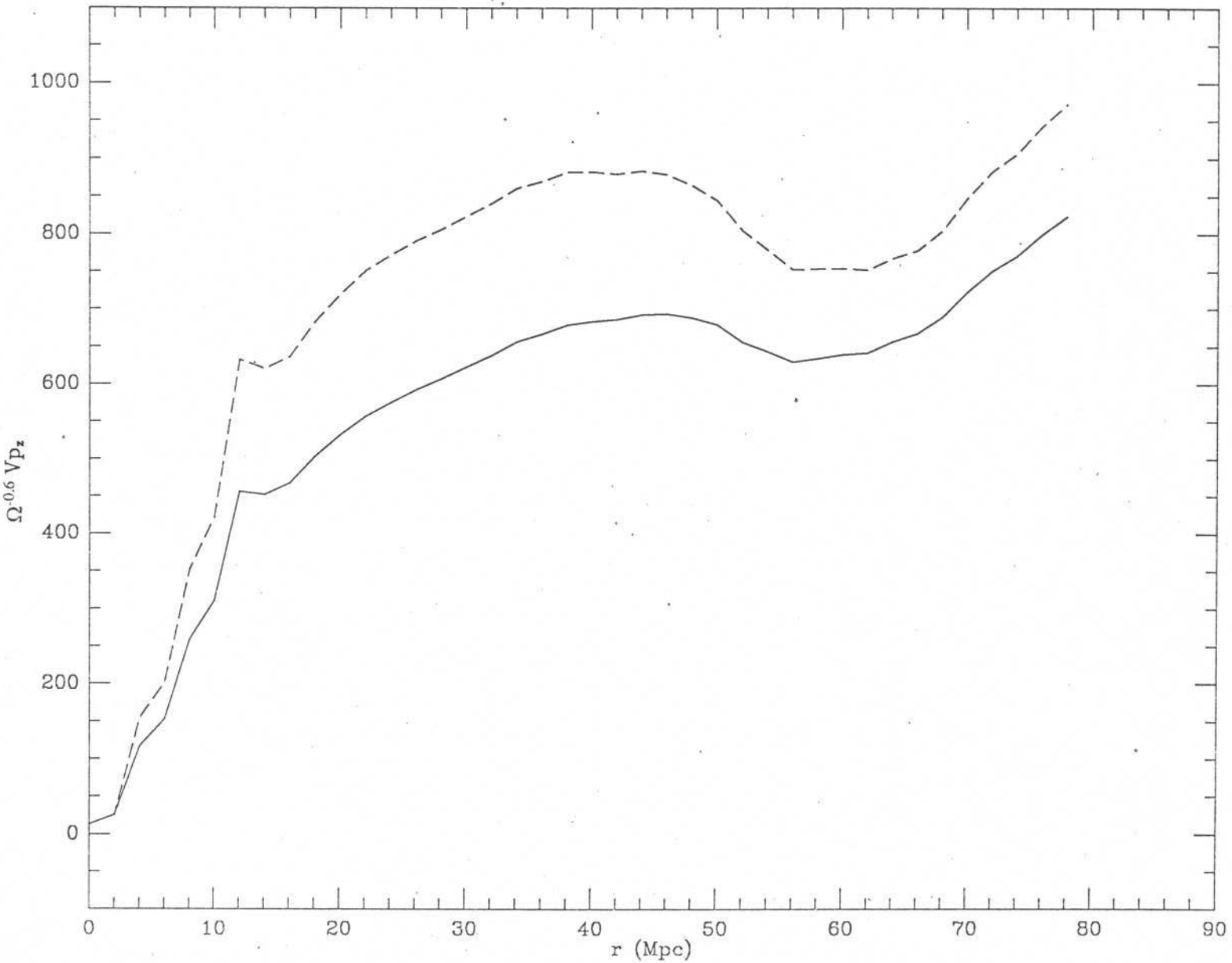

Figure 5

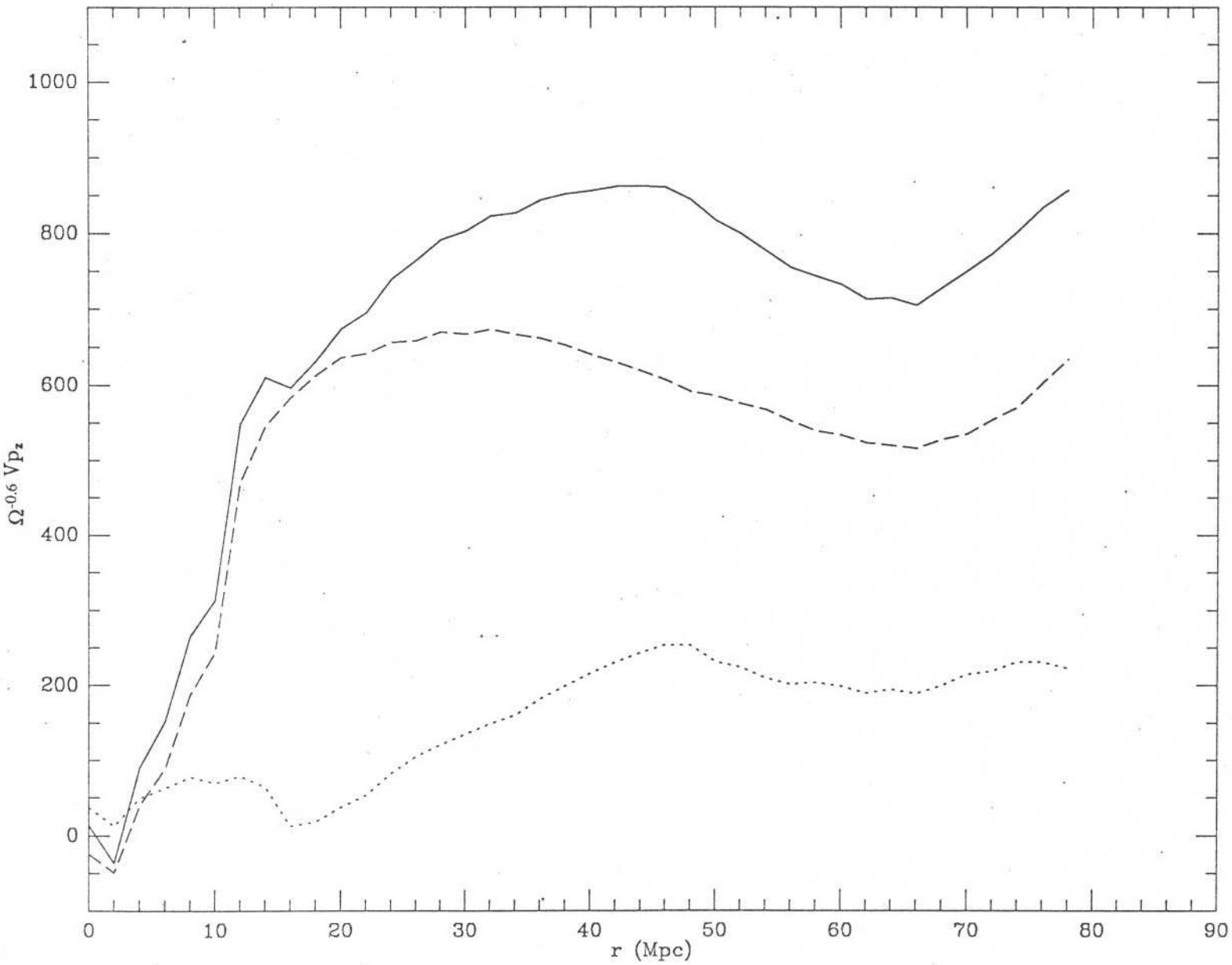
1000
800
600
400
200
0
$\Omega^{-0.6}$ Vd_z
0
10
20
30
40
50
60
70
80
90
r (Mpc)

Figure 6

VI. RESUMO DOS PRINCIPAIS RESULTADOS

Neste trabalho foram apresentados os primeiros resultados do maior levantamento de velocidades radiais de galáxias existente no hemisfério sul. Este trabalho só foi possível graças ao enorme empenho do pessoal do ON e a colaboração de diversos pesquisadores de outras instituições, num grande esforço internacional. Como esperado, os resultados obtidos foram de grande importância, principalmente porque nos permitiu examinar a natureza das estruturas de baixo contraste de densidade e, pela primeira vez, investigar se as propriedades estatísticas da amostra de galáxias considerada pelo CfA Redshift Survey são reproduzíveis. Estes dois pontos são, provavelmente, as principais contribuições do Levantamento de Velocidades de Galáxias do Hemisfério Sul.

A análise dos dados do SSRS, SGC e do Slice survey sugerem que as galáxias estao distribuidas ao longo de superfícies relativamente finas (de 5 a $10h^{-1}$ Mpc) que nos parecem planares, ao contrário das superfícies curvas sugeridas por de Lapparent et al. (1986). Esta interpretação é reforçada pelo fato de que as estruturas observadas se interceptam formando quinas bastante acentuadas, compondo ao que parece uma rede de células connectadas. Esta estrutura do universo é muito semelhante às primeiras descrições de Zel'dovich da distribuição esperada da evolução não-linear de pertubações adiabáticas, com uma escala de tamanho típica imposta por processos dissipativos. As estruturas observadas são tipicamente maiores do que $50h^{-1}$ Mpc, tem um contraste densidade da ordem de 4 em relação a densidade média e delineam grandes regiões

vazias, com tamanhos que vão até $60h^{-1}$ Mpc. Uma dessas regiões é particularmente extraordinária e por ser próxima poderá ser usada em trabalhos futuros para estudar o conteúdo dos "voids". Entretanto, amostras óticas a limites de magnitude ainda mais fracos e observações em 21 cm para galáxias de baixo brilho superficial serão necessários para este estudo. Estes resultados serão de grande importância para investigar se a distibuição de galáxias reflete a da matéria ou se existe algum efeito de "bias" que segrega diferentes tipos de galáxias, como previsto por algumas teorias de formação de estruturas envolvendo matéria escura. Além disso, o exame detalhado das propriedades dos "voids" em tres dimensões na região do SSRS indica que estes são irregulares e interconectados, como esperado para uma distribuição com uma topologia do tipo esponja como discutido por Gott et al. (1986).

Com a amostra do SSRS, foi possível confrontar as propriedade do CfA1 e SSRS, utilizando alguns dos mais usados métodos de análise estatística de distribuições de galáxias. Os resultados obtidos indicam que apesar de algumas diferenças nos detalhes dessas distribuições, suas propriedades estatísticas são bem similares indicando que os volumes observados até agora parecem ser representativos do universo em grande-escala. Este resultado é de grande importância já que a amostra do CfA1 vem sendo usada para calibrar as simulacões numéricas e confrontar as propriedades das distribuições obtidas nestas simulações.

Finalmente, a inclusão da amostra do hemisfério sul permitiu aprimorar as estimativas do parametro de densidade Ω a partir do cálculo direto da velocidade peculiar induzida pelas flutuações de densidade

existentes na nossa vizinhança, assumindo que as galáxias estão distribuidas da mesma forma que a matéria escura. A utilização de uma amostra mais funda do hemisferio sul, evitando a grande concentração de galáxias associadas ao aglomerado de Virgo, permitiu a obtenção de uma melhor estimativa da densidade média de galáxias. Com estas modificações obtivemos valores de Ω ligeiramente menores dos que aqueles obtidos por Davis and Huchra (1982).

O trabalho apresentado nesta tese representa o final da primeira fase do levantamento do hemisfério sul. A segunda, já iniciada, envolverá a complementação do levantamento de galáxias mais brilhantes que m_B = 15.5 na faixa de declinação de -30° a -40°, onde pelo menos dois grandes voids foram detectados, e a complementação do levantamento na faixa coberta pelo MCG. O primeiro programa visa determinar o contraste de densidade efetivo das grandes regiões vazias e verificar se o tamanho dos voids varia com parâmetros intrínsicos das galáxias tais como o tipo morfológico, brilho superficial e luminosidade. O objetivo do segundo programa é completar um levantamento de velocidades radiais de uma amostra homogênea, limitada em magnitude ou diâmetro, cobrindo as calota polares a uma profundidade moderada como aquela obtida no SSRS. Estes programas, quando finalizados, poderão contribuir significativamente para avaliar os modêlos teóricos para formação e evolução de grandes estruturas no universo.

Todos os Interessados em Publicações do Observatório Nacional. Devem Dirigir-se à

MCT - CNPq
Observatório Nacional
Biblioteca
Setor de Reprodução Gráfica
r. Gal. José Cristino, 77 - CP. 23002
20921 - São Cristovão, RJ
BRASIL
Telf. 5807313 - r.271